IDENTIFICATION OF CONCRETE INCOMPATIBILITIES USING CEMENT PASTE RHEOLOGY

A Dissertation

by

SE HOON JANG

Submitted to the Office of Graduate Studies of
Texas A&M University
in partial fulfillment of the requirements for the degree of

DOCTOR OF PHILOSOPHY

May 2009

Major Subject: Civil Engineering

IDENTIFICATION OF CONCRETE INCOMPATIBILITIES USING CEMENT PASTE RHEOLOGY

A Dissertation

by

SE HOON JANG

Submitted to the Office of Graduate Studies of
Texas A&M University
in partial fulfillment of the requirements for the degree of

DOCTOR OF PHILOSOPHY

Approved by:

Co-Chairs of Committee,	Dan G. Zollinger
	Anal K. Mukhopadhyay
Committee Members,	Zachary Grasley
	Mohammed Haque
Head of Department,	David V. Rosowsky

May 2009

Major Subject: Civil Engineering

ABSTRACT

Identification of Concrete Incompatibilities Using Cement Paste Rheology. (May 2009)

Se Hoon Jang, B.S., Kyungpook National University, Daegu, South Korea;

M.S., Texas A&M University

Co-Chairs of Advisory Committee, Dr. Dan G. Zollinger
Dr. Anal K. Mukhopadhyay

The complex interaction between cement and chemical/mineral admixtures in concrete mixtures sometimes leads to unpredictable concrete performance in the field which is generally defined as concrete incompatibilities. Cement paste rheology measurements instead of traditional workability tests (i.e., slump cone test) can have great potential in detecting those incompatibilities in concrete before the concrete is placed, which can, in turn, avoid related workability problems and setting time as well as heat evolution abnormalities. The objectives of the present study were to examine the applicability of the dynamic shear rheometer (DSR) to measure cement paste rheology, and to identify cement and mineral/chemical admixture incompatibilities, based on the determined rheological parameters.

The DSR was modified and optimized for cement paste rheology measurements. Two different modes of operations (i.e., static and dynamic methods) with the modified DSR were investigated to measure representative rheological parameters as well as to identify cement and chemical/mineral admixture incompatibility. The conventional plastic viscosity and yield stress are measured in static mode and storage modulus curve, as a function of time, is measured in dynamic mode. The rate of change of plastic viscosity (RPV) as another static rheological parameter and the modeled magnitude parameter α, from the dynamic rheological method,

showed great potentialities as acceptance criteria to identify incompatible mixtures. The heat of hydration data from isothermal conduction calorimeter tests and setting time results for the studied mixtures have strongly supported the rheology based observations as supporting tools. Based on the main tests results, the acceptance criteria were set up using the rheological parameters in accordance with heat of hydration data. This will ultimately help material suppliers, concrete producers, and other users to detect problematic combinations of concrete ingredients before a given concrete mixture is placed.

DEDICATION

To my mother, Teaja Woo; my wife, Eunjeong Jung; and my lovely son, Minjun Jang.

I would like to express my respect to my father, Copmoon Jang, who passed away on November 23, 2004, during my study.

ACKNOWLEDGEMENTS

I would like to thank my advisors, Dr. Dan G. Zollinger and Dr. Anal K. Mukhopadhyay for their suggestions, guidance, and support throughout the course of this research. Additionally, I would like to thank my other dissertation committee members, Dr. Zachary Grasley and Dr. Mohammed Haque, for their valuable comments and advice. The study presented herein was sponsored by TxDOT (Texas Department of Transportation). Their support is gratefully acknowledged. Finally, thanks to my mother for her encouragement, and to my wife and son for their patience and love.

NOMENCLATURE

DSR	Dynamic Shear Rheometer
OPC	Ordinary Portland Cement
RMA	Rheology Modifying Admixture
MWRA	Medium-range Water Reducing Admixture
WRRA	Water Reducing and Set Retarding Admixture
SCM	Supplementary Cementitious Material
PV	Plastic Viscosity
YS	Yield Stress
RPV	Rate of change of Plastic Viscosity
RYS	Rate of change of Yield Stress
TxDOT	Texas Department of Transportation
C2	Type I/II ordinary portland cement
C4	Type V low C_3A cement
F35	Class F fly ash with 35% replacement of cement weight
C35	Class C fly ash with 35% replacement of cement weight
S50	Granulated Slag with 50% replacement of cement weight
X15TD	Lignin based Type A&F chemical admixture with typical dosage
X15DD	Lignin based Type A&F chemical admixture with double dosage
D17TD	Lignin based Type B&D chemical admixture with typical dosage
D17DD	Lignin based Type B&D chemical admixture with double dosage

TABLE OF CONTENTS

TABLE OF CONTENTS (Continued)

CHAPTER Page

TABLE OF CONTENTS (Continued)

CHAPTER Page

TABLE OF CONTENTS (Continued)

CHAPTER Page

LIST OF FIGURES

Page

LIST OF FIGURES (Continued)

Page

LIST OF FIGURES (Continued)

Page

LIST OF FIGURES (Continued)

Page

LIST OF FIGURES (Continued)

Page

LIST OF FIGURES (Continued)

Page

LIST OF FIGURES (Continued)

Page

LIST OF FIGURES (Continued)

Page

LIST OF TABLES

Page

LIST OF TABLES (Continued)

Page

LIST OF TABLES (Continued)

Page

CHAPTER I

INTRODUCTION

In this study, an effort was made to identify concrete incompatibilities, the abnormal interaction between cement and chemical/mineral admixtures in concrete mixture that leads to unpredictable concrete performance in the field through the direct measurement of cement paste rheology. To achieve this objective, rheological properties of cement pastes with different temperature conditions were measured by the modified dynamic shear rheometer (DSR). The DSR was modified and optimized for cement paste rheology measurements. Based on the rheological parameters, the acceptance criteria of incompatibility were set up irrespective of cement types and ambient temperature conditions.

BACKGROUND OF THE STUDY

The use of various chemical and mineral admixtures in portland cement concrete is a common practice, which sometimes deliberately or non-deliberately alters the hydration process and chemical interaction that leads to unexpected concrete behavior. Complex chemical interaction between different compositions in cements, supplementary cementitious materials (SCMs), and chemical admixtures along with temperature effects sometimes creates poor cement-admixture compatibility and can give rise to premature loss of workability due to irregular setting characteristics or abnormal heat evolution. The common manifestations of setting abnormalities are extreme cases of set retardation or fast stiffening (*1, 2, 3*) whereas for heat evolution abnormalities these are manifest the absence of release of heat.

This dissertation follows the style of *Transportation Research Record*.

Therefore, cement-admixture incompatibility is a major problem in the concrete industry that affects the efficiency of concrete placing, the quality of concrete, and construction schedules. As a result of concrete incompatibilities, additional and unplanned costs may arise. For that reason, it is advantageous to identify concrete incompatibilities before concrete placement in order to avoid problems the associated in the placing and curing process.

Concrete incompatibilities are mostly associated with complex and unpredictable chemical interaction between the components in the cement paste (i.e., cement, supplementary cementitious materials, chemical admixtures, and water). The chemical interaction between paste components sometimes shows a relation with temperature. A cement paste with normal interaction between the components at an intermediate placement temperature (e.g., 20-24°C) may behave abnormally at either low (e.g., 5-10°C representing winter) or high placement temperature (e.g., 30-40°C representing summer). Concrete rheology can be directly measured by concrete rheometers. However, they may not be sensitive to identify the fine changes due to cement-admixture incompatibilities as aggregate effects may mask the paste effects. Reproducibility of concrete rheological parameters in different laboratories using different concrete rheometers was found to be poor (*4*). Additionally, existing concrete rheometers are large, heavy, and not suitable for field application. Therefore, identifying cement-admixture (mineral and chemical) incompatibilities through the measurement of cement paste rheological parameters instead of concrete rheological parameters is a sound concept.

Cement paste rheology tests have the following advantages over concrete rheology tests: (i) need small amount of paste specimen, (ii) less testing time, (iii) reasonably good accuracy and repeatability, as the tests avoid aggregate disturbance of the rheological measures, and (iv) less

labor intensive. Moreover, aggregate shearing effects in concrete can be simulated during cement paste rheology tests by some suitable means, e.g., using a high shear mixing procedure.

Over the past decade the cement paste rheology techniques have been developed to characterize the flow behavior of cement paste at an early age. The rheology of cement paste is influenced by a variety of factors. In particular, hydration reaction kinetics and interparticle forces develop the stiffening process of cement paste and change the flow properties of cement paste during the first few hours. Stiffening refers to the increase in rigidity of fresh cement paste or concrete with time. Normally stiffening process goes gradually until setting takes place. It is important to characterize and monitor the stiffening behavior of cement paste for identifying concrete incompatibilities because the results of concrete incompatibilities are accompanied by abnormal setting. Measurement of setting time is one of the ways to characterize the degree of stiffening. However, the traditional penetration tests used to measure setting of cement paste or concrete very crude and arbitrary (*5*). This investigation focuses on characterizing the stiffening behavior of cement paste using the modified DSR by monitoring the microstructural development of the studied cement paste specimen under different temperature conditions.

Thus, the measurement of rheological properties of cement pastes yields crucial information about (i) the evolution of hydrating cementitious systems, (ii) microstructural changes and particle interaction in cement paste, (iii) the relative performance of different chemical admixtures (e.g., water reducing admixture) - the optimum dosage and the consequences of excessive dosages, and (iv) the compatibility of various cement, chemical and mineral admixtures' combinations. Therefore, it is anticipated that cement paste (cement + supplementary cementitious materials + chemical admixtures + water) rheological measurements could be a good indicator of incompatibilities of concrete.

In this study, the rheological parameters in two different rheology modes of operations (i.e., static and dynamic modes) have been investigated to identify incompatibilities among cement and mineral/chemical admixtures considering the effect of cement, supplementary cementitious materials (SCMs), type and dosage of chemical admixtures, and temperature. Based on the rheological parameters, the acceptance criteria of incompatibility were set up irrespective of cement types and ambient temperature conditions. This will ultimately help material suppliers, concrete producers, and other users to detect problematic combination of concrete ingredients before the concrete is placed.

OBJECTIVES OF THE STUDY

The objectives of this study were (i) to use the dynamic shear rheometer (DSR) device as part of an easy-to-use process to measure cement paste rheology with acceptable reproducibility and sensitivity, and (ii) to investigate whether potential cement-mineral/chemical admixture incompatibilities can clearly be identified through the direct measurement of cement paste rheology from the laboratory-based testing procedure.

The ultimate goal is to develop a field laboratory test and equipment to predict potential concrete mixture incompatibilities, such as those between cement and mineral/chemical admixtures through the measurements of cement paste rheology.

SCOPE OF DISSERTATION

The study presented herein consists of the following sequence to achieve the above objectives:

- Identify the areas of modifications needed to make the DSR suitable for measuring cement paste rheology - Literature review on the use of rheometers with parallel plate geometry (similar to the DSR) in measuring cement paste rheology along with some preliminary DSR tests will be conducted.
- Adopt those modifications and upgrade the DSR to measure cement paste rheology.
- Conduct a preliminary investigation to optimize the DSR test configuration and develop a DSR-based rheology test procedure.
- Conduct an extensive laboratory investigation using the modified DSR-based rheology test procedure with varieties of cements, supplementary cementitious materials (SCMs), different types and dosages of commonly used chemical admixtures under different temperature conditions. Incompatible mixtures will be generated in the laboratory by (i) selecting materials based on the available historical information (materials that are suspected to cause incompatibilities in the fields), and/or (ii) formulating artificial incompatible mixtures (e.g., overdose of chemical admixture) in such a way so that incompatibilities can be generated in the laboratory.
- Develop a procedure to formulate rheology-based acceptance criteria in terms of the test results available from the above laboratory investigation.

This should ultimately help material suppliers, concrete producers, and other users to detect problematic combinations of concrete ingredients before concrete is placed and thereby avoid poorly consolidated and finished concrete and possibly durability-related issues due to incompatibilities. Further refinement of these acceptance criteria based on more specific work covering a wider range of incompatibilities and field laboratory validation is beyond the scope of

the present study.

This study was divided into a number of parts, which are explained in the following chapters. Chapter II gives background information based on a literature review and personal communication with experts on cement paste rheology. Chapter III describes the modification of the DSR and the developed mixing procedure. Chapter IV explains the applicability of the DSR to the measurement of cement paste rheology. Chapter V describes the characterization of the collected materials that were used for the laboratory test program. Chapter VI presents the experimental design and test methods for the laboratory test program. Chapter VII presents laboratory test analysis, results, and discussion. Finally, conclusions and recommendations from this study are presented in Chapter VIII.

CHAPTER II

LITERATURE REVIEW

A complex interaction between cement, supplementary cementitious materials (SCMs), and chemical admixtures sometimes creates poor cement-admixture compatibility (1, *2, 3*), which sometimes leads to early stiffening or excessive retardation along with heat evolution abnormalities. It is reported that cement-admixture incompatibilities sometimes leads to severe early age cracking and low strength development (*6*). Therefore, it is advantageous to identify those incompatibilities before placement of the concrete in order to avoid problems associated with the placing and curing process.

An extensive literature review was carried out to study the stiffening mechanism of cement paste and how stiffening process or the microstructural development of cement paste affects the rheological properties. The literature review addressing four major categories, i.e., (i) stiffening mechanism of cement paste, (ii) theoretical background of rheology associated with cement paste, (iii) factors influencing concrete incompatibilities, and (iv) modifications of the dynamic shear rheometer (DSR) to measure cement paste rheology, was described below.

STIFFENING MECHANISM OF CEMENT PASTE

There are two different mechanisms for the stiffening process of cement paste. First, an increase in net attraction forces between cement particles exists due to the change of ionic concentrations in the pore solution and the change of surface potential, leading to an increase in flocculation. Second, cement particles are bridged by hydration products resulting, in continuously increasing in rigidity. In the first mechanism, the total ionic strength increases

continuously with time at an early age (*7*). As a result, the electrostatic repulsion forces decrease since the double layer is compressed though the vander Waals forces between cement particles change little. In the second mechanism, the hydration products increase with time, and the bonding between particles is strengthened, leading stiffening. It is described below how interparticle forces between particles and cement hydration affect the stiffening mechanism of cement paste.

Interparticle Forces

Understanding the interparticle forces that result in the flocculation of colloidal cement particles is critical to understanding the rheological behavior of cement paste. Interactions between particles in fresh cement paste are determined by DLVO theory named after co-inventors Derjauin, Landau, Verwey, and Overbeek, which is the combination of electrostatic forces and van der Waals forces.

Most substances develop a surface charge when brought to contact with a polar medium (e.g. water). Charged surface affects the distribution of nearby ions in the continuous medium. Ions with opposite charge (counter-ions) are attracted towards the surface and ions of like charge (co-ions) are repelled away from the surface, leading to the formation of an electrical double layer and resulting in electrostatic forces between surfaces. The electrical double layer can be divided into two regions, a dense inner region called Stern layer that may contain adsorbed ions, and outside of the Stern layer called diffuse layer in which the electrical pontential exponentially decays until the surface charge in neutralized. Figure 2-1 shows the schematic electrical double layer model of interfaces (*8*).

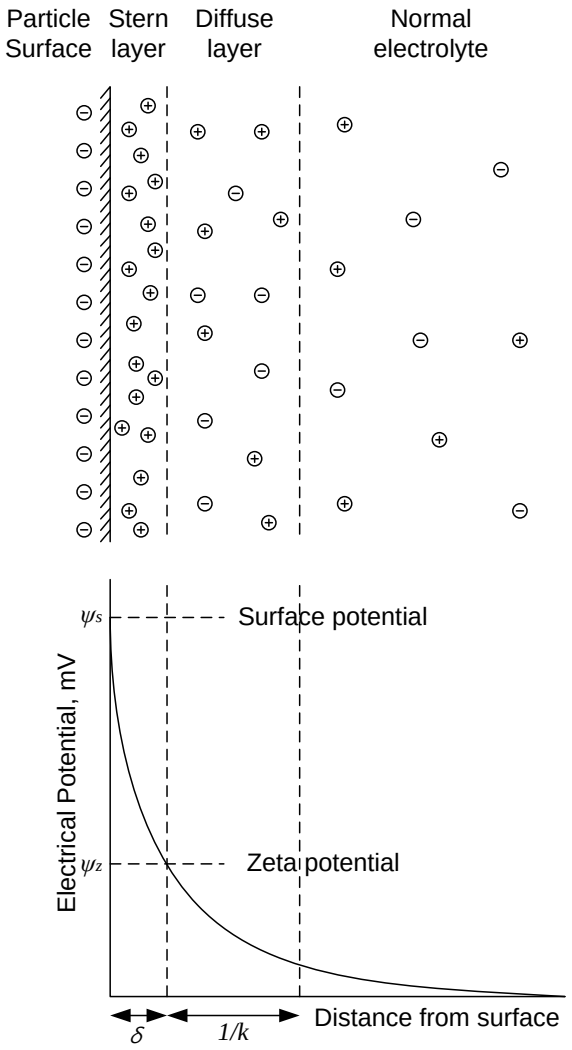

Figure 2-1 Electrical double layer model of interfaces (*8*).

The electrical potential is given by,

$$\psi = \psi_z \cdot \left(\frac{a}{r}\right) \cdot e^{\left[-k(r-a)\right]} \quad \text{.....(2.1)}$$

where ψ_z is the potential at the shear plane, a is the radius of the particle plus the width of the Stern layer, r is the distance from the center of the particle, and k is the Debye-Huckel parameter given by,

$$k = \sqrt{\frac{F^2 \cdot \sum n_i^0 z_i^2}{\varepsilon_0 \varepsilon_r kT}} \quad \text{.....(2.2)}$$

where F is the Faraday's constant, ε_0 is the permittivity of vacuum ($8.85 \times 10^{-12} C^2/Jm$), ε_r is the solvent dielectric constant (78 for water at 25°C), k is Boltzmann's constant, T is the absolute temperature, and n_i and z_i are the valence and the number density of the electrolyte ions of type i respectively. The inverse of k is called the Debye length and represents the thickness of the double layer (Stern plus diffuse layer). In cement particles, the thickness of the double layer is approximately 1nm (*9*). The boundary between the Stern and diffuse layer is the shear plane. The electrical potential at the shear plane is termed the zeta potential (ς) and is the only value of potential that can be measured experimentally (*10*). The application of an electric field across a colloidal suspension moves the particles in a net direction. This phenomenon is called electrophoresis. The viscosity of the moving particles can be used to calculate the zeta potential expressed as,

$$\varsigma = \frac{4\pi\eta V}{\varepsilon_0 \varepsilon_r E} \quad \text{.....(2.3)}$$

where η is the viscosity of the solution, V is the measured velocity of the particles, and E is the applied electric field. The zeta potential can range from -100 to +100 mV for typical ceramic suspensions. The particles are immobile when ς = 0, termed the "iso-electric point" (IEP). When the suspension is at the IEP or low ς (-25 mV < ς < +25 mV) flocculation occurs. At ς values above ±25 mV, the particles remain dispersed (*11*).

The total interaction energy for particles in a suspension is the sum of attraction energy of van der Waals and repulsion energy of electrical double layer (Figure 2-2). Assuming ka>>1, the equations are given by,

$$U_A = \left(\frac{A_H \cdot a}{6R}\right) \cdot \left[1 + \left(\frac{R}{2a+R}\right) + \left(\frac{R}{a}\right) \ln\left(\frac{R}{2a+R}\right)\right] \quad \text{.....(2.4)}$$

$$U_R = \left(2\pi\varepsilon_0\varepsilon_r a\zeta^2\right) \cdot \ln\left\{1 + e^{[-k(R)]}\right\} \quad \text{.....(2.5)}$$

$$U_{Total} = U_A + U_R \quad \text{.....(2.6)}$$

where A_H is Hamaker constant, a is the particle radius, R is the separation distance between particles, U_A is the attraction energy due to van der Waals forces, U_R is the repulsion energy due to electrical double layer, and U_{Total} is the total interaction energy a flocculated suspension (e.g. cement paste) (*8*).

The repulsive force is dependent on the ionic strength and zeta potential of the particles in addition to the interparticle spacing. Figure 2-2 shows the superimposition of the attractive and repulsive potential curves for a flocculated suspension. The existence of a secondary minimum is normally associated with a weak flocculated while a large primary minimum is indicative of a strongly flocculated suspension. By changing the ionic concentration in the solvent, the interparticle potential changes and leads to a dispersed or flocculated suspension. Yanez et al. (1996) showed that the yield stress of colloidal alumina slurries was directly related to the depth of the potential well predicted by DLVO theory (*12*). The state of dispersion between particles is commonly altered through the addition of various types of oils, acids, and other dispersing chemical admixtures (*13*). Cement paste is normally flocculated with the absolute value of zeta potential less than 20 mV (*14*). Various types of dispersing chemical admixtures are added to cement paste to increase slump and, consequently, the depth of the potential well. The types of dispersing chemical admixtures commonly used in cement paste are discussed in more detail in Chapter V.

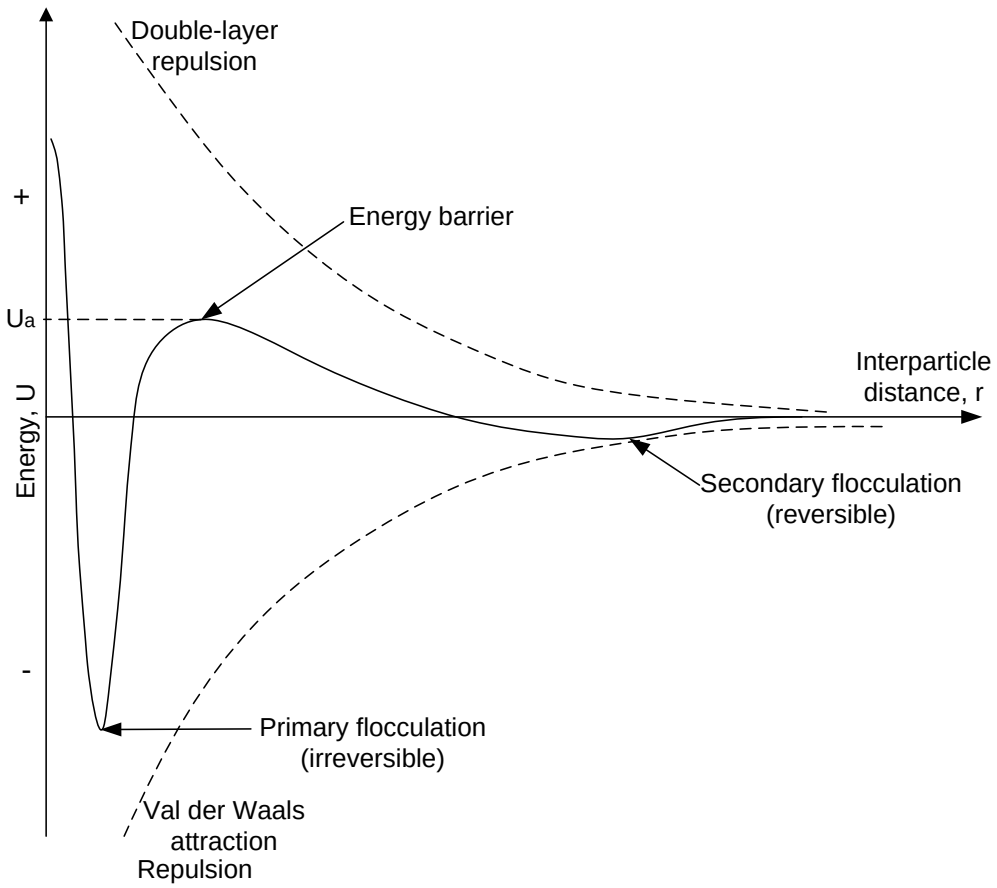

Figure 2-2 Potential energy curves between particles in a colloidal suspension (*8*).

Figure 2-3 shows several potential energy curves according to the electrolyte concentration in cement paste. The interaction between cement particles has the following features:

(1) At a long distance, interaction energy approaches zero.

(2) In more concentrated electrolyte solutions there is a significant secondary minimum (cases b-d).

(3) If cement particles have a low density charge or potential, the energy barrier is always low and the cement paste is flocculated (cases c-d).

(4) If the surface charge or potential approaches zero, van der Waals forces dominate the paste, and cement particles start to be flocculated rapidly (case e).

(5) If cement particles have a high surface charge the paste is dispersed (case a).

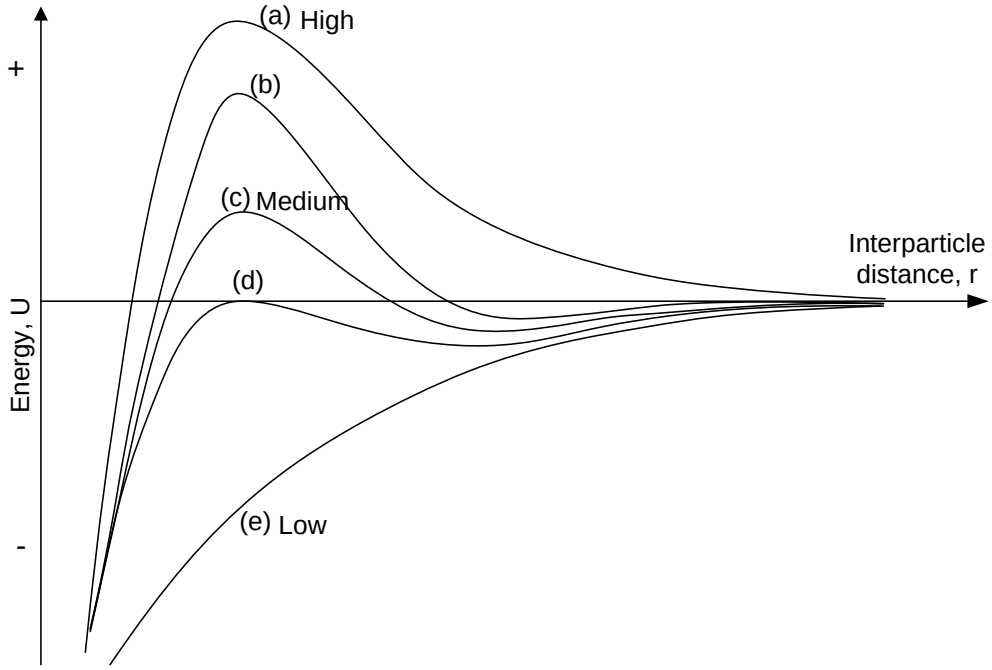

Figure 2-3 Effect of electrolyte concentration and the flocculation of a colloid (*8*).

In summary, if particles in a suspension have a weak surface potential or a high surface potential but screened by a high ionic strength, van der Waals attraction forces dominate the system and it is flocculated. On the other hand, high surface potential and low ionic strength result in repulsion between colloid particles and a dispersed suspension.

Cement Hydration

The stiffening of cement paste is also affected by ongoing hydration reactions in addition to interparticle forces. Since hydration and stiffening are closely related to each other it is necessary to review the processes associated with the hydration and early age behavior of normal cement paste. Cement paste is the most active component of any mortar or concrete; and is a complex mixture of multiple inorganic components such as the aluminates phases (C_3A, C_4AF), silicates phases (C_3S, C_2S), other sulphate forms ($CaSO_4 \cdot xH_2O$), and alkalis (Na_2O, K_2O) (*5*). When water is added to portland cement, a series of chemical reactions are triggered that lead to the formation of hydration products and interparticle bonding which results in a dense, stable microstructure. The hydration products are responsible for the stiffening of the paste and consequently the properties of the hardened paste. A simplified description of the hydration process is shown in Figure 2-4, demonstrating the basic characteristics of the hydration process:

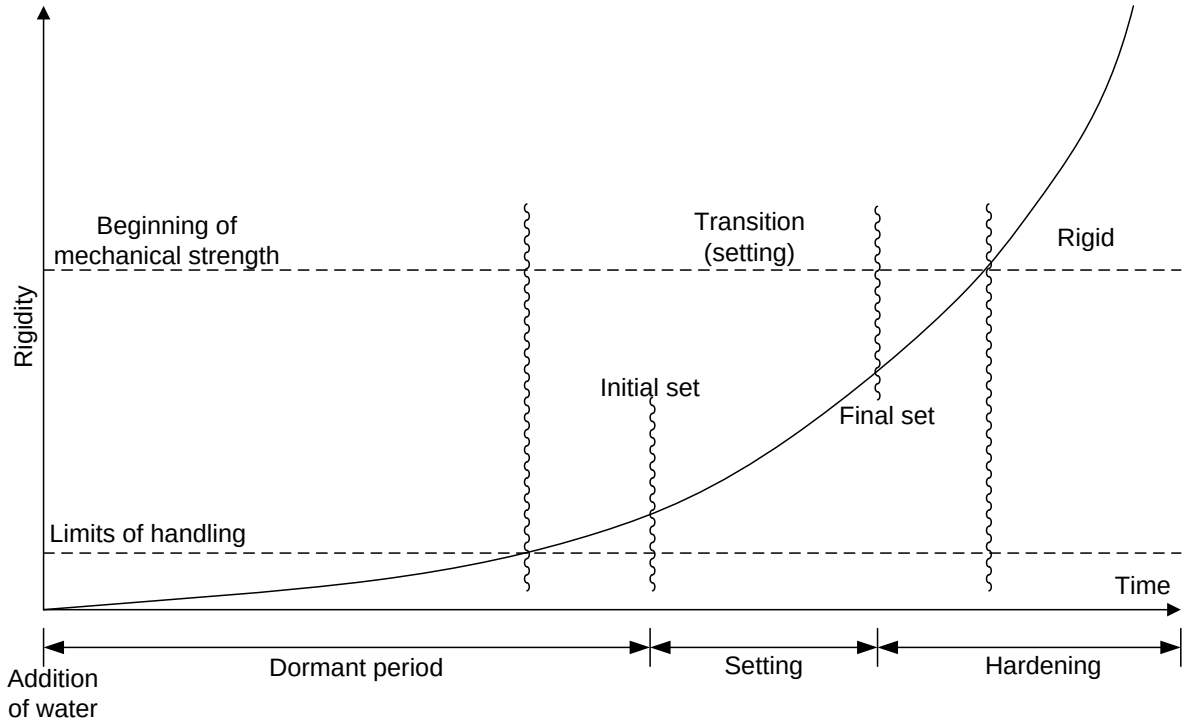

Figure 2-4 Schematic description of the hydration process in a cement paste (*5*).

(1) The paste is fluid as long as the individual particles are separated from one another.

(2) The hydration products occupy a greater volume than the original cement particle and therefore the advent of hydration is accompanied by a pore-filling effect (i.e., reduction in the porosity).

(3) During the early stages of hydration, when sufficient contact has formed between hydration products, the paste gains sufficient rigidity to lose its fluidity; this is referred to as setting.

(4) The continuation of the hydration process after the setting results in the generation of strength due to bonding interactions between the hydration products, which are facilitated by the close proximity of the hydration products as the porosity decreases. At this stage the rigidity increases to such a degree that at the time referred to as final setting the paste is already a solid, although of a very low strength.

(5) The process of hydration from the final setting time is accompanied by measurable strength increase; this is referred to as the hardening stage.

The hydration of cement has four distinct periods; the first is an initial period of rapid chemical reaction. Upon initial contact with water, multiple phases and components of cement undergo a variety of chemical reactions that yield rapid evolution of heat for approximately 15 minutes immediately following mixing (Figure 2-5). This is then followed by what is often termed as a ‘dormant’ or ‘induction’ period where the rates of reaction are slowed. The slow reaction rate of the induction period allows for the flowable nature of cement paste at early ages. Initial set occurs in 2-4 hours after mixing and setting continues at a higher rate during the ‘acceleration’ period. After 4-8 hours, the reaction rate slows and continues into the ‘steady

state' period. These changing rates of reactions are reflected in the development of heat due to a series of exothermic reactions. A typical representation of this heat evolution is illustrated in Figure 2-5.

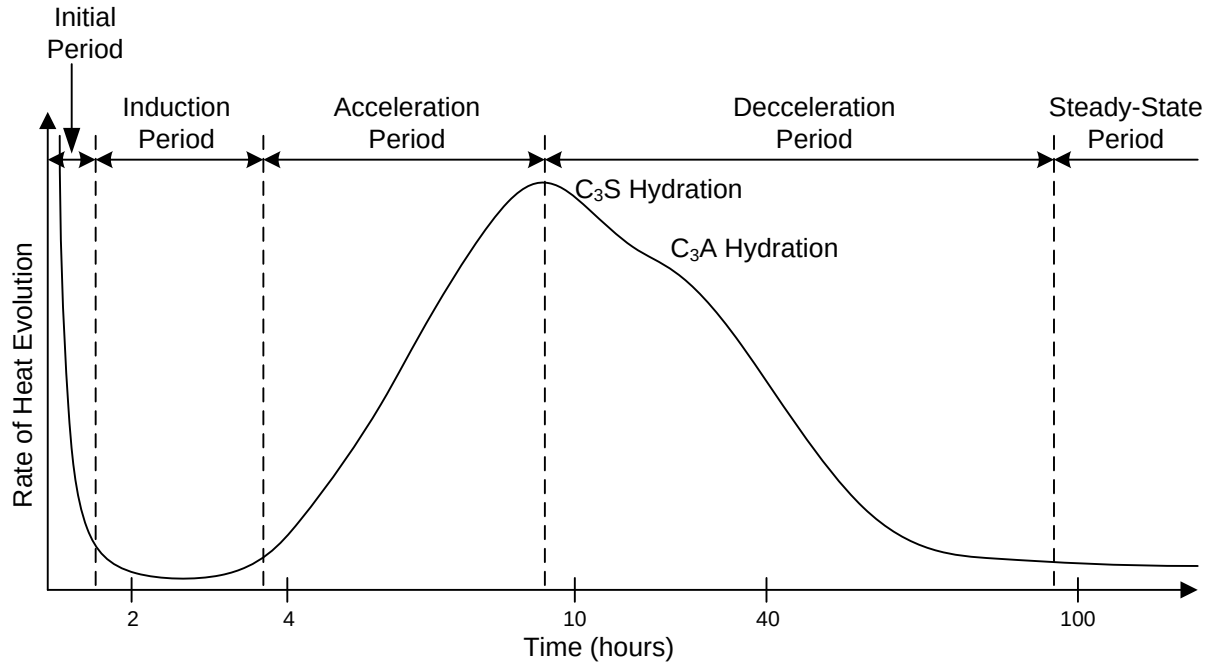

Figure 2-5 Rate of heat evolution during the hydration of ordinary portland cement.

Although the exact composition of cement is slightly different from each producer, it principally consists of five major components, each containing various oxide phases. Tables 2-1 and 2-2 list the typical composition of Type I ordinary portland cement, and the weight percentage, oxide proportion, and chemical notation for each phase (*5*).

Table 2-1 Typical chemical composition of ordinary portland cement (*5*).

Chemical Name	Chemical Formula	Chemical Notation	Weight Percent (%)
Tricalcium silicate	$3CaO{\cdot}SiO_2$	C_3S	55
Dicalcium silicate	$2CaO{\cdot}SiO_2$	C_2S	18
Tricalcium aluminate	$3CaO{\cdot}Al_2O_3$	C_3A	10
Tetracalcium aluminoferrite	$4CaO{\cdot}Al_2O_3{\cdot}Fe_2O_3$	C_4AF	8
Calcium sulfate dehydrate (gypsum)	$CaSO_4{\cdot}2H_2O$	$C\hat{S}H_2$	6

Table 2-2 Typical oxide composition of ordinary portland cement (*5*).

Oxide	Chemical Notation	Common Name	Weight Percent (%)
CaO	C	Lime	64.67
SiO_2	S	Silica	21.03
Al_2O_3	A	Alumina	6.16
Fe_2O_3	F	Ferric oxide	2.58
MgO	M	Magnesia	2.62
K_2O	K	Alkalis	0.61
Na_2O	N	Alkalis	0.34
SO_3	$\hat{S}$	Sulfur trioxide	2.03
CO_2	$\hat{C}$	Carbon dioxide	-
H_2O	H	water	-

Initial Period

Cement hydration begins immediately upon contact with water. Within several minutes, the easily soluble components (Na^+, K^+, Ca^{2+}, SO_4^{2-}, OH^-) of the cement are dissolved into the aqueous phase, and initial hydration reactions begin (*15*). The hydration process of cement involves a series of complex chemical reactions expressed in Equations 2.7 to 2.12. Tricalcium silicate dissolves congruently and a layer of a calcium silicate hydrate (C-S-H) precipitates at the

cement particle surface. At the same time, silicate ions also enter the liquid phase, although their concentration remains very low. The fraction of C_3S hydrated in the initial period remains low, probably between about 2 and 10 percent. Tricalcium aluminate dissolves and reacts with Ca^{2+} and SO_4^{2-} ions present in the liquid phase, yielding ettringite that also precipitates at the cement particle surface. The amount of C_3A that hydrates in the initial period varies in different cements between about 5 and 25 percent.

The early fast hydration reaction appears to be slowed down due to the deposition of a layer of hydration products at the cement particle surface. In this way a barrier is formed between the non-hydrated material and the liquid phase. Eventually the cement particles become fully coated with a protective layer of hydration products that hinders the diffusion of reacting species, thus sharply reduce the rate of the various reactions (*16*).

$2C_3S + 11H \rightarrow C_3S_2H_8 + 3CH$ …….……(2.7)

$2C_2S + 9H \rightarrow C_3S_2H_8 + CH$ …….…….....(2.8)

$2C_3A + 21H \rightarrow C_4AH_{13} + C_2AH_8$ …….…….....(2.9)

$C_4AH_{13} + C_2AH_8 \rightarrow 2C_3AH_6 + 9H$ ……..(2.10)

$C_3A + 3CSH_2 + 26H \rightarrow C_6A\hat{S}_3H_{32}$ (sufficient sulfate) …….(2.11)

$2C_3A + C_6A\hat{S}_3H_{32} + 4H \rightarrow 3C_4A\hat{S}H_{12}$ (sulfate ion depletion) ……..... (2.12)

Induction Period

The initial phase of high reactivity is followed by a period of latency normally referred to as the ‘dormant’ or ‘induction’ period until the onset of setting. Although the reactions initiated in the first phase continue during the induction period, little ettringite is produced during this

latent period allowing the cement paste to maintain most of its plasticity. Hardening starts after about two or three hours, due to the formation of calcium silicate hydrate. The only notable event at this stage is a progressive thickening of the surface gel layer. Any loss in the consistency at this stage is mainly attributable to the physical coagulation of the cement particles rather than to any chemical process (*16*).

Acceleration Period

The end of the induction period is marked by a sharp increase in the reaction rate of cement, in general, indicated by the second peak of heat evolution in cement hydration process. The internal structure was formed when the deposition of hydration products on the surface of cement grains comes into contact with neighboring grains (*16*). Cement grains bond to one another by the interaction of the C_3S hydration products. This gradually forms an internal structure that, as it continues to grow, will bring about stiffening, and eventually concrete sets. Ultimately, it produces a strong durable matrix of cement hydrates.

The second peak of heat evolution in Figure 2-5 often denotes the hydration of the C_3S phase. In some cements, there may be a third, less pronounced peak in this curve, the result of renewed C_3A hydration once all the SO_3 is reacted, the gypsum is depleted and ettringite formation has concluded; this third peak typically occurs within a few days from the first contact with water (*5*). This renewed C_3A hydration may occur simultaneously with C_3S hydration and the two will appear as one peak of the heat evolution graph.

THEORETICAL BACKGROUND OF RHEOLOGY ASSOCIATED WITH CEMENT PASTE

Rheology is the science of the deformation and flow of matter, and the emphasis on flow means that it is concerned with the relationships between stress, strain, rate of strain, and time. Cement paste in its fresh state can be considered as a fluid and therefore the basic principles of rheology can be applied to this material (*17*). Many researchers used the principles of rheology to study cement paste for the past decades (*18, 19, 20*). The focus of the previous studies was given to monitor the shear stress vs. shear rate flow of a cement paste using the Bingham model and the static rheology method. In static rheology, tests are conducted where the shear rate varies from some start point to a certain level, then returns to the start point. The corresponding shear stress is recorded as a function of the shear rate. Recently, Struble, Schultz, and Lei reported interesting results using the small amplitude oscillatory shear technique on cement paste; this is called a dynamic rheology method (*19, 20*). They reported that the storage modulus as a function of time is related to stiffening behavior of cement paste at an early age. The two different techniques for measuring the cement paste rheology, static and dynamic rheology methods, were reviewed and described below.

Static Rheological Method

Rheology is the science dealing with the deformation and flow of materials under stress. Cement paste in its fresh state can be considered as a fluid and therefore the basic principles of rheology can be applied (5). The simplest fluid is one that obeys Newton's law of viscous flow, which can be described by the following equation:

$$\tau = \eta\dot{\gamma} \quad \text{.....(2.13)}$$

where τ is the shear stress (Pa), η is the coefficient of viscosity (Pa·s), and $\dot{\gamma}$ (s^{-1}) is the shear strain rate or the velocity gradient.

The flow behavior of any fluid requires a measurement of shear stress with varying shear strain rate and generates the flow curve, i.e., a plot of shear stress vs. shear strain rate, which is called static rheology. The different types of flow curves for the cementitious materials are presented in Figure 2-6. As shown in Figure 2-6 (a), the Newtonian liquid described in Eq. (2.13) is represented with a plot of the shear rate versus the shear stress that has a straight line passing through the origin, with a slope η.

Diluted suspensions of a solid in liquid generally follow the Newtonian flow behavior as interparticle forces are practically non-existent. However, the Newtonian model breaks down for fluids in which the volume of suspended solids is large. Fresh cement paste can be considered to be a very concentrated suspension, in which there are forces acting between the cement particles. For such concentrated materials, these interparticle forces change the type of flow behavior. As seen in Figure 2-6 (b), cement paste has a yield stress, which must be exceeded before flow can occur. A common description of materials that exhibit this type of behavior is given by the Bingham model as:

$$\tau = \tau_0 + \mu\dot{\gamma} \quad \text{.....(2.14)}$$

where τ (Pa) is the shear stress, τ_0 is the yield stress, μ (Pa·s) is the plastic viscosity, and $\dot{\gamma}$ (s^{-1}) is the shear strain rate. The yield stress is a measure of the force necessary to start a movement of cement paste, whereas the plastic viscosity is a measure of the resistance of cement paste against an increased speed of movement.

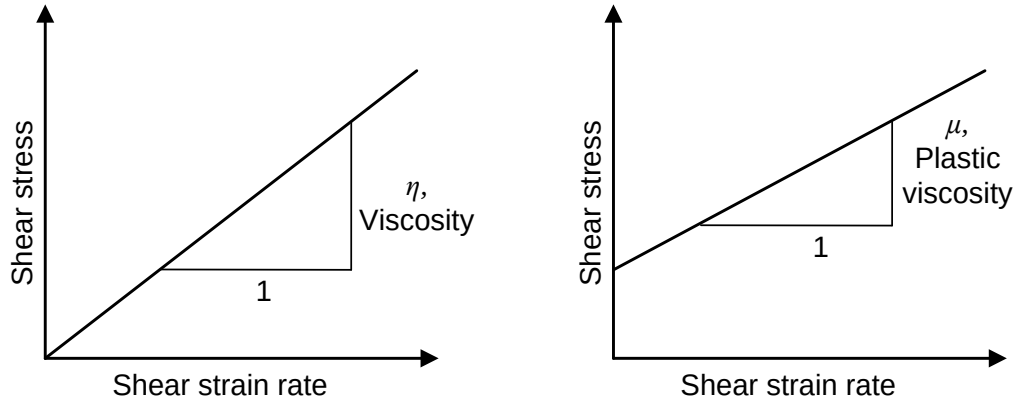

(a) Newtonian model **(b) Bingham model**

Figure 2-6 Newtonian model (left) and Bingham model (right).

A single-point test would not be very useful to describe such a fluid. Both parameters (i.e., yield stress and plastic viscosity) are considered to fully describe the rheology of materials that obey the Bingham model. There is considerable evidence that the behavior of fresh cement paste can be reasonably approximated by the Bingham model (5). It is possible that two cement pastes may have the same yield stress but exhibit different plastic viscosities as shown in Figure 2-7 (a). On the other hand two cement pastes may have the same plastic viscosity but different yield stresses as shown in Figure 2-7 (b). Therefore, measurement of both yield stress and plastic viscosity provides the complete picture of the flow behavior of paste.

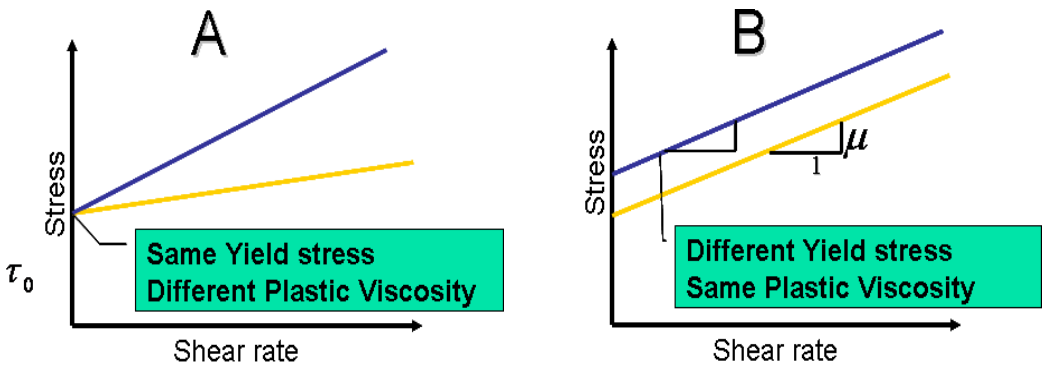

Figure 2-7 Characteristics of two rheological parameters.

Flow Curves of Cementitious Materials

A great deal of research has been conducted to determine the flow behavior of cementitious materials during the past decades. Figure 2-8 shows the most commonly used types of curves to express the shear stress and shear rate relationship of cementitious materials. As shown in this figure, a Newtonian liquid has a constant viscosity. A Bingham material needs to overcome the yield stress to start flow, and its plastic viscosity is also constant. In a shear thickening material, viscosity increases continuously with shear rate, while in a shear thinning material, viscosity decreases continuously with shear rate. In the material having shear thinning with yield stress, viscosity decreases with shear rate once the yield stress has been exceeded. On the other hand, in the material having shear thickening with yield stress, viscosity increases with shear rate once the yield stress has been exceeded (*21*).

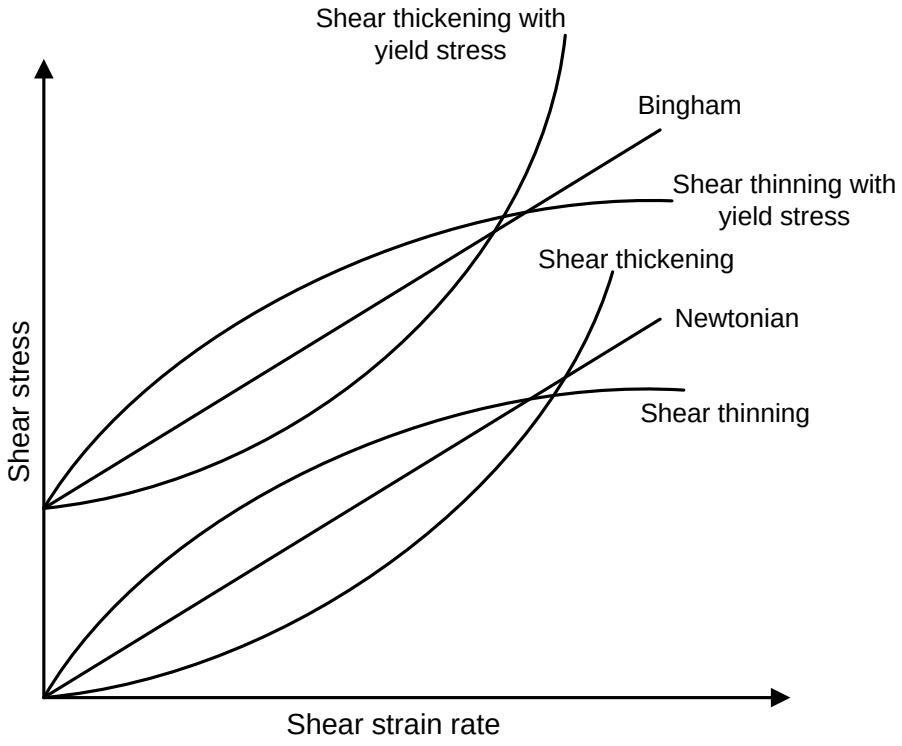

Figure 2-8 The different types of flow behavior of cementitious materials (*21*).

To determine fundamental rheological properties of fresh cement paste, many scientists researched cement paste rheology with different models listed at Table 2-3. The Power equations in Table 2-3 (i.e., Herchel-Bulkley model, modified Bingham model, Sisko model, Robetson-Stiff model) can be used to describe shear thinning (n<1) or shear thickening (n>1) behavior. The Herchel-Bulkley equation can be used for the case of shear thinning or shear thickening with yield stress. Several researchers have compared the equations describing flow curves of cementitious materials (*22, 23*). All of the relationships listed in Table 2-3 used at least two parameters to describe cement paste flow. Those equations that have a term of yield stress (i.e., Bingham model, Herschel-Bulkley model, and Casson model, etc) have a physical basis, while the other equations contain more than two parameters without exact physical meanings.

Table 2-3 Various models for the rheology of cement paste.

Model	Equation	Parameters/Reference
Bingham model	$\tau = \tau_0 + \mu\dot{\gamma}$	τ_0 = yield stress, μ=viscosity (*14*)
Herchel-Bulkley model	$\tau = \tau_0 + K\dot{\gamma}^n$	τ_0 = yield stress, *K*= constant (*13, 14*)
Casson model	$\tau = \tau_0 + \mu_\infty\dot{\gamma} + 2(\sqrt{\tau_0\mu_\infty})\sqrt{\dot{\gamma}}$	τ_0 = yield stress, μ_∞ =viscosity at infinite shear rate (*13, 14*)
Modified Bingham model	$\tau = \tau_0 + \mu\dot{\gamma}^{n_1} + A\dot{\gamma}^{n_2}$	τ_0 = yield stress, *A*=constant (*14*)
Vom Berg model	$\tau = \tau_0 + B\sinh^{-1}(\dot{\gamma}/C)$	τ_0 = yield stress, *B* and *C*=constants (*13*)
Sisko model	$\mu = \mu_\infty + K\dot{\gamma}^{n-1}$	μ_∞ =viscosity at infinite shear rate, *K* = constant (*13, 14*)
Williamson model	$\tau = \mu_\infty\dot{\gamma} + \tau_f\frac{\dot{\gamma}}{\dot{\gamma}+\Gamma}$	Γ = parameter which governs the deviation from Bingham behavior, τ_f = intercept of the asymptote of the flow curve with the τ axis (*13*)
Robetson-Stiff model	$\tau = a(\dot{\gamma}+C)^b$	*a, b, and C* = constants (*13*)

Different models may be only suitable for certain ranges of material or measurement. Some researchers stated that the Herschel-Bulkley model is more suitable than the Bingham model for certain concretes, like self-consolidated concrete (SCC) (*24*). Jones and Taylor stated that the Robertson-Stiff model might be used to predict the relationship a wide range of water to cement ratios (w/c) while the Herschel-Bulkley model can only predict shear stress and shear rate data for a limited range of w/c. However, fresh cement paste is most commonly described using the Bingham model because the flow of most cement paste and concrete follows this equation fairly well (*9*) and because the two parameters in the Bingham model, yield stress and viscosity, can be measured independently. Therefore, the Bingham model was commonly used for rheological investigations on cement paste.

Rheology of Cementitious Materials

Table 2-4 shows the normal range of rheological parameters of cement paste, mortar and different types of concretes (*25*). From cement paste to concrete, the yield stress and plastic viscosity increases as the particle size increases. Banfill and Tattersall pointed out that this was because the aggregate could resist stresses without deformation (*9*). Since the aggregate occupies up to 70~80% of concrete volume, the yield stress of concrete is higher than that of cement paste without aggregate. Mortar yield stress is in between cement paste and concrete yield stress. In general, due to the increased interparticle contact and surface interlocking, the plastic viscosity of concrete is higher than that of cement paste. When concrete is subjected to a shear stress, since the solid aggregate particles cannot deform, the shear rate within the solid aggregate particles is zero. As a result, in order to have a certain shear rate in the whole composite, the shear rate of paste in concrete is higher compared to the material with just pure cement paste.

This higher shear rate results in a higher stress and resistance to flow in the cement paste that in turn accounts for the increase in measured plastic viscosity of the bulk material (*25*).

Table 2-4 Rheological parameters of cementitious materials (*25*).

Material	Paste	Mortar	Self-compacting concrete	Flowing concrete	Pavement concrete
Yield Stress (Pa)	10-100	80-400	50-200	400	500-2000
Plastic Viscosity (Pa·s)	0.01-1	1-3	20-100	20	50-100

Another important parameter of rheology is thixotropy. As shown in Figure 2-9, thixotropy is generally defined as the continuous decrease of viscosity with time under steady shearing and the subsequent recovery of viscosity when flow is discontinued (*26*). The shear rate was first increased to a certain value, then immediately decreased to the starting point. The down curve as shown in Figure 2-9 (b-i) lies beneath up curve. The area between the up and down curves (as shown in the shade area in Figure 2-9 (b-i)) is termed “hysteresis loop”, which is caused by the decrease in the fluid’s viscosity with increasing time of shearing resulting from the material’s structural breakdown. Generally, the larger the hysteresis loop area, the higher degree that the material structure is broken down (*25*).

The opposite behavior, involving a gradual increase in viscosity under steady shearing, followed by recovery is termed “negative thixotropy” or “anti-thixotropy” as shown in Figure 2-9 (b-ii). Anti-thixotropy is generally resulting from the cement hydration process when the rheology test duration is prolonged (*26*). Thixotropy usually occurs in situations where the material is shear thinning while anti-thixotropy is normally associated with shear thickening

suspensions (*27*). For both types of behavior, the processes are reversible and occur over a much longer period of time than the effects associated with viscoelasticity.

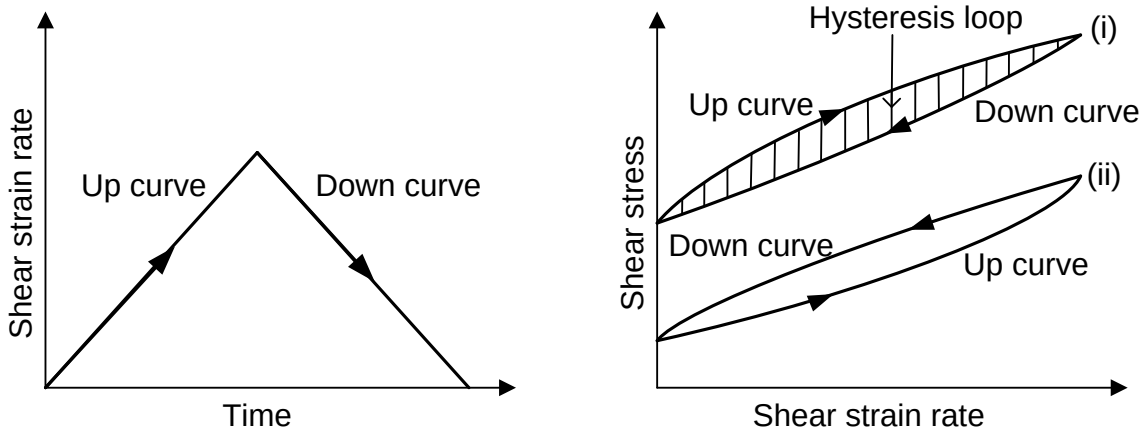

(a) Shear rate vs. time **(b) Shear rate vs. shear stress**

Figure 2-9 Thixotropy, anti-thixotropy, and hysteresis loop.

From a microstructural perspective, thixotropy is the result of structural degradation due to the rupturing of flocculation or linked particles. When a specified structure is disrupted, the viscosity decreases with shearing time until it asymptotically reaches the lowest possible value for a given shear rate.

Time Dependent Flow Behavior of Cement Paste

The previous discussion detailed some of the important rheological parameters that represent the flow behavior of cement paste, excluding time-dependent flow behavior. When a constant shear stress is applied to a flocculated suspension, the strain response is normally time-dependent. Since the shear rate varies in time for a constant shear stress, the material is viscoelastic. Most materials are viscoelastic to some degree (i.e. simultaneous existence of both

viscous and elastic properties), meaning that the shear stress depends on both the shear strain and shear rate. When a viscoelastic material is deformed, part of the energy input is recoverable, while part is dissipated. Using this concept, several viscoelastic models (e.g. Maxwell model, Kelvin Model, and Burgers model) have been developed to describe the viscoelasticity of materials as shown in Figure 2-10.

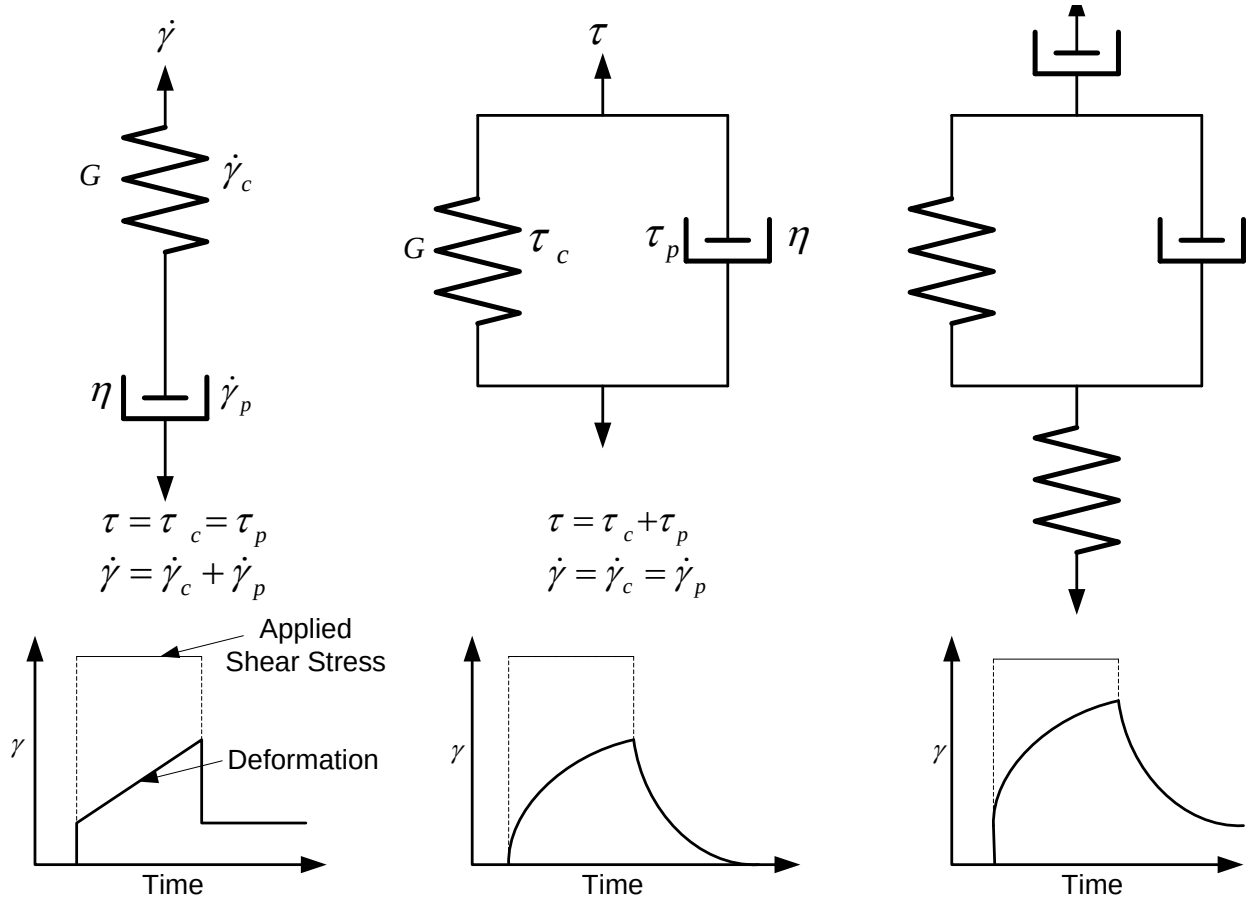

(a) Maxwell model **(b) Kelvin model** **(c) Burgers model**

Figure 2-10 Viscoelastic models: (a) Maxwell model, (b) Kelvin model, and (c) Burgers model (*28*).

However, cementitious materials can be less or more viscous depending on the overall interaction energy between particles (i.e. flocculation) and chemical reactions as a function of time (i.e. hydration). This implies that the degree of viscoelasticity in cement paste drastically changes with time although it is under constant temperature. This makes cementitious materials difficult to describe using those viscoelastic models (*29*). In addition, static rheological tests should be conducted within the linear viscoelastic response region for cement paste (i.e. at stresses below the yield stress). In static rheology, there have been relatively few studies examining the viscoelasticity of cement paste as a function of time due to equipment limitations (*19*). In many of the reported studies, the experiments were not conducted within the linear viscoelastic region (i.e. below yield stress) (*29*). Consequently, the results do not accurately reflect the true viscoelastic properties of cement paste.

On the other hand, the oscillation mode was used recently to describe the viscoelasticity of cement paste (*30*). When cement particles in cement paste are well dispersed or diluted after mixing it behaves like a fluid showing low or zero yield stress, but it has a low storage modulus and a high loss modulus under oscillatory shear. As time elapses, cement particles are flocculated and cement paste behaves like a highly viscous material, showing a high storage modulus and a relatively low loss modulus under oscillatory shear. Since cement hydrates after it is mixed with water, cement paste eventually shows viscoelastic behavior even though it is dispersed at the beginning and the stiffness increases with time. As long as cement paste shows a linear viscoelastic range, the small oscillatory shear technique can be used to monitor the stiffening process by measuring the storage modulus as a function of time, by which the stiffness of the cement paste is evaluated.

Dynamic Rheological Method

At stresses below the yield stress, the viscoelasticity of cement paste can be evaluated using oscillatory shear techniques. Oscillatory shear is a dynamic method, in which stress is oscillated according to a sinusoidal function. This test is conducted within the linear viscoelastic response region for a given material (i.e. at stresses below the yield stress). Unlike static rheology, dynamic rheology with an oscillatory shear mode is one of the newest approaches to characterize stiffening and microstructure of cement paste. Recently, cement paste has been studied using the small oscillatory shear technique to monitor the stiffening process of various mixtures (*19*). To use this technique, a small amplitude oscillatory shear is applied to cement paste, and the resulting strain and phase difference are measured. The applied oscillatory stress can be illustrated as follows

$$\sigma = \sigma_0 \cos \omega t \quad \text{.....(2.15)}$$

In the case of an ideal elastic solid, the resulting oscillatory strain will be completely in phase with stress and is expressed as follows

$$\gamma = \gamma_0 \cos \omega t \quad \text{.....(2.16)}$$

The resulting oscillatory strain for a viscous fluid will be 90° out of phase with the stress, and is expressed in the following equation

$$\gamma = \gamma_0 \cos\left(\omega t - \frac{\pi}{2}\right) \quad \text{..... (2.17)}$$

Where, ω is the oscillation frequency. Thus, the resulting oscillatory strain for a viscoelastic material such as cement paste is given by

$$\gamma = \gamma_0 \cos\left(\omega t - \delta\right) \quad \text{.....(2.18)}$$

When a viscoelastic material is subjected to a sinusoidal stress, the resulting sinusoidal strain will have a lag of δ with that of stress, which varies in the range of 0 to π/2 (*30*). Figure 2-11 illustrated the shear stress and shear strain response of viscoelastic material. The complex behavior of a viscoelastic material subjected to a sinusoidal stress wave is further expressed by the complex storage modulus

$$G^* = G' + iG'' \quad \text{.....(2.19)}$$

The real component (storage modulus) in the above equation is calculated according to Eq. (2.20), and the imaginary component (loss modulus) is calculated according to Eq. (2.21)

$$G' = \frac{\sigma_0}{\gamma_0}\cos\delta \quad \text{.....(2.20)}$$

$$G'' = \frac{\sigma_0}{\gamma_0}\sin\delta \quad \text{.....(2.21)}$$

For perfectly elastic solid materials, *G*" is zero, therefore no loss occurs and Eq. (2.19) becomes $G^* = G'$. For perfectly viscous liquid materials, the storage modulus equals zero. Hence, there is no rigidity in the material as it becomes fluid, and Eq. (2.19) becomes $G^* = iG'$.
The phase angle (δ), i.e., the lag between the applied stress and resulting strain, is expressed as follows

$$\tan\delta = \frac{G''}{G'} \quad \text{.....(2.22)}$$

It is important to note that the phase angle is zero when the material is an elastic solid, and is π/2 when the material is a viscous liquid.

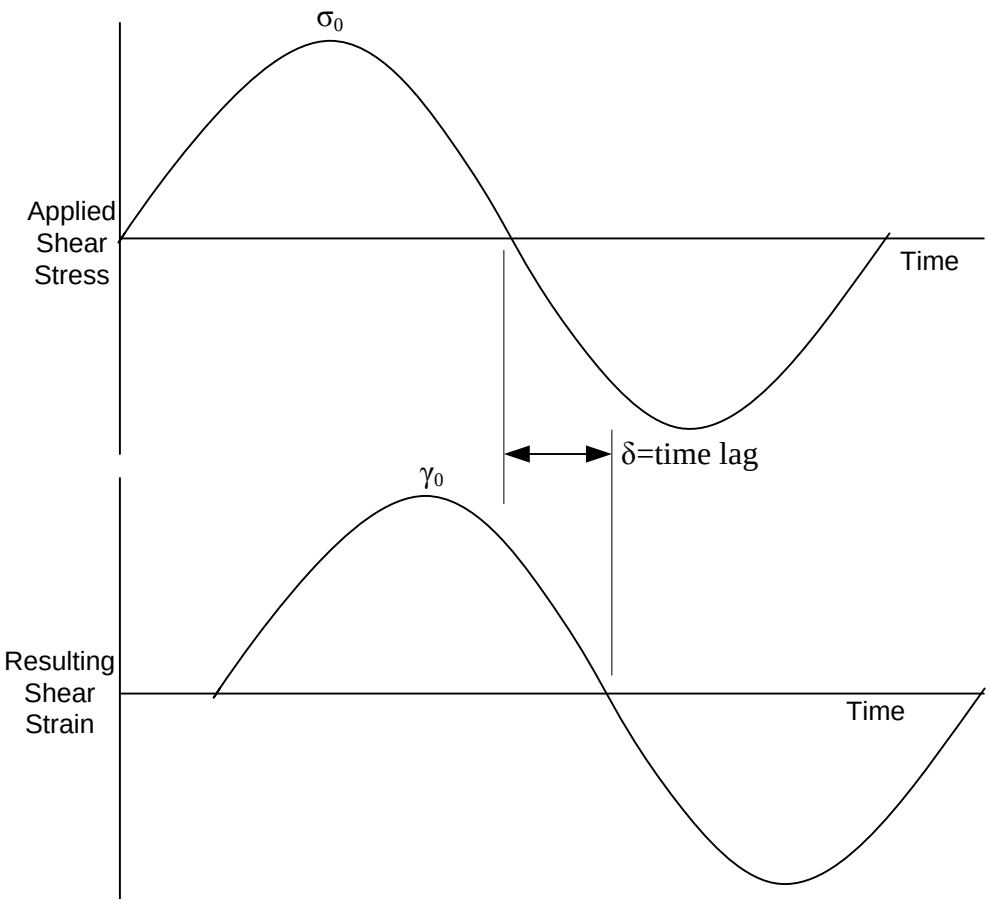

Figure 2-11 Shear stress and strain response of a viscoelastic material.

In previous studies, it was indicated that for weekly flocculated cement pastes, the appearance of yielding is mainly strain-controlled (*28*). Therefore, in order to keep cement paste in its linear viscoelastic range, it is easier to control the strain than to control the stress. To perform an oscillation measurement, a target strain less than the breaking strain is input as a parameter. The stress-controlled rheometer has advantages since it can measure much smaller strains and directly measure the yield stress. In recent research using a highly sensitive stress-controlled rheometer, Zhang and Struble showed that the critical strain limit for cement paste is on the order of 10^{-4}. Using a target strain below the critical strain of 10^{-4}, the viscoelastic properties of cement paste were successfully measured using the storage modulus parameter (G')

as a function of time (*30*). They reported the comparison of storage modulus curves as a function of time for cement paste mixtures with various dosage levels of superplasticizer, as shown in Figure 2-12 (*31*). The stiffening processes of each mixture were fairly distinguishable from the storage modulus vs. elapsed time relationship. Therefore, monitoring storage modulus with time using the dynamic rheology technique could be a potential concept to identify cement-mineral/chemical admixture incompatibility.

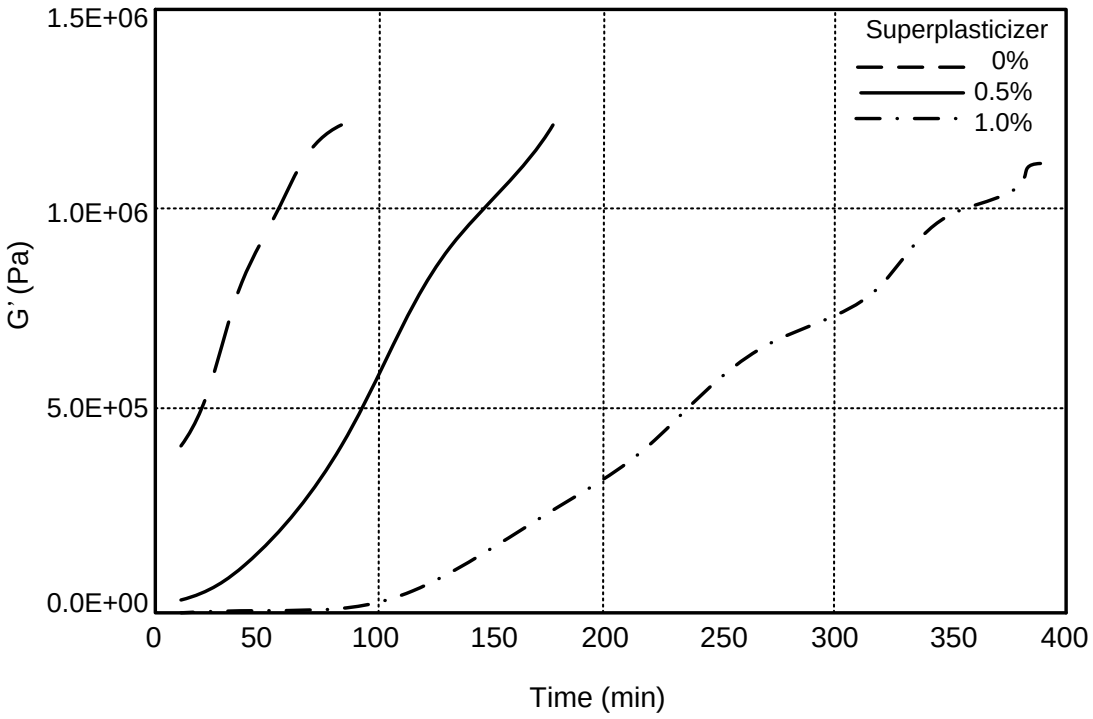

Figure 2-12 Storage modulus of cement paste as a function of time with various dosage levels of superplasticizer (*31*).

Zhang and Struble (2001) reported that the dynamic rheology method has several advantages over the static rheology method. First, it provides a better way to understand the microstructure of cement paste (i.e., evaluation of the cement paste stiffness). Second, the tested

cement paste retains its microstructure without breaking down throughout the test, provided that the strain is kept in the linear viscoelastic range. Therefore, it can continuously monitor change of microstructure due to continuous hydration. In their study, the dynamic rheology technique was used to characterize the microstructure and stiffening process by measuring the storage modulus as a function of time using a stress-controlled rheometer (*31*).

However, in order to get an accurate result, it is necessary to select a reasonable strain value to monitor change of the storage modulus with time. An unnecessarily small strain results in low sensitivity whereas a too large strain leads to a microstructural breakdown (*31*). It is necessary to assign an optimum target strain for a particular rheometer with specific geometry in order to achieve better sensitivity, which is detailed in Chapter III.

Other Test Methods for Measuring Cement Paste Flow Behavior

Kantro investigated the rheological properties of cement paste in 1980 since the flow properties of a concrete are largely dependent upon the cement paste component of the mixture (*32*). As a result, a series of new test methods has been produced for the determination of the rheological properties of cement paste; the two most popular methods being discussed at present are the Marsh cone and the Mini slump cone test. The Marsh flow cone is used as a measure of the fluidity of different cement pastes. The test involves the measurement of the time taken for approximately 1 liter of prepared cement paste to pass through a funnel having an orifice of 12 mm diameter. The water reducing admixture effect is represented as a decrease in the flow time. The mini slump test method is a scaled down version of the slump cone used in ASTM C 143 for the measuring of slump of concrete by keeping the same ratio of dimension.

The mini slump cone test was originally designed by Kantro to evaluate the performance of water reducing admixtures on the workability of cement pastes. The mini slump cone test is simple, inexpensive and can be performed rapidly with a small sample. The mini slump cone is a scaled down (1:5) version of the concrete slump cone and the design details are illustrated in Figure 2-13. Due to action of gravity, cement pastes slump, much like concrete does, to a point where its yield value is no longer exceeded. Although cement paste and concrete may be very different in terms of their rheology, there should be a good correlation between the slump of a concrete and pat area of cement paste since the flow characteristics of concrete are determined largely by the yield value of cement paste contained within it (*32*). Due to the relatively small size of the pat produced by the mini slump test, it is impractical to measure changes in height; rather the pat area is measured. Both tests, however, remain measures of the deformation imposed by gravitational force. Application of the mini slump test has proven promising in that the test shows good correlation with the regular slump values of concrete and has proven to have excellent reproducibility with a single operator (*33*). Due to its sensitivity to change in the rheological behavior of cement pastes, the test has been adapted for use in numerous studies testing the affects of admixture combinations on workability and early stiffening problems (*34*). Jiang and Kim (2000) reported that the rheological behavior of cement paste as a function of time and superplasticizer dosage provides relevant information on key properties, such as slump and slump loss, which can be transferred to fresh concrete (*35*). Therefore, the applicability of the mini slump cone test for identifying cement-mineral/chemical admixture incompatibility is investigated.

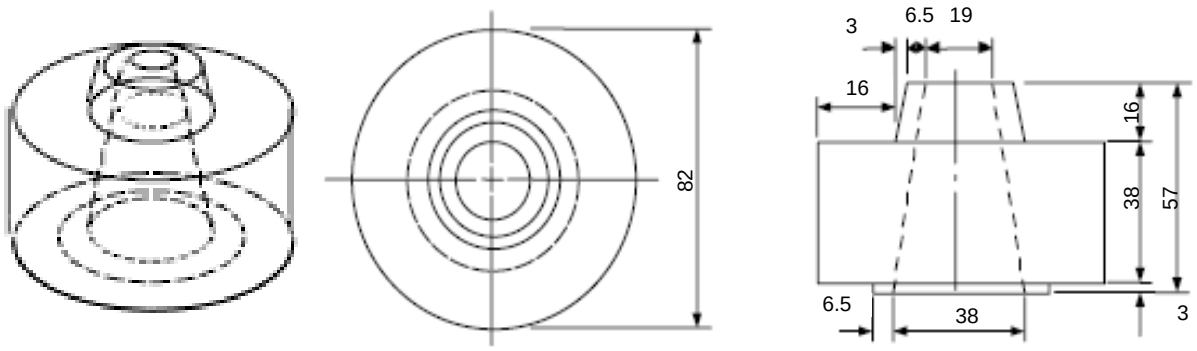

Note: units are in millimeters

Figure 2-13 Schematic illustration of mini slump cone (*32*).

AREAS OF MODIFICATION OF THE DSR TO MEASURE CEMENT PASTE RHEOLOGY

According to many previous studies, it is clear that change in the rheology of cement paste affects the concrete rheology, although the relationship between cement paste and concrete rheology has not been completely established (*36*). Cement paste rheology is typically measured under conditions that are not experienced by the cement paste in concrete. The values usually reported in the literature for cement paste do not take into account the contribution of the aggregates (*37*). Determining the correct method for measuring the rheology of cement paste requires simulation of the conditions that cement paste experiences in concrete. A method was developed by several researchers to predict concrete rheology based on cement paste rheology measured under simulated shearing conditions (*38*). Various factors were addressed in designing the proposed test procedure:

- Selection of the proper geometry and friction characteristic of surfaces is important to simulate the actual flow of cement paste in fresh concrete. It was shown that rheological properties of cement paste obtained from flow tests vary with the test geometry, gap and friction level of the shearing surfaces (*39*).

- The mixing of cement paste must imitate the shear stresses experienced in concrete. It has been reported that the high shear mixer for preparing cement paste can be used in order to simulate the shearing effect which is caused by aggregates in concrete (*40*). Thus, the mixer type and mixing procedure affects the rheology of cement paste.

Therefore, modification of the DSR is discussed based on the available information regarding (i) selection of the geometry for cement paste rheology testing, (ii) modification of the shearing surfaces and temperature controller, and (iii) influence of mixer type and mixing procedure.

Selection of the Geometry for the Rheology of Cement Paste

The variation of the geometry and the friction characteristic of shearing surface in the rheology of cement paste were recently studied by M. Nehdi relative to the actual flow of cement paste in fresh concrete (*39*). It was reported that rheological parameters of cement paste (i.e. yield stress and viscosity) obtained from shear stress-shear rate flow tests vary with test geometry and friction level of the shearing surfaces. In his study, the yield stress and plastic viscosity were measured for different cement paste mixtures using a smooth coaxial cylinder, vane rotor, smooth parallel plates, and serrated parallel plates, as illustrated in Figure 2-14.

Cement paste mixtures with a few mineral and chemical admixtures were tested in accordance with the static rheological mode (i.e. shear stress-shear rate flow mode). The measured flow curves were fitted to the Bingham model (i.e., Eq. (2.14)). The standard error of measured flow curves was also calculated for different cement paste mixtures using four different geometries. The standard error was used as a scale for measuring the relative level of accuracy of each geometry. The calculation of standard error was based on the standard

deviation normalized by the difference between the maximum and minimum measured plastic viscosity multiplied by 1000 as follows:

$$S.E = \frac{1000 \times \left[\sum \left(X_m - X_c \right)^2 / \left(n - 2 \right) \right]^{1/2}}{Range} \quad \text{.....(2.23)}$$

where, X_m = measured shear stress, X_c = calculated shear stress, using the fit to the Bingham model, n = number of data points and *Range* = maximum value of X_m - minimum value of X_m.

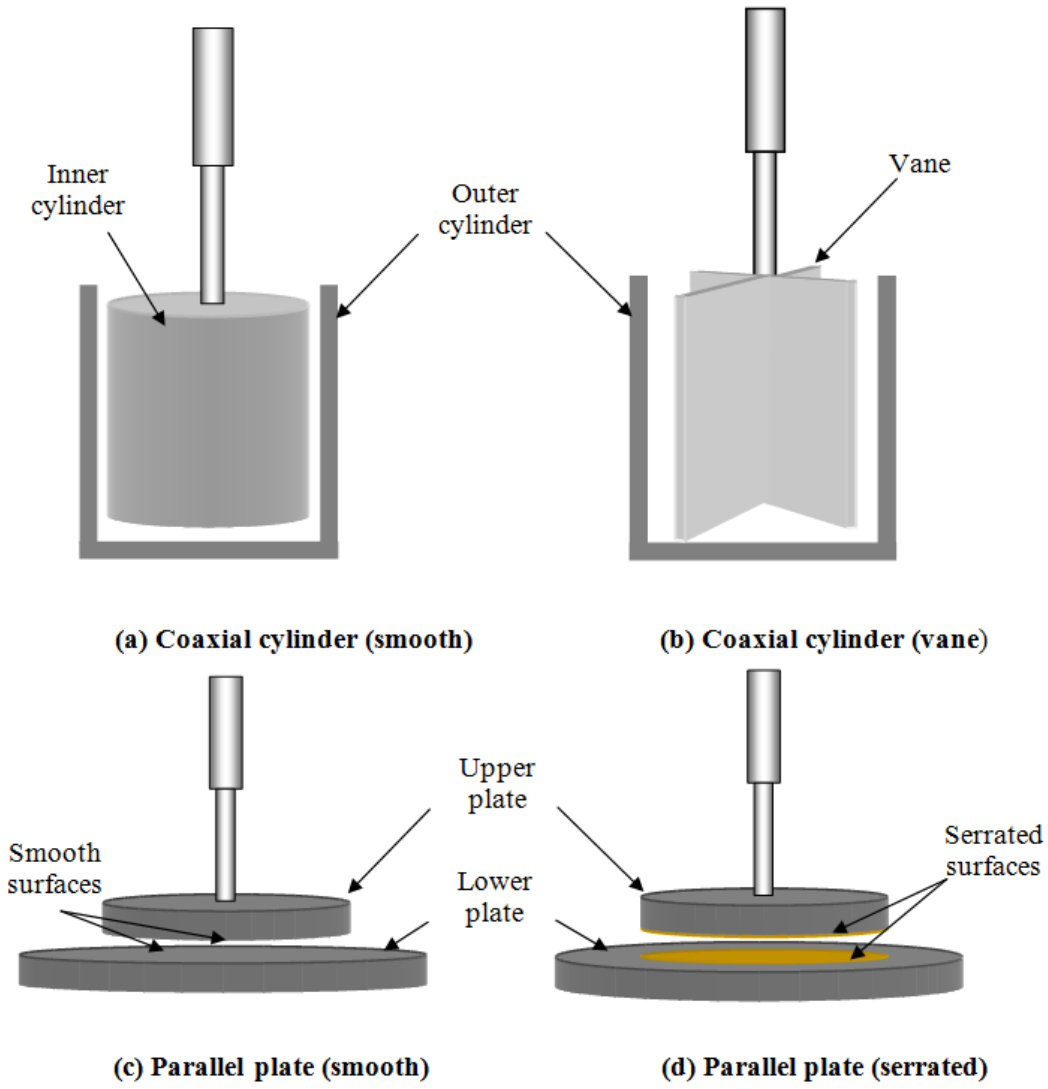

Figure 2-14 Various geometries used for cement paste rheology tests.

Table 2-5 shows the plastic viscosity and standard error for cement pastes with different water binder ratio (w/b) and mineral admixtures. The general observation indicates that the serrated parallel plate geometry has the lowest standard error among four different geometries, as well as distinguishable rheological parameters (i.e., yield stress and plastic viscosity) for the studied mixtures. It was reported that this trend also extended to other cement mixtures such as those containing various dosage levels of chemical admixtures (RMA, rheology-modifying admixture), as listed at Table 2-6. Thus, the serrated parallel plates system can be considered as a potential geometry to measure cement paste rheology since it shows good reproducibility of the rheological parameters with low standard error.

Table 2-5 Yield stress, viscosity, and standard error (S.E.) of the studied cement pastes with various geometries (*39*).

Test Geometry	Cement Paste	Yield Stress	Plastic Viscosity	Standard Error (S.E.)	Average S.E.
Coaxial Cylinder	100% OPC (w/b = 0.5)	7.3	0.34	122.90	87.5
	100% OPC (w/b = 0.4)	12.5	1.28	45.60	
	25% Slag (w/b = 0.5)	7.0	0.38	111.90	
	25% Slag (w/b = 0.4)	7.5	1.21	40.83	
	25% FA (w/b = 0.5)	6.9	0.29	131.90	
	25% FA (w/b = 0.4)	7.9	0.91	49.65	
	8% SF (w/b = 0.5)	19.0	1.37	109.90	
Vane Rotor	100% OPC (w/b = 0.5)	12.1	0.16	115.10	86.7
	100% OPC (w/b = 0.4)	29.9	0.69	102.60	
	25% Slag (w/b = 0.5)	11.2	0.13	78.21	
	25% Slag (w/b = 0.4)	47.0	0.57	65.09	
	25% FA (w/b = 0.5)	8.7	0.14	131.90	
	25% FA (w/b = 0.4)	33.5	0.35	70.41	
	8% SF (w/b = 0.5)	47.1	0.22	43.38	
Smooth Parallel Plates	100% OPC (w/b = 0.5)	4.8	0.37	128.60	87.1
	100% OPC (w/b = 0.4)	5.1	1.62	37.77	
	25% Slag (w/b = 0.5)	2.3	0.34	103.11	
	25% Slag (w/b = 0.4)	5.0	1.61	28.14	
	25% FA (w/b = 0.5)	1.9	0.32	76.05	
	25% FA (w/b = 0.4)	6.7	1.05	65.09	
	8% SF (w/b = 0.5)	26.6	0.80	170.90	
Serrated Parallel Plates	100% OPC (w/b = 0.5)	6.8	0.22	84.66	71.5
	100% OPC (w/b = 0.4)	42.1	0.90	55.05	
	25% Slag (w/b = 0.5)	7.5	0.23	96.60	
	25% Slag (w/b = 0.4)	58.0	1.29	40.96	
	25% FA (w/b = 0.5)	4.0	0.14	93.41	
	25% FA (w/b = 0.4)	52.1	0.80	59.35	
	8% SF (w/b = 0.5)	88.2	0.84	77.95	

Note: OPC=ordinary portland cement, F= fly ash, SF=silica fume, w/b=water binder ratio

Table 2-6 Yield stress, viscosity, and standard error (S.E.) of the studied cement pastes with various geometries (*39*).

Test Geometry	Cement Paste	Yield Stress	Plastic Viscosity	Standard Error (S.E.)	Average S.E.
Coaxial Cylinder	100% OPC (RMA 0.00%)	7.3	0.33	122.90	91.5
	100% OPC (RMA 0.03%)	8.9	0.43	87.37	
	100% OPC (RMA 0.05%)	13.1	0.45	66.49	
	25% Slag (RMA 0.00%)	6.6	0.38	111.90	
	25% Slag (RMA 0.03%)	8.7	0.43	84.18	
	25% Slag (RMA 0.05%)	9.1	0.44	76.41	
Smooth Parallel Plates	100% OPC (RMA 0.00%)	4.6	0.37	128.60	102.4
	100% OPC (RMA 0.03%)	5.3	0.54	97.78	
	100% OPC (RMA 0.05%)	8.4	0.62	107.70	
	25% Slag (RMA 0.00%)	2.0	0.34	103.10	
	25% Slag (RMA 0.03%)	3.2	0.44	77.24	
	25% Slag (RMA 0.05%)	4.9	0.48	99.75	
Serrated Parallel Plates	100% OPC (RMA 0.00%)	6.5	0.21	84.66	72.2
	100% OPC (RMA 0.03%)	12.1	0.22	65.67	
	100% OPC (RMA 0.05%)	13.6	0.25	60.17	
	25% Slag (RMA 0.00%)	7.6	0.23	96.60	
	25% Slag (RMA 0.03%)	8.3	0.23	66.90	
	25% Slag (RMA 0.05%)	10.7	0.24	59.31	

Note: RM A = rheology-modifying admixture

Modification of the Shearing Surfaces and Temperature Controller

Although the parallel plate geometry with smooth shearing surfaces has been used for the rheology of cement paste, it is susceptible to the effects of slippage. During testing, a liquid layer may develop due to the displacement of cement particles away from the smooth shearing surfaces of the measurement device. The development of this layer produces a lubricating effect, making fluid flow easier and not representative of the bulk cement paste specimen. This phenomenon, called '*slippage*', is most pronounced at stresses near the yield point (*41*). The thickness of the slip layer is normally on the order of 0.1 to 10 μm. As the solid concentration

increases, the size of the slip layer decreases; however, the influence of slippage becomes more dominant (*41*). The high solid concentrations typical of most cement pastes are prone to a slippage effect in experiments using the geometry with smooth shearing surfaces.

Slippage was first shown to occur in rheological measurements of cement paste by Wesche et al. (1973) who compared the results of flow curve experiments using smooth-walled and serrated cylinders (*42*). Slippage was most pronounced at low strain rates and led to unusually low viscosity measurements. As the strain rate was increased, the influence of slippage decreased. Thus, it is important to prevent the slippage effect at stresses near the yield stress of the material.

Ferraris and her collaborators have been evaluating cement paste since 1991 using fluid rheometers with a parallel plate geometry (*43*). They modified the shearing surfaces of the parallel plates using serrated paper (240 grit or 54 micron) or cross-hatched metal plates to avoid slippage. In the same manner, the smooth shearing surfaces of both upper and lower parallel plates in the DSR can be grooved (*44*). The schematic pictures of both smooth and serrated parallel plates are shown in Figure 2-15.

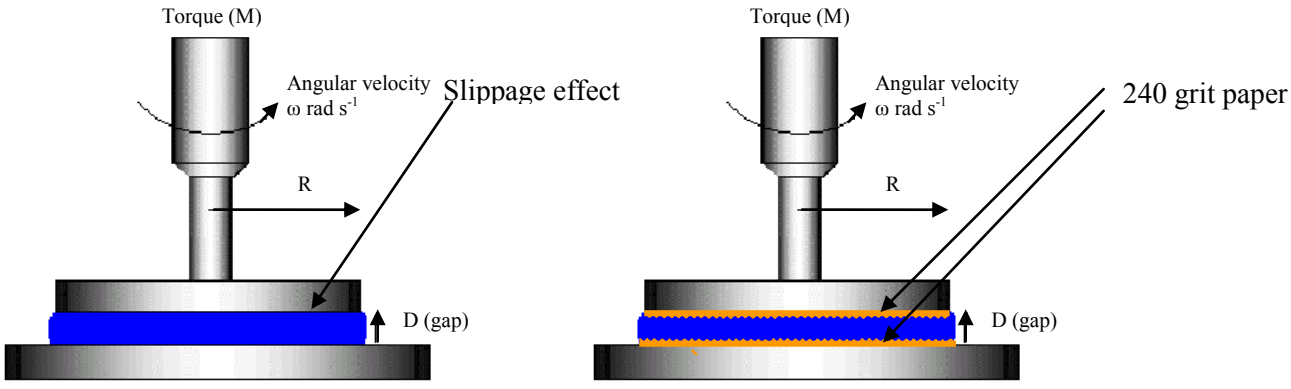

Figure 2-15 Smooth parallel plates (left) and grooved parallel plates (right).

In addition to the geometry, the gap between shearing surfaces of the device plays an important role to measure the rheology of cement paste that is representative of the paste in concrete. The aggregates in concrete cause shearing effects in cement paste during the mixing process. The distance between the aggregates (varying with the paste content in concrete) in concrete has an important influence on the degree of shearing effects. The distance between aggregates can be represented by setting a proper gap between two parallel plates (*43*). Therefore, selecting an optimum gap between two plates in the DSR-based rheology test procedure is necessary to simulate the shearing effects that cement paste experiences in concrete due to aggregates. An effort was made to find the optimum gap for the rheology of cement paste using the modified DSR as a preliminary test program, detailed in Chapter IV.

Moreover, the DSRs used by State Departments of Transportation (DOTs) have mainly used water circulation to control the temperature of the specimen through direct contact with water. Since fresh cement paste is a water-sensitive material (unlike asphalt cement), other arrangements such as Peltier heating-cooling system or closed water circulation system (i.e., water circulation occurs inside a container that is located below the lower plate) is appropriate for temperature controlling. In most of the previous studies on cement paste rheology, temperature control during mixing instead of temperature control in the rheometer was considered as a means to study the effect of temperature. However, temperature control in both mixing and rheometer testing stages is necessary in order to study the effect of temperature precisely.

Influence of the Mixer Type and Mixing Procedure

Shear history for cement paste in its fresh state can best be defined as the shear experienced by a given mixing process. The effects of mixing on the rheology of cement paste have been studied by several researchers for the past decades. Roy and Asaga (1979) have used a blender as a high speed shear mixer (up to 5000 rpm) and a Hobart paddle mixer as a low speed shear mixer (with 100 rpm) in their cement paste rheology research (*45*). They mentioned that the cement pastes mixed in the blender more accurately represent concrete performance when the yield stresses are compared with concrete slump tests.

Some studies on the rheology of cement paste suggest that higher shear mixing increases viscosity and yield stress due to abrasion of the cement grain surfaces (*46*). These results show that mixing is effective insofar as it breaks down the early structure of cement paste by rupturing the flocculated cement grains. However, long mixing times in high shear mixers reduce cement paste flowability (*47*). It is obvious that these conclusions are highly dependent on the type of mixer used in each study.

An intensive investigation of the effects of mixing on cement paste rheology was studied by Yang and Jennings in 1995 (*48*). His study was accomplished by measuring the structural breakdown in fresh cement pastes through evaluation of the plastic viscosity. The susceptibility of fresh cement paste to further breakdown upon controlled mixing in a rheometer was used as a method to compare the efficacy of various mixing techniques. Mixing cement paste involves breaking up particle agglomerates. In a well-mixed paste, the number of agglomerates in the liquid is small and the particles are dispersed. In such cement pastes, there are few hydrate membrane linkages susceptible to breakdown by the application of additional shear. Figure 2-16 shows that plastic viscosity of the cement paste mixed using the high shear mixer at 2500 rpm

was less dependent on the applied pre-shear rate than hand-mixed pastes. The large decrease in plastic viscosity for hand-mixed paste subjected to additional shear was observed in Figure 2-16. These results suggest that high shear-mixed pastes contain fewer agglomerates and show a good reproducibility regardless of pre-shear influence. This confirms a study by Helmuth (*49*) stating that in concrete, during mixing, the cement paste is sheared with an energy and rate more closely reproduced in a blender (3000 rpm) as opposed to the low shear rate of the Hobart mixer (500 rpm). Therefore, it is essential to use a high shear mixer to prepare cement paste in order to measure representative rheological parameters.

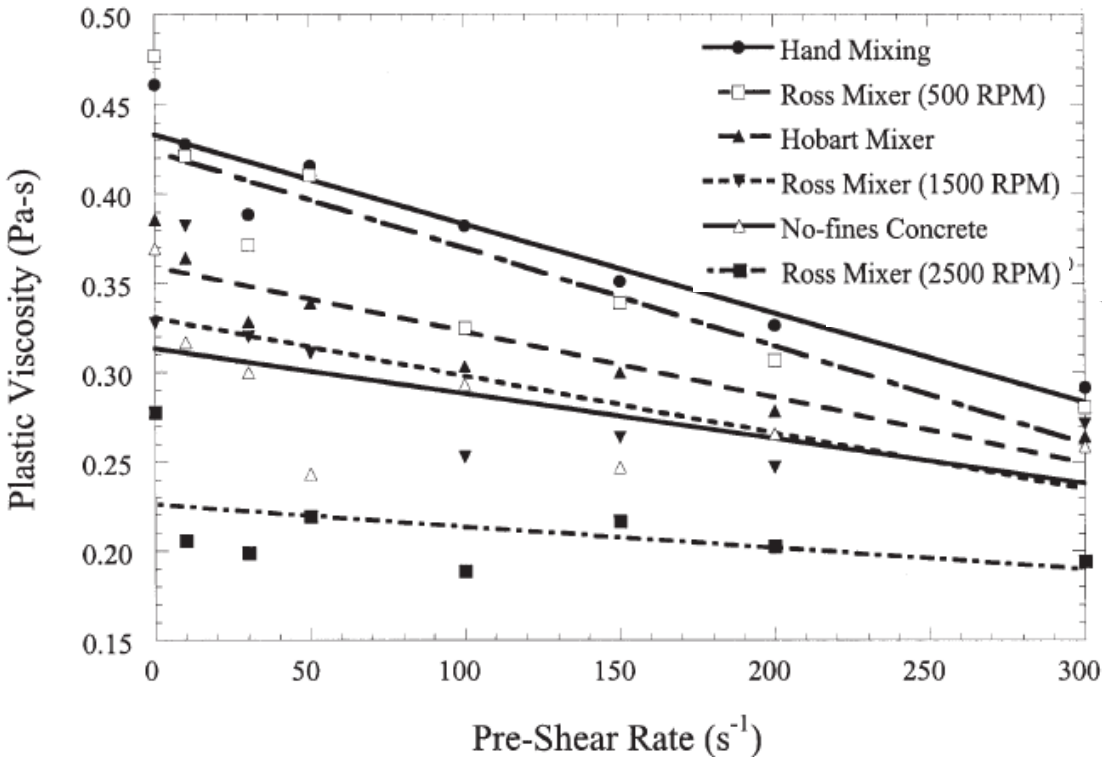

Figure 2-16 Plastic viscosity as a function of pre-shear rate for various mixing techniques (*48*).

Delayed Addition of Chemical Admixtures

During the mixing procedure, the timing of chemical admixture additions can be critical. Water reducing admixtures (WRAs) are negatively-charged organic molecules that adsorb primarily at the solid-water interface. Solid particles carry residual charges on their surfaces, which may be positive, negative, or both. Molecules of the WRA interact to neutralize these surface charges and cause all surfaces to carry uniform charges. Particles now repel each other, rather than attract, and remain fully dispersed in the paste. The WRA is consumed rapidly when added along with the mixing water. WRA molecules show an affinity for the aluminate phases and attach in substantial amounts to the tricalcium aluminate phase before it reacts with calcium silicate, thus very little of the admixture is left to adhere to the silicate phases (*50*). Due to the rapid hydration that tricalcium aluminate (C_3A) undergoes when contacted with water, the bound WRA becomes contained by the hydrated aluminates and cannot contribute itself to the water reduction, which creates a rapid slump loss (*51*).

By delayed addition of the WRA, the effectiveness of the chemical admixture can be drastically increased. By allowing the cement to react with the water, the C_3A can undergo its normal reaction with the sulphates to form the calcium alumino-sulphate compounds. These compounds are less prone to adsorb the admixture and the C_3A's affinity for the admixture is decreased. (*52*). As a result, the admixture is adsorbed to a lesser extent, so there will be sufficient admixture left in the solution to promote dispersion of the silicate phases and to lower the viscosity of cement paste. The effect of delayed addition of admixture is significant even if only delayed for several minutes (*52*).

FACTORS INFLUENCING CONCRETE INCOMPATIBILITIES

The reasons for the incompatibility of concrete are poorly understood but typically can be prevented by the replacement of either the cement or the admixture. However, an understanding must be developed so that the occurrences of such phenomena can be minimized, if not eliminated. Since cement consists of multiple components and phases, the chemical reaction in its hydration is complicated. The complexity of these interactions is complicated by chemical admixtures due to the variety of components, especially lignosulfonates (*53*). Hence, one can expect that any explanation of the mechanism related to the cause of compatibility problems should be either physical or chemical or a combination of both. However, a definitive explanation for concrete incompatibilities is yet to be established, although general explanations have been proposed by a few researchers in the past. There have been cases in the field that concrete has experienced an abnormal setting behavior after mixing (*54*). In some circumstances, these phenomena usually occur due to the complex interactions between chemical admixtures and some specific types of cements, although when used alone these cements don't show any abnormal setting behavior. Factors responsible for concrete incompatibility, although complicated, have been researched over the years, and the key factors are:

1. The C_3A content of the cement,
2. The sulphate content of the cement,
3. Alkali content of the cement,
4. Presence of a lignin-based chemical admixture, and
5. The curing temperature of the concrete

Effect of C_3A on Early Stiffening

In portland cement, the alumina-containing phases, especially the tricalcium aluminate, are the phases that react rapidly enough to give rise to the undesirable rapid set. As soon as contact is made with water the tricalcium aluminate evolves heat rapidly and reaches a sharp peak. For this reason, it has long been accepted that the aluminate phases and their hydration products are key to the early hydration process and setting behavior, relative to the effect of other phases of cement. The behavior of hydrating cements during the first two to three hours is governed by reactions of the aluminate phases (especially C_3A).

If the C_3A in the cement is very reactive, flash set may occur. Flash set is caused by the formation of large quantities of monosulfoaluminate or other calcium aluminate hydrates. This is a rapid set that cannot be disrupted by further mixing, indicating that some strength has developed. However, flash set has been largely eliminated as a problem with normal portland cement by the use of gypsum to control C_3A hydration (*55*).

Effect of Sulphate Content

It is important to note that the aluminate phases of portland cement hydrate very rapidly, and if it was not controlled by gypsum, crystals of calcium hydroaluminates would form, resulting in flash set. Thus, it is evident that the rate at which C_3A hydrates must be restricted. For this purpose some form of calcium sulphate ($CaSO_4$) is inter-ground with cement clinker to moderate this reaction. The sulphate ions that go into solution control the reaction rate by reacting with the C_3A to form mainly ettringite with some monosulfoaluminate (*5*). To produce normal set portland cement concrete, a sulfate-bearing phase (mainly gypsum) must provide

optimum sulphate ions in aqueous solution for the formation of an ettringite film on the cement particles. This protective film reduces the rate at which further C_3A can enter the pore solution.

In cement paste an optimum concentration of $CaSO_4$ is soon established in the liquid phase so that the hydroaluminates produced are immediately turned into calcium sulfoaluminate or ettringite by reacting with $CaSO_4$ and lime. The ettringite, when deposited on the surfaces of cement particles, provides an effective barrier to further reactions. This film of ettringite, which slows the hydration, lasts as long as the $CaSO_4$ concentration of the liquid remains at a certain level. After this, hydration resumes and a normal setting begins. In the absence of an effective retarder, such as finely ground gypsum, the release of silica and alumina into solution leads to the rapid precipitation of alumina-silica gel that causes both early stiffening and retards hydration of C_3S and strength development (*56*).

Other problems associated with the sulphate content of the cement are a result of the manufacturing process. The recent use of high sulphur fuels, air pollution control systems, and recycling of cement kiln dust has led to significantly higher sulphate contents in the cement clinker (*57*). An excess of sulphate in the clinker will cause the alkalis present to be highly soluble which can accelerate the hydration of both alite and C_3A, or the excess sulphate will form as insoluble fractions in the silicate or aluminate phases, or as anhydrate (*57*). Unfortunately, it has become more difficult to properly restrict the time of set by further addition of sulphates due to the presence of strict industry limitations with maximum sulphate content. Also, industrial byproducts are being used in some cases as a source of calcium sulphate, as a partial replacement of gypsum. The incorporation of these materials may lead to complexity in predicting cement setting performance.

Effect of Alkali Content

The presence of alkalis in portland cement clinker promotes the dissolution of C_3A, thus increasing its rate of reaction, and accelerates early hydration (*58*). The early hydration rates for the C_3S component of cement are not significantly affected by the presence of alkali. Increasing the alkali content has the effect of drastically increasing the solubility of sulphate ions. For cements of the same C_3A content, those high in alkalis reacting with gypsum more rapidly have a higher consumption rate of gypsum and require larger additions of gypsum than those low in alkalis (*59*). It appears that at least part of the alkalis in the cement are present in the aluminate phases and that the aluminate phases containing alkalis react with water more rapidly than do similar phases which are alkali-free or of lower alkali content (*59*). Therefore, the possibility of flash set is increased if insufficient levels of SO_3 are present even in high alkali cements.

Effect of Lignosulfonates

Lignosulfonate water reducers, the first polymeric water reducers used by the concrete industry, are limited in use due to dosage sensitivity. They are manufactured from one of the waste products produced by the pulp and paper industry. When first introduced to the concrete industry, lignosulfonates were relatively inexpensive. However, due to the non-uniformity of the law materials used (i.e., variances in sugar content) the lignin-based products have problems associated with excessive set retardation (*60*). Although excessive set retardation present in the early generations of lignosulfonates has been minimized, they still may occur when high dosages are used. The presence of sugar and other contaminants in commercial lignosulfonates can be blamed for this, since these compounds are difficult to completely remove (*60*). Under certain circumstances, a high dosage of a lignosulfonate admixture may permanently suppress hydration

of C_3S and inhibit strength development, particularly in cements with very low C_3A and alkali content (*2*). Figure 2-17 shows the heat evolution of normal portland cement with two different dosage levels of lignosulfonate water reducer. The mixture with the higher dosage of lignosulfonates has the restrained second peak compared to the one with normal dosage.

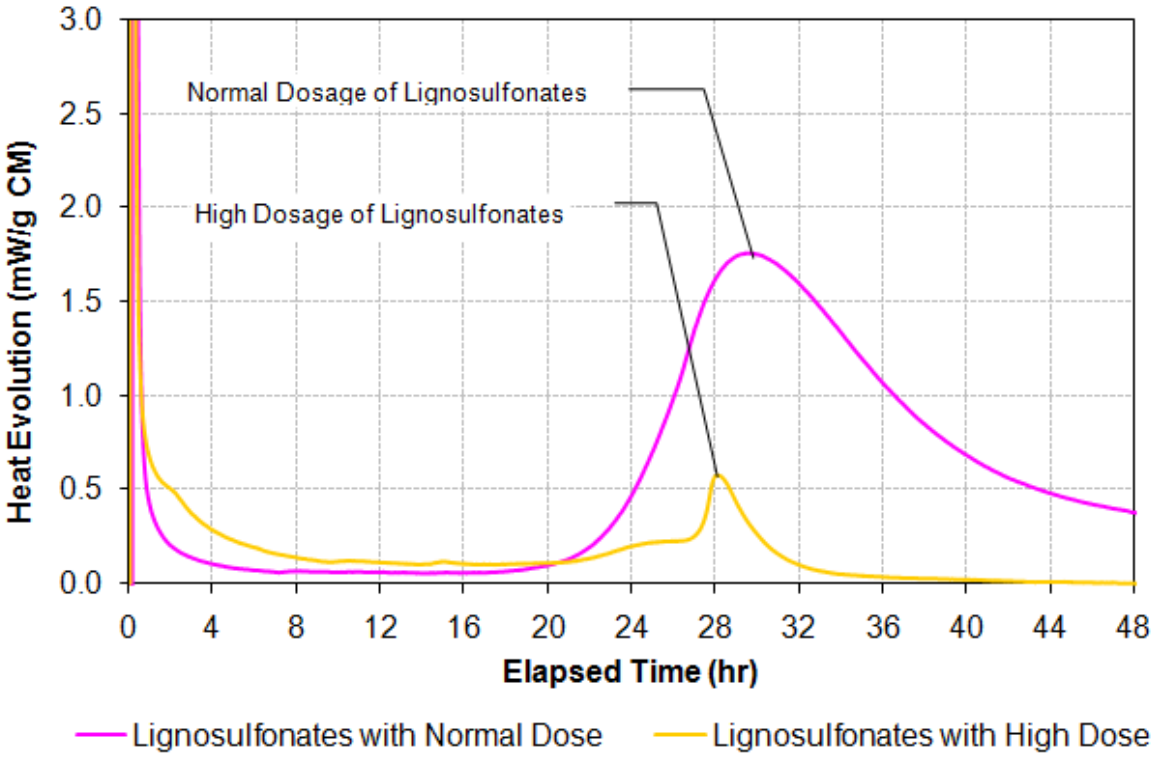

Figure 2-17 Normal and abnormal heat evolution with two different dosage levels of lignosulfonates.

Effect of Curing Temperature

The concrete placement temperature may alter the rate of hydration and evaporation of cement. A high temperature during concrete placement tends to accelerate the cement hydration due to high reaction kinetics, which causes high heat evolution. Similarly, a low temperature

causes the reverse effects, i.e., retardation of cement hydration (low heat evolution). As a result, in hot weather placement (e.g., summer construction), the concrete generally experiences higher slump loss and fast stiffening that sometimes results in early stiffening or loss of workability. On the other hand, in cold weather placement (e.g., winter construction), concrete may experience excessive set retardation in some extreme cases. One cement – admixture (both SCMs as well as chemical admixtures) combination may behave normally at a particular temperature (e.g., generally high temperature) but may behave abnormally at other temperature (e.g., generally low temperature) because of the difference in reaction kinetics. Thus, it is necessary to investigate the curing temperature effect on concrete incompatibility.

CHAPTER III

MODIFICATION OF THE DSR AND MIXING PROCESS

The dynamic shear rheometer (DSR) has been originally adopted in superpave to characterize the viscous and elastic behavior of asphalt cement at high and intermediate service temperatures. The DSR has been used as a standard test for measuring rheological properties of asphalt cement by most of the Department of Transportation (DOT). However, the DSR has a great potential to be considered as a user-friendly cement paste rheology measurement device after upgrading the device with necessary modifications. The areas of modification of the DSR along with the importance of mixing procedure were reviewed in the Chapter II. In this Chapter, it is presented the modifications of two different DSRs that have been actually made to optimize cement paste rheology test. The selection of mixer type and mixing process for the cement paste rheology test is described as followed by the modifications of DSRs.

MODIFICATION OF THE DSR FOR MEASURING CEMENT PASTE RHEOLOGY

The areas of modification of the DSR have been identified from Chapter II. These are (i) making a serrated surface to avoid slippage, (ii) installing a different temperature controlling system where sample contact with water can be avoided (e.g., peltier heating-cooling system or closed water circulation system), and (iii) installing a better evaporation control system. The three areas of modifications are described below one by one.

Making Serrated Surface

To make the parallel plate surfaces serrate, 240 grit size paper (70 micron) with adhesive back was installed in both upper and lower plates (25mm diameter for both the plates) in order to

prevent slippage. Figure 3-1 shows a schematic representation of attaching 240 grit paper on both the plates. The use of 240 grit size paper in rheometer with parallel plate configuration to prevent slippage effect as well as to simulate aggregate texture effects is reported by several researchers (*39, 43*).

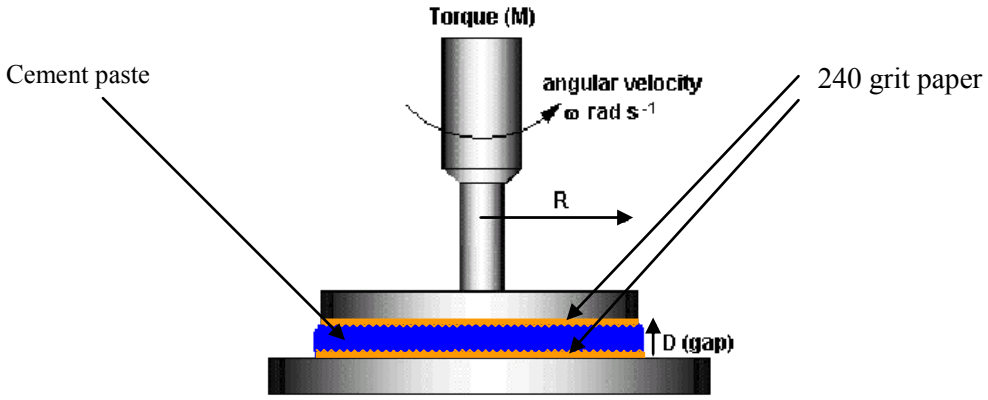

Figure 3-1 Installation of grit papers on both upper and lower plates in the DSR.

Temperature Control

Bohlin DSR was used for the static rheology procedure whereas AR2000 DSR for the dynamic rheology procedure since each rheometer has different software for measuring cement paste rheology. Although the Bohlin DSR is generally being used at most Department of Transportation (DOT), it doesn't have the proper software to measure the storage modulus of cement paste as a function of time. Thus, AR 2000 was used to explore the dynamic rheology mode.

A fluid jacket heating/cooling device for the Bohlin DSR and a Peltier device for the AR2000 DSR were installed (Figure 3-2) to avoid direct contact of cement paste specimen with water during testing. Most Bohlin DSRs used at State Departments of Transportation have open

water circulation system for temperature control where a specimen comes in contact with water directly. Since fresh cement paste is a water-sensitive material unlike asphalt cement, the existing temperature control system needed to be changed. The fluid jacket device operates with closed water circulation to control the specimen temperature and direct contact between samples and water is avoided. The AR 2000 is equipped with the peltier heating-cooling device, which operates with a thermoelectric controller to keep the temperature of the cement paste sample constant during the entire time span of the rheological test.

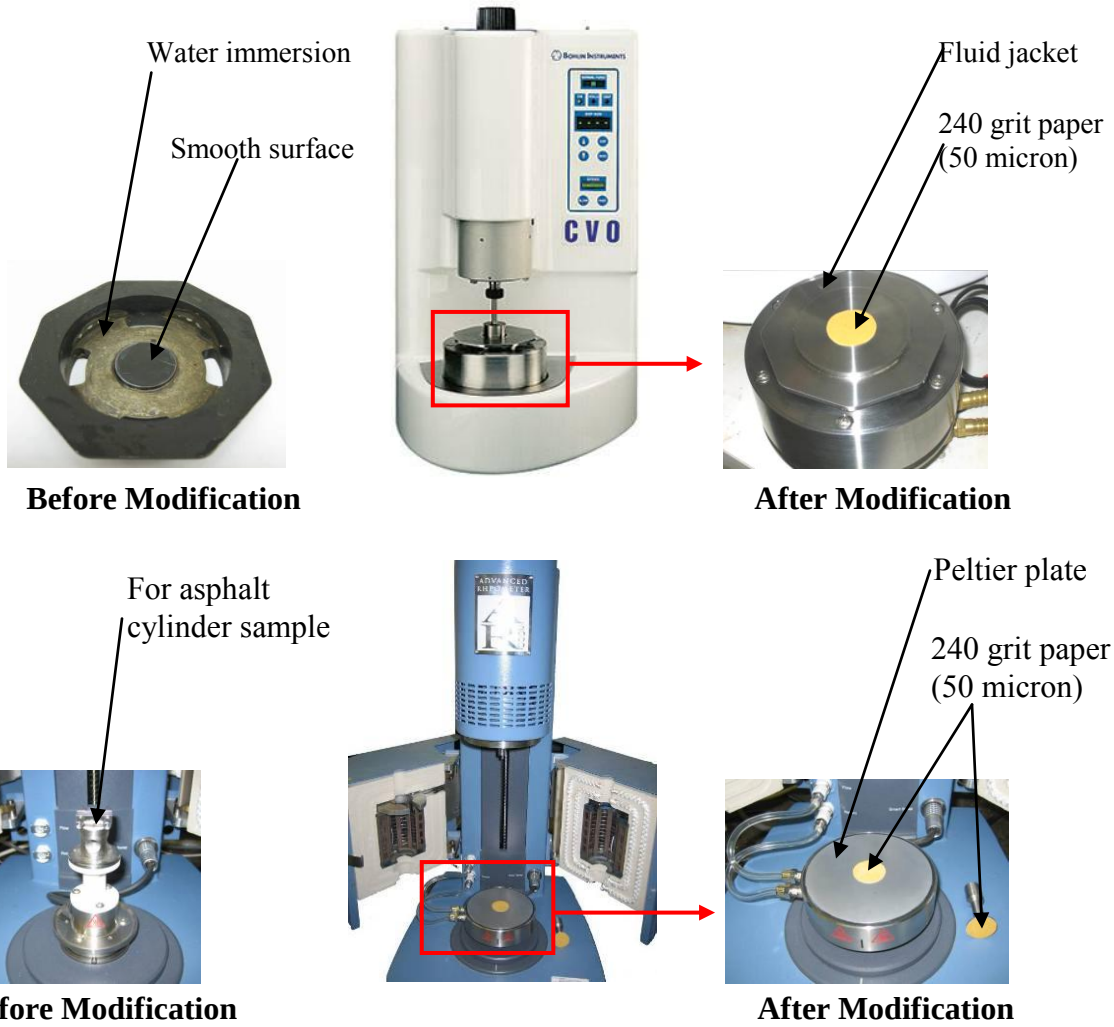

Figure 3-2 Modified DSR with the fluid jacket system (top), Peltier plate system (bottom).

Water Evaporation Control

It has been studied that the water evaporation control is important during the rheology test procedure. It was observed that the device recorded changes due to the water evaporation while measuring the rheological changes due to cement hydration and any interparticle interaction (during induction period). Therefore, it would be ideal to remove the evaporation effects at the best. An extensive study was conducted to develop a very effective evaporation control system in order to avoid the water evaporation during cement paste rheology measurements. Three different methods of water evaporation prevention was verified; (i) applying a thin layer of mineral oil (immiscible with the sample) especially at the periphery of the parallel plates, (ii) placing a humidifier in close proximity to maintain high relative humidity (RH) in the surrounding areas, and (iii) encapsulating the sample chamber by a plastic sealing cap. The sealing cap option (Figure 3-3) was found to be the most effective method and accepted as a final evaporation control measure for the cement paste rheology test program. This sealing cap had an adequate mechanism to allow rotation of the shaft without any interference.

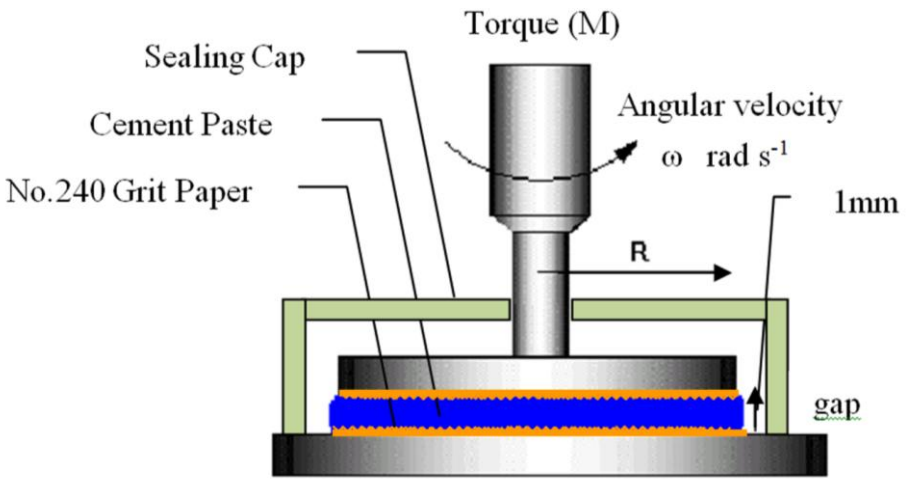

Figure 3-3 Evaporation control on modified DSR using sealing cap.

MIXER TYPE AND MIXING PROCEDURE

The mixing procedure to prepare the cement paste sample was developed by Texas Transportation Institute based on the procedure developed by Portland Cement Association (PCA) and later on National Institute of Standards and Technology (NIST). A high-shear mixer, i.e., a kitchen blender (Figure 3-4), was used to develop the mixing procedure. The maximum mixing speed used during mixing procedure was 6000 rpm instead of 10000 rpm (used by PCA/NIST) in order to reduce high heat generation due to friction. The steps involved in the mixing procedure are presented in Figure 3-5 and are briefly described below.

1. Keep the mixing bowl along with all the ingredients inside the refrigerator / oven / room for pre-conditioning under the selected studied target temperatures.
2. Keep the predetermined quantity of cement and SCM blend in the mixing bowl of the mixer.
3. Pour the water into the mixing bowl containing cement and SCM blend followed by switching on the mixer with 3000 rpm speed for 30 seconds.
4. Stop the mixer and add the chemical admixture to the cement and water mixture in the container slowly within 50 seconds and mix again with 3000 rpm setting for another 10 sec.
5. Increase mixing speed to 6000 rpm and continue mixing for another 30 seconds.
6. Stop mixing for 2 minutes and scrape the sides of the mixing bowl with a rubber paddle.
7. Mix again in the same high-shear blender at 6000 rpm for another 30 seconds.
8. The sample of cement paste was poured thereafter into the rheometer using a syringe.

Mixing Speed	1.	2.	3.	4.	5.
Level	Stir	Chop	Mix	Puree	Liquify
RPM	3000	6000	8000	10000	13000

Figure 3-4 High-shear mixer, KSB560OB Kitchen Aid Company (left) and different mixing speed levels corresponding to rpm (right).

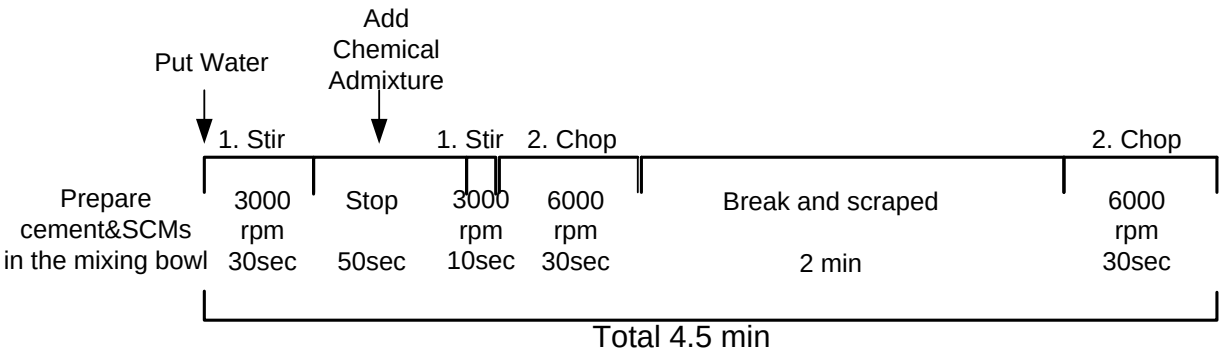

Figure 3-5 Schematic mixing procedure.

CHAPTER IV

APPLICABILITY OF THE DSR FOR MEASURING CEMENT PASTE RHEOLOGY

The applicability of the DSR to measure cement paste rheology has been verified through preliminary test program using the modified system and developed test procedure. Objectives and test methods for the preliminary tests are presented. Materials, test procedure, and results for the preliminary test follow.

OBJECTIVES OF PRELIMINARY TEST PROGRAM

The items that are identified for optimization are listed below:

(i) The gap between two parallel plates to obtain rheological parameters with the static rheology mode, i.e., the shear stress vs. shear rate flow.

(ii) The strain for the dynamic rheology mode, i.e., the storage modulus vs. elapsed time using another advanced rheometer of parallel plate configuration (AR 2000).

(iii) Reproducibility of the rheological results.

(iv) Verification of rheological test results with the conventional methods, i.e., heat of hydration and vicat setting time.

TEST METHODS

The testing plan in the experimental program is summarized in Table 4-1. The experimental program is based on four different test methods and equipments: (i) rheological behavior of cement paste measured by two DSRs (i.e., Bohlin and AR2000), (ii) heat generation behavior of cement paste measured by isothermal conduction calorimeter, and (iii) setting

behavior of cement paste determined by the Vicat apparatus (ACTM C 191) (*61*). The modified AR 2000 rheometer was selected for the preliminary test program to validate optimum strain rate for the dynamic rheology mode. The test methods for measuring heat of hydration and setting time served as supporting tools for the rheological parameters determined by the DSR.

Table 4-1 Test methods in the experimental program.

Test Method	Test Equipment	Measured Properties
Rheological behavior of fresh cement paste	Modified Bohlin CVO rheometer, DSR (Malvern Instrument)	Static rheology mode (yield stress and plastic viscosity)
Rheological behavior of fresh cement paste	Modified AR2000 rheometer, DSR (TA Instrument)	Dynamic rheology mode (Storage modulus)
Heat generation behavior of the cementitious system (ASTM C 186)	Isothermal conduction calorimeter (OMNICAL)	Heat of Hydration
Setting behavior (ASTM C191)	Vicat needle apparatus	Initial and final set time

MATERIALS

The materials that were used in the preliminary study are an ordinary ASTM Type I portland cement (OPC), a water reducing and set retarding admixture (WRRA), and deionized water. The cement was characterized for its bulk chemical compositions by X-ray fluorescence. The results of mineral phase contents along with other physical properties are presented in the Table 4-2.

Table 4-2 Chemical and physical characteristics of ordinary portland cement.

Component/properties		Percentage of Mass
Chemical composition (%)		
SiO_2 (%)		19.830
Al_2O_3 (%)		5.121
Fe_2O_3 (%)		1.853
CaO (%)		63.912
MgO (%)		1.208
SO_3 (%)		3.303
Na_2O (%)		0.115
K_2O (%)		0.474
CO_2 (%)		0.52
Equivalent total alkalis (%)		0.42
Insoluble Residue (%)		0.08
Limestone (%)		1.22
$CaCO_3$ in limestone (%)		96
Loss of ignition (%)		2.44
Chemical composition based Bougue's phase composition (%)		
C_3S (%)		63.00
C_2S (%)		9.326
C_3A (%)		10.44
C_4AF (%)		5.640
Sulfate minerals (%) from SAM extraction / QXRD		
Gypsum (%)		5
Hemihydrate (%)		1.4
Anhydrate (%)		0
Gypsum-to- hemihydrate Ratio		3.57
Physical properties		
Blaine Fineness (cm^2/g)		3920
Mean particle size (micron)		18.97
Median particle size (micron)		16.11
Compressive strength (MPa) standard cube	3 days	28.2
	7 days	36.5
	28 days	47.8

According to ASTM C 494 (*62*) the chemical admixture used for this study is classified as Type B & D, i.e., water reducing and set retarding admixture (WRRA). The ingredient of the chemical is an aqueous solution of lignosulfonate and compound carbohydrates. The manufacturer's recommended range of dosage is 130-520mL/100kg of cement (2-8 fl oz/cwt) and typical dosage is 195mL/100kg (3fl oz/cwt).

Three cement pastes (P1, P2, and P3) with varying proportions of WRRA are considered for the present preliminary investigation and their mixture proportions are presented in Table 4-3. P1 and P2 mixtures were formulated using a typical and a maximum recommended dosage of the studied WRRA respectively whereas P3 was formulated with excessively high dosage of the WRRA (i.e., double of the maximum recommended dosage). P3 mix was designed to create an artificial incompatible mixture in the laboratory.

Table 4-3 Mix design of three studied cement pastes.

Mixture	Water L/m^3 ($gal./yd^3$)	Cement kg/m^3 (lb/yd^3)	w/c	Chemical Admixture		
				Type	Dosage (%)	Range of Dosage
P1	550 (111)	1375 (2308)	0.4	WRRA	0.2% of cement weight	Typical recommended dosage
P2	550 (111)	1375 (2308)	0.4	WRRA	0.5% of cement weight	Maximum recommended dosage
P3	550 (111)	1375 (2308)	0.4	WRRA	1% of cement weight	Double of the maximum recommended dosage

Note: WRRA= water reducing and set retarding admixture

TEST PROCEDURE

The test procedure and test equipments (i.e., rheometers, isothermal conduction calorimeter, and vicat needle apparatus) are presented below. The temperature controlled high shear mixing procedure described in Chapter III was applied to the cement paste sample preparation for each test method as an essential requirement.

Temperature Controlled Storage and Mixing

All the ingredients, i.e., cement, deionized water, and chemical admixture, were kept under the selected temperatures at least for one day before mixing. A refrigerator was used to store as well as mix the materials at the studied low temperature (i.e., 10°C / 50°F) to represent a winter temperature whereas an oven was used for the same at the studied high temperature (i.e., 35°C / 95°F) to represent a summer temperature as shown in Figure 4-1. Storing materials and mixing inside a lab room with 24°C / 75°F temperature represented mixing at intermediate ambient temperature condition.

Figure 4-1 Use of the refrigerator to mix at low temperature (left) and the oven to mix at high temperature (right).

The mixer type and mixing procedure to prepare the cement paste sample for all the preliminary test methods were followed by the one developed by Texas Transportation Institute described at Chapter III. A high-shear mixer, i.e., a kitchen blender (Figure 3-4), was used to develop the mixing procedure. The steps involved in the mixing procedure are presented at Figure 3-5.

Static Rheology Test Procedure

The studied cement paste was tested for total 5 plate (25 mm diameter) gaps (i.e., 0.2, 0.5, 1.0, 1.2, and 1.5 mm). An effort was made to establish an optimum gap between two parallel plates with permissible sensitivity and reproducibility of each studied mixture. The shear stress and strain rate of the tested specimens are recorded through a computer based data acquisition system. The test was carried out at a controlled temperature 24˚C (75˚F). A computer program allows the user to customize test parameters, such as the number of readings, the gap of the parallel plate, the sampling interval between the readings, and specimen temperature. The rheometer test procedure is given below:

1. Take cement paste specimen from the mixing bowl using 3 ml syringes immediately after mixing procedure at 24˚C (75˚F).
2. Place the predetermined quantity of cement paste (i.e., 1.5ml) onto the lower plate of the rheometer from the syringe.
3. Sandwich the specimen between the two parallel plates with preselected plate gap and cover the sealing cap to prevent water evaporation during the rheology test period.
4. After 30 minutes of equilibrium time, the pre-shear rate of 200 s^{-1} is applied for 30 seconds.

5. Immediately after pre-shear rate, the upper parallel plate starts to rotate and shear with shear rate from 0 to 200/s proportionally representing the up curve followed by 200 to 0/s representing the down curve as shown in Figure 4-2. The shear stress as a function of the shear rate is then recorded. A run with one cycle consisting of one up curve and one down curve takes approximately 2.5 minutes.

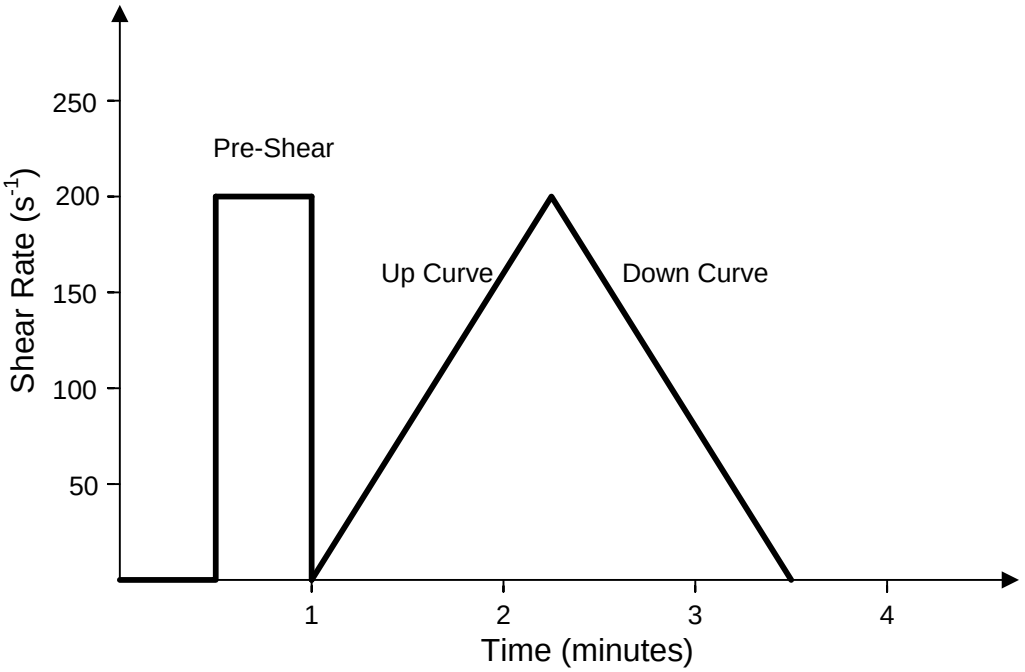

Figure 4-2 Applied pre-shear rate and main shear rate with time for static rheology test.

Calculation of Plastic Viscosity and Yield Stress

Typical data showing shear rate versus shear stress are presented in Figure 4-3. The plastic viscosity and yield stress are determined using Bingham model described in Eq. (1.2). Plastic viscosity is calculated from the slope of the linear region of the curve, whereas yield stress is calculated from the interception as shown in Figure 4-3. Average viscosity, yield stress,

and their respective coefficient of variation (CoV%) based on three repeated tests were calculated corresponding to each test run.

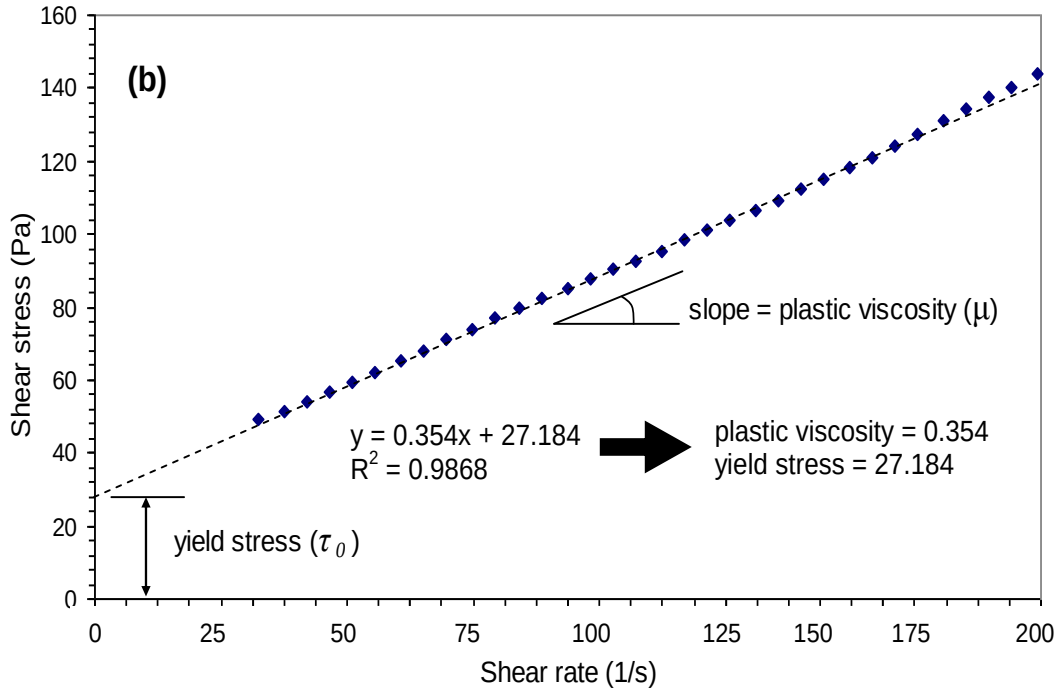

Figure 4-3 Typical shear stress vs. shear rate curve (top) and calculation of rheological parameters using Bingham model (bottom).

Dynamic Rheology Test Procedure

The P1 mixture that shows the normal heat evolution behavior, the cement paste with 0.2 % of WRRA listed at Table 4-3, was tested for total 4 different strains with oscillation mode (i.e., 2×10^{-5}, 5×10^{-5}, 1×10^{-4}, and 5×10^{-4}). The storage modulus, G', as a function of time with the tested specimen is recorded until 5 hours through a computer based data acquisition system. The test was carried out at a controlled temperature of 24˚C (75˚F). A computer program allows the

user to customize test parameters, such as the target strain, the sampling interval between the readings, and specimen temperature. The dynamic rheology test procedure is given below:

1. Take cement paste specimen from the mixing bowl using 3 ml syringes immediately after mixing procedure at 24˚C (75˚F).
2. Place the predetermined quantity of cement paste (i.e., 1.5ml) onto the lower plate of the rheometer from the syringe.
3. Sandwich the specimen between the two parallel plates with plate gap of 1 mm and cover the sealing cap to prevent water evaporation during the rheology test period.
4. Equilibrium time is applied for 10 minutes to stabilize the microstructure of cement paste.
5. The upper parallel plate starts to oscillate with preselected target strain (i.e., 2×10^{-5}, 5×10^{-5}, 1×10^{-4}, and 5×10^{-4}). The storage modulus as a function of time is then recorded until 5 hours.

Measurement of Storage Modulus as a Function of Time

The storage modulus curve for the studied mixture P1 is measured for 5 hours test duration using the dynamic rheology mode (i.e., continuous oscillation mode) with the preselected target strain. All dynamic rheology tests are conducted at a frequency of 6.28 radians per second which is equivalent to 1 Hz, which is generally adopted for cement paste rheology tests (*19*). Typical data showing the storage modulus curve as a function of time are presented in Figure 4-4. The storage modulus curve represents the stiffening behavior of cement paste at an early age.

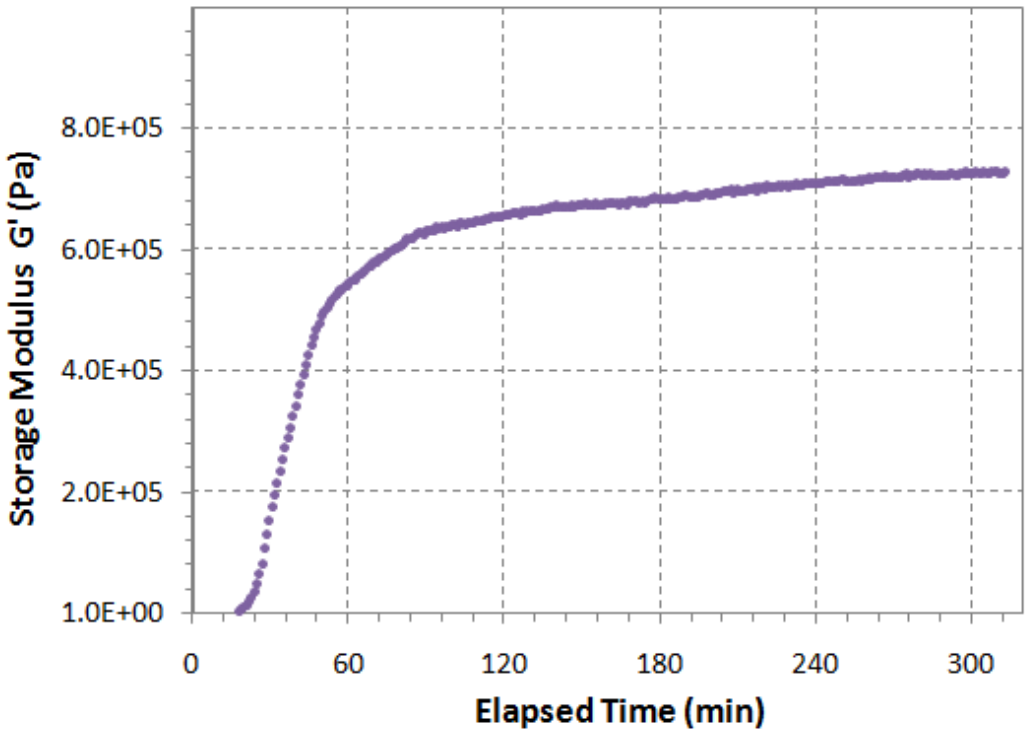

Figure 4-4 Typical storage modulus curve as a function of time with oscillation mode.

Conduction Calorimeter Test Procedure

An isothermal conduction calorimeter (the Super CRC) manufactured by Omnical Company (Figure 4-5) was used to measure heat of hydration in fresh cement paste. Immediately after completing mixing procedure, the cement paste was transferred into a glass cylinder, which was sealed at the top using a plastic layer cap and quickly placed in the isothermal conduction calorimeter. Heat evolution data were monitored and recorded for 50 hours at a 12 second interval.

Figure 4-5 Isothermal conduction calorimeter for the heat of hydration of cement paste.

Vicat Apparatus Test Procedure

The setting time in this study was measured by the Vicat apparatus (Figure 4-6) according to ASTM C 191 (*61*). A specimen of fresh cement paste was prepared with high shear mixer at 24°C (75°F) constant room temperature. Immediately after mixing the cement paste is placed in a frustum of 40 mm (1.57 in.) in height. Initial set is considered as the time when the needle penetration is 25 mm ± 0.5 mm (1.53 in. ± 0.019 in.). The final set corresponds to less than 0.5 mm (0.019 in.) penetration.

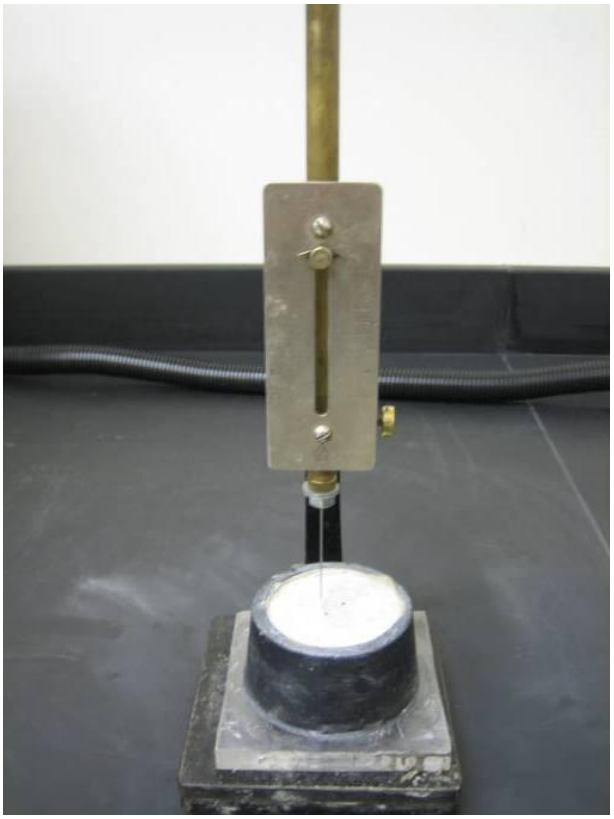

Figure 4-6 Vicat apparatus for setting time.

PRELIMINARY TEST RESULTS AND DISCUSSION

A preliminary test program consists of four different test methods listed at Table 4-1. The results from two rheology tests (i.e., static and dynamic rheology methods) are described first and the results from heat of hydration and setting time are followed as supporting tools.

Static Rheology Test

The plastic viscosity and yield stress as a function of gap between two parallel plates and dosage of water reducing and set retarding admixture (WRRA) for all 15 combinations with the modified DSR (Bohlin) are graphically presented in Figure 4-7 (a) and (b) respectively. CoV% of viscosity and yield stress corresponding to the same 15 combinations are compared in Figure

4-7 (c). The static rheological data results in details are presented at Appendix A. perusal of Figure 4-7 showed the following observations:

- Both plastic viscosity and yield stress corresponding to each cement paste mixture (P1, P2, and P3) decreased obviously with increasing dosage of WRRA for all the five plate gaps.
- The modified DSR with 1mm plate gap can clearly distinguish the three mixtures (P1, P2, and P3) with the lowest CoV%. This implies its better sensitivity and reproducibility.
- Below a 1mm plate gap, the sensitivity still remained good; however, reproducibility became poor as manifested by CoV% > 10. Permissible reproducibility of low viscous materials (P3) can still be maintained with lower plate gap (e.g., 0.2, 0.5mm) whereas reproducibility for high viscous materials (P1) with lower plate gap cannot be maintained.
- Above a 1mm plate gap, reproducibility remained good as manifested by CoV% < 10, however, sensitivity became poor since no such considerable difference between rheology of three mixtures was noticed.

Therefore, the modified DSR with 1 mm plate gap have clearly identified these three mixtures with distinct difference in viscosity and yield stress and with permissible reproducibility. The main purpose, i.e., distinguishing an abnormal mixture (P3) from a normal mixture (P1) based on cement paste rheology, is satisfied by the modified DSR. These results described above ultimately point out the potential feasibility of identifying cement - chemical admixture incompatibilities through the direct measurement of cement paste rheology by the modified DSR.

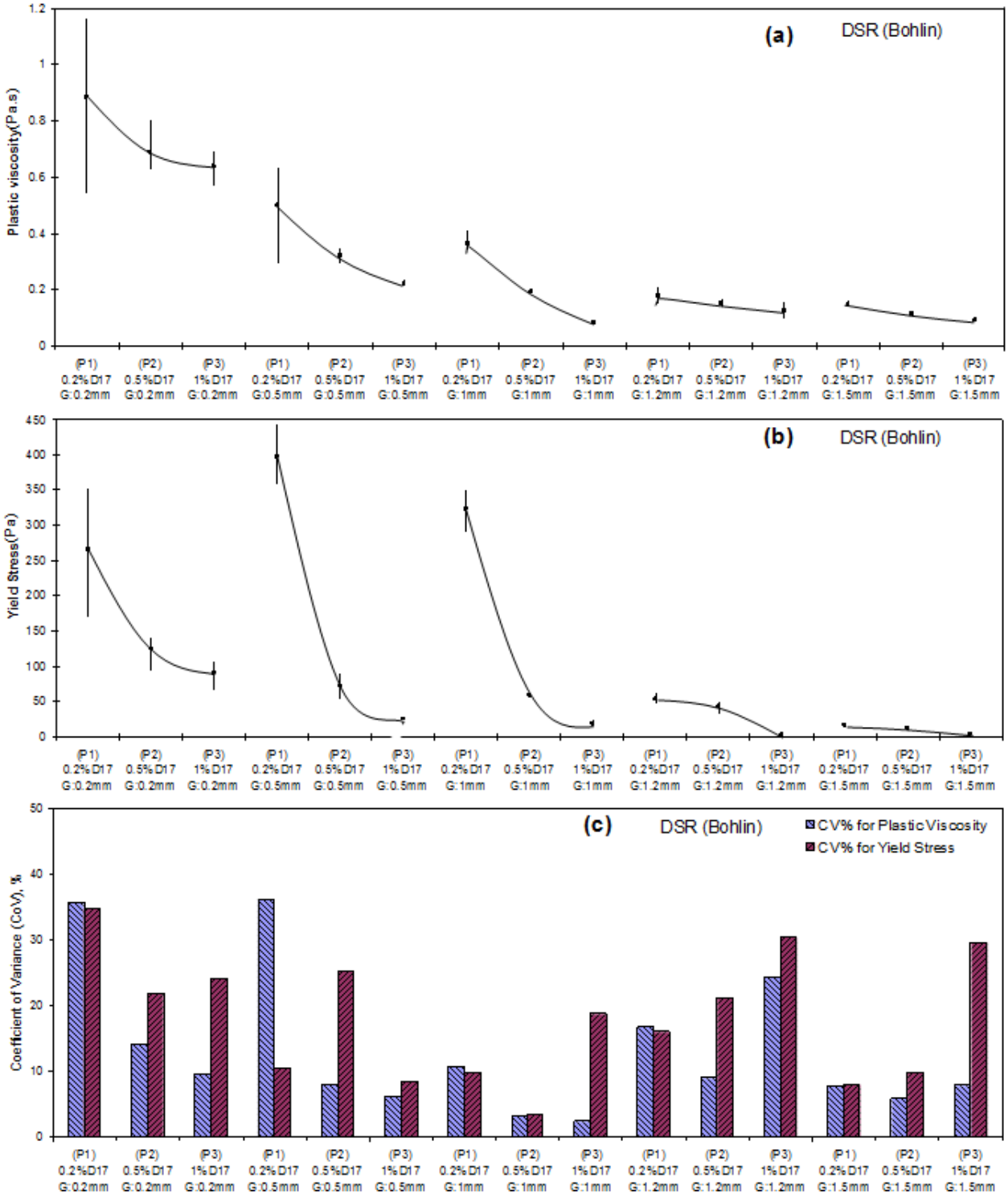

Figure 4-7 (a) Plastic viscosity, (b) Yield stress, and (c) CoV% data from the DSR.

Dynamic Rheology Test

In the dynamic rheology mode, the storage modulus curve was measured as a function of time. In order to obtain a plot of storage modulus as a function of time, it is important to keep a target strain small enough to avoid breakdown of microstructure. Figure 4-4 illustrated previously tells about the change of stiffness of the cement paste with time. Struble and Zhang found that measuring the storage modulus as a function of time using a dynamic rheology mode (i.e., continuous oscillatory shear mode) is a better way to monitor the cement paste stiffening process (*30, 31*). By applying a small oscillatory shear using the modified DSR (AR2000 rheometer), it is feasible to monitor microstructure, stiffening behavior of cement paste mixtures. However, in order to get an accurate result it is necessary to select an optimum strain for dynamic rheology test. An unnecessarily small strain results in low sensitivity whereas a too large strain leads to a microstructural breakdown. Zhang reported that the target strain of 1.0×10^{-4} (100 microstrain) was suitable to provide reproducible measurements using the coaxial cylinder geometry (bob-cup) and no breakdown in microstructure had been observed (*31*). In the present study, the modified AR 2000 rheometer with parallel plate geometry was used, which is different from the rheometer that used by Zhang et.al. Therefore, it is necessary to assign an optimum target strain for the AR 2000 rheometer.

Figure 4-8 shows the storage modulus of P1 mixture (i.e., Type I cement with 0.2% WRRA, typical dosage) under continuous oscillation with different strain levels. When the target strain was 5.0×10^{-4} (500 microstrain), the storage modulus remained at a very low level until 70 minutes of hydration. This storage modulus change indicates that the strain was too large to stay in the linear-viscoelastic range. The storage modulus curve with the target strain of 1.0×10^{-4} (100 microstrain) also shows delay of the initial storage modulus increase until 30 minutes of

hydration. This phenomenon was no longer observed the storage modulus curve with the target strain below 5.0×10^{-5} (50 microstrain). However, at a low strain of 2.0×10^{-5} (20 microstrain) the storage modulus curve increased more rapidly but, there was a microstructural breakdown after 80 minutes showing a very poor resolution with the fluctuated data. The strain of 5.0×10^{-5} (50 microstrain) is validated as an optimum target strain to provide a good reproducibility and no breakdown of microstructure in cement paste rheology test. Therefore, the optimum target strain of 5.0×10^{-5} (50 microstrain) will be used for the main rheology test program presented at Chapter VII.

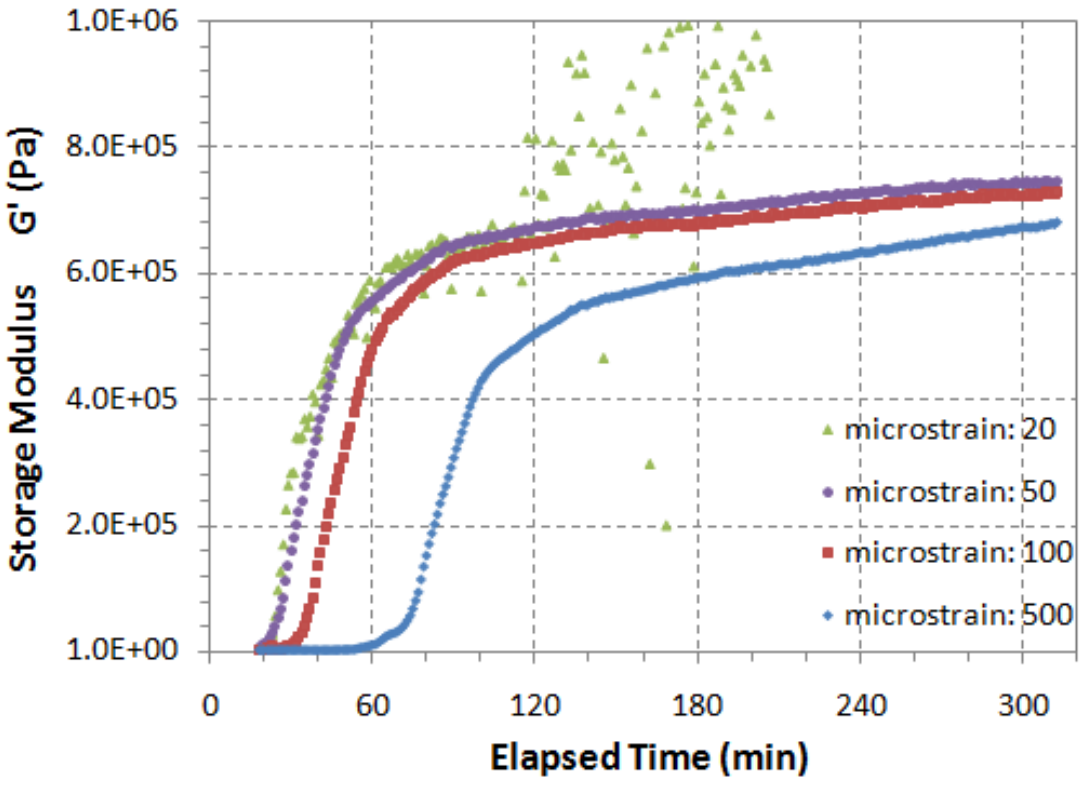

Figure 4-8 Effect of target strain on the storage modulus for P1 mixture at 24°C.

Heat of Hydration Test

The isothermal conduction calorimeter tests were performed for each mixture (P1, P2, and P3) as a supporting tool to verify whether these three mixtures can clearly be distinguished (in accordance with the rheology based distinction) based on their heat evolution characteristics at early ages. All the mixtures were tested three times to verify the reproducibility in the same manner of the rheology tests. Figure 4-9 (a) shows that the occurrence of the second peak of heat evolution is a function of WRRA dosage and induction period of cement hydration increases as the dosage of WRRA increases. As for example, in P3 mixture containing high dosage of WRRA the induction period is around 16 hours showing the evidence of incompatibility whereas in P2 mixture it is around 4-5 hours. P1 mixture behaves as a normal mixture. A good reproducibility of the heat of hydration results for all the three mixtures is manifested by closer superimposition of the three graphs generated from three consecutive tests. Figure 4-9 (b) shows that the integrated heat evolution drastically decreases as the dosage of WRRA increases, i.e., three mixtures having three clearly distinct integrated heat evolution curves. Therefore, the three mixtures have clearly been distinguished based on their heat evolution characteristics, which support the rheology-based observation in the previous section.

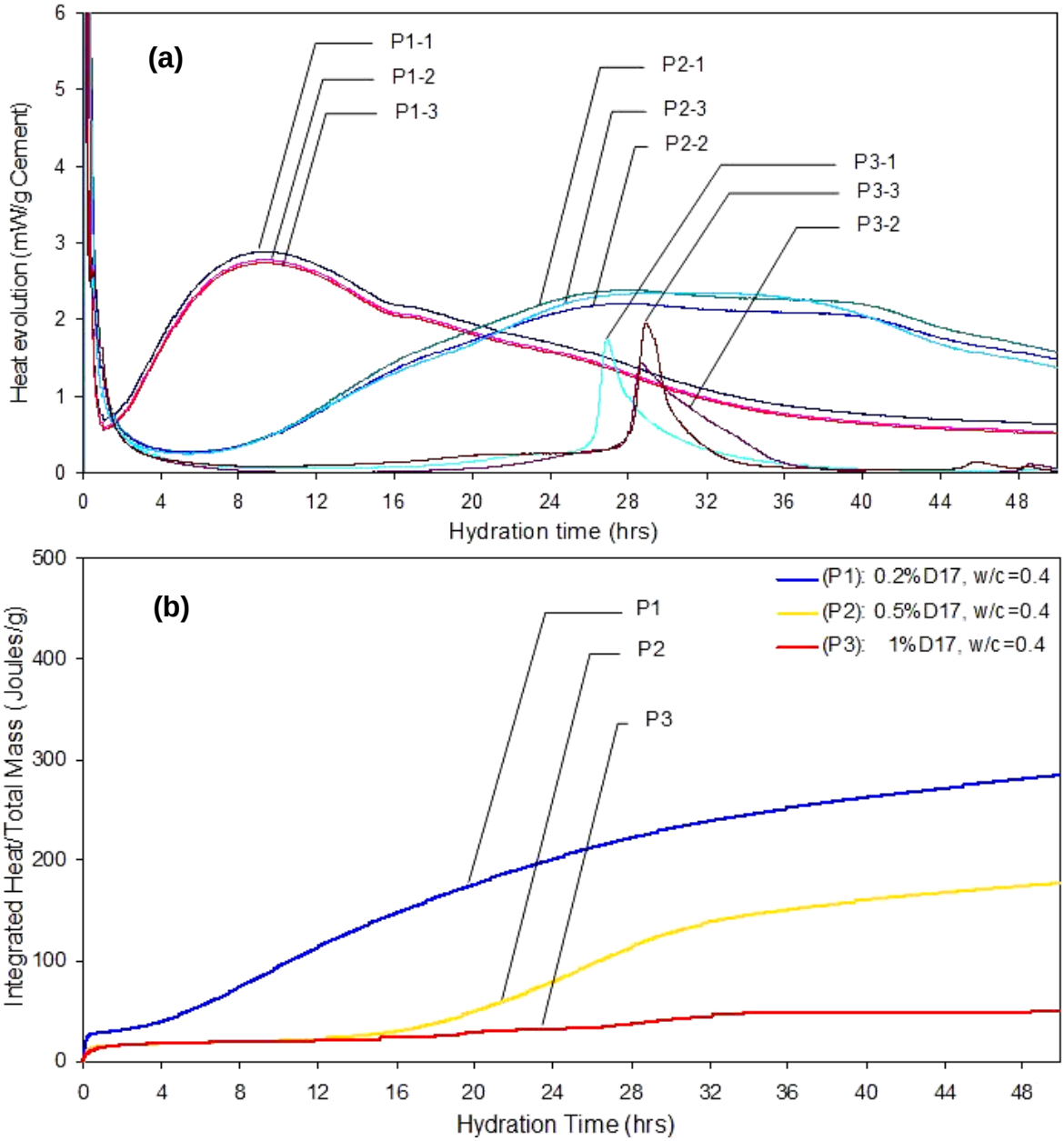

Figure 4-9 Heat evolution (top) and integrated heat evolution as a function of time (bottom).

Vicat Setting Time Test

Vicat Setting time tests were conducted for the studied three mixtures. The results of initial and final setting times are presented Figure 4-10. Figure 4-10 shows that the initial and final set is drastically retarded with P3 mixture containing high dosage of WRRA. This

phenomenon is in accordance with both heat of hydration and rheological behavior as discussed previously.

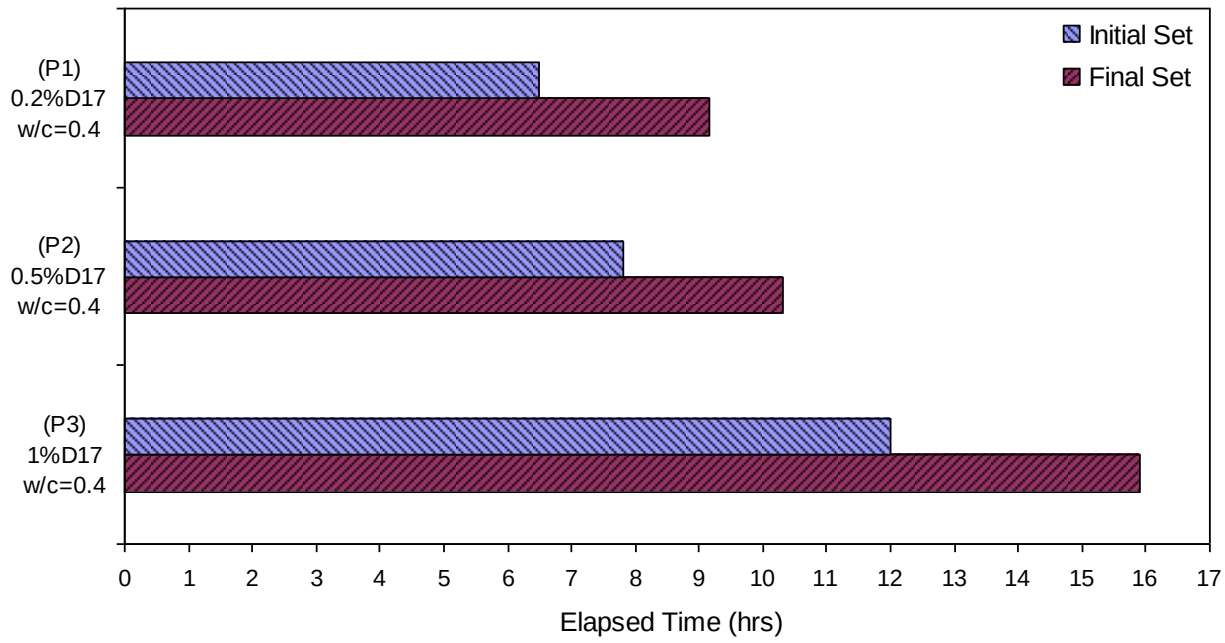

Figure 4-10 Initial and final setting time by Vicat apparatus.

CHAPTER V

MATERIALS CHARACTERIZATION AND SELECTION

MATERIAL COLLECTION

The historical information pertaining to the specific responsible factors for cement-mineral /chemical admixture incompatibilities under field conditions was collected from past records with the help of Texas Department of Transportation (TxDOT) in order to select the factors and levels in such a way that incompatibilities can be reproduced in the laboratory in a similar manner. The most influential factors that affect cement-admixture compatibility in cement paste are summarized based on the literature review and listed in Table 5-1.

Table 5-1 Key parameters related to cement-mineral/chemical admixture incompatibilities.

	Influential Factors		Possible Effects
1	Type of Cement	C_3A contents	The amount of C_3A content in the cement may affect the incompatibility of concrete mixtures.
		Alkali contents	The amount of water-soluble alkalis content in the cement may affect the incompatibility of concrete mixtures.
2	Type of MWRA		Incompatibility issues caused by lignin-based MWRAs are more than any other type of MWRAs.
3	Dosage of MWRA		High dosage of MWRA is likely to cause incompatibility issues in concrete. Standard dosage (5~10 fl oz/cwt), high dosage (>15 fl oz/cwt)
4	Type of SCMs		Soluble sulfate, water-soluble alkali and other reactive phases (e.g., C_3A) in SCMs (fly ashes slag) play an important role in cement-admixture incompatibilities in concrete.
5	Temperature		Excessively high (e.g., > 30^0C) or low ambient temperatures (e.g., < 20^0C) are reported to be more vulnerable than moderate temperatures to create incompatibilities.

Note: MWRA= mid-range water reducing admixture, SCMs=supplementary cementitious materials

Based on field evidence of incompatibilities from TxDOT, materials are collected and listed in Table 5-2. Seven different types and brands of cements were collected in order (i) to cover a wide range of C_3A contents, sulfate contents (especially gypsum to hemihydrate ratio), and soluble alkali contents in the tested cements on one hand and (ii) to enhance the chances of getting incompatible mixtures in the lab on the other hand. Three cements from these seven characterized cements will ultimately be selected for the main laboratory tests.

Three SCMs (Class C fly ash, Class F fly ash, and granulated slag), commonly used in TxDOT concrete pavement construction and suspected to be the cause of creating some problematic mixtures, are selected in order to investigate the role of SCMs in creating incompatibilities.

Mid-range water reducing admixture (MWRA) is generally being used in concrete pavement construction. Therefore, two different commercial sources of MWRA are considered as chemical admixtures. Both are lignin-based MWRAs because of frequent reports of its incompatibilities in combination with mineral admixtures from field construction. Each material has its own code (Table 5-2) for the convenience of formulating design of experiment.

Table 5-2 Materials collected.

Materials	Material Code	Type	Sulfate contents	C_3A Contents
Cement	C1	Type I/II	Normal	Normal
	C2	Type I/II	Normal	Normal
	C3	Type I/II	Normal	Normal
	C4	Type V	High	Low
	C5	Type I/II	Medium	Normal
	C6	Type I	Medium	High
	C7	Type I	High	High
Fly ash	C35	Class C fly ash	N/A	N/A
	F35	Class F fly ash		
Slag	S50	Slag		
MRWA (Lignin-based)	D17	WRRA		
	X15	MRWA		

Note: C35- Class C fly ash at 35% cement replacement, F35 -Class C fly ash at 35% cement replacement S50 - slag at 50% cement replacement

MATERIAL CHARACTERIZATION

The collected cements and SCMs were characterized for their bulk chemical compositions (elemental oxide percentages) and phase compositions. The following analytical tools were used to do chemical and mineralogical characterization of the collected cements, fly ashes, and slag samples:

- Bulk chemical analysis of cements, fly ashes and slag by X-ray fluorescence (XRF)
- Identification of phases present in cements, fly ashes, and slag by X-ray Diffraction technique (XRD)
- Quantitative estimation of C_3A, gypsum, and hemi-hemihydrate in cements were analyzed using the quantitative X-ray diffraction (QXRD)

Chemical and Mineralogical Compositions of Cements

Chemical and mineralogical compositions of all the selected cements are discussed below. Bulk chemical analyses along with relevant chemical parameters (e.g., gypsum to hemihydrate ratio) and calculated bogue phases of the selected cements are presented in Table 5-3. The summary of XRD results is presented Table 5-4. The XRD diffractograms corresponding to all the studied cements that are generated to identify the phases qualitatively are presented in Figures 5-1 and 5-2. Cements 1, 2, 3, and 5 belong to Type I/II whereas cements 6 and 7 belong to Type I category with varying gypsum to hemihydrate ratio and C_3A contents. Cement 4 is classified as a type V low C_3A cement.

Table 5-3 Oxide analyses of cements from XRF tests.

Chemical Analysis	Percentage of Mass						
	C1	C2	C3	C4	C5	C6	C7
Cement type	I/II	I/II	I/II	V	I/II	I	I
SiO_2	20.349	20.284	20.480	20.422	20.681	19.298	19.830
Al_2O_3	4.501	4.161	4.660	4.057	4.630	5.345	5.121
Fe_2O_3	3.132	3.201	3.772	4.764	3.459	2.306	1.853
CaO	61.534	62.231	63.398	61.959	62.844	63.087	63.912
MgO	3.665	4.168	1.330	0.848	0.796	1.105	1.208
SO_3	2.480	2.456	2.231	3.850	3.053	2.949	3.303
Na_2O	0.101	0.067	0.210	0.298	0.170	0.099	0.115
K_2O	0.627	0.771	0.557	0.232	0.717	0.959	0.474
SrO	0.086	0.042	0.053	0.062	0.176	0.079	0.086
MnO	0.140	0.128	0.037	0.077	0.310	0.041	0.029
TiO_2	0.216	0.260	0.215	0.167	0.233	0.243	0.227
P_2O_5	0.109	0.144	0.067	0.028	0.200	0.279	0.122
L.O.I (950˚C)	1.9	0.8	2.3	1.5	1.7	2.5	2.44
Total	98.84	98.71	99.31	98.26	98.97	98.29	98.72
Alkalies as Na_2O_{eq} *	0.51	0.59	0.54	0.45	0.62	0.73	0.42
Gypsum	2.0	0.2	2.0	0.2	0.2	2.0	5.0
Hemihydrate	3.5	0.2	2.5	1.0	0.2	0.2	0.2
Anhydrate	0	0.2	0	0.2	0.2	0.2	0.2
Gypsum-to-hemihydrate Ratio*	0.57	1.0	0.8	0.2	1.0	10	25
Calculated Compounds per ASTM C 150-02a							
C_3S	54.06	59.65	59.38	51.97	53.90	62.55	63.00
C_2S	17.55	13.16	13.92	19.34	18.63	8.141	9.326
C_3A*	6.628	5.611	5.967	2.692	6.417	10.26	10.44
C_4AF	9.532	9.740	11.48	14.50	10.53	7.018	5.640
LSF	0.9283	0.9474	0.9457	0.9097	0.9238	0.9851	0.9797
Blaine Fineness (cm^2/g)	3730	3660	3920	3840	3670		

*Note: * - Key factors which influences cement-admixtures incompatibilities*

Table 5-4 Summary of cement phases identified by XRD.

Materials	Identified Phases
Cement 1	Gypsum, hemihydrate, C_3S, C_2S, C_3A, C_4AF
Cement 2	Hemihydrate, C_3S, C_2S, C_3A, C_4AF
Cement 3	Gypsum, C_3S, C_2S, C_3A, C_4AF
Cement 4	Hemihydrate, anhydrate (high peak), C_3S, C_2S, C_3A, C_4AF
Cement 5	Gypsum, hemihydrate C_3S, C_2S, C_3A, C_4AF
Cement 6	Gypsum (high peak), hemihydrate, C_3S, C_2S, C_3A, C_4AF
Cement 7	Gypsum (high peak), hemihydrate, C_3S, C_2S, C_3A, C_4AF

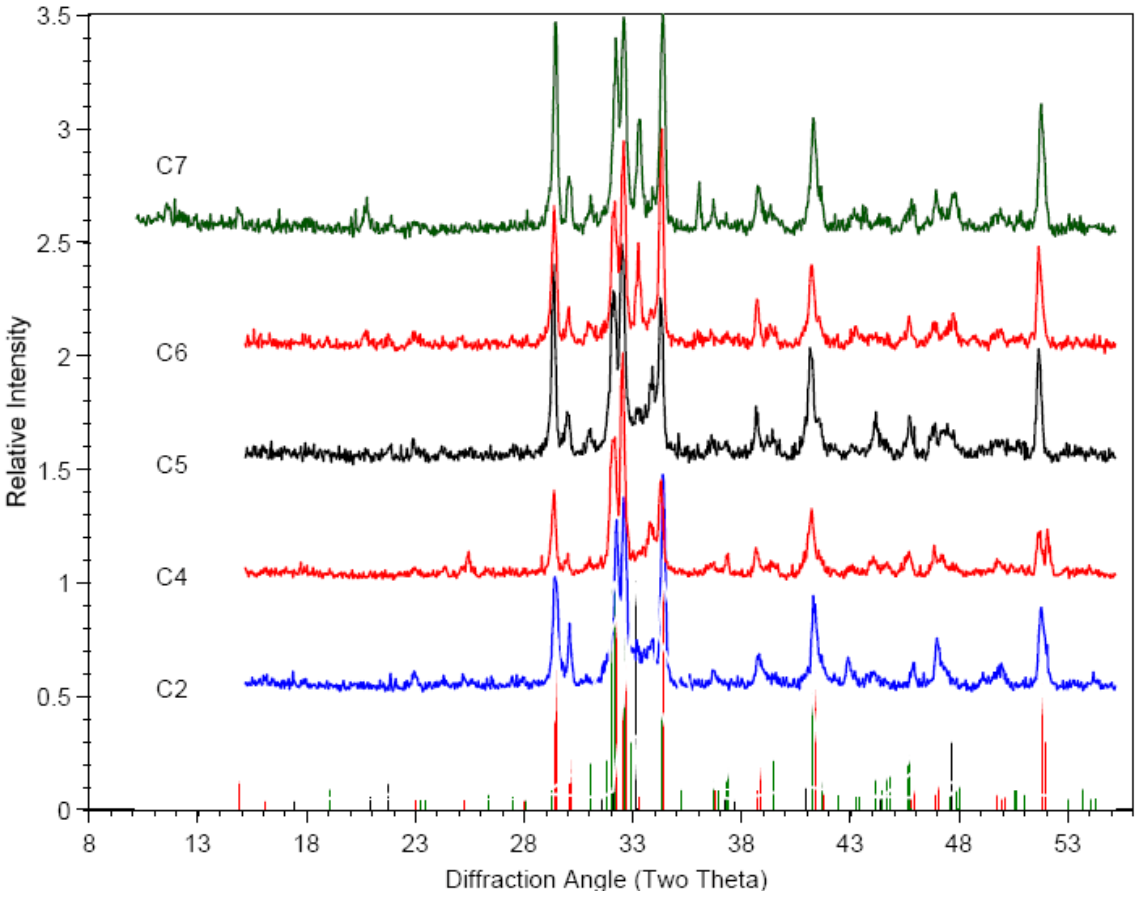

Figure 5-1 XRD patterns for cement samples with stick patterns for C_3S (red), C_2S (green) and C_3A (black).

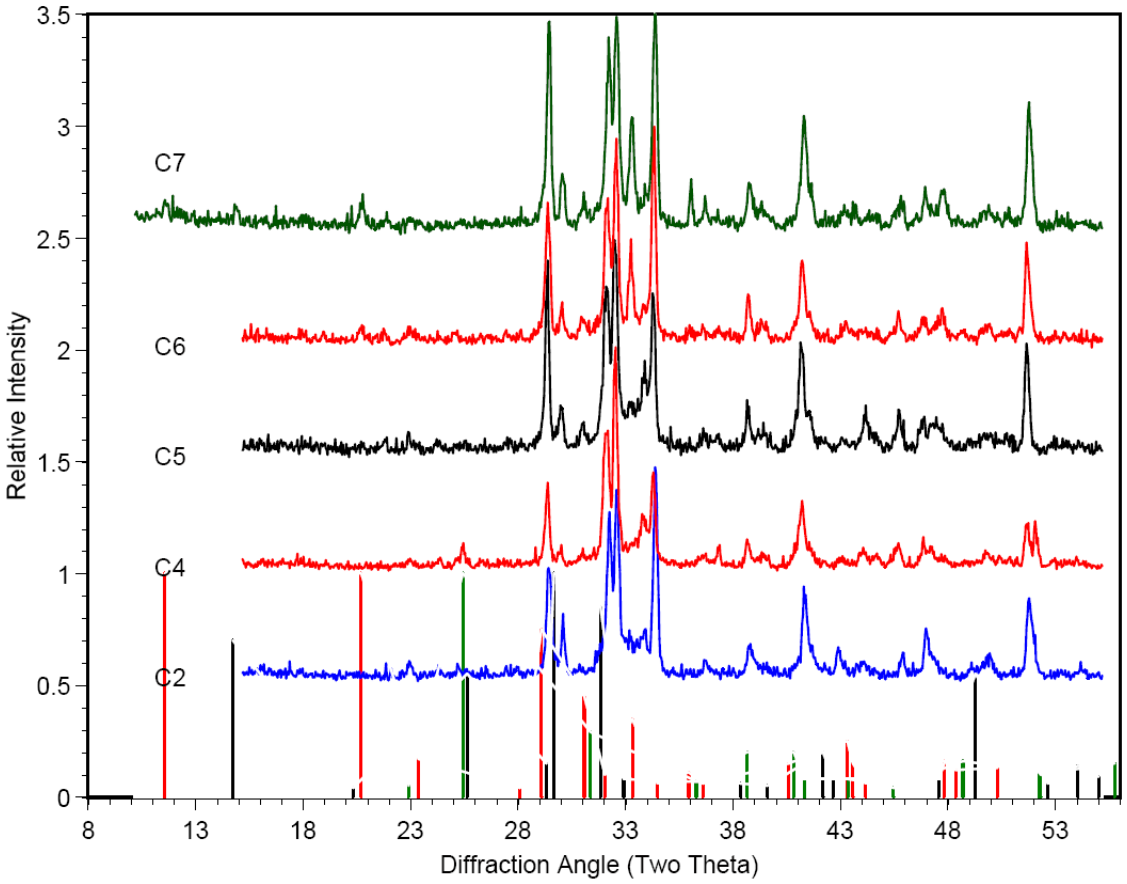

Figure 5-2 XRD patterns for cement samples with stick patterns for gypsum (red), anhydrite (green) and bassanite (black).

Chemical and Mineralogical Compositions of SCMs

The chemical compositions of the selected SCMs (Class C fly ash, Class F fly ash, and granulated slag) are presented in Table 5-5 and phases identified by XRD are presented at Table 5-6. The XRD patterns of all the SCMs are presented at Figures 5-3, 5-4, and 5-5 respectively.

Table 5-5 Oxide analyses of the studied SCMs.

Chemical Analysis	Percentage of Mass		
	Class C fly ash	Class F fly ash	Slag
Material Code	C35	F35	S50
SiO_2	38.551	54.123	33.8
Al_2O_3	20.144	25.347	11.1
Fe_2O_3	5.404	3.427	0.8
CaO	22.652	7.501	43.1
MgO	4.312	1.785	6.8
SO_3	1.326	0.326	0.4
Na_2O	1.350	0.462	0.32
K_2O	0.434	0.939	0.30
L.O.I (950˚C)	0.14		
Total	94.313	93.91	96.62
Alkalies as Na_2O	1.636	1.08	0.52
Specific gravity	2.69		

Table 5-6 Summary of SCMs phases identified by XRD.

Materials	Identified Phases
Class C fly ash	Predominantly amorphous with quartz, C_3A, $CaFeO_3$, $MgAl_2O_4$ as minor crystalline phases
Class F fly ash	Predominantly amorphous with quartz, mullite as minor crystalline phases
Granulated slag	Mostly amorphous with practically no crystalline phases

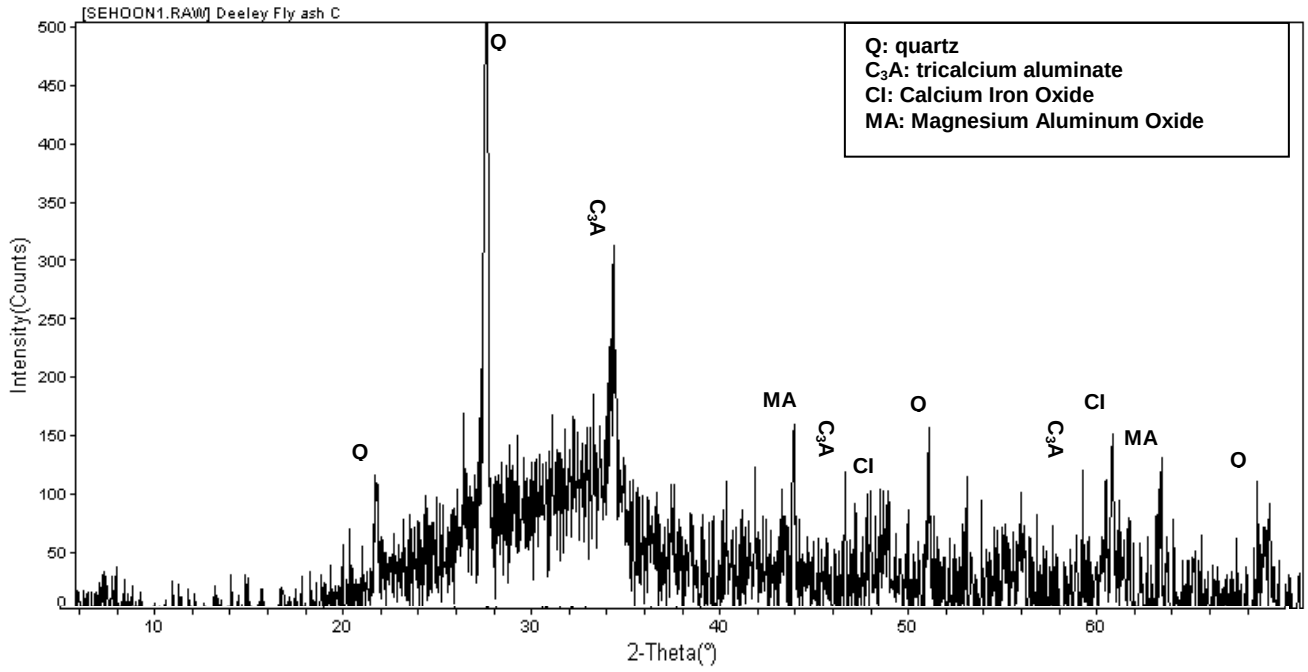

Figure 5-3 XRD pattern of Class C fly ash.

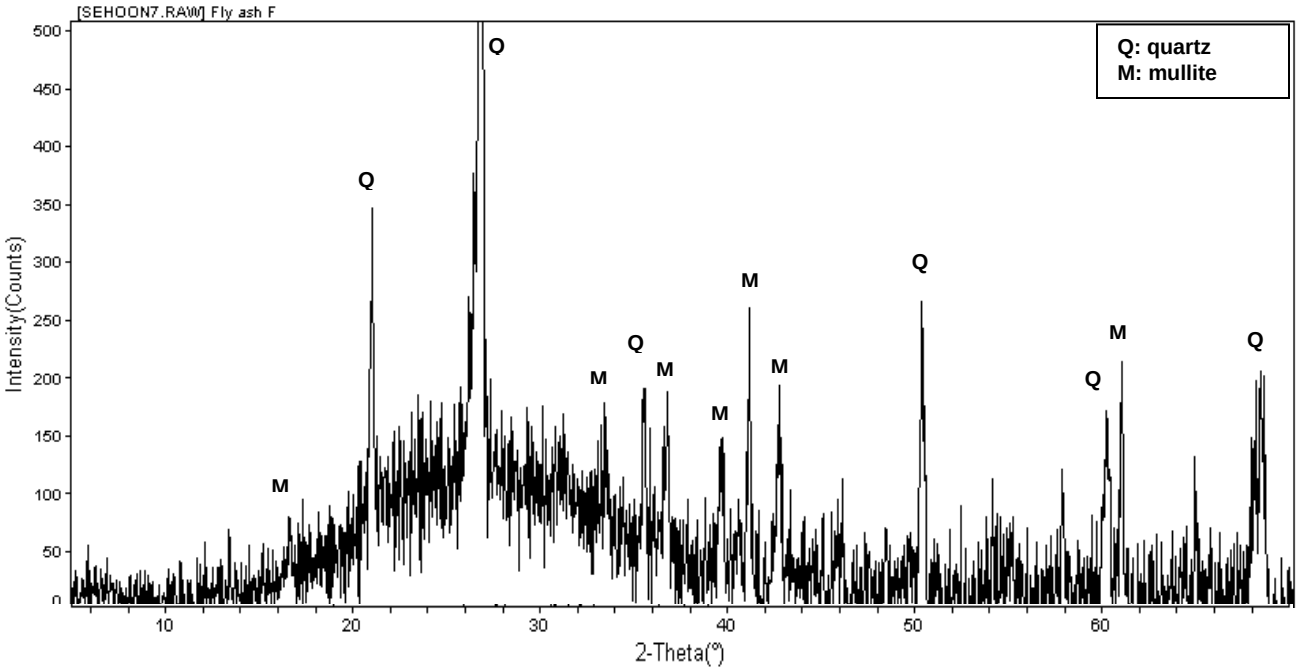

Figure 5-4 XRD pattern of Class F fly ash.

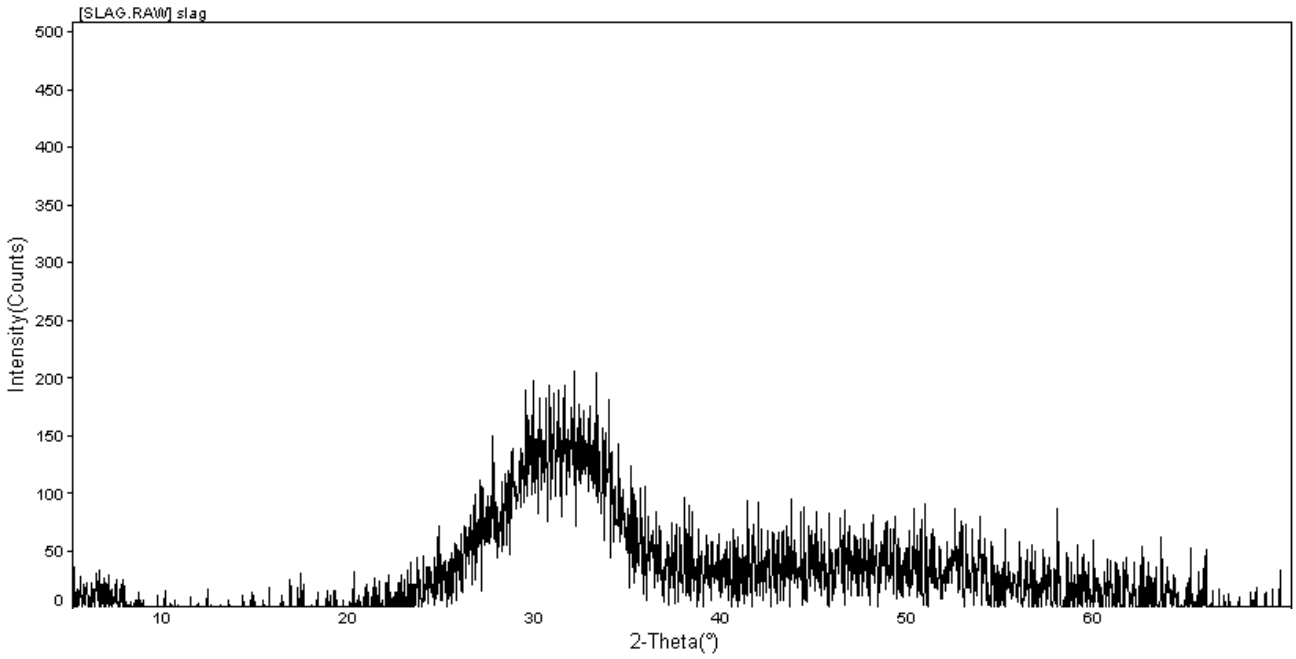

Figure 5-5 XRD pattern of granulated slag.

Class C Fly Ash

The Class C fly ash used in this research consisted mainly of an amorphous phase (glassy phase) along with crystalline compounds that include alpha-quartz (SiO_2), $MgAl_2O_4$, and $CaFeO_3$ as shown in Figure 5-3.

Class F Fly Ash

As with the Class C fly ash, the Class F fly ash was also composed primarily of an amorphous phase and some crystalline components that include alpha-quartz, and mullite as shown in Figure 5-4.

Granulated Slag

The granulated slag was completely amorphous (glassy). The XRD pattern in Figure 5-5 is a typical one of a calcium silicate glass with no crystalline components.

Particle Size Distribution of Both Cements and SCMs

Particle size distributions of all collected cements and SCMs were measured using a laser scattering particle size distribution analyzer (PSDA), Horiba CAPA-700. Each material was dispersed with pure ethyl alcohol (99.9%) followed by ultrasonic vibration of three minutes (as a part of sample preparation procedure) before starting the actual analysis by the machine. The results of particle size distribution curves for cements and SCMs are shown in Figure 5-6 and 5-7 respectively. Mean and median particle size of cements and SCMs are listed in Table 5-7.

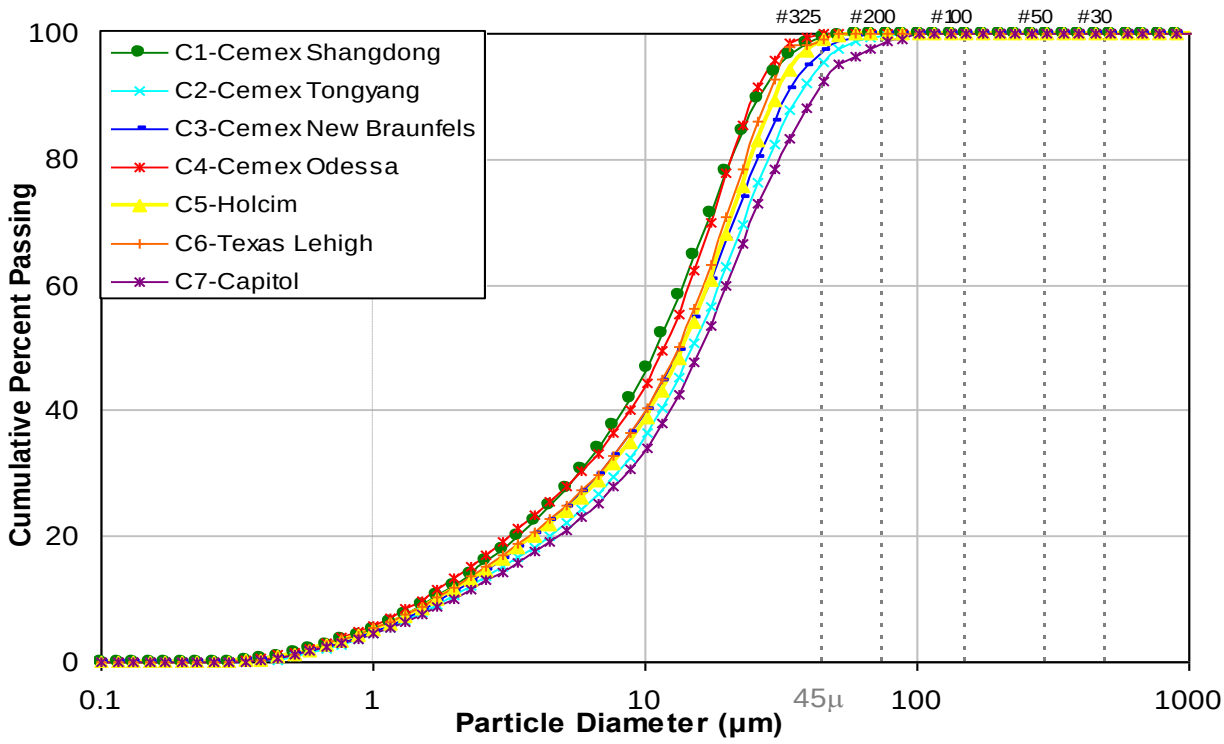

Figure 5-6 Particle size distribution curves of cements.

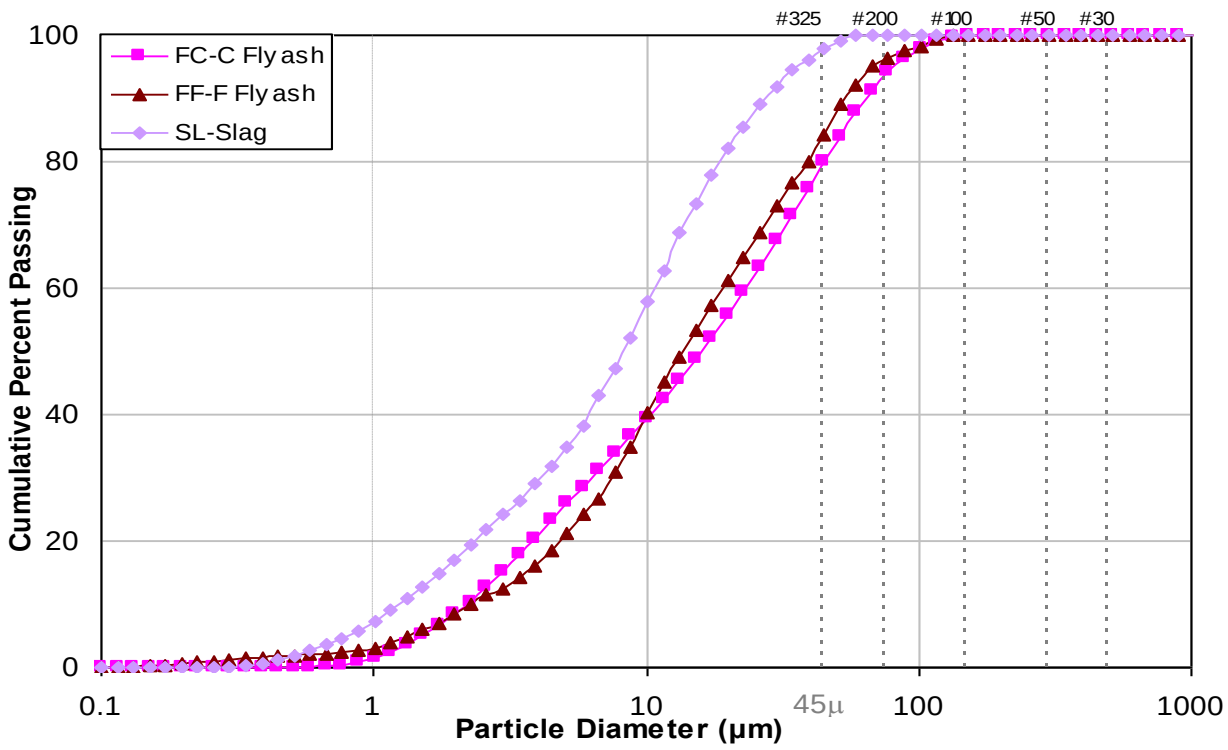

Figure 5-7 Particle size distribution curves of SCMs.

Table 5-7 Mean and median particle size of cements and SCMs.

Size (micron)	Percentage Passing									
	C1	C2	C3	C4	C5	C6	C7	C35	F35	S50
Mean	12.70	17.53	15.80	12.61	15.11	13.98	18.97	17.14	15.42	9.81
Median	10.91	14.92	13.44	11.71	13.76	12.34	16.11	16.38	13.67	8.12

All seven cements (Cements 1-7) have very similar particle size distributions, although Cement 7 has slightly more coarse particles than other cements. The SCMs have slightly wider range of particle size distribution curves than cements have. The granulated slag is finer (mean size 9.8 micron) than all the tested cements and fly ashes.

Characteristics of Chemical Admixture

The chemical admixtures that have been selected and used in the main laboratory testing are X15 and D17. X15 is classified as a Type A & F admixture or mid-range water reducing admixture (MWRA) whereas D17 is classified as a Type B & D or water reducing and set retarding admixture (WRRA) according to ASTM C 494 (*62*). X15 is an aqueous solution of lignosulfonate salt specially formulated for use in portland cement concrete containing pozzolans. D17 is also an aqueous solution of lignosulfonate and compound carbohydrates. The characteristics of the two chemical admixtures are listed in Table 5-8.

Table 5-8 Characteristics of chemical admixtures.

	X15 (MWRA)	D17 (WRRA)
ASTM C 494	Type A & F	Type B & D
Recommended Dosage	196-652 ml/100 kg of cement (3-10 fl oz/cwt)	130-520mL/100kg of cement (2-8 fl oz/cwt)
Typical Dosage	325mL/100kg (5fl oz/cwt)	195mL/100kg (3fl oz/cwt)
Ingredient	Calcium lignosulfonate	Sodium o-phenylphenol
CAS#	8061-52-7	000132-27-4

SELECTION OF CEMENTS FOR EXPERIMENTAL TEST PROGRAM

To cover a wide range of C_3A contents, sulfate-bearing phases (especially gypsum to hemihydrate ratio), and soluble alkali contents; seven commercial portland cements, described in Table 5-3, were initially identified based on chemical and mineralogical compositions. As described previously in Table 5-1, three factors i.e., C_3A content, total soluble alkali content, and gypsum to hemihydrate ratio in cement are more crucial cement parameters in addition to (i) type

and dosage of MWRA, (ii) type of SCMs, and (iii) temperature, in order to address the cement-chemical/mineral admixture incompatibilities.

All the seven commercial cements were classified into three different levels (low, normal, and high) with respect to C_3A content, total soluble alkali content, and gypsum to hemihydrate ratio separately and presented in Table 5-9. The normal level of C_3A content in cement is considered as 5-6%, anything more or less than this normal range is described as high or low. It is believed that high C_3A content could significantly influence cement-admixture incompatibilities. In case of total soluble alkali content, the normal level is between 0.5 and 0.6 percent. The effect of soluble alkali on cement-admixture incompatibilities is not fully understood. The normal range of gypsum to hemihydrate ratio is between 0.8 and 1.2. It is anticipated that any cement with gypsum to hemihydrate ratio below 0.8 or above 1.2 (i.e., more hemihydrates and less gypsum) is more prone to cement-admixture incompatibilities. In this context, mitigation of concrete incompatibilities with a proper level of gypsum to hemihydrate ratio can be referred.

Table 5-9 Commercial portland cement characteristics.

Cement	Type	Percentage of C_3A content (%) (5< Normal< 6)		Percentage of Alkali Content (%) (0.5<Normal< 0.6)		Gypsum-to-Hemihydrate Ratio (0.8<Normal<1.2)	
Cement 1	I/II	6.628	Normal	0.51	Normal	0.57	Close to Normal
Cement 2	I/II	5.611	Normal	0.59	Normal	1.0	Normal
Cement 3	I/II	5.967	Normal	0.54	Normal	0.8	Normal
Cement 4	V	2.692	Low	0.45	Low	0.2	Abnormal
Cement 5	I/II	6.417	Normal	0.62	Normal	1.0	Normal
Cement 6	I	10.26	High	0.73	High	10	Abnormal
Cement 7	I	10.44	High	0.42	Low	25	Abnormal

Three representative cements (Table 5-10) from the total seven cements are selected to conduct laboratory investigation by applying the following analogy:

- Cement 2 has the normal level of C_3A and total soluble alkali contents while Cement 4 and 6 has low and high level of that in order.
- In case of calcium sulfate content, Cement 2 has normal level of gypsum to hemihydrates ratio whereas Cement 4 and 6 has low and high level of that (abnormal situation) in order.
- In case of percent of alkali content, Cement 2 has normal level of that whereas Cement 4 and 6 has low and high level of that in order.

Table 5-10 Three selected cements for the main experimental test program.

Cement	Type	Percentage of C_3A content (%) (5< Normal < 6)		Percentage of Alkali Content (%) (0.5<Normal< 0.6)		Gypsum-to-Hemihydrate Ratio (0.8<Normal<1.2)	
Cement 2	I/II	5.611	Normal	0.59	Normal	1.0	Normal
Cement 4	V	2.692	Low	0.45	Low	0.2	Abnormal
Cement 6	I	10.26	High	0.73	High	10	Abnormal

It is anticipated that these 3 cements should be effective to address cement-admixture incompatibilities. Setting time and heat of hydration characteristics corresponding to cement 2, 4, and 6 will be determined before conducting the main laboratory testing and any addition / rejection of cements based on any other abnormalities will be made.

CHAPTER VI

EXPERIMENTAL DESIGN AND TEST METHODS

This chapter presents the experimental design and test methods for the main laboratory test program based on the selected materials described at Chapter V.

EXPERIMENTAL DESIGN FOR THE LABORATORY TESTING

The experimental design has been presented at Table 6-1. The five factors, i.e., (i) type of cement, (ii) type of chemical admixture, (iii) dosage of chemical admixture, (iv) type of SCMs, and (v) testing temperature, are considered as the most influential factors in the experimental design. The selected factors and their levels are presented in Table 6-1. Three different types of cements (i.e., C2, C4 and C6) were selected in the original design (Chapter V). Based on the results of preliminary tests, it was observed that both cements C2 (type I/II) and C6 (type I) have similar mineralogical and chemical compositions and show very similar heat of hydration and setting time behaviors. Therefore, C6 cement was removed from the design of experiment. Two different commercial sources of lignin-based chemical admixtures with two different dosage levels (e.g., manufacturer's typical recommended dosage, and double the manufacturer's typical recommended dosage) were considered for the factors of type and dosage of chemical admixture respectively (details are given in Chapter V). Three different types of SCMs were considered (i.e. Class F fly ash, Class C fly ash, and granulated slag). Temperature is another controlling factor related to concrete incompatibilities. When concrete is exposed to uncontrolled field conditions such as hot and cold weather, it is reported that the possibilities of getting incompatible mixtures increases. As for example, one concrete mixture may perform satisfactorily at one temperature (generally at higher temperature, e.g., summer time) but the same mixture can behave as

incompatible at lower temperature (e.g., winter time). Three different levels (i.e. 10, 24, and 35˚C) of testing temperatures were selected to represent winter, summer and intermediate ambient temperature conditions in this study.

Table 6-1 Design of experiments.

<table>
<tr><th>Total Test Runs</th><th>Cement Type</th><th>Chemical admixture type</th><th>Chemical admixture dosage</th><th>SCMs type</th><th>Temp.</th></tr>
<tr><td rowspan="3">96</td><td rowspan="2">C2
(Type I/II)
C_3A - 5.61%</td><td rowspan="2">X15
(Brand X, Lignin based MRWA)</td><td rowspan="2">TD
(0.25% for X15, 0.2% for D17 of total cement binder weight)</td><td>F35
(35% replacement of Class F fly ash)</td><td>10˚C
(50˚F)</td></tr>
<tr><td rowspan="2">C35
(35% replacement of Class F fly ash)</td><td rowspan="2">24˚C
(75˚F)</td></tr>
<tr><td>C4
(Type V)
C_3A - 2.69%</td><td>D17
(Brand D Lignin based WRRA)</td><td>DD
(0.5% for X15, 0.4% for D17 of total cement binder weight)</td><td>S50
(50% replacement of slag)</td><td>35˚C
(95˚F)</td></tr>
</table>

Note: MWRA: mid-range water reducing admixture (Calcium lignosulfonate); WRRA: water reducing and set retarding admixture (Calcium lignosulfonate and compound carbohydrates); TD: manufacturer's typical recommended dosage, DD: double the manufacturer's typical recommended dosage

The total number of combinations was 32 including 8 controls. The combination of two cements and three SCMs give rise to e controls. The experimental design table that shows the mixture number and code is given at Table 6-2. These mixture number and code will refer to explain the results of laboratory tests at Chapter VII. Since the tests with total combination of 32 were repeated under three different temperature conditions, the total test runs were 96. The water

to binder ratio (w/b) was selected for all the controlled mixtures based on a constant flow (i.e., a pat area of 5000 mm^2 at 5 minutes after mixing) determined by mini-slump flow test on cement / (cement +SCMs) pastes. This resulted w/b for the mixtures with Class F fly ash is 0.38 whereas those with Class C fly ash and slag are 0.36 and 0.45 respectively to maintain a constant mini-slump flow. These w/b are valid for both the C2 and C4 cements. The w/b for both the cement pastes (C2 and C4) without SCM was found to be 0.4.

The materials are selected based on the available historical information. Some combinations in the above design of experiments are expected to show incompatibilities in the laboratory tests through the following possible mechanisms:

- In general, overdose of chemical admixtures (e.g., double dosage in Table 6-1) are the common cause of concrete incompatibilities
- A mixture with satisfactory performance at higher temperature (e.g., summer) can become an incompatible mix at lower temperature (e.g. winter) as a result of change in reaction kinetics in different temperatures
- Some kind of chemical incompatibilities arises from complex interaction between fly ash, cement, and chemical admixtures

Past records showed that some combinations in Table 6-2 have actually manifested incompatibilities in the field because of one or more of the above mechanisms.

Table 6-2 Experimental design table for the laboratory test program.

Group	Cement	SCMs	MRWA Type	MRWA Dosage	Mix. No.	Mixture Code
Control	C2	-	-	-	1	C2
	C4	-	-	-	2	C4
Group I	C2	F35	-	-	3	C2-F35
		C35	-	-	4	C2-C35
		S50	-	-	5	C2-S50
	C4	F35	-	-	6	C4-F35
		C35	-	-	7	C4-C35
		S50	-	-	8	C4-S50
Group II	C2	F35	X15	TD	9	C2-F35-X15-TD
			D17	TD	10	C2-F35-D17-TD
		C35	X15	TD	11	C2-C35-X15-TD
			D17	TD	12	C2-C35-D17-TD
		S50	X15	TD	13	C2-S50-X15-TD
			D17	TD	14	C2-S50-D17-TD
	C4	F35	X15	TD	15	C4-F35-X15-TD
			D17	TD	16	C4-F35-D17-TD
		C35	X15	TD	17	C4-C35-X15-TD
			D17	TD	18	C4-C35-D17-TD
		S50	X15	TD	19	C4-S50-X15-TD
			D17	TD	20	C4-S50-D17-TD
Group III	C2	F35	X15	DD	21	C2-F35-X15-DD
			D17	DD	22	C2-F35-D17-DD
		C35	X15	DD	23	C2-C35-X15-DD
			D17	DD	24	C2-C35-D17-DD
		S50	X15	DD	25	C2-S50-X15-DD
			D17	DD	26	C2-S50-D17-DD
	C4	F35	X15	DD	27	C4-F35-X15-DD
			D17	DD	28	C4-F35-D17-DD
		C35	X15	DD	29	C4-C35-X15-DD
			D17	DD	30	C4-C35-D17-DD
		S50	X15	DD	31	C4-S50-X15-DD
			D17	DD	32	C4-S50-D17-DD

TEST METHODS

The test methods that are used in the main experimental program are summarized in Table 6-3. These test methods are already described under preliminary test program in Chapter IV. The mini-slump cone test was included in the main test program to measure flow characteristics of the studied cement pastes as an alternative or supporting tool for rheology tests.

Table 6-3 Test methods in the experimental program.

Test Method	Test Equipment	Measured Properties
Heat generation behavior of the cementitious system (ASTM C 186)	Isothermal conduction calorimeter (OMNICAL)	Heat of Hydration
Setting behavior (ASTM C191)	Vicat needle apparatus	Initial and Final set time
Rheological behavior of fresh cement paste	Modified Bohlin CVO rheometer, DSR (Malvern Instrument)	Rheological parameters (yield stress and plastic viscosity)
Rheological behavior of fresh cement paste	Modified AR2000 rheometer, DSR (TA Instrument)	Dynamic rheology mode (Storage modulus)
Flow characteristics	Mini-Slump cone	5, 10, 20, and 30 minutes pat area

STATIC RHEOLOGICAL TEST PROCEDURES

The same temperature controlled high shear mixing developed during preliminary test program (described in Chapter IV) has been used in the main test program. However, some changes have been made in the static rheology test procedure and calculation of the rheological parameters, which are described below. This effort was made to consider the change of rheological parameters (i.e., yield stress and plastic viscosity) as a function of time. To monitor the stiffening behavior of cement paste mixtures at an early age, the time function should be added to the parameters of test procedure. Therefore, relatively longer test duration (up to 2 hours with 10, 30, 60, 90 and 120 minutes testing intervals) was applied for static rheological test procedure to derive an effective rate of change of rheological parameters (i.e., rate of change of plastic viscosity (RPV) and rate of change of yield stress (RYS). As a result, the rheometer test procedure was changed (in comparison with the procedure that used in the preliminary test program described in Chapter IV.

The static rheological test procedure is described below:

1. Take cement paste specimen from the mixing bowl using five 3 ml syringes immediately after mixing procedure.
2. All the syringes filled up with the cement paste were kept under the respective studied temperatures (e.g., inside an oven / refrigerator at 35°C / 10°C and under room temperature of 24°C). The syringes were kept in horizontal position to minimize any segregation / sedimentation effect.
3. Five syringes corresponding to each mixture and under a particular temperature were tested one by one with the selected five time intervals, i.e., 10, 30, 60, 90, and 120 minutes. This procedure ensured not to disturb the changes in the paste due to hydration or any other structural changes (during induction period) and thereby monitoring the changes of rheological parameters as a function of time.
4. Place the predetermined quantity of cement paste (i.e., 1.5ml) onto the lower plate of the rheometer from a syringe with a large opening. The purpose of using a syringe with a large opening was to minimize any microstructural breakdown during sample injection from the syringe.
5. Sandwich the specimen between the two parallel plates with 1 mm plate gap and shear with shear rate from 0 to 200/s representing the up curve followed by 200 to 0/s representing the down curve. The shear stress as a function of the shear rate is then recorded. A run with one cycle consisting of one up curve and one down curve takes approximately 3 minutes.
6. Start the first run approximately 10 minutes after adding water to the cement. Conduct another four runs using the remaining specimens in the four syringes with different time intervals of 30, 60, 90, and 120 minutes following the same procedure described above.

Calculation of RYS and RPV

Typical data showing shear rate versus shear stress are presented in Figure 6-1 (a). The plastic viscosity and yield stress determined using the Bingham model are shown in Figure 6-1 (b). The plastic viscosity is calculated from the slope of the linear region of the down curve, whereas yield stress is calculated from the y-intercept as shown in Figure 6-1 (b).

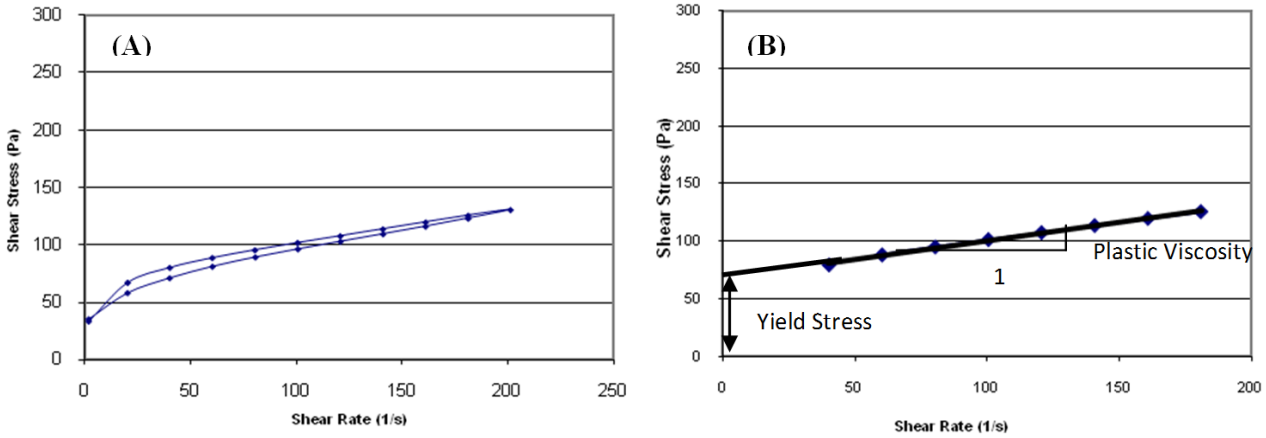

Figure 6-1 Typical plot of shear stress vs. shear rate (left) and calculation of rheological parameters (right).

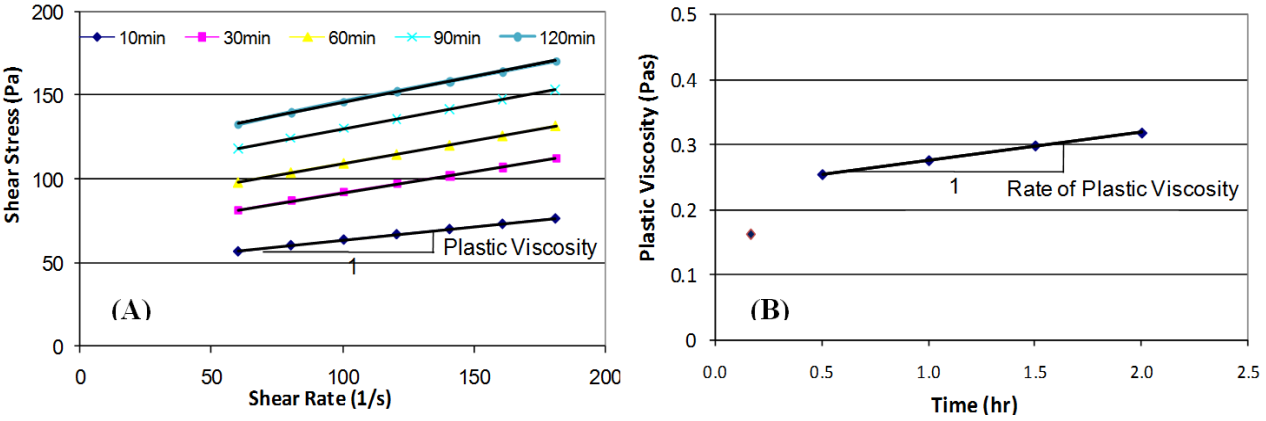

Figure 6-2 Plastic viscosities with five time intervals (left) and calculation of rate of change of plastic viscosity (right).

However, plastic viscosity and yield stress are measured at a certain time point. Thus, in order to consider the stiffening behavior of cement paste, time-functioned rheology parameters, the rate of change of plastic viscosity (RPV) and rate of change of yield stress, was developed during induction period (i.e., two hours after mixing). The rheological parameters, i.e., plastic viscosity and yield stress, corresponding to five different time intervals were calculated as described above. Figure 6-2 (a) demonstrates the calculation of the plastic viscosity corresponding to five time intervals. Figure 6-2 (b) shows change of plastic viscosity as a function of time. The slope of the linear region in Figure 6-2 (b) represents the rate of change of plastic viscosity (RPV) within 2 hours time period. The rate of change of yield stress (RYS) within 2 hours time period is calculated by applying the same procedure. For each time interval, the flocculation of cement particle due to the interparticle forces is breakdown during the application of pre-shear rate and the up curve. However, the hydration products that contribute the stiffening of cement paste and not breakdown under 200/s pre-shear rate are developed during induction period. Thus, the physical meanings of the RPV and RYS are to measure the stiffening behavior of cement paste during induction period due to the hydration products by monitoring the rate of change of plastic viscosity and yield stress as a function of time.

MODELING OF STORAGE MODULUS CURVE

In dynamic rheology mode, the storage modulus as a function of time is monitored by following the procedure described in the preliminary test program with dynamic mode (Chapter IV). The storage modulus curve with time trend was then modeled using a suitable numerical equation to derive some characteristics parameters. The model development and utility of the derived parameters to identify incompatible mixtures are described below.

Development of Dynamic Rheological Curve Model

The storage modulus curve as function of time is fit well by Eq. (6.1). Eq. (6.1) presents an exponential formulation that can be used in conjunction with experimental data to regress the modulus development of various cement paste system. This equation was originally derived by Schindler and Folliard to predict the degree of hydration in cement hydration system (*63*). However, this equation can be used with any S-shaped curve because of its versatile nature. The applicability of this equation to represent S-shaped curve of storage modulus versus time is verified during preliminary test program.

$$G'(t,\alpha,\beta,\tau) = \alpha \cdot \exp\left(-\left(\frac{\tau}{t}\right)^{\beta}\right) \quad \text{.....(6.1)}$$

where, α is a magnitude parameter, β is a slope parameter, and τ is a shift parameter.

The cement paste stiffening characteristics, i.e., the storage modulus curve as a function of time, were measured by the modified DSR (AR2000 rheometer) for the P1 mixture (i.e., Type I cement with 0.2% WRRA, typical dosage) listed at Table 4-3 and regressed based on the developed modulus curve model of Eq. (6.1). After the storage modulus curve with time was regressed, the model yields three different parameters according to the curve shape (i.e., α, β, and τ).

The storage modulus curve for the P1 mixture were measured for 5 hours test duration using the dynamic rheology mode (i.e., continuous oscillation mode) with the optimum target strain (i.e., fixed as 5.0E-05 in the preliminary test program, Chapter IV). The water evaporation control measurements and plate gap (i.e., 1 mm) remain the same as described for static mode of rheology measurement earlier. The storage modulus data, G', were measured with one minute

time interval and automatically recorded. The measured storage modulus vs. time curve for the P1 mixture was compared with the modeled curve as shown in Figure 6-3 and the three parameters (α, β, and τ) are derived as listed at Table 6-4.

Table 6-4 Regressed parameters with P1 mixture.

Parameters	Values
α	7.7 E+05
β	1.1
τ	17

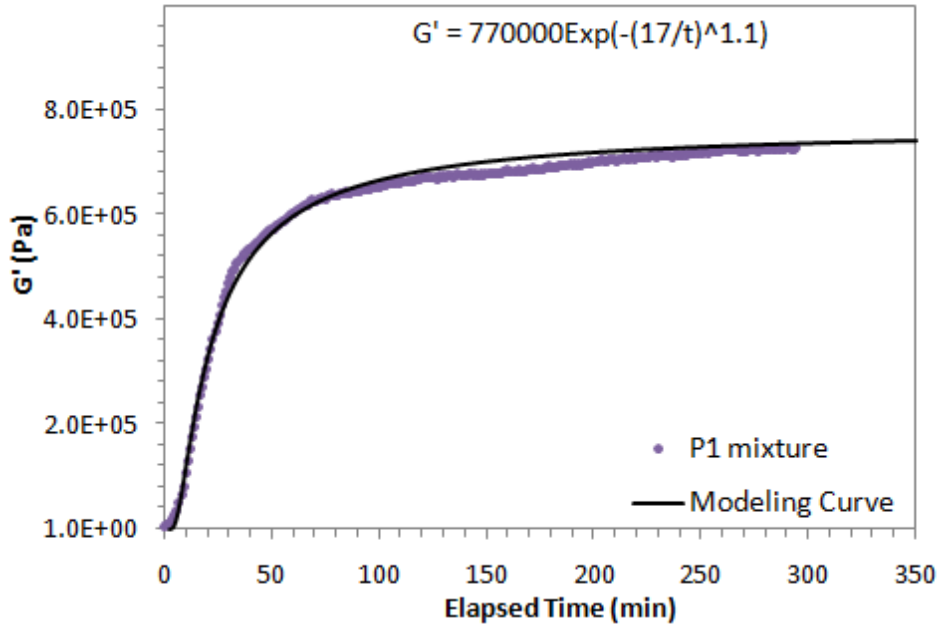

Figure 6-3 Measured storage modulus curve vs. modeled curve.

The disposition or change of shape of the modeled storage modulus curve with change in α, β, and τ is shown graphically in Figures 6-4, 6-5, and 6-6 respectively. The effect of each parameter on the modulus curve is described below.

Firstly, the α parameter is used to scale the ultimate values of the storage modulus during the induction period. Figure 6-4 shows that increasing α term causes the storage modulus curve to shift up. Thus, the physical meaning of α parameter is the degree of stiffening process of cement paste during induction period. Secondly, the τ parameter controls the rate of increase of the storage modulus. The smaller τ, the more rapid the increase of the storage modulus, as shown in Figure 6-5. Finally, the slope of the storage modulus curve is controlled by the β parameter, as shown in Figure 6-6. This parameter also has an impact on the τ parameter since the rate of increase in the storage modulus is influenced by both β and τ parameters. Thus, the physical meaning of β and τ parameters is associated with the rate of the development of stiffening process during the induction period.

In the main test program, these three parameters are compared for all the studied mixtures under different temperature conditions and presented at Chapter VII.

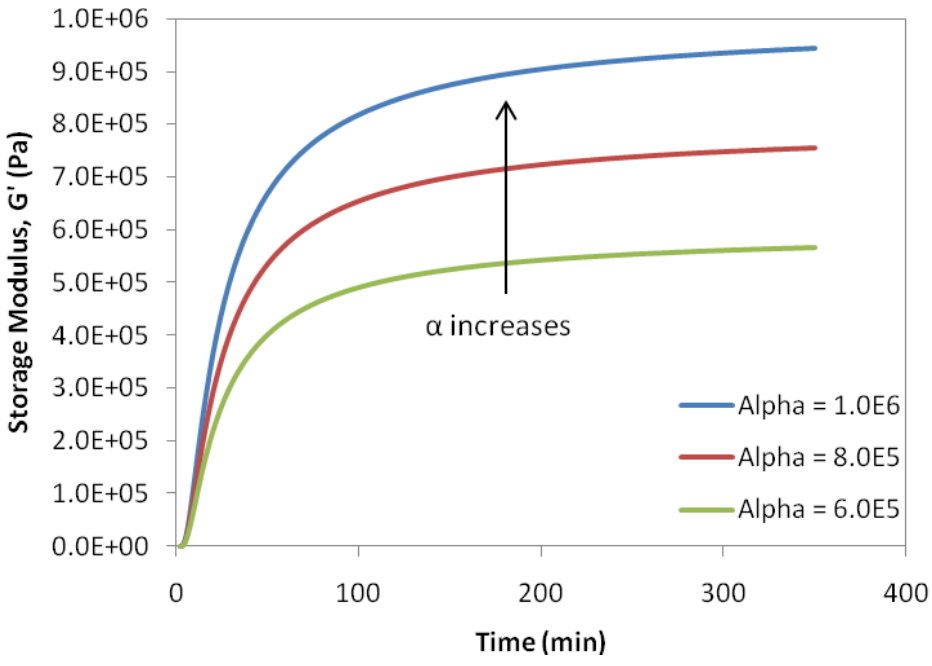

Figure 6-4 Effect of α parameter on the storage modulus curve.

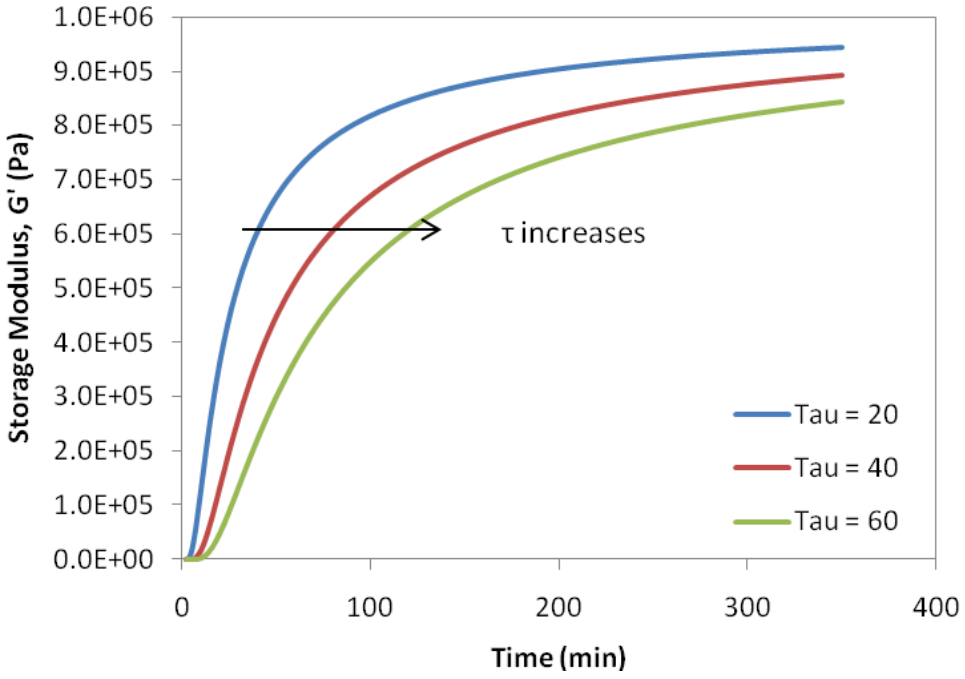

Figure 6-5 Effect of τ parameter on the storage modulus curve.

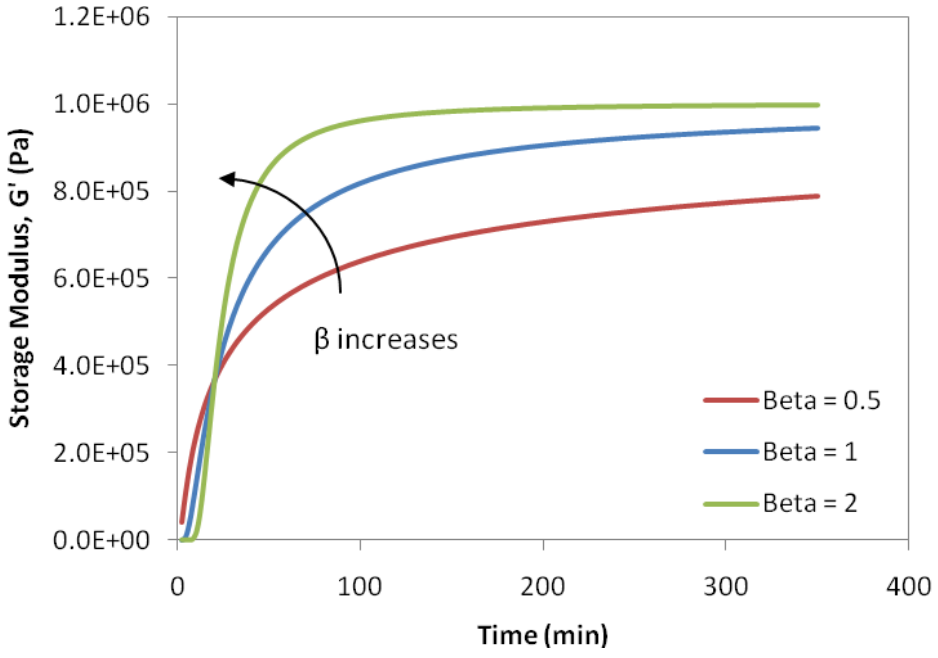

Figure 6-6 Effect of β parameter on the storage modulus curve.

MINI SLUMP CONE TEST PROCEDURE

The mini slump cone test was conducted for all the studied mixtures (according to Table 6-2) using a mini slump cone test. The mini slump cone had the following dimensions: 19 mm (3/4 in.) as top diameter, 38 mm (1-1/2 in.) as bottom diameter, and 57 mm (2-1/4 in.) as height. The dimensions are in the same proportions as in the concrete slump test (ASTM Test C 143). Design details of the mini slump cone are shown in Figure 6-7. The mini slump test procedure is described below:

1. The mixing procedure was the same as rheology tests presented at Chapter III (Figure 3-5).
2. Immediately after mixing, the sample was placed in the cone resting on a Lucite (acrylic) sheet. As the cone was filled, a small spatula was moved both laterally and vertically to aid the escape of entrapped air bubbles.
3. The cone was lifted with a motion rapid enough for the cone to remain clear of the flowing paste, but slow enough to avoid imparting a significant upward momentum to the paste.
4. The several diameter measurements of the pat were made with a caliper. An average diameter was calculated and from this, the area of corresponding pat area was determined.
5. The rest of the specimen were kept under the respective studied temperatures (e.g., inside an oven / refrigerator for 35°C / 10°C and under room temperature of 24°C).
6. The specimen corresponding to each mixture and under a particular temperature were tested one by one with the selected 3 time intervals, i.e., 10, 20, and 30 minutes. This procedure ensured not to disturb the changes in the paste due to hydration or any other structural changes (during induction period) and thereby monitoring the flow behavior as a function of time.

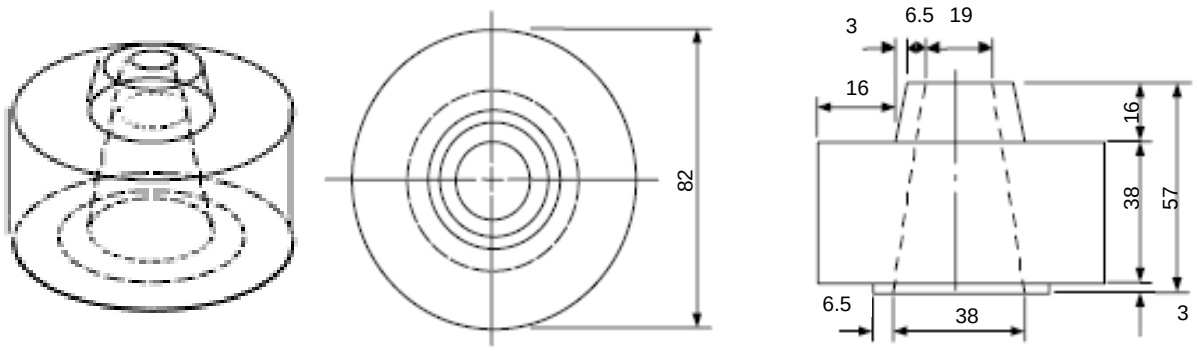

Note: units are in millimeters

Figure 6-7 Schematic representation of mini slump cone.

The pat area results from mini slump tests for C2 and C4 cement system as a function of time and temperature were measured. The results from the mini slump cone test were presented at Chapter VII.

CHAPTER VII

CONDUCTING LABORATORY TESTING AND DATA ANALYSIS

This chapter presents the test results and discussion of the laboratory tests that have been conducted based on the experimental design (Table 6-2) and test method (Table 6-3) given in Chapter VI. All the test runs according to the experimental design in Table 6-2 were conducted using the DSR test procedure mentioned in Chapter VI. Tests for heat of hydration, setting time and mini-slump were also conducted for all the combinations as supporting tools. The results are presented in the following order.

- Heat of hydration and setting time characteristics of all the combinations – The procedure to identify incompatible mixtures based on heat of hydration and setting time characteristics is developed and discussed.
- Rheological parameters that were determined by the modified DSR tests - The method to identify incompatible mixtures based on rheological characteristics is developed.
- A comparative assessment was made to verify whether the identification of the incompatible mixtures based on rheology method is supported by heat of hydration.

- Flow characteristics by the mini slump cone test - The flow behavior as a function of elapsed time were measured from the mini slump cone test. It was evaluated if the mini slump test has any potential feasibility to identify the incompatible mixtures from the normal ones similar to rheology method.

HEAT OF HYDRATION BY CONDUCTION CALORIMETER

The heat evolution characteristics, i.e., the amount and time of occurrence of the second peak and integrated heat evolution for all the test runs, were measured by the conduction calorimeter and are presented in Tables 7-1 and 7-2. The heat evolution graphs (i.e., plot of elapsed time vs. heat evolution) for all the test runs are presented in Figures 7-1 to 7-9. The plots for the integrated heat evolution for all the test runs are presented in Appendix B.

The results from heat of hydration tests are discussed in the following sub-system in order to reflect the effect of SCMs, chemical admixtures, and temperature separately.

Table 7-1 Heat evolution data with C2 cement system at different temperature conditions.

	Experimental Design	Second Peak Value (mW/g)	Second Peak Time (hr)	Integrated Heat Evolution (J/g)	Percent of Heat Evolution w.r.t. Control (C2)
10°C (50°F)	3_C2+F35	0.78	20	98	56.65
	9_C2+F35+X15TD	0.89	21	96	55.49
	21_C2+F35+X15DD	0.88	31	91	52.60
	10_C2+F35+D17TD	0.67	44	52	30.06
	22_C2+F35+D17DD	N/A	N/A	19	10.98
	4_C2+C35	0.73	28	81	46.82
	11_C2+C35+X15TD	0.74	30	79	45.66
	23_C2+C35+X15DD	0.49	33	57	32.95
	12_C2+C35+D17TD	0.18	35	30	17.34
	24_C2+C35+D17DD	N/A	N/A	20	11.56
	5_C2+S50	0.63	14	79	45.66
	13_C2+S50+X15TD	0.63	16.5	79	45.66
	25_C2+S50+X15DD	0.63	21	75	43.35
	14_C2+S50+D17TD	0.62	29	64.5	37.28
	26_C2+S50+D17DD	N/A	N/A	10.5	6.07
24°C (75°F)	***1_C2**	2.43	8.7	172	100.00
	3_C2+F35	1.79	12.5	135.5	78.32
	9_C2+F35+X15TD	1.78	13.2	122	70.52
	21_C2+F35+X15DD	1.80	16.2	118.5	68.50
	10_C2+F35+D17TD	1.18	34	102.5	59.25
	22_C2+F35+D17DD	N/A	N/A	25	14.45
	4_C2+C35	1.73	15.8	128.5	74.28
	11_C2+C35+X15TD	1.77	20.6	128	73.99
	23_C2+C35+X15DD	1.74	29.5	108.5	62.72
	12_C2+C35+D17TD	N/A	N/A	39	22.54
	24_C2+C35+D17DD	N/A	N/A	25	14.45
	5_C2+S50	1.5	6	129	74.57
	13_C2+S50+X15TD	1.51	9	127.5	73.70
	25_C2+S50+X15DD	1.52	10	111	64.16
	14_C2+S50+D17TD	1.68	22	107.5	62.14
	26_C2+S50+D17DD	N/A	N/A	25	14.45
35°C (95°F)	3_C2+F35	3.25	8	151.5	87.57
	9_C2+F35+X15TD	3.15	9	144	83.24
	21_C2+F35+X15DD	2.79	12.5	130	75.14
	10_C2+F35+D17TD	2.21	16	127.5	73.70
	22_C2+F35+D17DD	N/A	N/A	18	16.18
	4_C2+C35	3.25	10.5	171	98.84
	11_C2+C35+X15TD	2.95	14	160.5	92.77
	23_C2+C35+X15DD	2.49	21	136	78.61
	12_C2+C35+D17TD	N/A	N/A	35	20.23
	24_C2+C35+D17DD	N/A	N/A	29	16.76
	5_C2+S50	2.59	5.5	154	89.02
	13_C2+S50+X15TD	2.45	6.5	150.5	86.99
	25_C2+S50+X15DD	2.38	9	150.5	86.99
	14_C2+S50+D17TD	2	14.5	143	82.66
	26_C2+S50+D17DD	N/A	N/A	18	16.18

Note: *identified as incompatible mixtures* *identified as marginal mixtures*

Table 7-2 Heat evolution data with C4 cement system at different temperature conditions.

	Experimental Design	Second Peak Value (mW/g)	Second Peak Time (hr)	Integrated Heat Evolution (J/g)	% of Heat Evolution w.r.t. Control (C4)
10°C (50°F)	6_C4+F35	0.8	16	122	73.94
	15_C4+F35+X15TD	0.92	21	121.5	73.64
	27_C4+F35+X15DD	0.92	30.5	113	68.48
	16_C4+F35+D17TD	0.73	33	89	53.94
	28_C4+F35+D17DD	N/A	N/A	25.5	15.45
	7_C4+C35	0.74	18.5	111	67.27
	17_C4+C35+X15TD	0.74	22	93.5	56.67
	29_C4+C35+X15DD	0.68	29	82	49.70
	18_C4+C35+D17TD	0.38	36.5	57.5	34.85
	30_C4+C35+D17DD	N/A	N/A	29.5	17.88
	8_4+S50	0.7	12	107	64.85
	19_C4+S50+X15TD	0.7	16	103.5	62.73
	31_C4+S50+X15DD	0.7	20	99.5	60.30
	20_C4+S50+D17TD	0.68	25.5	83	50.30
	32_C4+S50+D17DD	N/A	N/A	25	15.15
24°C (75°F)	***2_C4**	2.86	7.2	165	100.00
	6_C4+F35	1.95	8.5	131	79.39
	15_C4+F35+X15TD	1.94	10.6	129.5	78.48
	27_C4+F35+X15DD	1.94	12.5	129.5	78.48
	16_C4+F35+D17TD	1.78	17.6	120.5	73.03
	28_C4+F35+D17DD	N/A	N/A	25	15.15
	7_C4+C35	1.78	10.3	136.5	82.73
	17_C4+C35+X15TD	1.75	13.2	121	73.33
	29_C4+C35+X15DD	1.78	14	118.5	71.82
	18_C4+C35+D17TD	1.74	21	115.5	70.00
	30_C4+C35+D17DD	N/A	N/A	24	14.55
	8_C4+S50	1.64	6	127	76.97
	19_C4+S50+X15TD	1.64	6.8	124.5	75.45
	31_C4+S50+X15DD	1.58	8.1	121	73.33
	20_C4+S50+D17TD	1.42	13.2	98	59.39
	32_C4+S50+D17DD	N/A	N/A	23	13.94
35°C (95°F)	6_C4+F35	3.34	5	139.5	84.55
	15_C4+F35+X15TD	3.34	7	138.5	83.94
	27_C4+F35+X15DD	3.28	8	138	83.64
	16_C4+F35+D17TD	2.71	14	132	80.00
	28_C4+F35+D17DD	2.06	38	59	35.76
	7_C4+C35	3.13	6.7	150	90.91
	17_C4+C35+X15TD	2.83	8	138.2	83.76
	29_C4+C35+X15DD	2.67	9.8	126.8	76.85
	18_C4+C35+D17TD	2.39	13.2	124.5	75.45
	30_C4+C35+D17DD	0.93	45.8	31.9	19.33
	8_C4+S50	2.81	3.4	149.8	90.79
	19_C4+S50+X15TD	2.72	4.1	140.6	85.21
	31_C4+S50+X15DD	2.7	4.9	139.8	84.73
	20_C4+S50+D17TD	2.23	11	112.1	67.94
	32_C4+S50+D17DD	0.32	42.8	37.08	22.91

Note: *identified as incompatible mixtures* *identified as marginal mixtures*

Effects of Cement Type on Heat of Hydration

The heat evolution of cement only (C2 and C4) was used as control. The second peak of C2 cement (Type I/II) occurs at approximately 8.7 hours after the addition of water with a value of 2.43 mW /g whereas for C4 cement (Type V), it occurs at 7.2 hours with a value of 2.86 mW/g illustrated in Figure 7-1. The integrated heat evolution of control mixtures after 48 hours is 172 J/g for C2 and 165 J/g for C4 [marked * at Tables 7-1 and 7-2] and are considered as 100%. The percentage of heat evolution for the other mixtures are then calculated with respect to cement-water heat evolution as 100% and presented in the last column of Tables 7-1 and 7-2. The bar graphs illustrated percentage of heat evolution for cements with SCMs, i.e., Class F fly ash, C fly ash, and granulated slag are presented at Figures 7-10, 7-11, and 7-12 respectively. The criterion of below 30 percent of integrated heat evolution is considered to be appropriate to identify the incompatible mixtures.

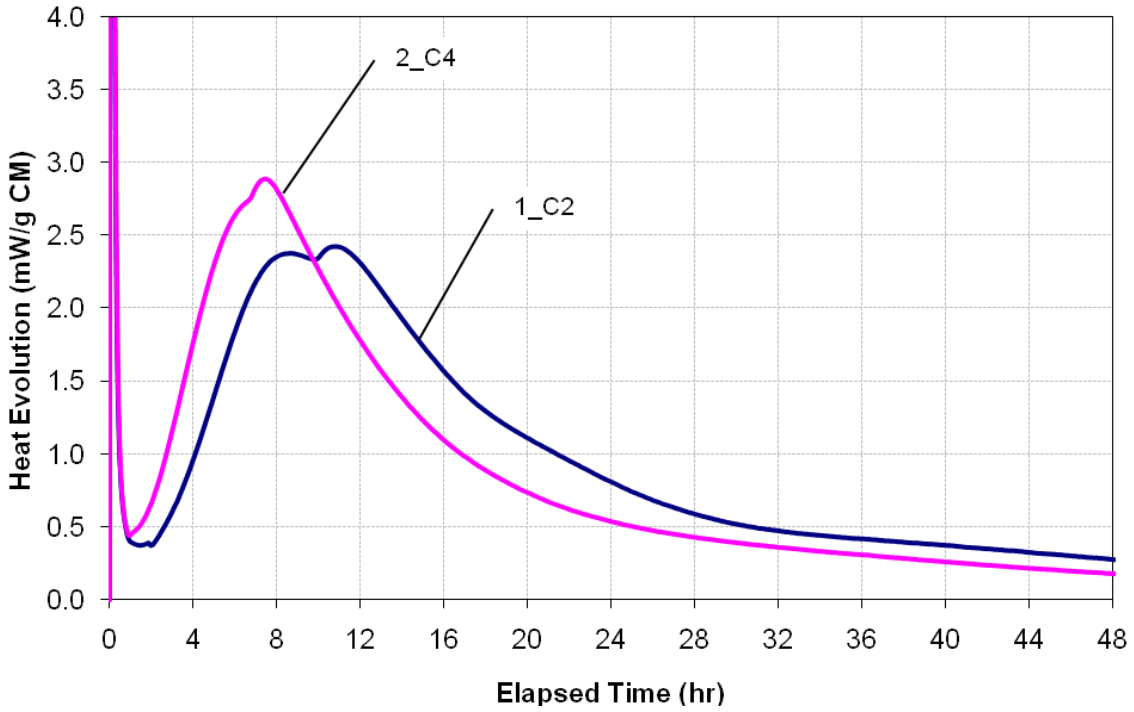

Figure 7-1 Heat evolution for C2 and C4 cements at 24°C.

Effects of SCMs on Heat of Hydration

The addition of fly ashes to cement (both C2 and C4) generally results in the reduction of the second peak intensity and the delay of the occurrence of the second peak (i.e., retardation) whereas the addition of slag results in the reduction of the second peak intensity but the acceleration of the occurrence of the second peak illustrated in Figures 7-2 and 7-3. The mixtures with Class F fly ash showed less retarding effect compared to the mixtures with Class C fly ash.

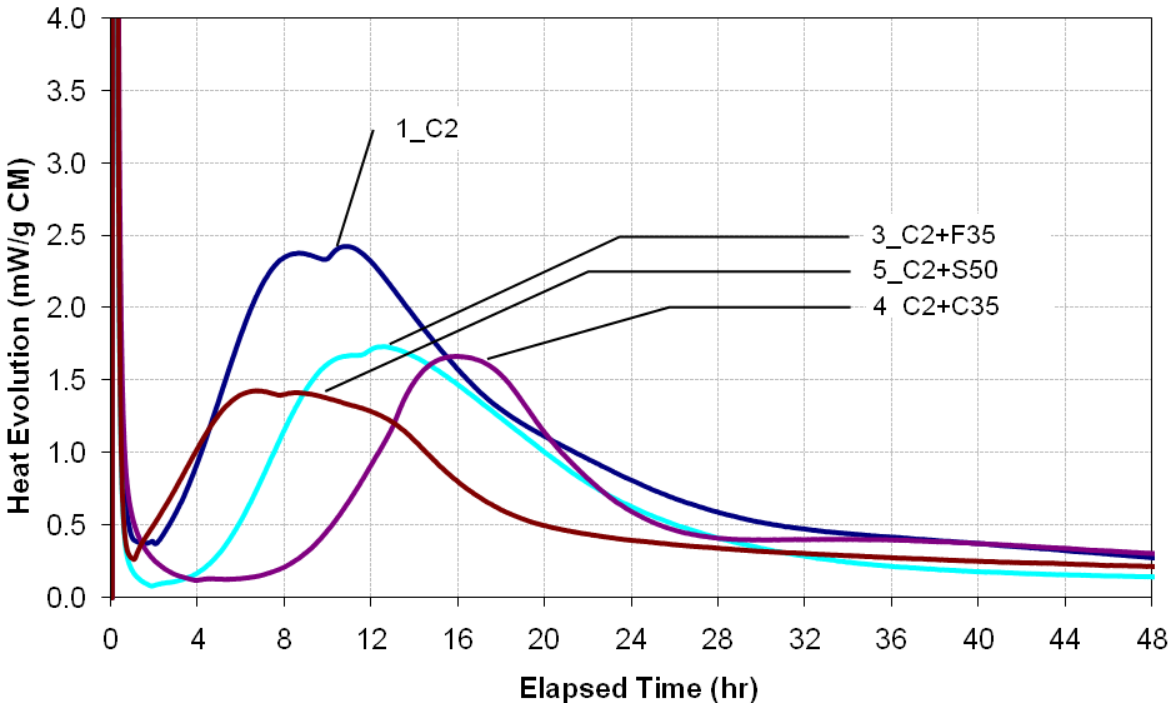

Figure 7-2 Heat evolution for C2 with different SCMs at 24°C.

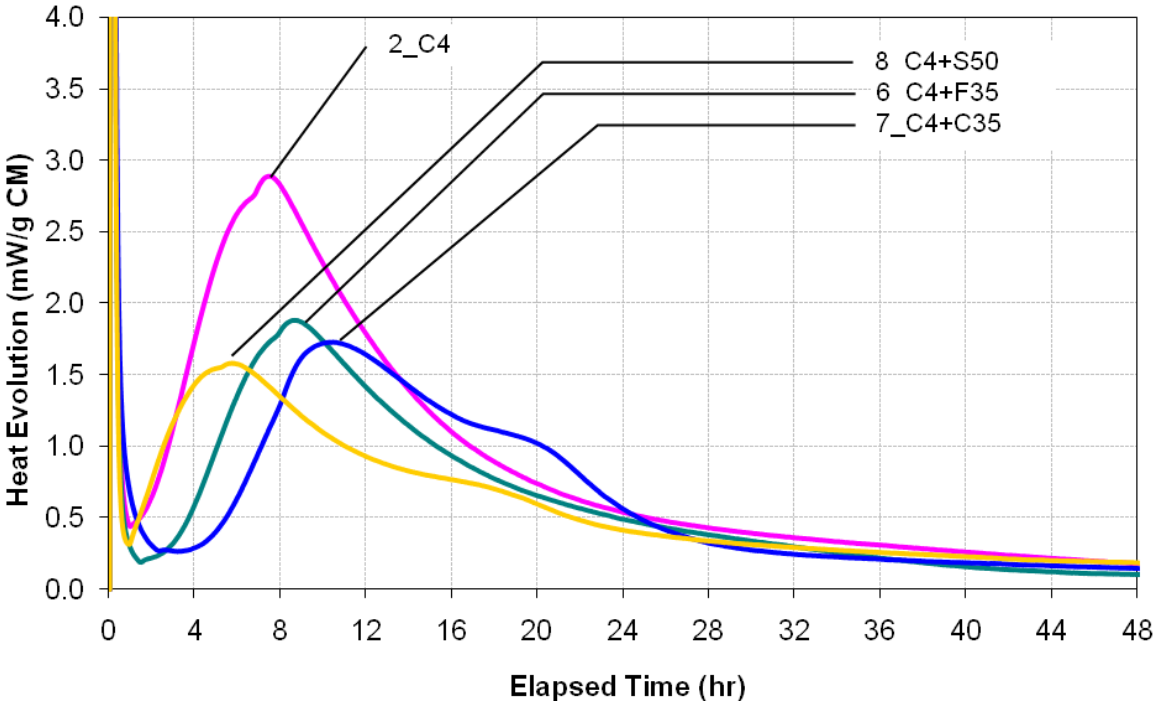

Figure 7-3 Heat evolution for C4 with different SCMs at 24°C.

Effects of Chemical Admixtures on Heat of Hydration

An overall effect of reduction in heat evolution is evident for the mixtures with chemical admixture X15 (MWRA) at both normal and high dosages regardless of SCM types. The degree of reduction was more in the mixtures with double dosages (i.e., 0.5% of total cement weight) than the mixtures with normal dosages. However, higher dose addition of admixture X15 had no detrimental effect on the hydration process since the second peak of the hydration was clearly observed and the percentage of integrated heat evolution for all the mixtures with X15 admixture remain above the 30 % criteria.

On the other hand, the chemical admixture D17 (WRRA) showed a significant reduction even with the typical dosage for all the mixtures with D17. It is to be stated that this admixture not only reduces water demand but also retards the setting time. At typical dosage of D17, the Class C fly ash with C2 cement showed a significant reduction in heat evolution manifested by

absence of the second peak after 48 hours of testing period at shown in Figure 7-5. This seems to be an example of chemical incompatibility arises due to complex interaction between cement, Class C fly ash, and D17 chemical admixture. The percent heat evolution for this mixture is below 30% limit for all the three temperatures. Therefore, mixture number 12, i.e., C2+C35+D17TD, was identified as an incompatible mixture at all three temperatures (Table 7-1). The addition of D17 with double dose (i.e., 0.4% of cement weight) resulted heat evolution abnormalities (i.e., the second peak didn't appear even after 48 hours of testing period) for all the tested mixtures regardless of the cement and SCMs types. As a result, the mixtures 22, 24, and 26 with cement 2 and mixture 28, 30, and 32 with cement 4 (Table 7-2) were identified as incompatible mixtures due to overdose of D17 as illustrated at Figures 7-10, 7-11 and 7-12.

Effects of Temperature on Heat of Hydration

The effect of temperature was investigated at 10°C (50°F) and 35°C (95°F) to grossly simulate winter and summer time concrete placement and presented at Figures 7-4 to 7-9. As expected all mixtures tested at low temperature condition had less integrated heat evolution as well as second peak intensity than those tested at intermediate temperature (i.e., 24°C / 75°F). Conversely, all the mixtures tested under high temperature condition had more integrated heat evolution as well as second peak intensity than those tested under intermediate temperature. Therefore, the effect of low temperature resulted in the retardation of cement hydration process whereas the one with high temperature caused the acceleration of cement hydration process on all the tested mixtures. As a result, some of the normal mixes at both 35°C and 24°C (e.g., mixture No. 10 and 23 in Table 7-1) became marginal (close to incompatible criteria of 30%, marked as green) at low temperature. Similarly, the mixture 28 behaves as marginal at higher temperature (35°C) but become incompatible at both low and intermediate temperatures.

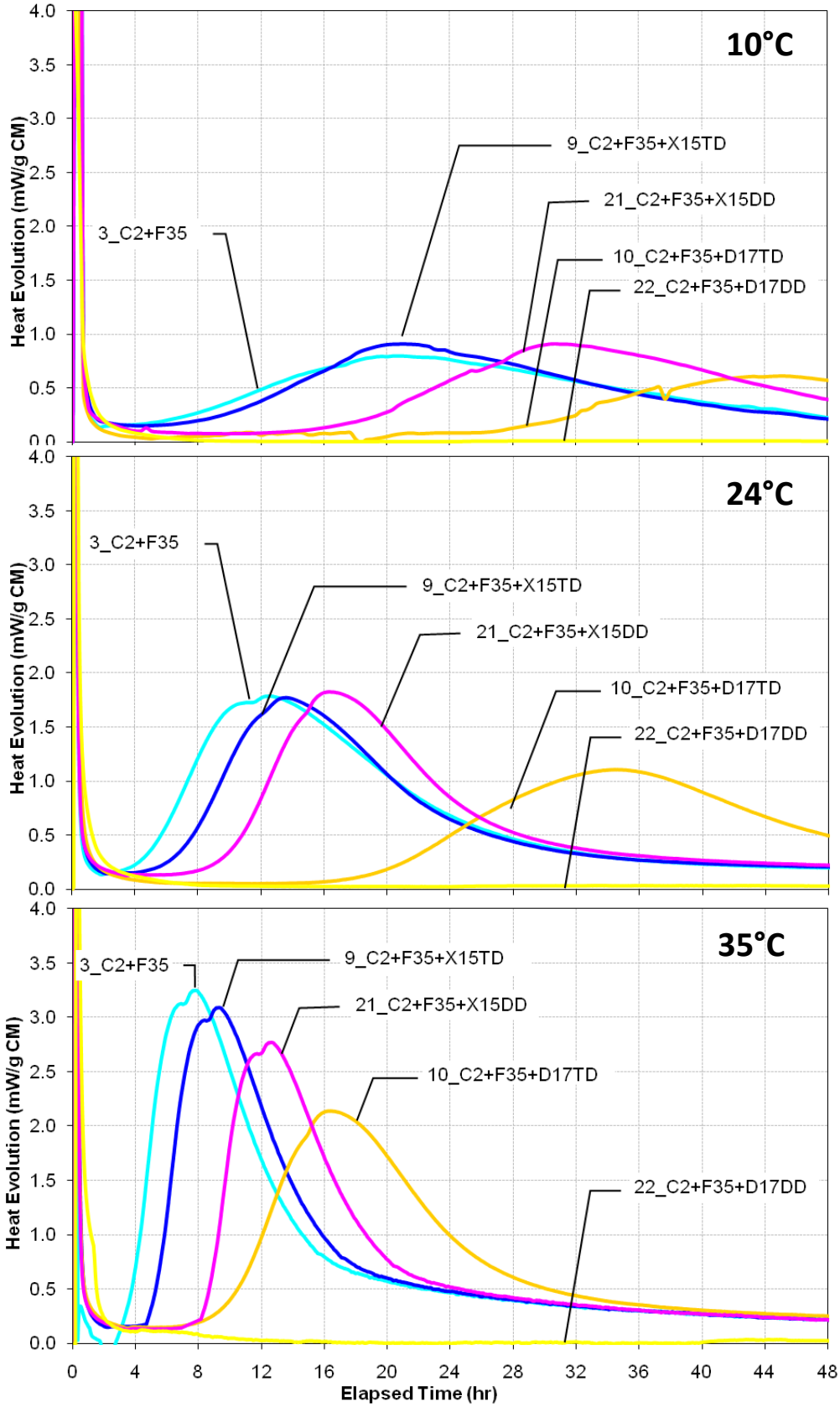

Figure 7-4 Heat evolution for C2 with F fly ash system at 10, 24, and 35°C.

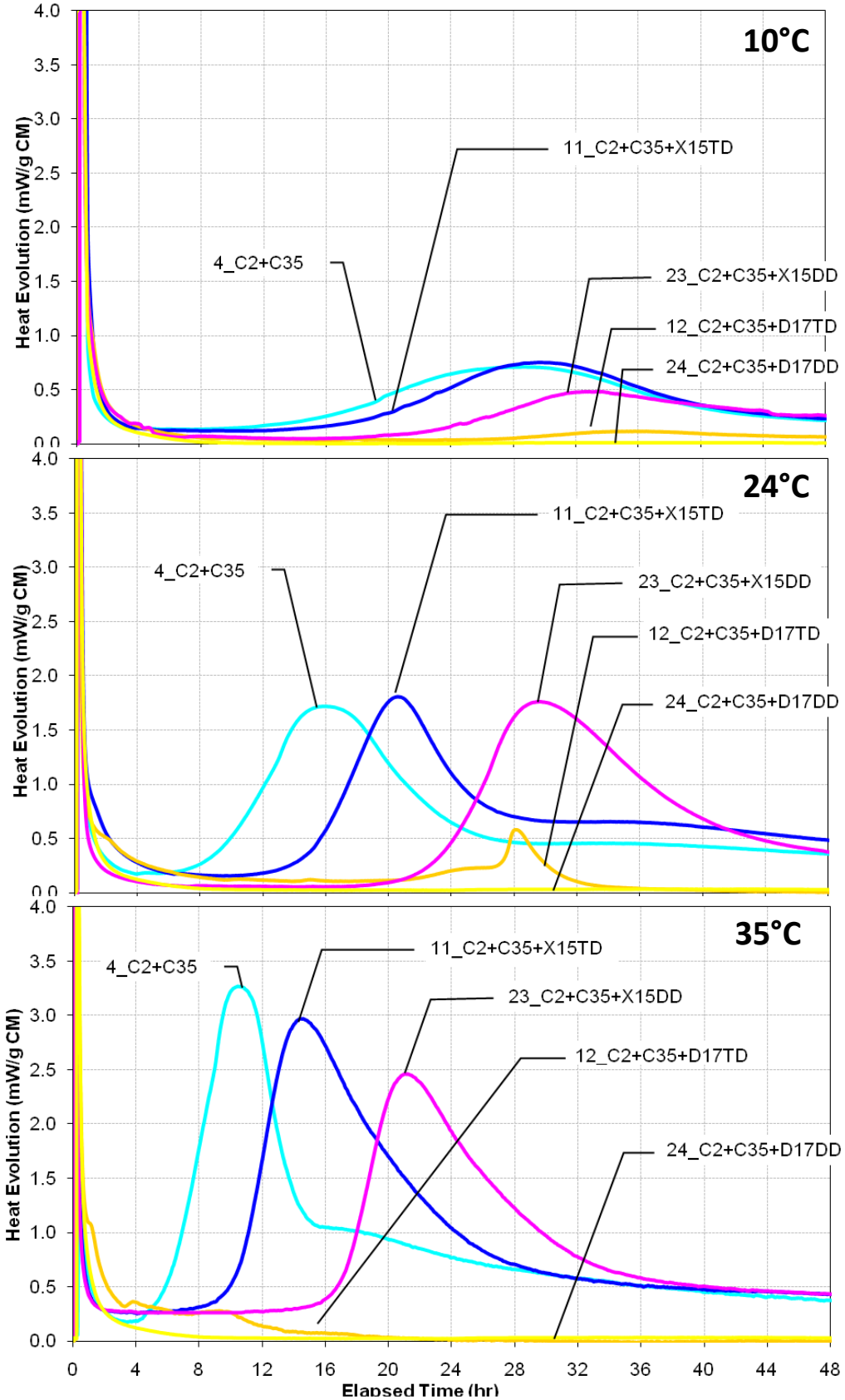

Figure 7-5 Heat evolution for C2 with C fly ash system at 10, 24, and 35°C.

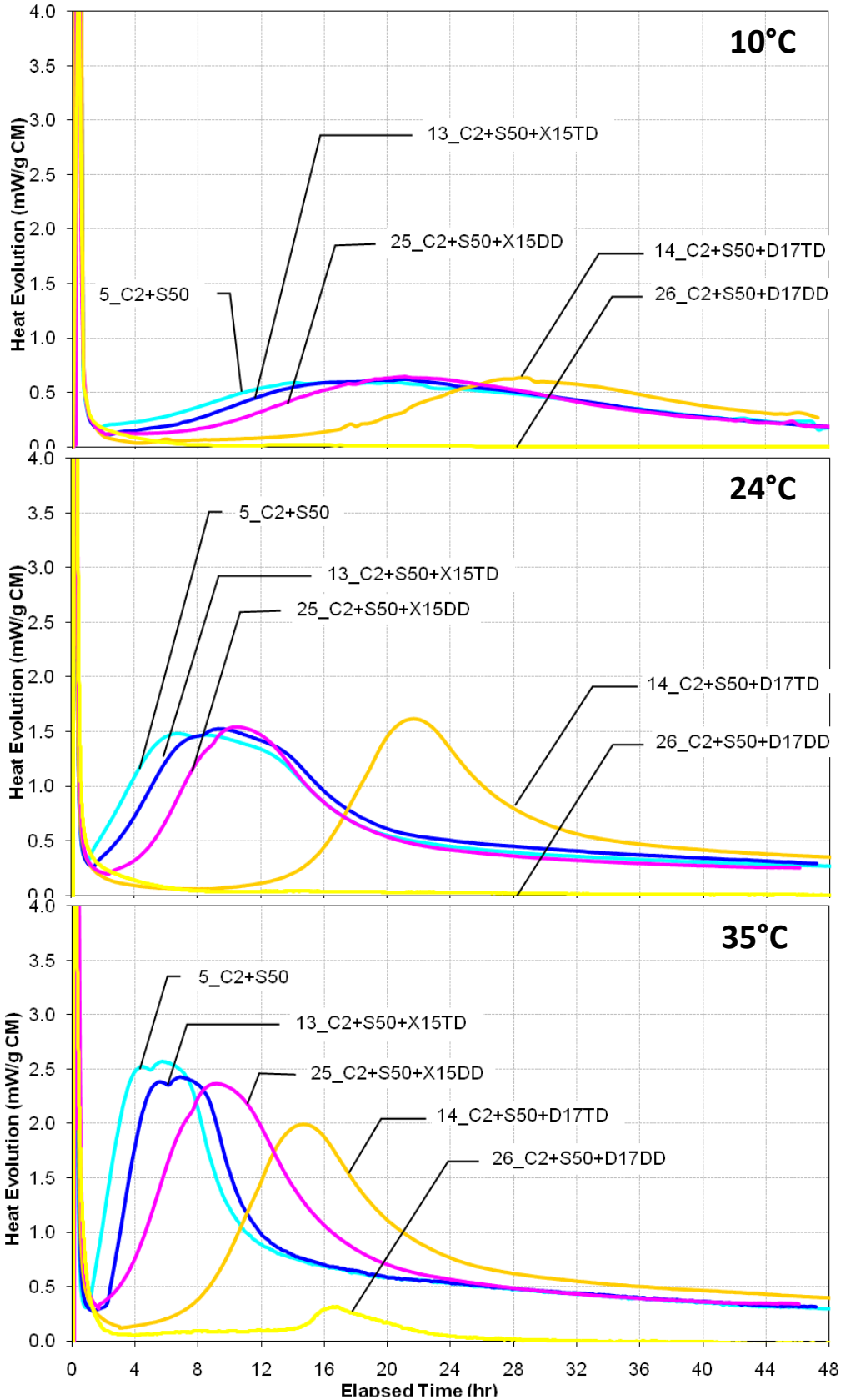

Figure 7-6 Heat evolution for C2 with slag system at 10, 24, and 35°C.

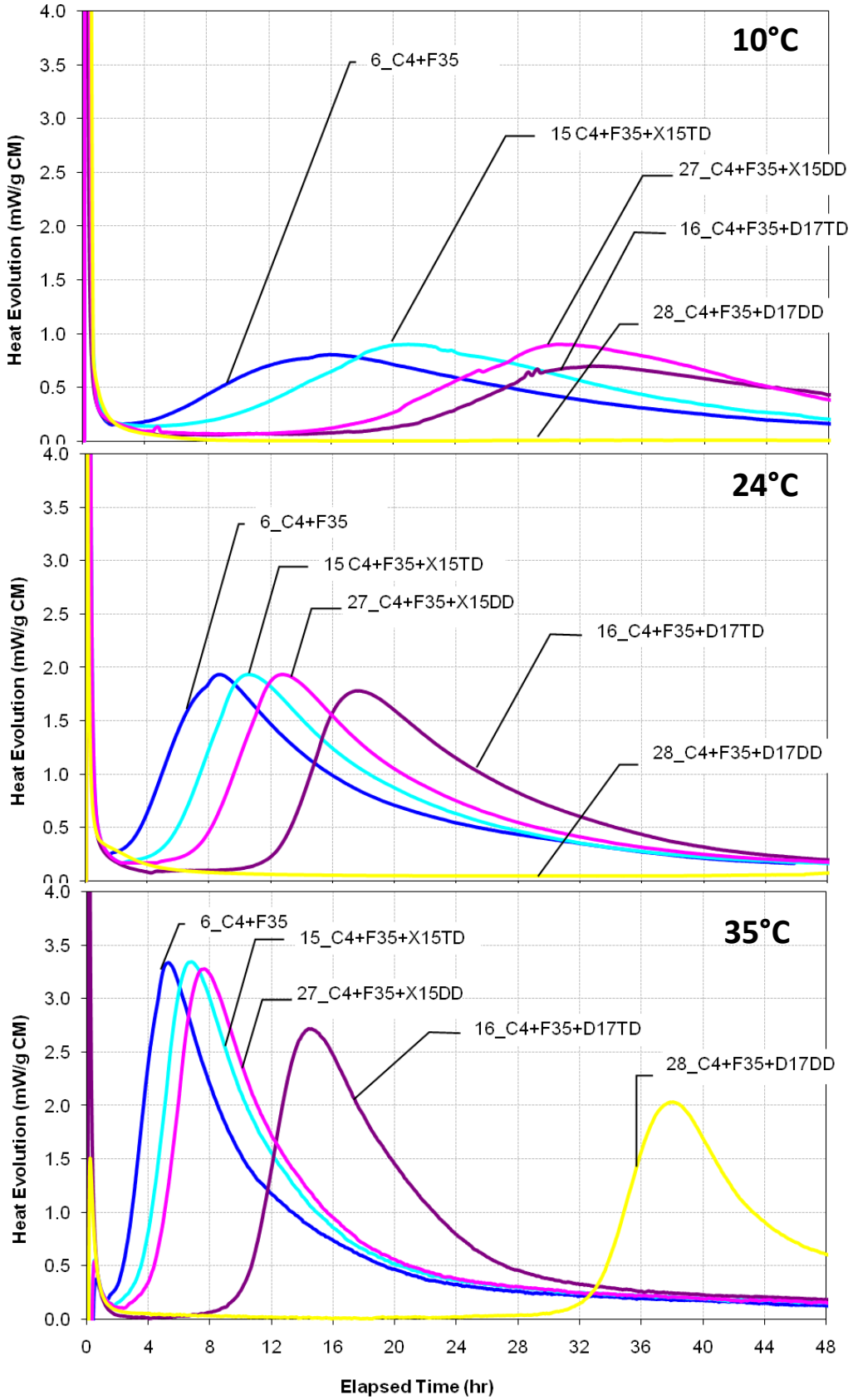

Figure 7-7 Heat evolution for C4 with F fly ash system at 10, 24, and 35°C.

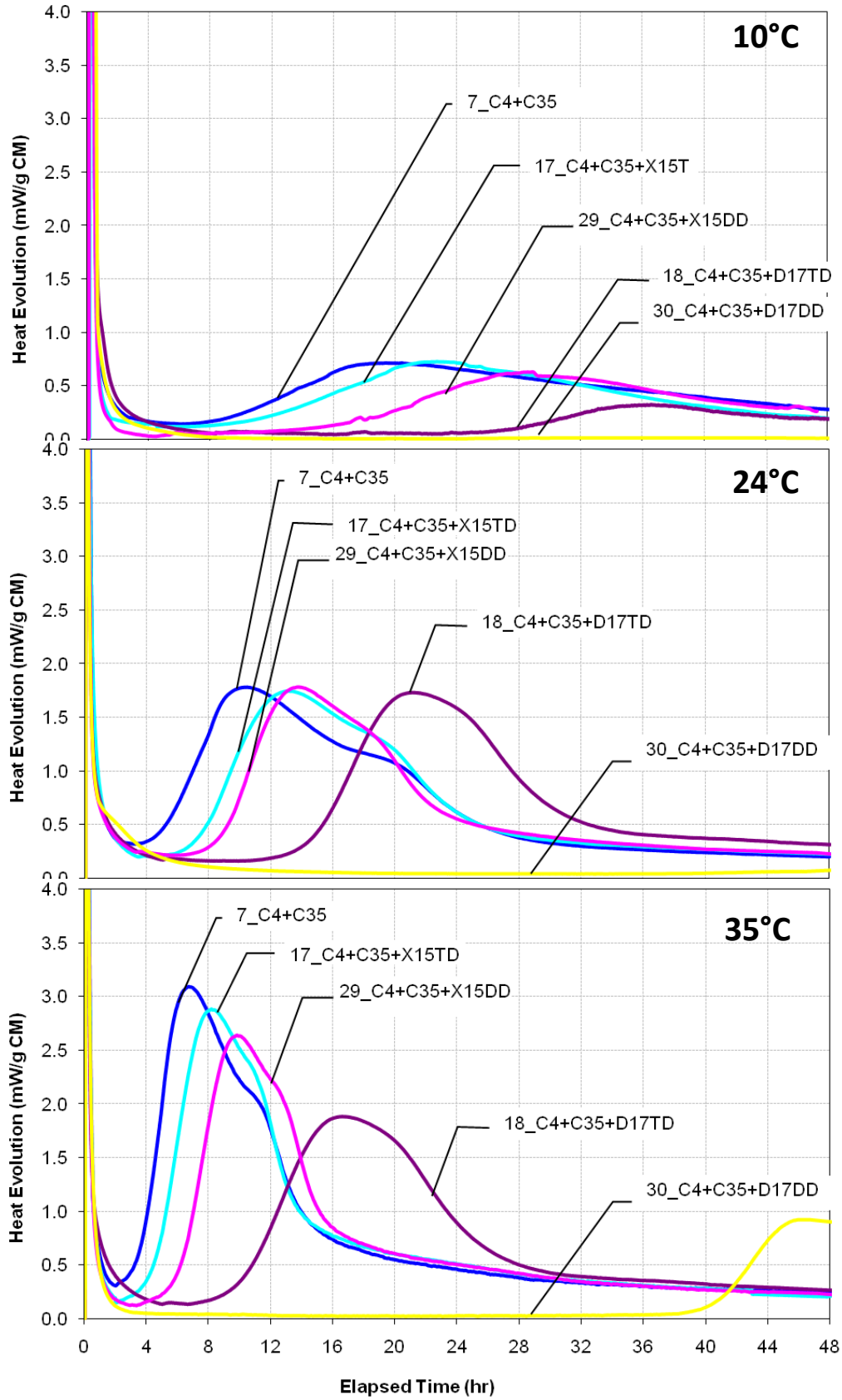

Figure 7-8 Heat evolution for C4 with C fly ash system at 10, 24, and 35°C.

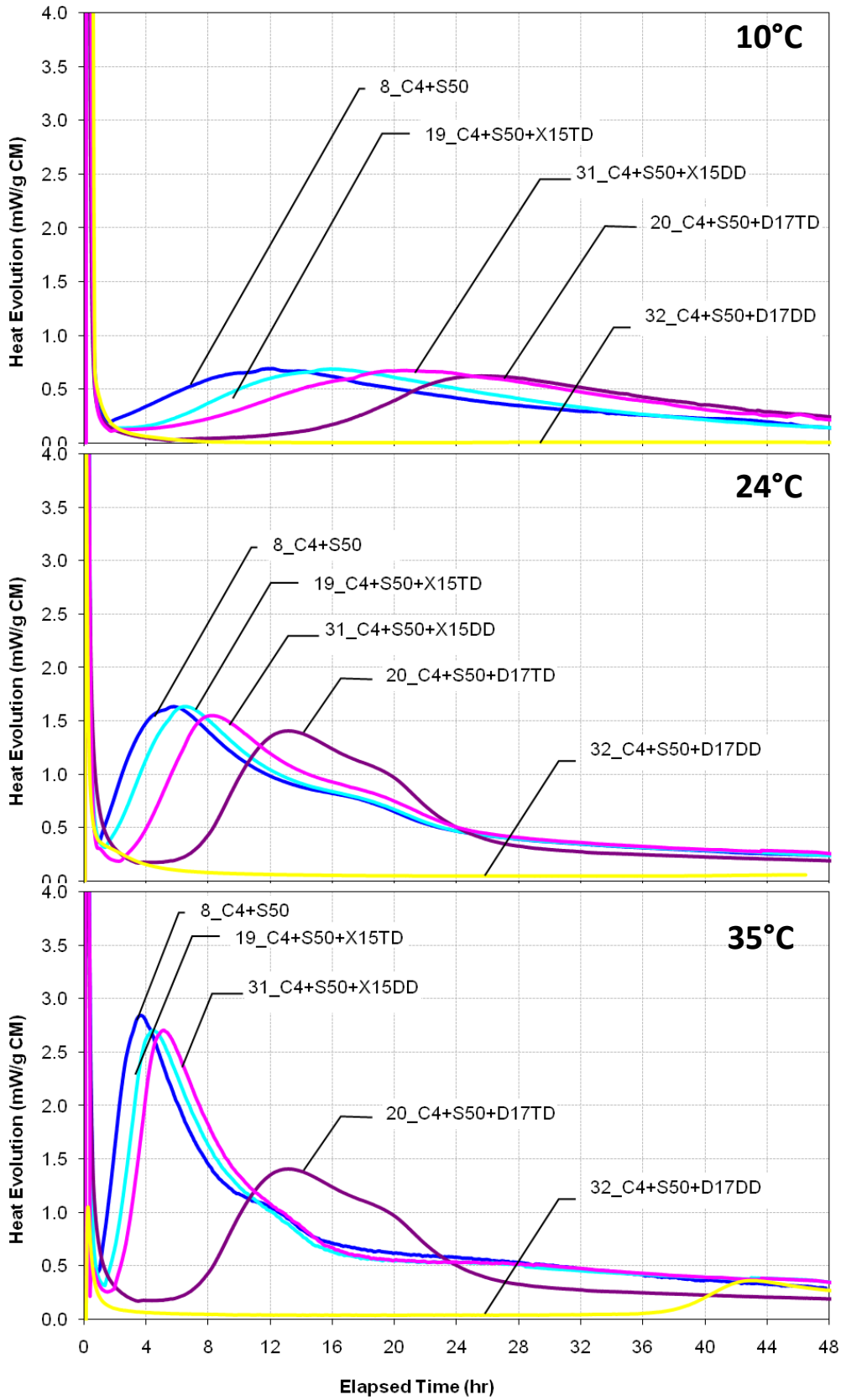

Figure 7-9 Heat evolution for C4 with slag system at 10, 24, 35°C.

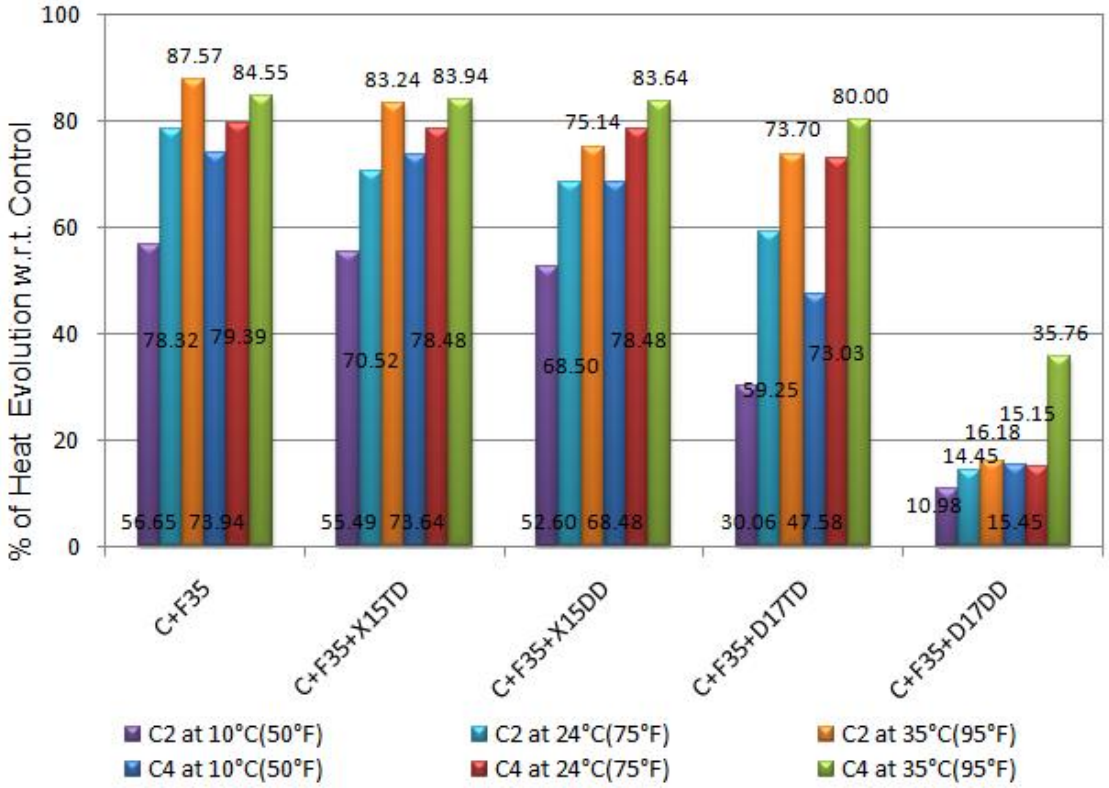

Figure 7-10 Percent of heat evolution w.r.t. control for cements with F fly ash system.

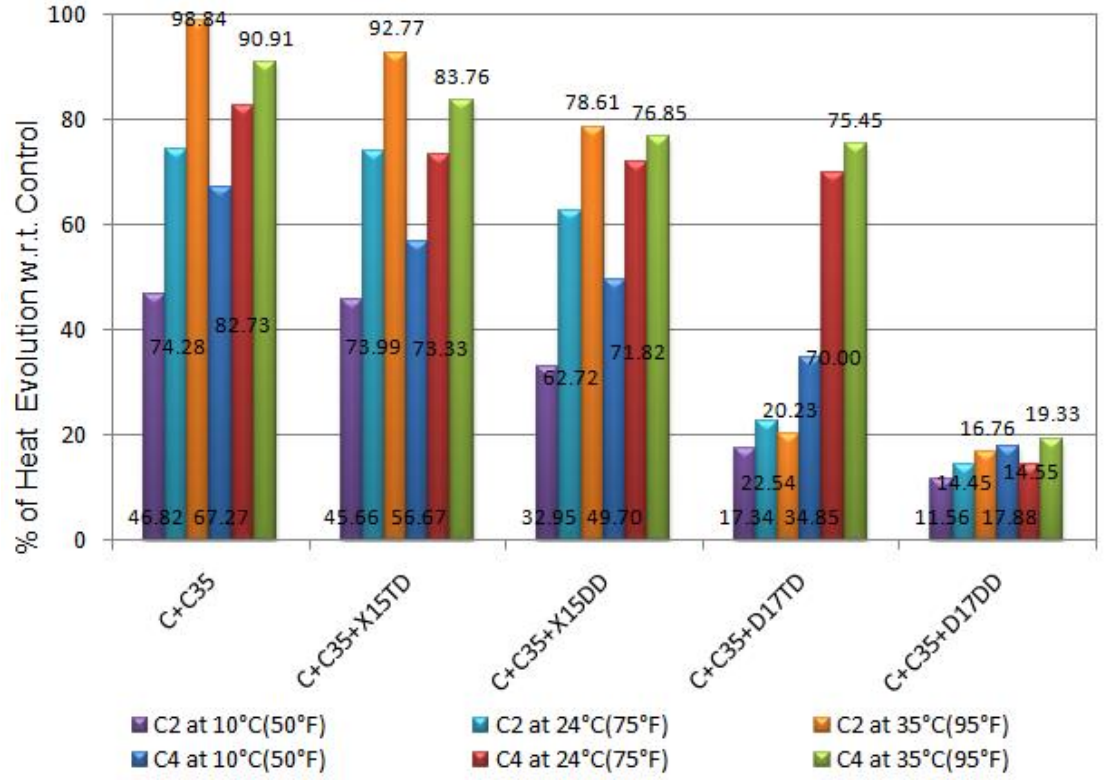

Figure 7-11 Percent of heat evolution w.r.t. control for cements with C fly ash system.

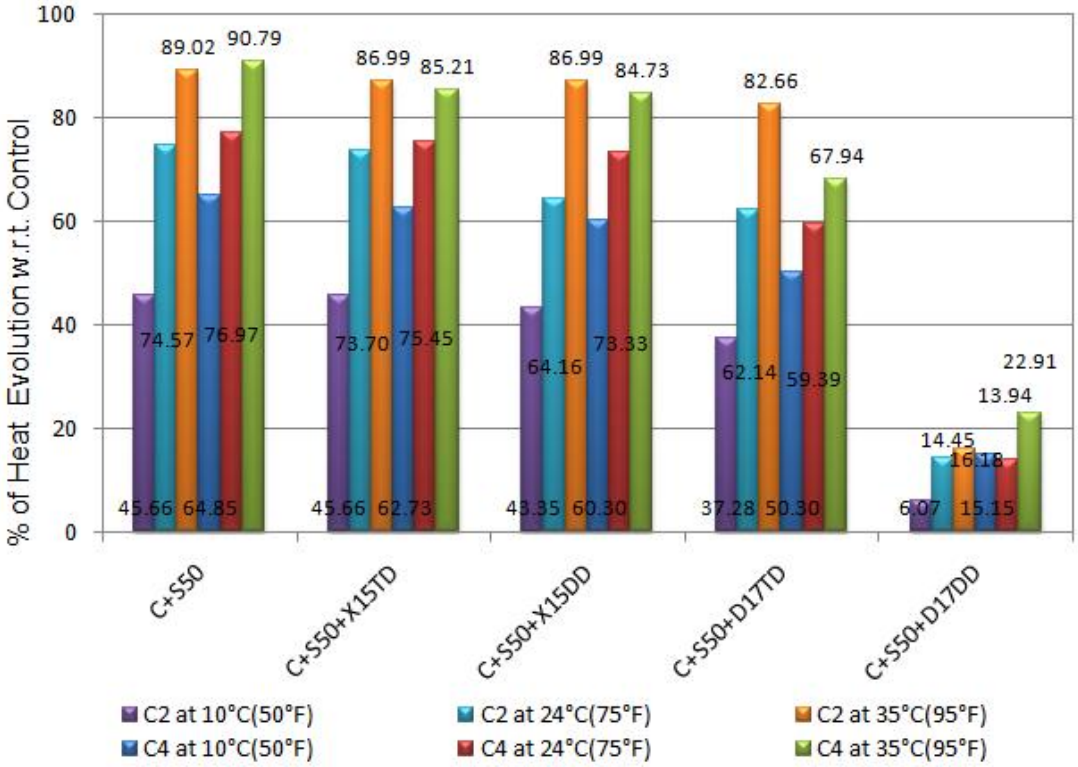

Figure 7-12 Percent of heat evolution w.r.t. control for cements with granulated slag system.

SETTING TIME BY VICAT APPARATUS

Setting time was measured using the Vicat apparatus equipment (ASTM C 191) for all the studied mixtures under intermediate temperature condition (24°C / 75°F) and are presented in Tables 7-3 and 7-4. Both the initial and final setting time is retarded more or less with the addition of chemical admixtures.

The usage of chemical admixture X15 resulted 2 to 5 hours delay of setting time (depending on the type of SCMs) at both typical and double dose. In case of the chemical admixture of D17, the setting time was delayed significantly (i.e., 5-11 hours for the fly ash mixtures and around 2 hours for the slag mixtures with typical dosage level and 11-19 hours for Class C fly ash, 21-29 hours for Class F fly ash and around 8 hours for slag mixtures at double dosage) compared with those of the mixtures tested without chemical admixtures.

The delay of setting time for the mixtures with Class C fly ash and typical dosage of D17 is higher (9-11 hours) than the other mixtures (5-8 hours with Class F fly ash and around 2 hours with slag). It is interesting to note that the same mixtures (i.e., with Class C fly ash and a typical dose of D17) are also identified as incompatible based on 30 percent of heat evolution criteria (Table 7-1). This is an indication that, in general, setting time and heat evolution results support each other. It seems the delay of setting time by 2-8 hours with the D17 chemical admixture (as with F fly ash / slag and a typical dose of D17) is within the normal range.

The addition of admixture D17 with double dose (i.e., 0.4% of cement weight) resulted detrimental effect on the cement set behavior (delayed by 8-30 hours) for all the tested specimens regardless of the cement and SCMs types. These abnormalities of setting behavior with double dose of admixture D17 is in general agreement with the integrated heat evolution results (mixtures with yellow marks in Tables 7-1 and 7-2).

With the C4 cement, the initial and final setting time tend to occur 1 to 5 hours earlier than those of C2 cement system. This phenomenon is also is in good agreement with the heat of hydration results.

The mixtures with slag and a double dose of D17 are identified as incompatible based on heat evolution criteria, although, the setting time delay is only around 7-8 hours. Either this setting time delay for slag mixtures is still abnormal or setting time determination based on the Vicat apparatus is not sensitive enough to identify all kind of incompatible mixtures because of some inherent limitations in the procedure. The criteria based on integrated heat evolution is more sensitive than setting time and considered as an efficient supporting tool for the rheological results. Therefore, the determination of setting time at other two studied temperatures (i.e., 10°C / 50°F and 35°C / 90°F) for the studied mixtures is not performed.

Table 7-3 Setting time data with C2 cement system at 24°C.

Experimental design	Initial Set	Final Set
1_C2	4.17	5.34
3_C2+F35	6.83	8.25
9_C2+F35+X15TD	8	9.33
21_C2+F35+X15DD	9.5	11.17
10_C2+F35+D17TD	14.67	16.33
22_C2+F35+D17DD	35	37
4_C2+C35	9	10.34
11_C2+C35+X15TD	12.17	13.67
23_C2+C35+X15DD	14	15.5
12_C2+C35+D17TD	18.67	21
24_C2+C35+D17DD	20.17	23.17
5_C2+S50	3.75	5.34
13_C2+S50+X15TD	4.5	6
25_C2+S50+X15DD	5.33	6.83
14_C2+S50+D17TD	5.92	7.75
26_C2+S50+D17DD	11.83	13.5

Note: The mixtures with yellow marks are identified as incompatible mixtures based on heat evolution criteria (as in Table 7-1)

Table 7-4 Setting time data with C4 cement system at 24°C.

Experimental design	Initial Set	Final Set
2_C4	3.17	4.17
6_C4+F35	4.1	5.58
15_C4+F35+X15TD	6.17	7.67
27_C4+F35+X15DD	7.33	8.83
16_C4+F35+D17TD	9.67	11.17
28_C4+F35+D17DD	25.83	27
7_C4+C35	5.67	7.17
17_C4+C35+X15TD	8.17	9.67
29_C4+C35+X15DD	9.83	11.33
18_C4+C35+D17TD	13.25	14.75
30_C4+C35+D17DD	23	26.5
8_C4+S50	2.67	4.17
19_C4+S50+X15TD	3.67	5.17
31_C4+S50+X15DD	4.42	5.83
20_C4+S50+D17TD	4.67	6.25
32_C4+S50+D17DD	9.33	11.17

Note: The mixtures with yellow marks are identified as incompatible mixtures based on heat evolution criteria (as in Table 7-2)

RHEOLOGICAL PARAMETERS BY STATIC RHEOLOGY MODE TEST

The plastic viscosity and yield stress of the all the studied mixtures (according to Table 6-2) were measured using the modified DSR. Five measurements at 5 different time intervals (10, 30, 60, 90, 120 minutes) for each mixture and at each temperature were conducted. The rate of change of plastic viscosity (RPV) and rate of change of yield stress (RYS) were then calculated based on these five measurements as described in the test method earlier (Chapter VI). The absolute values of plastic viscosity and yield stress (first measurement at 10 minutes after water added to the cement) are presented in Tables 7-5 and 7-6 and RPV and RYS are presented in Tables 7-7 and 7-8. The plots of PV, YS, RPV, and RYS vs. percent of heat evolution are illustrated Figures 7-13, 7-14, 7-15, and 7-16 respectively. The bar graphs for PV, YS, RPV and RYS as a function of admixture type / dosage and temperature for C2 cement + F35 (Class F fly ash 35% replacement) are presented in Figure 7-17 as an example. The bar graphs for C2 + C35, C2 + S50, C4 + F35, C4 + C35 and C4 + S50 systems are presented in Appendix C.

Absolute Values of Rheological Parameters (Plastic Viscosity and Yield Stress)

The following key observations were made based on plastic viscosity and yield stress results.

- Both plastic viscosity (PV) and yield stress (YS) decrease with the addition of the chemical admixtures to the control mixtures (mixtures with only SCMs) where the admixture D17 showed relatively higher reduction in both PV and YS than the admixture X15 (Tables 7-3 and 7-4). The similar decreasing trend of PV and YS is also noticed with the increasing dosage (i.e., from typical dosage to double dosage) of the individual chemical admixture.
- Slight increase of both plastic viscosity and yield stress with increasing temperature for all the mixtures with Class F fly ash and slag was noticed (Tables 7-5 and 7-6; Figure 7-

13). The PV showed sometimes decreasing trend or negligible change with increasing temperature for some mixtures with Class C fly ash, although, the YS showed the same behavior as in the mixtures with Class F fly ash and slag.

- The change of yield stress with increasing dosage of chemical admixtures (Table 7-6) is greater than the change of plastic viscosity (Table 7-5). The difference in YS between the incompatible (the mixture with double dosage of D17 identified based on heat evolution criteria earlier) and normal mixtures is greater than the difference in PV for those mixtures. However, the level of difference for both PV and YS is not good enough to clearly differentiate between the incompatible and normal mixtures. As for example, the difference in YS and PV between the incompatible mixture of No.12 (C2 cement with Class C fly ash and typical dose of D17) and the normal mixture of No.23 (C2 cement with Class C fly ash and double dose of X15) is not considerable (Tables 7-5 and 7-6). The incompatible / marginal mixtures, identified by heat evolution criteria (Tables 7-1 and 7-2), show abnormal / marginal PV/YS (Tables 7-5 and 7-6) values as expected. However, more number of normal mixtures based on heat evolution criteria, show PV and YS values in somewhat abnormal or marginal ranges [*, red asterisk marked mixtures in Tables 7-5 and 7-6]. This phenomenon is illustrated in Figures 7-13 and 7-14 by plotting PV and YS versus % of heat evolution w.r.t. control after 48 hours respectively. These are considered as mismatch between absolute values of rheological parameters and heat evolution characteristics. Interestingly, the number of mismatches is more with yield stress (Table 7-6 and Figure 7-14) than plastic viscosity (Table 7-5 and Figure 7-13). Therefore, criteria based on absolute values of PV and YS to identify incompatible mixtures was found to be inconclusive.

Table 7-5 Plastic viscosity of all the studied mixtures.

SCM Type	Exp. No.		Admix Type and Dosage	C2 (Type I/II Cement)			C4 (Type V Cement)		
	C2	C4		10^0C	24^0C	35^0C	10^0C	24^0C	35^0C
Class F (35%)	3	6	No Admix	0.2221	0.2295	0.2658	0.2249	0.2359	0.2551
	9	15	X15TD	0.1995	0.2356	0.2425	0.1995	0.2092	0.2225
	21	27	X15DD	0.1573*	0.1954	0.2581	0.1598*	0.1638	0.2181
	10	16	D17TD	0.1390	0.1652	0.2309	0.1689	0.1962	0.2442
	22	28	D17DD	0.1241	0.1351	0.1548	0.124	0.1437	0.1536
Class C (35%)	4	7	No Admix	0.1498	0.1589	0.1651	0.1712	0.1798	0.1789
	11	17	X15TD	0.1413	0.1478	0.1329	0.1687	0.1612	0.1581
	23	29	X15DD	0.1240	0.1221*	0.1124*	0.1354	0.1314	0.1322
	12	18	D17TD	0.1057	0.1011	0.1068	0.1259	0.1211*	0.1231*
	24	30	D17DD	0.0845	0.0824	0.0804	0.1195	0.1154	0.1157
Slag (50%)	5	8	No Admix	0.2316	0.2413	0.2896	0.2039	0.2113	0.2413
	13	19	X15TD	0.1763	0.1961	0.2411	0.1856	0.1874	0.2169
	25	31	X15DD	0.1423*	0.1523	0.1856	0.1487*	0.1501	0.1748
	14	20	D17TD	0.1584	0.1853	0.2633	0.1552	0.1652	0.2164
	26	32	D17DD	0.1233	0.1359	0.1406	0.1156	0.1256	0.1342

Note: Incompatible (yellow) and marginal (green) mixtures based on heat evolution criteria (Tables 7-1 and 7-2) are superimposed

Table 7-6 Yield stress of all the studied mixtures.

SCM Type	Exp. No.		Admix Type and Dosage	C2 (Type I/II Cement)			C4 (Type V Cement)		
	C2	C4		10^0C	24^0C	35^0C	10^0C	24^0C	35^0C
Class F (35%)	3	6	No Admix	71.37	80.79	123.51	71.375	81.97	121.97
	9	15	X15TD	44.28*	62.25	91.04	59.56	68.72	91.04
	21	27	X15DD	25.26*	43.54*	74.22	42.1*	46.92*	69.89
	10	16	D17TD	19.06	39.56*	61.87	40.23*	45.59*	83.045
	22	28	D17DD	4.57	16.59	31.88	14.57	23	47.587
Class C (35%)	4	7	No Admix	45.97	78.21	129.53	55.29	80.11	112.38
	11	17	X15TD	30.75*	58.29	110.25	37.86*	57.21	84.14
	23	29	X15DD	23.47	38.23*	74.5	26.52*	39.66*	64.54
	12	18	D17TD	14.28	32.87	77.88	21.57	35.25*	65.21
	24	30	D17DD	3.78	13.58	27.05	9.59	16.39	37.24
Slag (50%)	5	8	No Admix	53.5	79.23	94.25	62.33	80.87	118.29
	13	19	X15TD	35.51*	51.74	83.64	44.28	55.45	89.54
	25	31	X15DD	15.2*	29.32*	53.18	24.58*	31.23*	58.67
	14	20	D17TD	19.94*	31.08*	51.48	27.98*	33.52*	52.81
	26	32	D17DD	4.98	12.45	29.41	13.23	15.82	35.23

Note: Incompatible (yellow) and marginal (green) mixtures based on heat evolution criteria (Tables 7-1 and 7-2) are superimposed

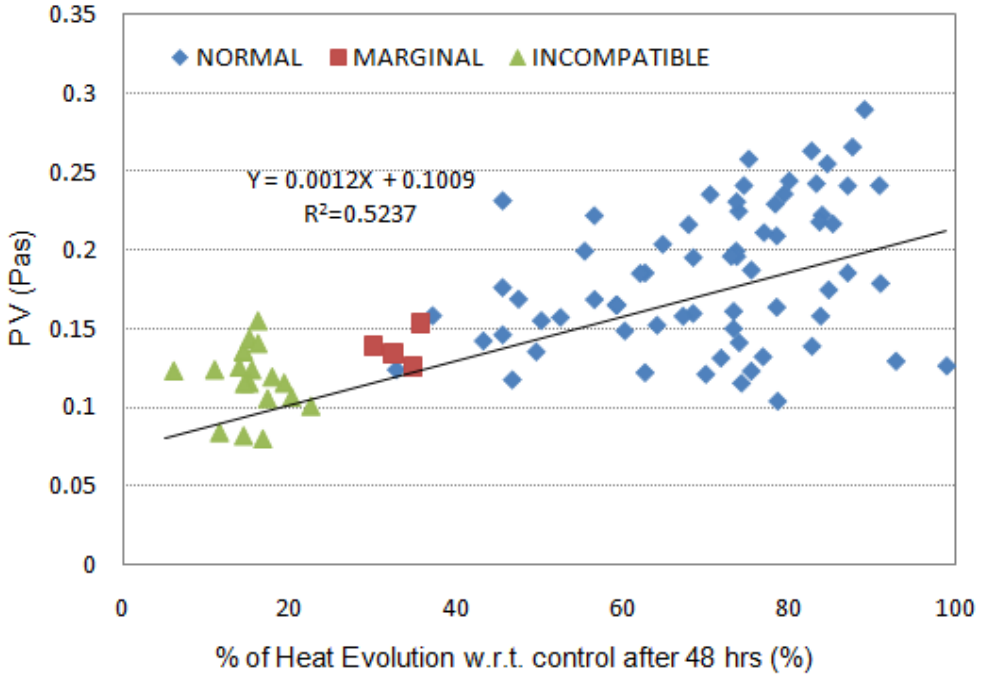

Figure 7-13 Plastic viscosity vs. percent of heat evolution w.r.t. control after 48 hours.

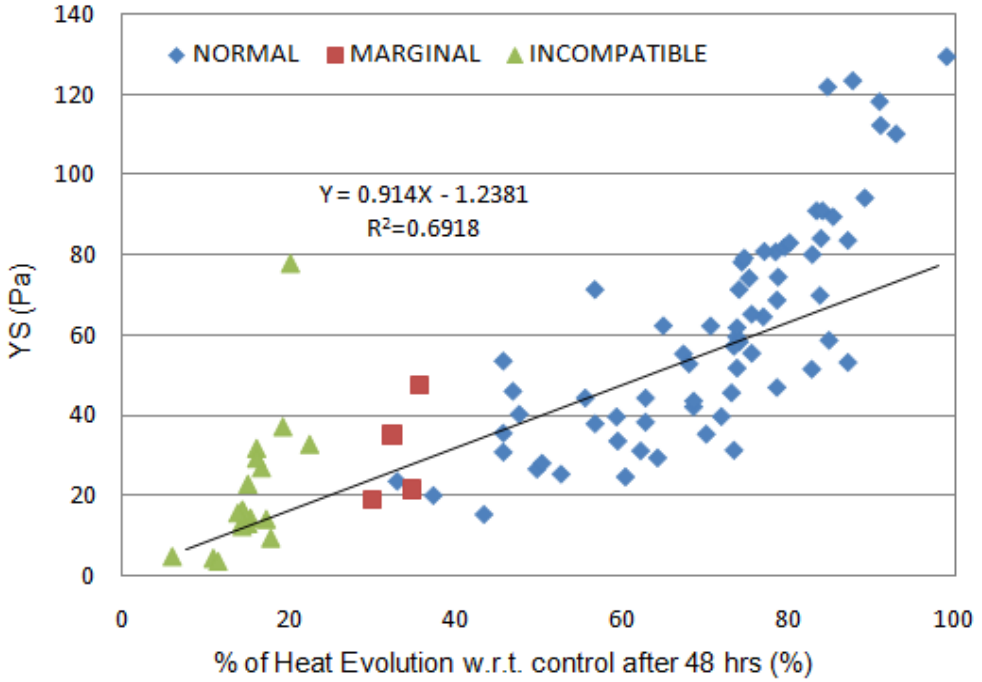

Figure 7-14 Yield stress vs. percent of heat evolution w.r.t. control after 48 hours.

Rate of Change of Rheological Parameters (RPV and RYS)

The rate of change of the rheological parameters were calculated based on the plastic viscosity and yield stress data at five different time intervals during 2 hours testing period and are presented in Tables 7-7 and 7-8; Figures 7-15 and 7-16. A perusal of these tables and figures showed the following observations:

- Both the value of the rate of change of plastic viscosity (RPV) and the rate of change of yield stress (RYS) have a tendency to decrease when the dosage of the chemical admixture increases (Tables 7-7 and 7-8).
- Both RPV and RYS show an increasing trend with increasing temperature for all the studied mixtures (Tables 7-7 and 7-8). This is in agreement with the fact that the rate of change of rheological parameters becomes faster at higher temperature due to higher reaction kinetics than that at lower temperature. In general, the rate of increase is greater at higher temperature range (i.e., 24-35°C) and slower at lower temperature range (10-24°C) for the normal mixtures as shown in Figure 7-17.
- It is important to note that a significant difference between RPV and RYS of the normal and incompatible mixtures exists regardless of the ambient temperature effects. This phenomenon is matched well with the heat evolution characteristics from the isothermal conduction calorimetry and set behavior form Vicat apparatus test.
- Almost all the incompatible and marginal mixtures, identified based on heat evolution criteria (Tables 7-1 and 7-2), show abnormal (yellow) and marginal (green) ranges of RPV and RYS (Tables 7-7 and 7-8). The number of mismatches [*, red asterisk marked mixtures in Tables 7-7 and 7-8] are greatly reduced. Figures 7-15 and 7-16 illustrate RPV and RYS versus percent of heat evolution w.r.t. control after 48 hours respectively. The

RPV plot (Figure 7-15) makes a clear demarcation between normal, incompatible, and marginal mixtures but some overlaps between marginal and normal mixtures (in supportive with Table 7-8) exit in RYS plot (Figure 7-16).

- Therefore, criteria based on rate of change of rheological parameters are more sensitive than that based on absolute values to identify incompatible mixtures.
- Both RPV and RYS are acceptable for criteria of incompatibilities; however, RPV is more sensitive than RYS to distinguish between normal and incompatible mixtures. Interestingly, the mismatches are more with RYS (Table 7-7) than RPV (Table 7-8). The details are described in the next section on establishing acceptance criteria.

Table 7-7 Rate of change of plastic viscosity (RPV) of all the studied mixtures.

SCM Type	Exp. No.		Admix Type and Dosage	C2 (Type I/II Cement)			C4 (Type V Cement)		
	C2	C4		10^0C	24^0C	35^0C	10^0C	24^0C	35^0C
Class F (35%)	3	6	No Admix	0.0852	0.1058	0.1787	0.0789	0.0924	0.1459
	9	15	X15TD	0.0702	0.0924	0.1321	0.0687	0.0807	0.1136
	21	27	X15DD	0.0389	0.0486	0.0658	0.0356	0.0436	0.0517
	10	16	D17TD	0.0211	0.0325	0.0402	**0.0214***	0.0318	0.0388
	22	28	D17DD	0.0018	0.0102	0.0143	0.0016	0.0115	0.0204
Class C (35%)	4	7	No Admix	0.0891	0.1254	0.2153	0.0857	0.1158	0.1587
	11	17	X15TD	0.0852	0.1135	0.1852	0.0849	0.1042	0.1459
	23	29	X15DD	0.0402	0.0831	0.1023	0.0428	0.0612	0.0923
	12	18	D17TD	0.0112	0.0145	0.0167	0.0254	0.0512	0.0873
	24	30	D17DD	0.0032	0.0057	0.0129	0.0085	0.0138	0.0198
Slag (50%)	5	8	No Admix	0.1138	0.1659	0.2345	0.1278	0.1586	0.2114
	13	19	X15TD	0.1069	0.1589	0.2068	0.1151	0.1411	0.1951
	25	31	X15DD	0.0723	0.1023	0.1357	0.0659	0.0953	0.1312
	14	20	D17TD	0.0521	0.0753	0.0987	0.0585	0.0847	0.1185
	26	32	D17DD	0.0175	0.0185	0.0176	0.0168	0.0191	0.0228

Note: Incompatible (yellow) and marginal (green) mixtures based on heat evolution criteria (Tables 7-1 and 7-2) are superimposed

Table 7-8 Rate of change of yield stress (RYS) of all the studied mixtures.

SCM Type	Exp. No.		Admix Type and Dosage	C2 (Type I/II Cement)			C4 (Type V Cement)		
	C2	C4		10^0C	24^0C	35^0C	10^0C	24^0C	35^0C
Class F (35%)	3	6	No Admix	42.51	45.26	59.87	35.69	39.469	49.469
	9	15	X15TD	35.32	36.53	45.29	31.78	33.294	39.87
	21	27	X15DD	25.41	26.49	32.14	21.59	24.75	29.56
	10	16	D17TD	15.39	**15.87***	24.58	**11.26***	**14.81***	22.98
	22	28	D17DD	8.98	9.87	11.21	6.969	8.14	14.72
Class C (35%)	4	7	No Admix	41.29	49.65	52.46	34.54	37.54	45.23
	11	17	X15TD	33.26	39.52	43.21	33.52	32.58	39.25
	23	29	X15DD	23.12	28.57	35.92	**20.58***	**23.58***	27.21
	12	18	D17TD	8.35	11.29	12.89	13.52	**16.56***	**18.56***
	24	30	D17DD	4.52	6.59	9.54	7.59	9.87	13.58
Slag (50%)	5	8	No Admix	48.97	55.87	65.32	48.95	56.89	68.24
	13	19	X15TD	39.65	47.52	56.89	41.54	49.58	57.27
	25	31	X15DD	29.89	39.56	49.59	30.54	37.41	48.54
	14	20	D17TD	**16.89***	23.48	31.58	19.52	28.45	35.23
	26	32	D17DD	9.63	11.21	12.56	10.58	12.34	18.59

Note: Incompatible (yellow) and marginal (green) mixtures based on heat evolution criteria (Tables 7-1 and 7-2) are superimposed

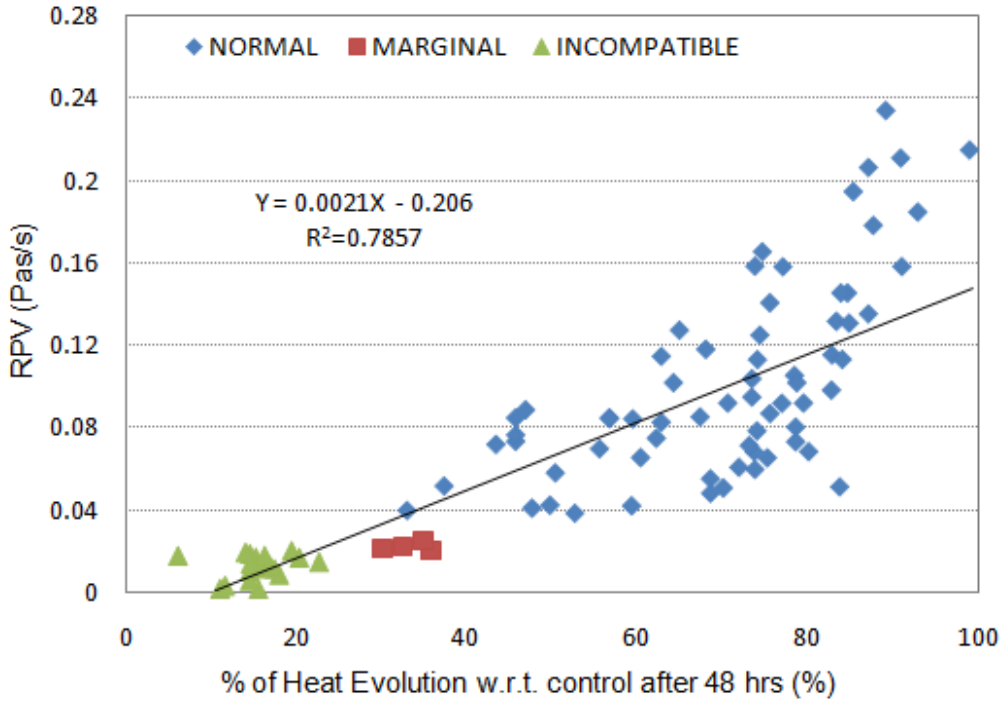

Figure 7-15 RPV vs. percent of heat evolution w.r.t. control after 48 hours.

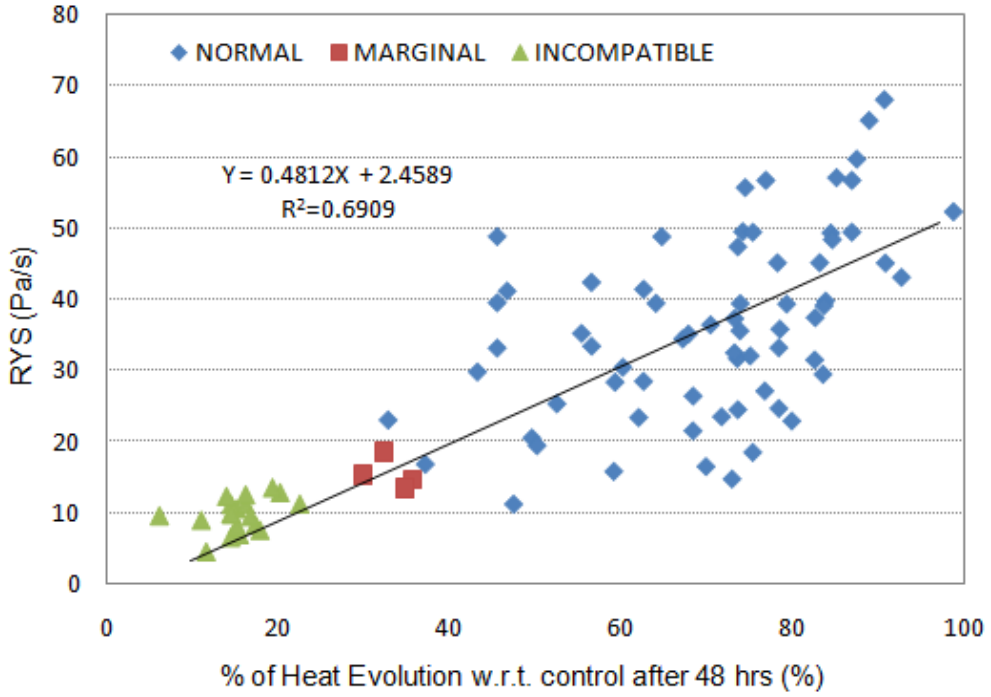

Figure 7-16 RYS vs. percent of heat evolution w.r.t. control after 48 hours.

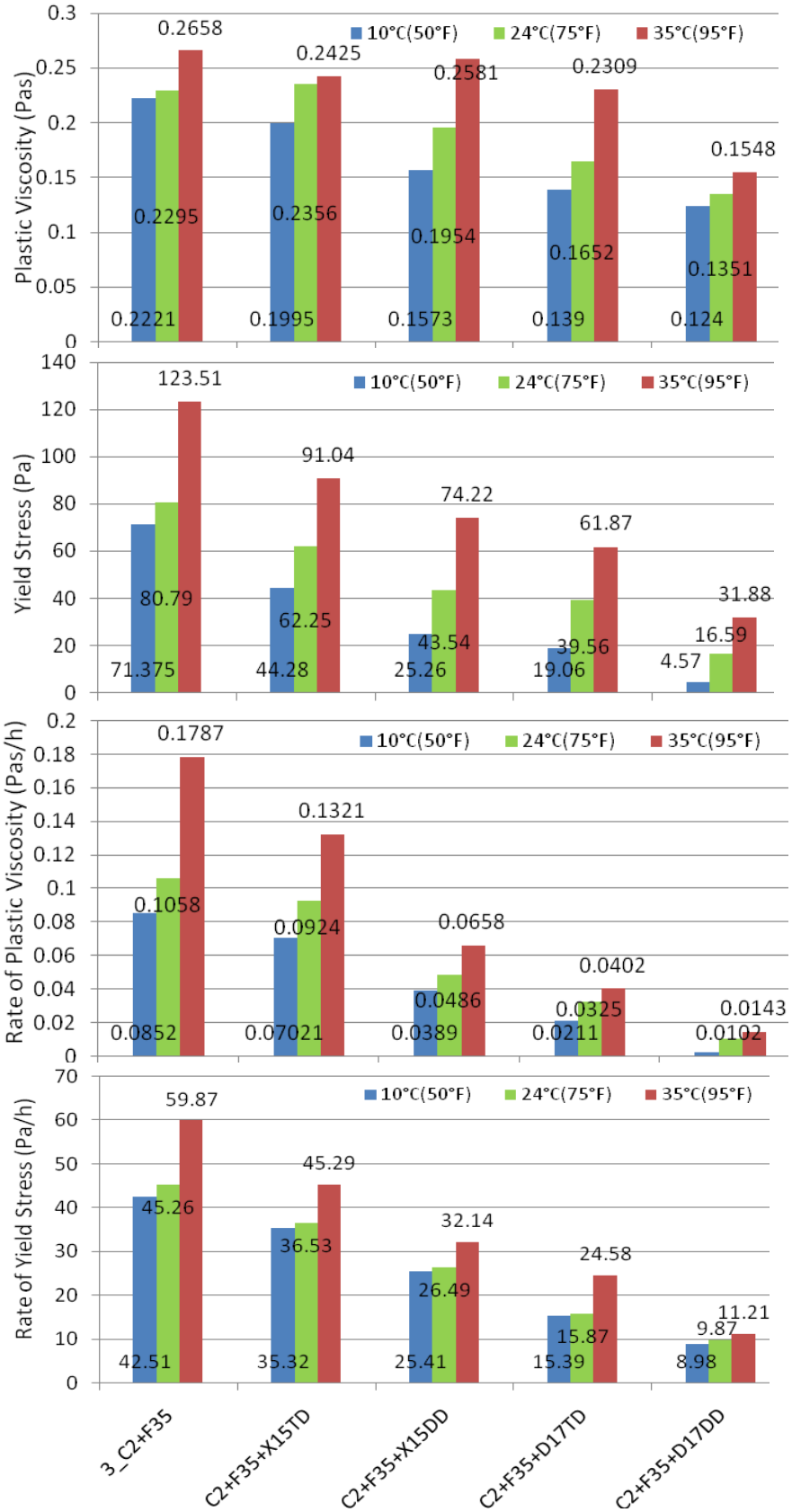

Figure 7-17 PV, YS, RPV, and RYS for C2 cement with Class F fly ash system.

ACCEPTANCE CRITERIA BASED ON STATIC RHEOLOGICAL PARAMETERS

An attempt has been made to develop the static rheology based acceptance criteria using the test results generated in the laboratory investigation and discussed below.

Procedure to Develop Acceptance Criteria

The incompatible mixtures that were identified based on 30 percent of heat evolution criteria are listed in Tables 7-9 and 7-10. The mixture numbers 12, 22, 24, and 26 with C2 cement and 30, 32 with C4 cement were identified as incompatible mixtures at all three temperature conditions. The mixture number 28 with C4 cement is identified as incompatible mixture both at low (10°C) and intermediate temperatures (24°C) but become marginal at high temperature (35°C). The rate of change of rheological parameters, i.e., rate of change of plastic viscosity (RPV) and rate of change of yield stress (RYS), corresponding to the identified incompatible mixtures are then compared with the percent of heat evolution after 48 hours to see whether identification of incompatible mixtures based on the two methods supports each other. The following observations are important in this connection.

- An incompatible mixture shows a very low value of RPV and RYS. It is interesting to see that all the incompatible mixtures identified by heat evolution criteria (12, 22, 24, 26 with C2 cement and 30, 32 with C4 cement) show very low RPV and RYS values as shown in Tables 7-9 and 7-10. This is in good agreement between heat evolution and rheology based criteria.
- The marginal mixtures based on combined criteria of percent heat evolution, RPV and RYS are listed in Table 7-11. Based on percent of heat evolution criteria, the mixtures having percent heat evolution between 30-35% are considered as marginal mixtures. Therefore, the mixture numbers 10, 23 with C2 cement at 10°C; 18 with C4cement at

10°C and 28 with C4 cement at 35°C are identified as marginal mixtures based on heat evolution criteria. The values of the marginal mixtures have served to fix the upper limit for the acceptance criteria.

- Based on the values of RPV and RYS of the confirmed incompatible mixtures (Tables 7-9 and 7-10) and marginal mixtures (Table 7-11), the possible acceptance criteria is formulated and given in Table 7-12.

Table 7-9 Incompatible mixtures with C2 cement under different temperatures.

	Mixture Combinations	% of Heat Evolution w.r.t. control	RPV	RYS
10°C (50°F)	22_C2+F35+D17DD	10.98	0.0018	8.98
	12_C2+C35+D17TD	17.34	0.0112	8.35
	24_C2+C35+D17DD	11.56	0.0032	4.52
	26_C2+S50+D17DD	6.07	0.0175	9.63
24°C (75°F)	22_C2+F35+D17DD	14.45	0.0102	9.87
	12_C2+C35+D17TD	22.54	0.0145	11.29
	24_C2+C35+D17DD	14.45	0.0057	6.59
	26_C2+S50+D17DD	14.45	0.0185	11.21
35°C (95°F)	22_C2+F35+D17DD	16.18	0.0143	11.21
	12_C2+C35+D17TD	20.23	0.0167	12.89
	24_C2+C35+D17DD	16.76	0.0129	9.54
	26_C2+S50+D17DD	16.18	0.0176	12.56

Table 7-10 Incompatible mixtures with C4 cement under different temperatures.

	Mixture Combinations	% of Heat Evolution w.r.t. control	RPV	RYS
10°C (50°F)	28_C4+F35+D17DD	15.45	0.0016	6.96
	30_C4+C35+D17DD	17.88	0.0085	7.59
	32_C4+S50+D17DD	15.15	0.0168	10.58
24°C (75°F)	28_C4+F35+D17DD	15.15	0.0115	8.14
	30_C4+C35+D17DD	14.55	0.0138	9.87
	32_C4+S50+D17DD	13.94	0.0191	12.34
35°C (95°F)	30_C4+C35+D17DD	19.33	0.0198	13.58
	32_C4+S50+D17DD	22.91	0.0228	18.59

Table 7-11 Marginal mixtures under different temperatures.

	Mixture Combinations	% of Heat Evolution w.r.t. control	RPV	RYS
10°C (50°F)	10_C2+F35+D17TD	30.06	0.0211	15.39
	23_C2+C35+X15DD	32.95	0.0402	23.12
	14_C2+S50+D17TD	37.28	0.0521	16.89
	18_C4+C35+D17TD	34.85	0.0254	13.52
35°C (95°F)	28_C4+F35+D17DD	35.76	0.0204	14.72

Table 7-12 Criteria of incompatibilities based on RPV and RYS.

Criteria	RPV	RYS
Incompatible Mixtures	≤ 0.02	≤ 14
Marginal Mixtures	0.02 - 0.025	14 - 19
Normal Mixtures	> 0.025	> 19

A perusal of Table 7-12 showed the following observations:

- As described earlier, the normal and incompatible mixtures can be clearly distinguished based on RPV and RYS. Both RPV and RYS can be used to identify incompatible mixtures. However, RPV is more sensitive than RYS. In addition, the reproducibility of RPV is generally better than that of RYS as manifested by lower coefficient of variation (CoV) % (discussed later and presented in Tables 7-13 and 7-14).
- A generalized criterion irrespective of SCM type and temperature is obtained based on the limited data, which is a good indication of the modified DSR-based rheology method to identify incompatible mixtures. Further refinement of these acceptance criteria based

on more specific work covering wide range of incompatibilities and field laboratory validation through implementation efforts are warranted but beyond the scope of the present study.

REPRODUCIBILITY OF STATIC RHEOLOGICAL PARAMETERS

The reproducibility tests of static rheological parameters using the modified DSR were conducted and described in this section. Reproducibility of the rheological parameters (both absolute values and rates) based on the two mixes at three different temperatures with three replicas are presented in Tables 7-13 and 7-14. The ingredients corresponding to each mixture at the selected temperature were mixed and tested separately three times in order to generate three replicas. Average of rheological parameters (i.e., PV, YS, RPV, and RYS) based on 3 replicas and their respective coefficient of variation (CoV %) were calculated for the studied mixture combinations and are presented in Table 7-13 for PV and YS, and Table 7-14 for RPV and RYS. The plastic viscosity and yield stress data in Table 7-13 represents data from the first run, i.e., 10 minutes after adding water to the cement, for the selected mixtures. It is to be noted that the mixture with C4 + F35 + X15DD was identified as normal mixture and the mixture with C4 + F35 + D17DD was identified as incompatible mixture based on both the rheological parameters and heat of hydration data.

Table 7-13 Reproducibility of plastic viscosity (PV) and yield stress (YS).

Mixture Combination			PV	PV Average	CoV%	YS	YS Average	CoV%
C4+F35+ X15DD	10°C	1	0.1598	0.1553	2.54	42.1	41.06	3.21
		2	0.1524			41.51		
		3	0.1537			39.58		
	24°C	1	0.1638	0.1616	1.36	46.92	39.70	16.93
		2	0.1594			33.62		
		3	0.1617			38.56		
	35°C	1	0.2181	0.2099	3.86	69.89	65.53	5.80
		2	0.2019			63.84		
		3	0.2096			62.87		
C4+F35+ D17DD	10°C	1	0.124	0.1221	1.35	14.57	15.54	6.51
		2	0.1215			16.59		
		3	0.1209			15.47		
	24°C	1	0.1437	0.1381	3.55	23.00	20.03	15.75
		2	0.1348			16.72		
		3	0.1357			20.37		
	35°C	1	0.1536	0.1538	4.10	47.587	51.25	8.84
		2	0.1602			56.32		
		3	0.1476			49.85		

Table 7-14 Reproducibility of RPV and RYS.

Mixture Combination			RPV	RPV Average	CoV%	RYS	RYS Average	CoV%
C4+F35+ X15DD	10°C	1	0.0356	0.0370	3.48	21.59	24.17	9.93
		2	0.0381			26.34		
		3	0.0374			24.57		
	24°C	1	0.0436	0.0437	4.81	24.75	26.80	6.72
		2	0.0459			28.12		
		3	0.0417			27.54		
	35°C	1	0.0517	0.0548	7.38	29.56	32.78	12.09
		2	0.0534			31.58		
		3	0.0594			37.21		
C4+F35+ D17DD	10°C	1	0.0016	0.0015	6.67	6.969	6.49	17.02
		2	0.0014			5.23		
		3	0.0015			7.28		
	24°C	1	0.0115	0.0120	4.21	8.14	9.07	9.58
		2	0.0119			9.21		
		3	0.0125			9.86		
	35°C	1	0.0204	0.0227	9.92	14.72	16.20	11.26
		2	0.0249			15.65		
		3	0.0228			18.24		

Tables 7-13 and 7-14 indicate that the coefficient of variation (CoV) % of both absolute values of PV and RPV is below 10%. The CoV% of the YS and RYS is also under 10 for the 60% of the cases. The CoV% of the YS and RYS for the remaining 40% cases is under 17. It was also demonstrated that both RPV and RYS were more sensitive to differentiate the two studied mixtures than absolute values of PV and YS.

STORAGE MODULUS FROM RHEOMETER TEST WITH DYNAMIC MODE

The storage modulus curve as a function of time were measured by the modified DSR (AR2000 rheometer) for all studied mixtures and modeled using the numerical approach developed in Chapter VI. The three modeled parameters (i.e., α: magnitude parameter, β: slope parameter, τ: shift parameter) characteristic of each mixture were determined. The objectives of this section are (1) to conduct a comparative assessment between the modeled parameters **(**α, β, and τ) and the heat evolution results, and (2) to verify if these parameters are useful to distinguish between the incompatible and normal mixtures.

The storage modulus curve for each studied mixture were measured for 5 hours test duration using the dynamic rheology mode (i.e., continuous oscillation mode) with the optimum target strain of 5.0E-05 (50 microstrain). The dynamic rheology tests for all the studied mixtures were conducted at a frequency of 6.28 radians per seconds (equivalent to 1Hz) same as determined during preliminary investigation.

The parameters α, β, and τ from the regressed model for all the studied mixture at 24°C are listed in Table 7-15. To investigate the temperature effect on the storage modulus, two selected mixtures (i.e., mix number 9 as normal and 22 as incompatible) were tested under two other temperature conditions (10 and 35^0C) and their modeled parameters are listed in Table 7-16.

The results are discussed in the following sub-sections in order to discuss the effect of SCMs, chemical admixtures and temperature separately. The bar graphs illustrating the comparison of each parameter α, β, and τ for cement with three different SCMs system are presented at Appendix D.

Table 7-15 α, β, and τ from the storage modulus model for C2 and C4 systems at 24°C.

	Experimental Design	% of Heat Evolution w.r.t. control after 48 hrs	Modeled Parameters		
			α	τ	β
C2 at 24°C (75°F)	***1_C2**	100.00	1.52E+07	125	2.8
	3_C2+F35	78.32	7.20E+06	45	1.9
	9_C2+F35+X15TD	70.52	6.00E+06	45	1.7
	21_C2+F35+X15DD	68.50	5.00E+06	45	1.6
	10_C2+F35+D17TD	59.25	4.50E+06	50	1.4
	22_C2+F35+D17DD	14.45	1.05E+06	24	1.1
	4_C2+C35	74.28	7.30E+06	65	1.9
	11_C2+C35+X15TD	73.99	6.00E+06	54	1.9
	23_C2+C35+X15DD	62.72	5.00E+06	50	1.7
	12_C2+C35+D17TD	22.54	1.60E+06	50	1.3
	24_C2+C35+D17DD	14.45	9.00E+05	20	1
	5_C2+S50	74.57	1.47E+07	90	0.9
	13_C2+S50+X15TD	73.70	1.20E+07	79	1
	25_C2+S50+X15DD	64.16	1.00E+07	73	0.9
	14_C2+S50+D17TD	62.14	9.00E+06	90	1
	26_C2+S50+D17DD	14.45	1.90E+06	50	0.6
C4 at 24°C (75°F)	***2_C4**	100.00	1.77E+07	110	1.3
	6_C4+F35	79.39	7.50E+06	70	2.7
	15_C4+F35+X15TD	78.48	6.80E+06	65	1.7
	27_C4+F35+X15DD	78.48	5.40E+06	60	1.6
	16_C4+F35+D17TD	73.03	4.90E+06	45	1.4
	28_C4+F35+D17DD	15.15	1.65E+06	31	1.8
	7_C4+C35	82.73	7.30E+06	55	2.3
	17_C4+C35+X15TD	73.33	6.40E+06	64	2.0
	29_C4+C35+X15DD	71.82	5.30E+06	52	1.9
	18_C4+C35+D17TD	70.00	4.80E+06	48	1.6
	30_C4+C35+D17DD	14.55	7.30E+05	39	1.2
	8_C4+S50	76.97	1.41E+07	108	1.56
	19_C4+S50+X15TD	75.45	1.11E+07	87	1.4
	31_C4+S50+X15DD	73.33	1.02E+07	79	1.2
	20_C4+S50+D17TD	59.39	8.56E+06	60	0.9
	32_C4+S50+D17DD	13.94	1.80E+06	45	0.7

Note: *identified as incompatible mixtures*

Table 7-16 α, β, and τ from the storage modulus model for normal and incompatible mixtures under different temperature conditions.

	Experimental Design	% of Heat Evolution w.r.t. control after 48 hrs	Modeled Parameters		
			α	τ	β
10°C (50°F)	9_C2+F35+X15TD	55.49	5.20E+06	50	1.9
	22_C2+F35+D17DD	10.98	6.50E+05	60	1.8
24°C (75°F)	9_C2+F35+X15TD	70.52	6.00E+06	45	1.7
	22_C2+F35+D17DD	14.45	1.05E+06	24	1.1
35°C (95°F)	9_C2+F35+X15TD	83.24	6.90E+06	25	1
	22_C2+F35+D17DD	16.18	1.60E+06	15	2

Note: *identified as incompatible mixtures*

Effects of Cement Type on the Storage Modulus Curve

The storage modulus (G') of cement only (C2 and C4) was measured for 5 hours as controls. As shown in Figure 7-18, no such major difference on stiffening process between the two cement alone mixtures is observed. However, C4 cement developed stiffness a bit more rapidly for the first 3 hours than C2 cement. After that, the modulus increased at nearly the same rate for both the cement. This phenomenon is agreement with the heat of hydration results, i.e., the second peak of C2 cement occurs at approximately 8.7 hours whereas the one of C4 cement occurs at 7.2 hours.

At a certain point of time, the development of the storage modulus is stabilized and converged to a particular value of the storage modulus. Since the magnitude α parameter is mathematically represent the ultimate value of the storage modulus, α parameter among the three parameters is investigated in details for comparison of each studied mixture. The parameter α of paste with C4 and C2 cement alone (i.e., 1.77E+07 for C4 and 1.52E+07 for C2) is the biggest one among all the studied mixtures and considered as controls.

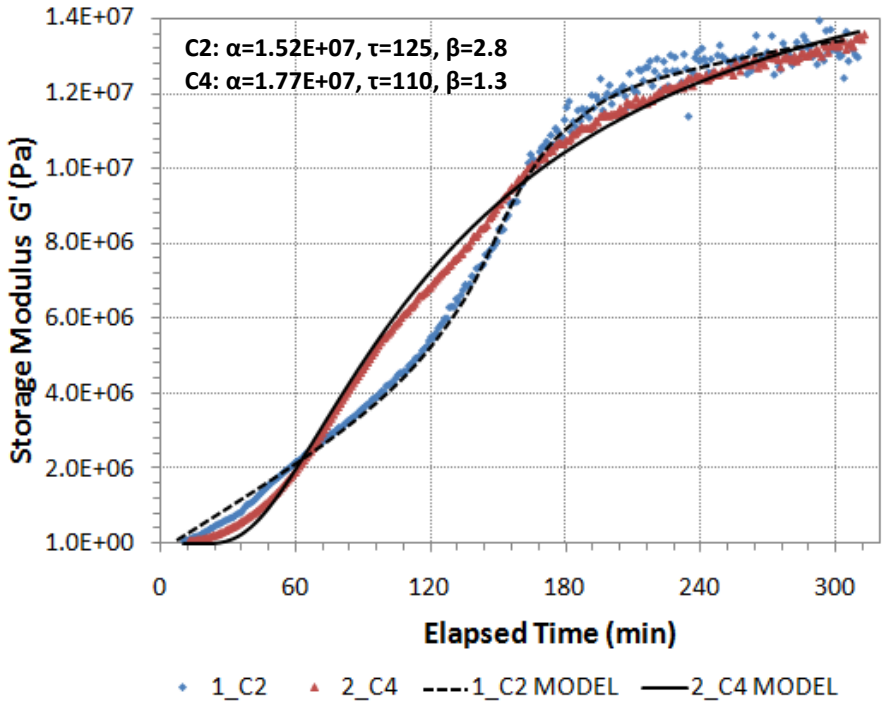

Figure 7-18 Measured and modeled storage modulus curve for C2 and C4 cements at 24°C.

Effects of SCMs on the Storage Modulus Curve

The addition of mineral admixtures to both the cements generally results in the reduction of the storage modulus development at an early age as shown in Figures 7-19 and 7-20. C2 + F35 and C2 + C35 show no discernable difference on the modulus development as manifested by almost the same α values (i.e., 7.2E+06 and 7.3E+06 respectively). The slag mix (i.e., C2 + S50 mix) shows higher α value (i.e., 1.47E+07, close to cement alone) than the fly ash mixtures. Thus, the magnitude parameter, α, declines in the order of C2 > C2+S50 > C2+F35 > C2+C35, as illustrated in Figure 7-19 and Table 7-15. This order is also the same as percent of heat evolution (Table 7-15). The other two parameters (i.e., τ and β) for all the studied mixtures do not show any good correlation either with α or percent of heat evolution. Therefore, α parameter was found to be potential to develop criterion for identifying incompatible mixtures. With C4, the same trend of the storage modulus curve as manifested by C2 is observed (Figure 7-20).

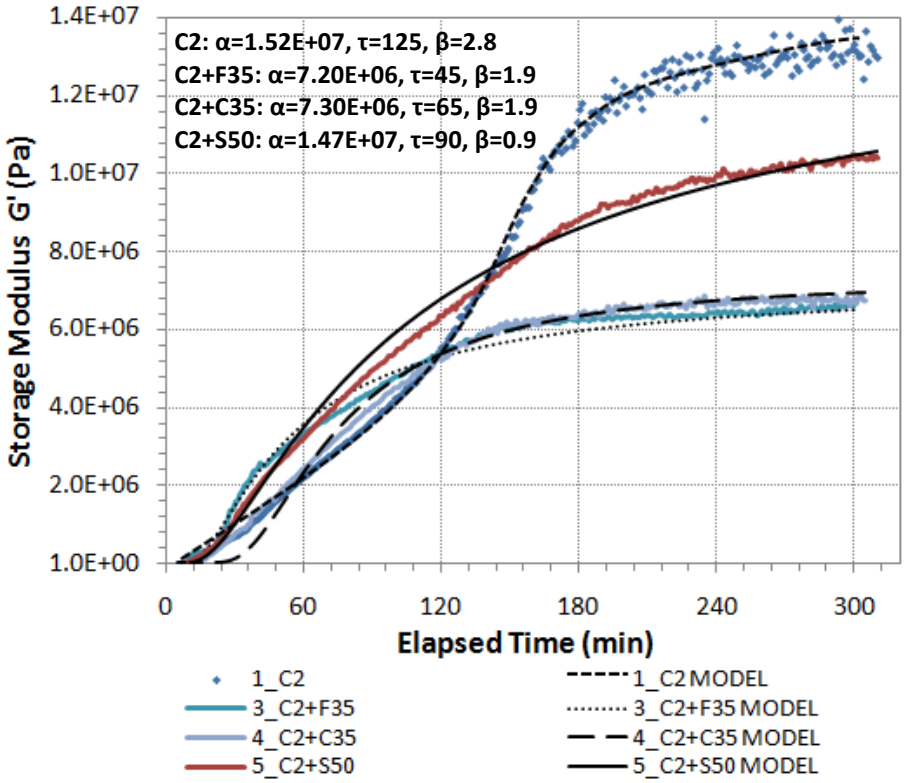

Figure 7-19 Measured and modeled storage modulus curve for C2 with SCMs at 24°C.

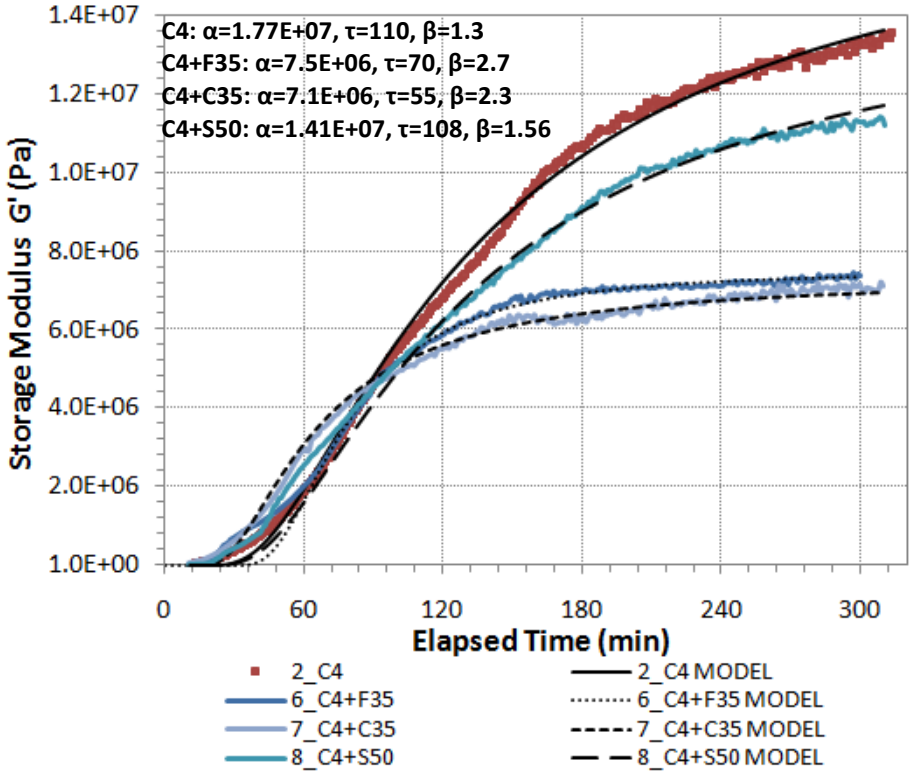

Figure 7-20 Measured and modeled storage modulus curve for C4 with SCMs at 24°C.

Effects of Chemical Admixtures on the Storage Modulus Curve

The Figures 7-21, 7-22, and 7-23 show the effects of chemical admixture type and dosage on the storage modulus curve as a function of time for C2 + F35, C2 + C35 and C + S50 mixtures. An overall effect of reduction in α parameter is evident for the mixtures with chemical admixture X15 both normal and high dosages regardless of SCM types. The value of α parameter tends to decrease slightly regardless of cement and SCM type in the order of Cement+SCM > Cement+SCM+X15TD > Cement+SCM+X15DD as illustrated in Figures 7-21, 7-22, and 7-23. This order is well matched with the percent of heat evolution data (Table 7-15).

On the other hand, the chemical admixture D17 with the double dosage showed a significant reduction in α value during the first 5 hours for all the mixtures (Figures 7-21 to 7-23 and Table 7-15). It is previously noted that the mixture containing D17 with double dosage (i.e., mixture no. 22, 24, and 26 for C2 cement system and 28, 30, and 32 for C4 cement system) were classified as the incompatible mixtures based on 30 percent of heat evolution criterion listed at Tables 7-1 and 7-2. Thus, extremely low value of α parameter for the mixtures with double dosage of D17 is in accordance with the heat evolution data. The C2 + Class C fly ash paste system with even typical dosage of D17 was identified as incompatible mixture based on the heat of hydration result (Table 7-1). Interestingly, it is observed that α for mixture no. 12 (C2 + C35 + D17TD) is significantly reduced (Figure 7-22) in comparison with C2 + F35 + D17TD (Figure 7-21) and C2 + S50 + D17TD (Figure 7-23). It is interesting to note that α value for mixture No. 12 (i.e., 6E+06) and mixture No. 24 (C2+C35+D17DD) is very close. Therefore, α parameter turned out to be a potential parameter to formulate acceptance criterion of incompatibility.

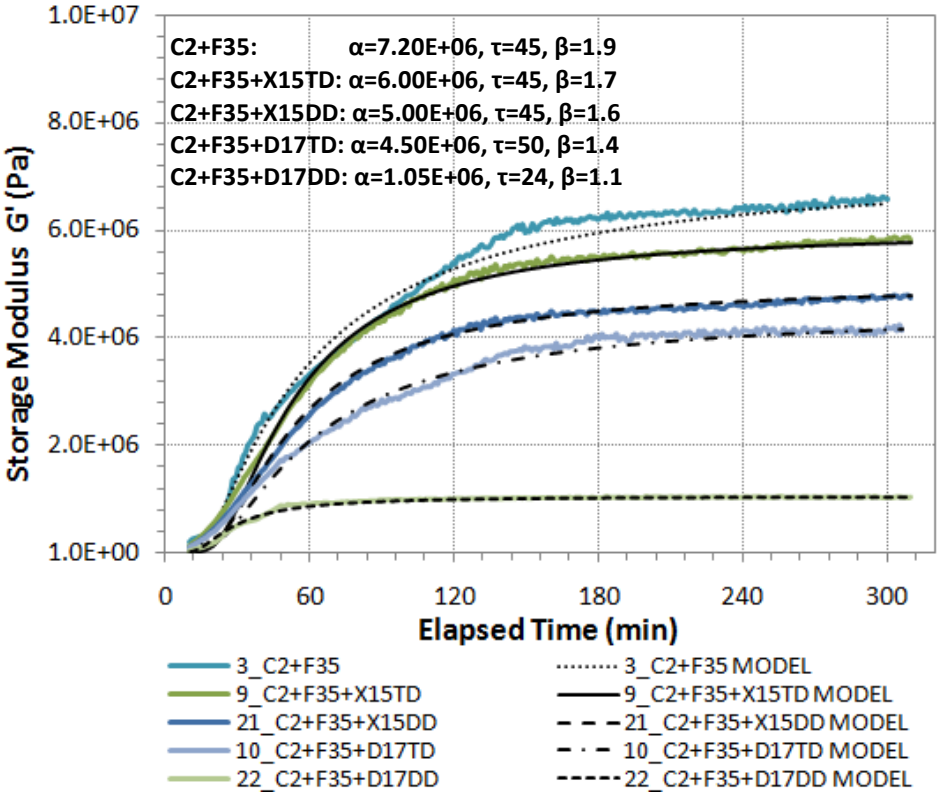

Figure 7-21 Measured and modeled storage modulus curve for C2 + F35 system at 24°C.

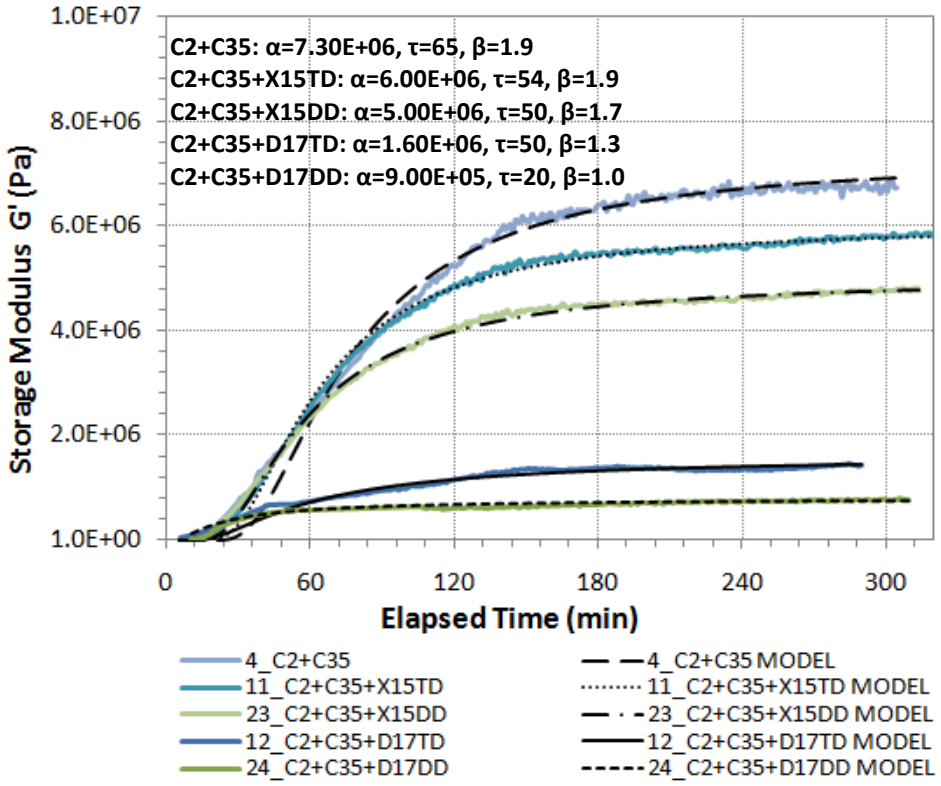

Figure 7-22 Measured and modeled storage modulus curve for C2 + C35 system at 24°C.

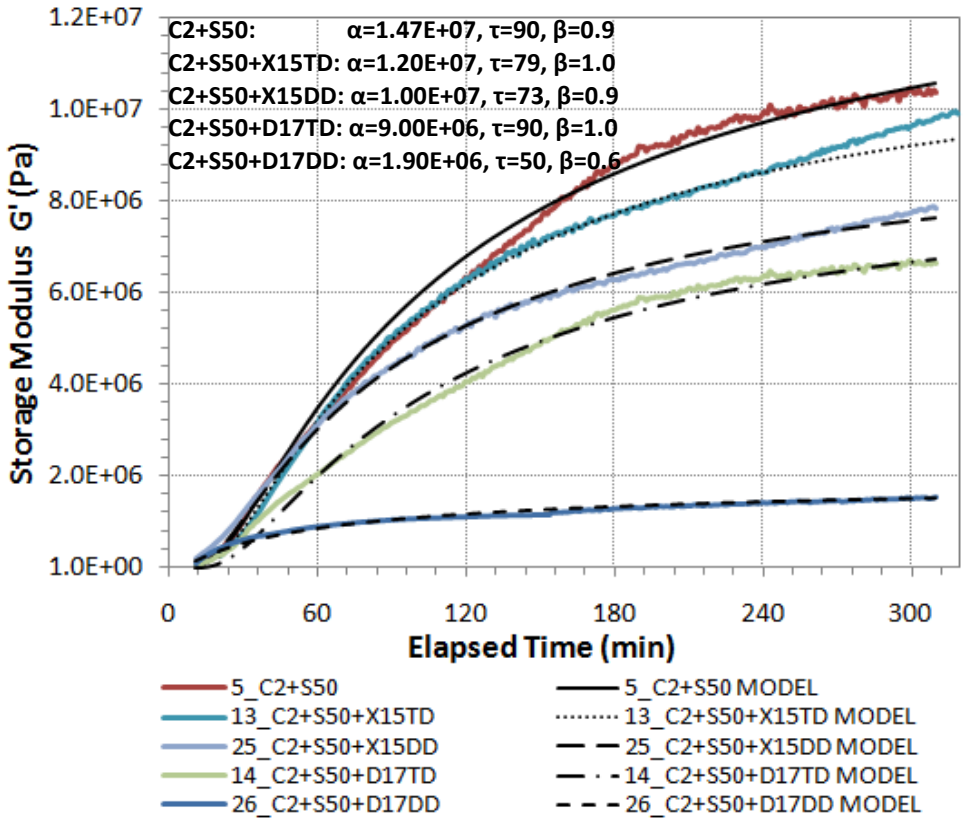

Figure 7-23 Measured and modeled storage modulus curve for C2 + S50 system at 24°C.

Effects of Temperature on the Storage Modulus Curve

The effect of temperature on the storage modulus curve was investigated for the two selected mixtures (i.e., mixture no.9 as normal and 22 as incompatible mixtures based on heat evolution criteria) These two mixtures were tested at 10°C (50°F) and 35°C (95°F) to simulate winter and summer time concrete placement and the results are presented in Figure 7-24. As expected, both the mixtures showed lowest α value at low temperature condition and highest α value at high temperature condition. However, the degree of change in the storage modulus curve along with the temperature change was not significant for both selected mixtures as illustrated in Figure 7-24. This phenomenon is well matched with the finding from heat of hydration data. Based on the heat of hydration results it was noted that the mixture no. 9 (i.e.,

9_C2+F35+X15TD) and no. 22 (i.e., 22_C2+F35+ D17DD) show normal and abnormal behavior of heat evolution respectively regardless of temperature changes listed in Table 7-16.

Therefore, the effect of low temperature resulted in the reduction of α whereas the one with high temperature caused the increase of α for the studied mixtures. Moreover, it was observed that the shift parameter, τ, shows some correlation with the ambient temperature like α parameter. For both the mixtures, the τ parameter tends to decrease as the ambient temperature increases. Since low ambient temperature of 10°C retarded the stiffening process at an early age, the storage modulus curve shifted towards the right which caused the value of τ parameter to increase. In case of high ambient temperature of 35°C, the stiffening process of the tested mixture was accelerated which caused the value of τ parameter to decrease.

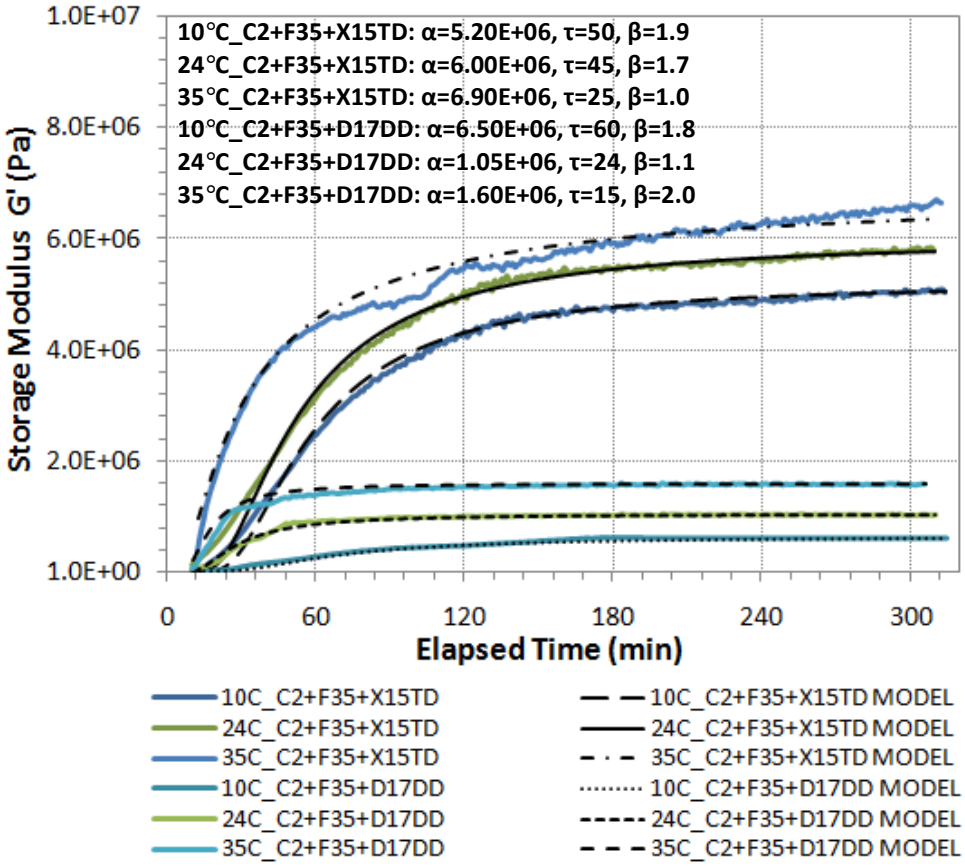

Figure 7-24 Measured and modeled storage modulus curve for the selected mixtures under different temperature conditions.

ACCEPTANCE CRITERIA BASED ON DYNAMIC RHEOLOGICAL PARAMETERS

An attempt has been made to develop acceptance criteria of incompatibility based on the test results on dynamic rheological parameters generated from the laboratory investigation and discussed below.

The incompatible mixtures that were identified based on 30 percent of heat evolution criteria are listed in Tables 7-15 and 7-16. The mixture numbers 12, 22, 24, and 26 for C2 cement system and 30, 32, and 34 for C4 cement system were identified as incompatible mixtures. The storage modulus curve parameters α, τ, and β corresponding to the incompatible mixtures are then compared with the percent of heat evolution to see whether identification of incompatible mixtures based on the two methods supports each other. The key findings are as follows:

- An incompatible mixture shows a very low value of α parameter. It is interesting to see that all the incompatible mixtures identified by 30 percent criterion of heat evolution (12, 22, 24, 26 for C2 cement system and 30, 32, 34 for C4 cement system) show very low α values (Table 7-15). This is in good agreement between heat evolution and the storage modulus based criteria. Therefore, the parameter α is capable to identify incompatible mixtures from normal ones.
- The modeled parameter α is more sensitive to change in the mineral and chemical admixture type and dosage than the other two parameters, i.e., τ, and β.
- Due to the limited tests under low and high ambient temperature conditions, the range of α parameter for the marginal mixture was determined based on the lowest α value among the normal mixtures and the highest α value among the incompatible mixtures (Table 7-

17). The range of α parameter for the marginal has served to fix the upper limit for the acceptance criterion of incompatibility.

- Based on the values of α parameter for the studied mixtures (Tables 7-15 and 7-16), the possible acceptance criterion is formulated and given in Table 7-18.

Table 7-17 Incompatible mixtures with C2 and C4 cements under different temperatures.

	Mixture Combinations	% of Heat Evolution w.r.t. Control After 48 hrs	Parameters from Modulus Curve Model		
			α	τ	β
24°C (75°F)	22_C2+F35+D17DD	14.45	1.05E+06	24	1.1
	12_C2+C35+D17TD	22.54	1.60E+06	50	1.3
	24_C2+C35+D17DD	14.45	9.00E+05	20	1
	26_C2+S50+D17DD	14.45	1.90E+06	50	0.6
	28_C4+F35+D17DD	15.15	1.65E+06	31	1.8
	30_C4+C35+D17DD	14.55	7.30E+05	39	1.2
	32_C4+S50+D17DD	13.94	1.80E+06	45	0.7
10°C (50°F)	22_C2+F35+D17DD	10.98	6.50E+05	60	1.8
35°C (95°F)	22_C2+F35+D17DD	16.18	1.60E+06	15	2

Table 7-18 Criteria of incompatibilities based on α, τ, and β parameters.

Criteria	α	τ	β
Incompatible Mixtures	< 2.0E+06	N/A	N/A
Marginal Mixtures	2.0E+06 – 4.0E+06	N/A	N/A
Normal Mixtures	> 4.0E+06	N/A	N/A

A perusal of Table 7-18 showed the following observations:

- In dynamic rheology method, the normal and incompatible mixtures can be clearly distinguished based on the α parameter from the regression model of the stororage modulus curve for the tested cement paste. Moreover, the reproducibility of the α parameter is generally good as manifested by lower coefficient of variation (CoV) % (discussed later and presented in Tables 7-19).
- A generalized criterion of cement-admixture incompatibilities irrespective of SCM type and temperature is obtained based on the dynamic rheology mode. This is a good indication of the modified DSR-based rheology method to identify incompatible mixtures.

REPRODUCIBILITY OF DYNAMIC RHEOLOGICAL PARAMETERS

The reproducibility tests of dynamic rheological parameters using the modified DSR (AR2000) were conducted and described in this section. Reproducibility of the storage modulus curve as a function of time was determined by comparing the value of the parameter α, τ, and β from the three replicas. The value of the parameter α, τ, and β based on the two mixtures (i.e., mixture no. 9 and 22) at three different temperatures with three replicas are presented in Table 7-19. The coefficient of variation (CoV %) were calculated based on three replicas for the studied mixtures and are included in Table 7-19. It is to be noted that the mixture with C2 + F35 + X15TD was identified as a normal mixture and the mixture with C2 + F35 + D17DD was identified as an incompatible mixture based on both the dynamic rheological parameters and heat of hydration data (Figure 7-21 and Table 7-17).

Table 7-19 Reproducibility of α, τ, and β parameters.

Mixture Combination			α	α CoV%	τ	τ CoV%	β	β CoV%
C2+ F35+ X15TD	10°C	1	5.20E+06	4.16	50	11.90	1.9	12.01
		2	5.52E+06		45		1.5	
		3	5.10E+06		57		1.8	
	24°C	1	6.00E+06	5.91	45	9.12	1.7	13.33
		2	5.80E+06		48		1.5	
		3	6.50E+06		40		1.3	
	35°C	1	6.90E+06	8.65	25	11.27	1	13.48
		2	7.60E+06		20		1.3	
		3	6.40E+06		22		1.1	
C2+ F35+ D17DD	10°C	1	6.50E+05	2.71	60	9.09	1.8	14.24
		2	6.30E+05		50		1.5	
		3	6.65E+05		55		2	
	24°C	1	1.05E+06	6.84	24	11.50	1.1	12.39
		2	1.20E+06		20		1.2	
		3	1.10E+06		25		1.4	
	35°C	1	1.60E+06	8.57	15	13.32	2	11.27
		2	1.90E+06		12		2.5	
		3	1.75E+06		12		2.2	

Table 7-19 indicates that the coefficient of variation (CoV) % of α parameter is below 10. The CoV% of the τ and β parameters shows relatively high values, i.e., varies from 9 to 15 Therefore, the reproducibility of α parameter is generally better than that of τ and β parameters as manifested by lower CoV %. It was also demonstrated that α parameter was more sensitive to differentiate the two studied mixtures than the other τ and β parameters.

MINI SLUMP CONE TEST

The mini slump test was conducted for all the studied mixtures (according to Table 6-2) using a mini slump cone. The pat area results from mini slump tests for C2 and C4 cement system as a function of time and temperature are presented in Tables 7-20 and 7-21 respectively. The graphs of the pat area as a function of time are presented in Appendix F. In general, it is considered that the larger the pat area the higher the fluidity.

Table 7-20 Mini slump test data for C2 cement system under different temperatures.

	Exp. #	5min	10min	20min	30min	Rate of pat area Loss
		mm^2	mm^2	mm^2	mm^2	5 to 30 min
C (50°F)	3_C2+F35	5153.0	4536.5	4185.4	4071.5	43.3
	9_C2+F35+X15TD	6939.8	5741.5	5410.6	4778.4	86.5
	21_C2+F35+X15DD	8741.7	7238.2	6013.2	5410.6	133.2
	10_C2+F35+D17TD	9331.3	7088.2	6647.6	6291.2	121.6
	22_C2+F35+D17DD	12568.1	11785.9	10659.6	9589.9	119.1
	4_C2+C35	5026.5	4071.5	3631.7	3318.3	68.3
	11_C2+C35+X15TD	9245.9	7620.1	4901.7	4656.6	183.6
	23_C2+C35+X15DD	11309.7	8908.2	7238.2	5876.5	217.3
	12_C2+C35+D17TD	12767.6	9589.9	8741.7	7543.0	209.0
	24_C2+C35+D17DD	15614.5	14313.9	12469.0	11499.0	164.6
	5_C2+S50	5026.5	4477.0	4417.9	3959.2	42.7
	13_C2+S50+X15TD	7389.8	6221.1	6151.4	5607.9	71.3
	25_C2+S50+X15DD	9503.3	7088.2	6866.1	6361.7	125.7
	14_C2+S50+D17TD	8992.0	7932.7	7088.2	7013.8	79.1
	26_C2+S50+D17DD	12568.1	11785.9	9852.0	9076.3	139.7
24°C (75°F)	*1_C2	5085.7	3655.8	2642.1	2623.9	98.4
	3_C2+F35	5345.6	4839.8	4596.3	4015.2	53.2
	9_C2+F35+X15TD	6647.6	5741.5	4963.9	4185.4	98.5
	21_C2+F35+X15DD	8332.3	7620.1	5808.8	5153.0	127.2
	10_C2+F35+D17TD	9160.9	7313.8	6221.1	6221.1	117.6
	22_C2+F35+D17DD	12667.7	11309.7	8824.7	7543.0	205.0
	4_C2+C35	5541.8	4242.9	3369.6	3068.0	99.0
	11_C2+C35+X15TD	7466.2	5674.5	4901.7	4185.4	131.2
	23_C2+C35+X15DD	9331.3	6792.9	5410.6	4778.4	182.1
	12_C2+C35+D17TD	11028.8	8171.3	6792.9	6013.2	200.6
	24_C2+C35+D17DD	15174.7	12667.7	9503.3	8171.3	280.1
	5_C2+S50	4901.7	4242.9	4071.5	4071.5	33.2
	13_C2+S50+X15TD	6720.1	5808.8	4778.4	4901.7	72.7
	25_C2+S50+X15DD	8576.7	7088.2	6866.1	6221.1	94.2
	14_C2+S50+D17TD	9331.3	7932.7	6939.8	6647.6	107.3
	26_C2+S50+D17DD	11785.9	10659.6	8908.2	8091.4	147.8
35°C (95°F)	3_C2+F35	3631.7	3217.0	2922.5	2687.8	37.8
	9_C2+F35+X15TD	4417.9	3631.7	3318.3	3019.1	56.0
	21_C2+F35+X15DD	6647.6	4477.0	3793.7	3421.2	129.1
	10_C2+F35+D17TD	6647.6	4359.2	3685.3	3318.3	133.2
	22_C2+F35+D17DD	10568.3	8659.0	5808.8	3793.7	271.0
	4_C2+C35	3685.3	2780.5	2419.2	1847.5	73.5
	11_C2+C35+X15TD	4359.2	3267.5	2507.2	2123.7	89.4
	23_C2+C35+X15DD	6647.6	3631.7	2551.8	2123.7	181.0
	12_C2+C35+D17TD	7088.2	3959.2	2734.0	2290.2	191.9
	24_C2+C35+D17DD	11979.1	8494.9	4778.4	2970.6	360.3
	5_C2+S50	3631.7	3318.3	3166.9	2922.5	28.4
	13_C2+S50+X15TD	4963.9	4128.2	3739.3	3473.2	59.6
	25_C2+S50+X15DD	6792.9	6013.2	5476.0	5026.5	70.7
	14_C2+S50+D17TD	7466.2	6013.2	4656.6	4656.6	112.4
	26_C2+S50+D17DD	10117.7	7854.0	6720.1	5876.5	169.6

Note: *identified as incompatible mixtures* *identified as marginal mixtures*

Table 7-21 Mini slump test data for C4 cement system under different temperatures.

	Exp. #	5min	10min	20min	30min	Rate of pat area Loss
		mm^2	mm^2	mm^2	mm^2	5 to 30 min
10°C (50°F)	6_C4+F35	5541.8	4656.6	4071.5	3848.5	67.7
	15_C4+F35+X15TD	7543.0	5876.5	5153.0	4417.9	125.0
	27_C4+F35+X15DD	10751.3	8171.3	6221.1	5216.8	221.4
	16_C4+F35+D17TD	11689.9	8659.0	6647.6	5741.5	237.9
	28_C4+F35+D17DD	15065.7	11309.7	9940.2	7775.6	291.6
	7_C4+C35	5674.5	4536.5	4071.5	3525.7	86.0
	17_C4+C35+X15TD	9940.2	6720.1	5741.5	4359.2	223.2
	29_C4+C35+X15DD	11979.1	8659.0	6866.1	5607.9	254.8
	18_C4+C35+D17TD	13684.8	9676.9	7620.1	5876.5	312.3
	30_C4+C35+D17DD	15948.5	13069.8	11028.8	8741.7	288.3
	8_4+S50	5410.6	4536.5	4128.2	3848.5	62.5
	19_C4+S50+X15TD	8091.4	6013.2	5476.0	4963.9	125.1
	31_C4+S50+X15DD	10386.9	8413.4	6866.1	6151.4	169.4
	20_C4+S50+D17TD	10028.7	8576.7	7088.2	6291.2	149.5
	32_C4+S505+D17DD	13788.6	11404.2	9245.9	7466.2	252.9
24°C (75°F)	*2_C4	3731.2	3252.3	3117.2	2922.5	32.3
	6_C4+F35	4128.2	3848.5	3848.5	3631.7	19.9
	15_C4+F35+X15TD	6647.6	5026.5	4717.3	4300.8	93.9
	27_C4+F35+X15DD	8659.0	6082.1	5476.0	4901.7	150.3
	16_C4+F35+D17TD	9245.9	7543.0	5345.6	5281.0	158.6
	28_C4+F35+D17DD	11979.1	10751.3	8824.7	5741.5	249.5
	7_C4+C35	4596.3	4185.4	3793.7	3369.6	49.1
	17_C4+C35+X15TD	7088.2	5476.0	4839.8	4071.5	120.7
	29_C4+C35+X15DD	8992.0	7088.2	6082.1	5153.0	153.6
	18_C4+C35+D17TD	10028.7	6647.6	4717.3	3369.6	266.4
	30_C4+C35+D17DD	13581.3	8659.0	6082.1	4015.2	382.6
	8_C4+S50	4778.4	4071.5	3959.2	3739.3	41.6
	19_C4+S50+X15TD	7163.0	5674.5	4901.7	4417.9	109.8
	31_C4+S50+X15DD	9589.9	8171.3	6575.5	5944.7	145.8
	20_C4+S50+D17TD	9503.3	7620.1	5944.7	5674.5	153.2
	32_C4+S50+D17DD	12370.2	10659.6	8251.6	6503.9	234.7
35°C (95°F)	6_C4+F35	3473.2	3166.9	2922.5	2780.5	27.7
	15_C4+F35+X15TD	4242.9	3793.7	3525.7	3267.5	39.0
	27_C4+F35+X15DD	6503.9	4778.4	4128.2	3525.7	119.1
	16_C4+F35+D17TD	6792.9	5089.6	4300.8	3421.2	134.9
	28_C4+F35+D17DD	9852.0	7697.7	5281.0	3578.5	250.9
	7_C4+C35	3525.7	2874.8	2463.0	2164.8	54.4
	17_C4+C35+X15TD	4300.8	3369.6	2734.0	2290.2	80.4
	29_C4+C35+X15DD	6432.6	4477.0	3217.0	2463.0	158.8
	18_C4+C35+D17TD	6866.1	4656.6	3318.3	2332.8	181.3
	30_C4+C35+D17DD	11499.0	5674.5	3959.2	3166.9	333.3
	8_4+S50	3631.7	3318.3	3166.9	2642.1	39.6
	19_C4+S50+X15TD	4778.4	4242.9	3848.5	3019.1	70.4
	31_C4+S50+X15DD	6575.5	5808.8	5410.6	4417.9	86.3
	20_C4+S50+D17TD	7088.2	6221.1	5410.6	4071.5	120.7
	32_C4+S50+D17DD	9676.9	7620.1	7088.2	4417.9	210.4

Note: *identified as incompatible mixtures* *identified as marginal mixtures*

Effects of SCMs on the Mini Slump Pat Area

The mini slump pat area of C2 cement only with water to binder ratio (w/b) of 0.4 at 24°C is approximately 5000 mm^2 at 5 minutes after mixing. An effort was made to fit the same pat area of 5000 mm^2 for the cement with different mineral admixtures. This resulted w/b for the mixtures with 35% replacement of Class F fly ash is 0.38 whereas those with Class C fly ash and slag are 0.36 and 0.45 respectively to maintain a constant mini-slump flow. It is to be noted that the addition of both types of fly ash increases the fluidity of mixtures and needs less w/b than the cement only mixture due to its spherical shape and high specific gravity. On the other hand, the addition of the granulated slag decreases the fluidity and needs more w/b due to its amorphous shape and low specific gravity.

Effects of Chemical Admixtures on the Mini Slump Pat Area

The addition of both the chemical admixtures, i.e., X15 and D17, increases the fluidity of cement paste (i.e., increase of pat areas). The double dosage of chemical admixture always makes pat areas bigger than the typical dosage irrespective of the type of chemical admixtures. However, the mixtures with the D17 chemical admixture show always larger pat areas (i.e., higher fluidity) than that with the X15 chemical admixture irrespective of SCMs types and temperature.

Effects of Temperature on the Mini Slump Pat Area

The mini slump tests were carried out at all three selected temperatures, i.e., 10°C (50°F), 24^0C (75^0F), and 35°C (95°F) to verify the temperature effects on the flow properties of cement pastes (Table 6-7). The pat areas for all the tested mixtures irrespective of the types of SCMs and

chemical admixture generally show a decreasing trend as the ambient temperature increases. This is an indication of decrease in fluidity with increasing temperature as expected.

It is observed from the foregoing discussion that mini slump cone test can detect the changes in terms of measuring different pat areas as a result of (i) adding different types of SCMs and chemical admixtures, and (ii) temperature changes. It would be interesting to see how the mini slump results to compare with the rheological parameters determined earlier. The plots of five minute pat area versus the absolute rheological parameters (i.e., plastic viscosity and yield stress) are presented in Figures 7-25 and 7-26 respectively. The graphs of the rate of pat area loss versus the rate of change of rheological parameters (i.e., RPV and RYS) are plotted at Figures 7-27 and 7-28 respectively. The rate of pat area loss was calculated by dividing elapsed time of 25 minutes to the difference in the pat area between 5 and 30 minutes. Some important observations are listed below:

- It shows reasonably good correlation ($R^2 = 0.80$) between the mini slump pat area (5 minutes after mixing) and the yield stress data from the rheology as manifested in Figure 7-25. Figure 7-25 indicates that paste mixtures with higher pat areas have lower yield stresses and vice versa irrespective of SCMs, chemical admixtures, and temperature.

This is in good agreement with the observation by earlier researchers (*28*). On the other hand, a poor correlation ($R^2 = 0.53$) exists between five minute pat areas and plastic viscosity, as illustrated at Figure 7-26.

- Pat area measurement can be considered as an indirect way to measure yield stress as a good correlation between these parameters is manifested (Figure 7-25), but not to measure plastic viscosity (Figure 7-26). Therefore, pat area measurement provides partial information pertaining to the rheology behavior whereas the modified DSR measurement provides the complete characterization of cement paste rheology. Consequently, criteria based on mini slump pat area to identify incompatible mixtures have the same limitations as with yield stress (discussed earlier).
- The results of the rate of pat area loss have no such a good correlation with the results of RPV and RYS (low R^2 of 0.53 and 0.61 respectively as illustrated in Figures 7-27 and 7-28). This is an indication that the rate of pat area loss cannot serve as an effective criterion.

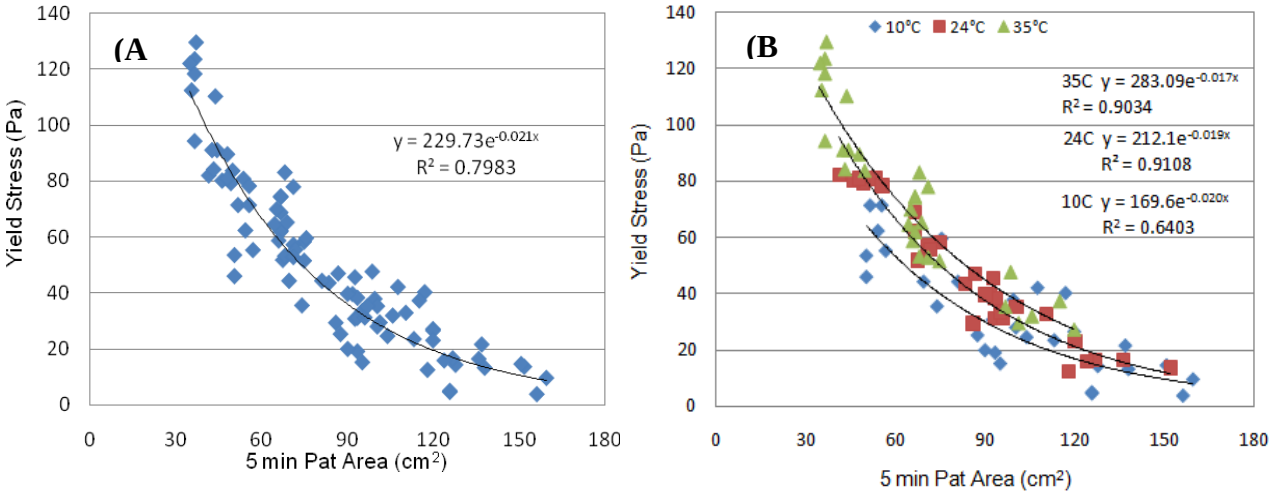

Figure 7-25 Correlation between YS and five minute pat area for all studied mixtures (left) and under different temperature conditions (right).

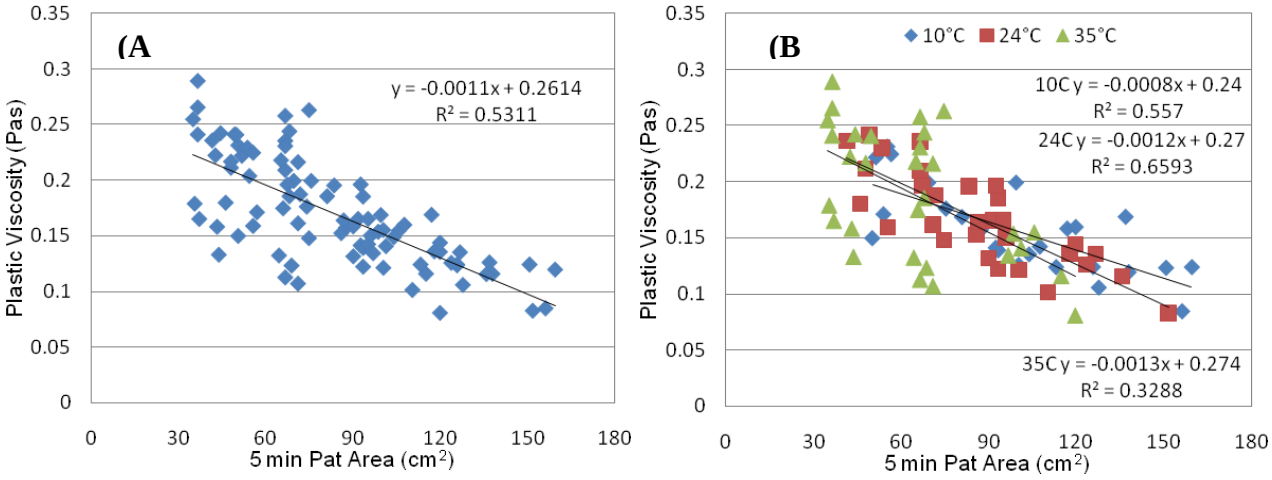

Figure 7-26 Correlation between PV and five minute pat area for all studied mixtures (left) and under different temperature conditions (right).

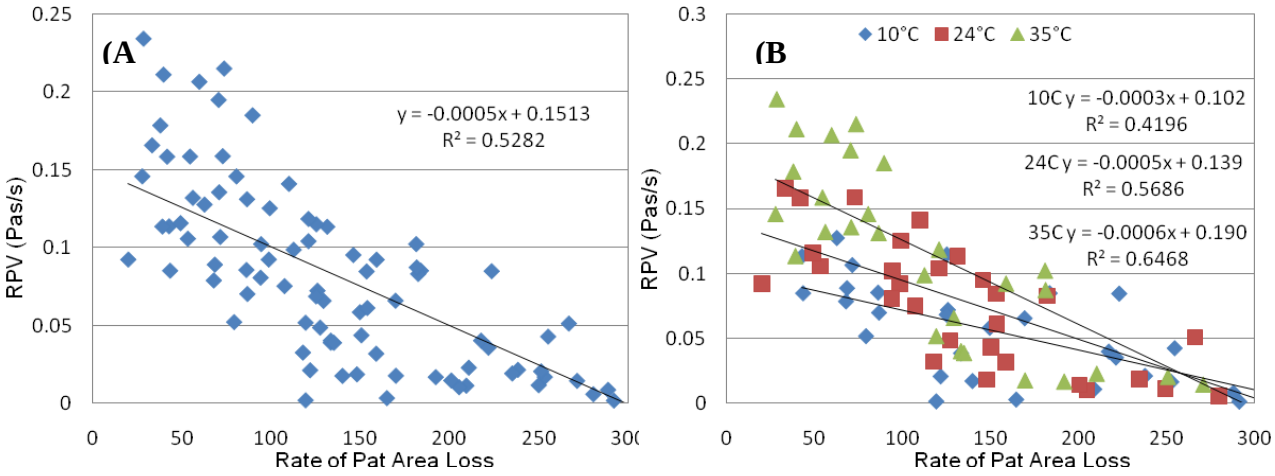

Figure 7-27 Correlation between RPV and rate of pat area loss for all studied mixtures (left) and under different temperature conditions (right).

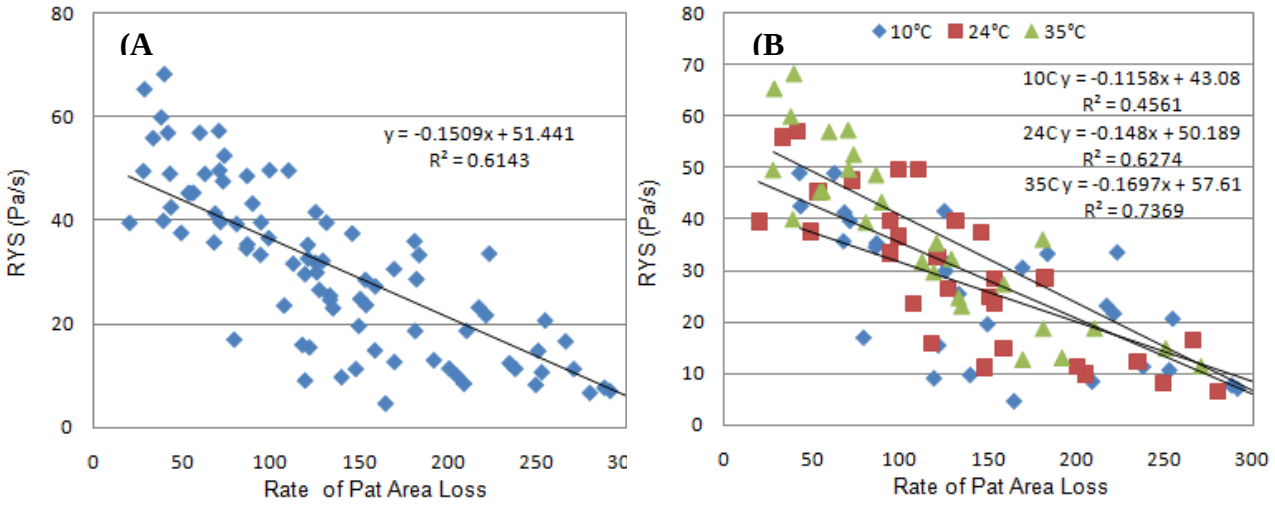

Figure 7-28 Correlation between RYS and rate of pat area loss for all studied mixtures (left) and under different temperature conditions (right).

ACCEPTANCE CRITERIA BASED ON MINI SLUMP TEST

An effort was made to identify the incompatible mixtures using the data from mini slump tests. The rate of pat area loss and five minute pat area are considered as potential candidates to develop some possible criteria. A comparative assessment of the mixture categorization (normal, marginal and incompatible) by both the heat evolution and rate of pat area loss has been made and observations are described below:

- A large number of normal and marginal mixtures (based on 30 percent of heat evolution criteria in Table 7-1) are identified as incompatible mixtures based on the rate of pat area loss criteria especially under low temperature condition, as shown in Figure 7-29.
  In addition to that, one incompatible mixture (i.e., mixture no. 26) is identified as a normal and marginal one at 24 and 35°C respectively. Therefore, large number of mismatches is evident. The rate of pat area loss for each studied mixture in details is presented in Appendix G.
- Additionally, the rate of pat area loss-based criterion changes drastically with the type of cement and temperature as opposed to RPV and RYS based rheology criteria.

For above reasons, the rate of pat area loss has not appeared to be an effective criterion of incompatibility as pointed out earlier.

The five minute pat area does not appear to a good criterion of incompatibility either because of the following reasons:

- A common criterion for both the cements (i.e., C2 and C4 cements) cannot be established.
- The results of five minute pat area are prone to alter rapidly with the types of SCMs, chemical admixture, and temperature indicating a good correlation with the yield stress

(Figure 7-25). However, the yield stress by the rheology tests was verified not to be suitable for an effective acceptance criterion.

- In five minute pat area-based criterion, a large number of normal mixtures (based on 30 percent of heat evolution criteria in Table 7-1) are identified as incompatible mixtures, as shown in Figure 7-30.

Therefore, it can be concluded that both the rate of pat area loss and five minute pat area cannot be accepted as an effective criteria of incompatibility. However, more number of data including different types of fly ash, cement, and chemical admixture as a function of temperature needs to be generated in order to confirm this conclusion.

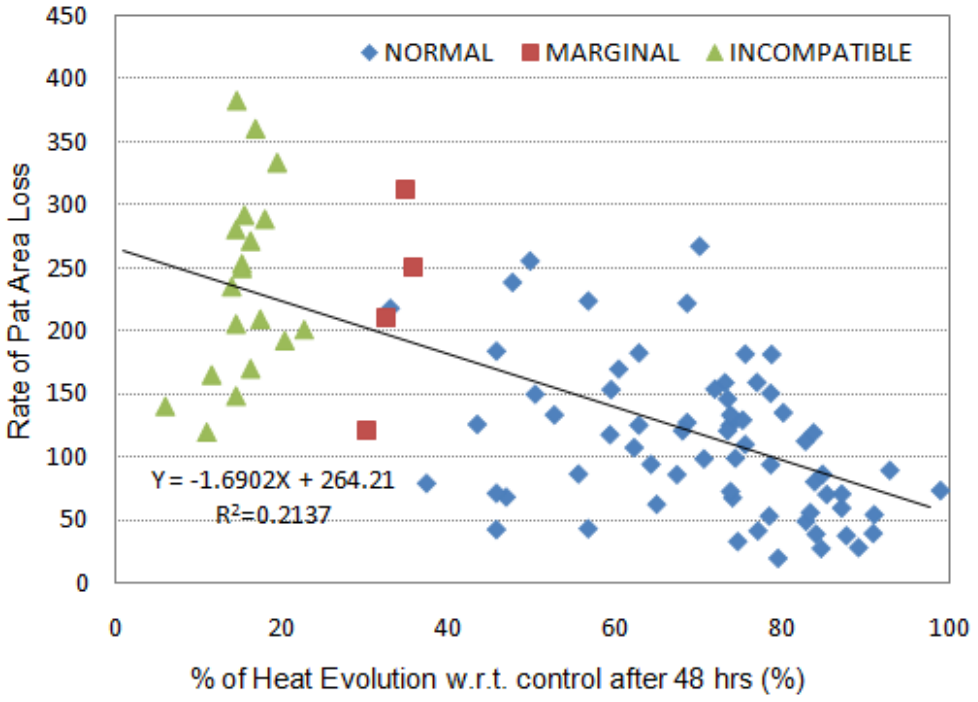

Figure 7-29 Rate of pat area loss vs. percent of heat evolution w.r.t. control after 48 hours.

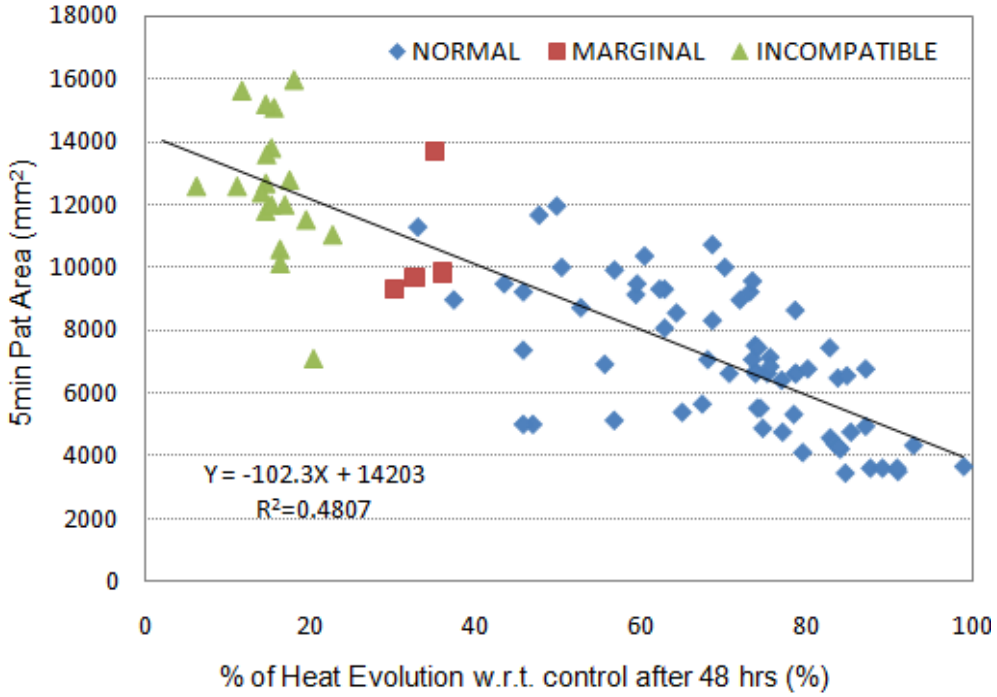

Figure 7-30 Five minute pat area vs. percent of heat evolution w.r.t. control after 48 hours.

CHAPTER VIII

CONCLUSIONS AND RECOMMENDATIONS

In this study, the rheological parameters of a series of cement paste mixtures with different temperature conditions were measured by the modified dynamic shear rheometer (DSR). Based on the experimental results, the rheological parameters in two different rheology modes of operations (i.e., static and dynamic rheological modes) have been investigated to identify incompatibilities among cement and mineral/chemical admixtures considering the effect of cement, supplementary cementitious materials (SCMs), type and dosage of chemical admixtures, and temperature.). The heat of hydration tests by the isothermal conduction calorimeter tests and setting time tests by the Vicat apparatus were performed and analyzed as supporting evidences. Mini slump cone test was conducted to investigate its feasibility to identify the incompatible mixtures from the normal mixtures similar to rheology method. The developed acceptance criteria of incompatibility can help the concrete industry to detect problematic concrete mixtures before concrete is placed.

CONCLUSIONS

Based on the results presented in this study, the following conclusions can be drawn:

- The static rheological parameters (i.e., plastic viscosity and yield stress) with 1 mm parallel plate gap are the most representative to distinguish the change of chemical admixture dosage based on the reproducibility and sensitivity.
- The time-functioned static rheological parameters, the rate of change of plastic viscosity (RPV) and rate of change of yield stress (RYS), are able to distinguish clearly the normal mixtures from the incompatible ones. However, the RPV is more sensitive and

reproducible than the RYS in the distinction between normal and abnormal mixtures. Therefore, the acceptance criteria based on RPV has a great potential to identify incompatible mixtures.

- It was verified that the storage modulus curve as a function of time for the dynamic rheological test (i.e., continuous oscillation mode) with the parallel plate geometry shows the best reproducibility with the target strain of 5.0E-05 (50 microstrain).
- The dynamic rheology results indicate the storage modulus curves as a function of time can be well described by the developed exponential law dependence model for all the studied mixtures.
- The α parameter (i.e., magnitude parameter) from the regression model of the storage modulus curve is more sensitive than the other two parameters (i.e., τ and β) to identify confirmed incompatible mixtures based on the percent of heat evolution criteria. Therefore, the α parameter-based acceptance criterion can also be considered as another potential option for identifying incompatible mixtures.
- At typical dosage of the lignin-based WRRA chemical admixture, combination of Class C fly ash and C2 cement showed abnormal heat evolution manifested by the absence of the second peak after 48 hours of testing period due to mineral and chemical admixture interaction.
- The heat of hydration tests by the isothermal conduction calorimeter and setting time tests by the Vicat apparatus have strongly supported the rheology-based observations. In other words, incompatible mixtures can also be detected based on the heat of hydration and setting time characteristics, however, these test methods are time consuming and labor intensive compared with rheology testing by the modified DSR.

- There exists a good correlation between the resulting of five minute pat area by the mini slump cone tests and the yield stress by the static rheology tests whereas a poor correlation exists between the resulting of five minute pat area and the plastic viscosity.
- Cement paste rheology based on both the static and dynamic methods using the modified DSR has a great potential to identify cement-mineral/chemical admixture incompatibilities. This will ultimately help material suppliers, concrete producers, and other users to detect problematic combination of concrete ingredients during the mixture design process and thereby, to avoid concrete cracking and other durability issues due to incompatibilities.

RECOMMENDATIONS

The following recommendations are made for continued research in this field:

- The study should be expanded to investigate the influences of other types of chemical admixture on the incompatibilities among cement, mineral, and chemical admixtures.
- Further study should be devoted to the effects of soluble alkali contents of cements on cement/chemical admixture incompatibilities.
- The influences of other supplementary cementitious material systems on incompatibility issues should be investigated by expanding the test program.
- Further work should be conducted to correlate the cement pate rheology to mortar or concrete rheology.

REFERENCES

1. Dodson, V.H., and T.D. Hayden. Another Look at the Portland Cement/Chemical Admixture Incompatibility Problem. *Cement, Concrete and Aggregates*, Vol. 11, No. 1, 1989, pp. 52-56.
2. Johnston, C.D. Admixture-Cement Incompatibility: A Case History. *Concrete International: Design and Construction*, Vol. 9, No. 4, 1987, pp. 51-60.
3. Tuthill, L.H. A Case of Abnormally Slow Hardening Concrete for Tunnel Lining. *Journal of the American Concrete Institute*, Vol. 32, No. 9, 1961, pp. 1091-1109.
4. Wong, G.S., A.M. Alexander, R. Haskins, T.S. Poole, P.G. Malone, and L. Wakeley. *Portland-Cement Concrete Rheology and Workability: Final Report*, FHWA-RD-00-025. Federal Highway Administration, Mclean, Virginia, April 2001.
5. Mindess, S., J.F. Young, and D. Darwin. *Concrete*. 2nd edition, Prentice-Hall, Inc, Upper Saddle River, New Jersey, 2002.
6. Kosmatka, S.H., B. Kerkhoff, and W.C. Panarese. Design and Control of Concrete Mixtures, 14th Edition, EB001.14T, *Portland Cement Association*, Skokie, Illinois, 2002, pp. 355.
7. Bartos, P. *Fresh Concrete: Properties and Tests.* Elsevier, New York, 1992.
8. Young, J.F., S. Mindess, R.J. Gray, and A. Bentur. *The Science and Technology of Civil Engineering Materials.* Prentice-Hall, Inc, Upper Saddle River, New Jersey, 1998, pp. 76-80.
9. Tattersall, G.H., and P.F.G. Banfill. *The Rheology of Fresh Concrete*. Pitman, London, England, 1983.
10. Hunter, R.J. *Foundation of Colloid Science.* Vol. 1, Clarendon Press, Oxford, 1987.
11. Lewis, J.A. Ceramic Suspensions, *Ceramic Engineering 321 Lecture notes*, 1994.
12. Yanez, J.A., T. Shikata, F.F. Lange, and D.S. Pearson. Shear Modulus and Yield Stress Measurements of Attractive Alumina Particle Networks in Aqueous Slurries. *Journal of American Ceramic Society*, No. 11, 1996, pp. 2917-2924.
13. Reed, J.S. *Principles of ceramic processing*, 2nd ed. John Wiley and Sons, Inc., New York, 1995.

14. Yang, M., C.M. Neubauer, and H.M. Jennings. Interparticle Potential and Sedimentation Behavior of Cement Suspensions, *Advanced Cement Based Materials*, Vol. 5, 1997.
15. Jolicoeur, C. and M.A. Simard. Chemical Admixture and Cement Interactions: Rhenomenology and Physico-Chemical Concepts, *Cement and Concrete Composites*, No. 20, 1998, pp. 87-101.
16. Hewlett, P.C. *Lea's Chemistry of Cement and Concrete*. John Wiley and Sons Inc., New York, 1998.
17. Metha, P.K.. *Concrete: Structure, Properties, and Materials.* Prentice-Hall, Inc, Englewood Cliff, New Jersey, 1986, pp. 449.
18. Ferraris, C.F., and K.H. Obla. The Influence of Mineral Admixtures on the Rheology of Cement Paste and Concrete, *Cement and Concrete Research*, Vol. 31, No. 2, 2001, pp. 245-255.
19. Schultz, M.A., and L.J. Struble. Use of Oscillatory Shear to Study Flow Behavior of Cement Paste, *Cement and Concrete Research*, Vol. 23, No. 2, 1993, pp. 273-283.
20. Struble, L.J. and W.G. Lei. Rheological Changes Associated with Setting of Cement Paste, *Advanced Cement Based Materials*, Vol. 22, No. 6, 1995, pp. 224-230.
21. Hackley, V.A., and C.F. Ferraris. Guide to Rheological Nomenclature: Measurements in Ceramic Particle Systems, *NIST Special Publication,* No. 946.
22. Papo, A. Rheological Models for Cement Pastes, *Materials and Structures*, Vol. 21, No. 121, 1988, pp. 41-46.
23. Nehdi, M., and M.A. Rahman. Effect of Geometry and Surface Friction of Test Accessory on Oscillatory Rheological Properties of Cement Pastes, *Journal of ACI Materials*, No.101-M47, 2004.
24. De Larrard, F., C.F. Ferraris, and T. Sedan. Fresh Concrete: A Herschel-Bulkley Material, *Materials and Structures*, Vol. 31, No. 211, 1998, pp. 494-498.
25. Banfill, P.F.G. The Rheology of Fresh Cement and Concrete-a Review, Proceeding, *11th International Cement Chemistry Congress*, Durban, May 2003.
26. Mewis, J. Thixotropy-A General Review, *Journal of Non-Newtonian Fluid Mechanics*, Vol. 6, 1979.
27. Larson, R.G. *The Structure and Rheology of Complex Fluids.* Oxford University Press, New York, 1999.

28. Barnes, H.A., J.F. Hutton, and K. Walters. *An Introduction to Rheology.* Elsevier, Amsterdam, 1989.
29. Saasen, A., C. Marken, and N. Blomberg. Viscoelastic Properties of Oilfield Cement Slurries, *Rheology of Fresh Cement and Concrete*, London, 1991, pp. 170-177.
30. Struble, L.J., H. Zhang, G.K. Sun, and W.G. Lei. Oscillatory Shear Behavior of Portland Cement Paste during Early Hydration, *Journal of Concrete Science and Engineering*, Vol. 2, No. 9, 2000, pp. 141–149.
31. Zhang, H. *Using Dynamic Rheology to Explore the Microstructure and Stiffening of Cementitious Materials*, Ph.D. Thesis, University of Illinois at Urbana-Champaign, 2001.
32. Kantro, D. L. Influence of Water-Reducing Admixtures on Properties of Cement Paste-a Miniature Slump Test, *Cement, Concrete and Aggregates*, Vol. 2, 1980, pp. 95-102.
33. Tang, F.J. and S. Bhattacharja. Development of an Early Stiffening Test, *PCA Research and Development Bulletin,* RP346, Skokie, Illinois, 1997.
34. Helmuth, R.A., and L.M. Hills. Abnormal Concrete Performance in the Presence of Admixtures, *PCA Research and Development Bulletin,* RP333, Skokie, Illinois, 1995.
35. Jiang, S., B.G. Kim, and P.C. Aitcin. Importance of Adequate Soluble Alkali Content to Ensure Cement/Superplasticizer Compatibility, *Cement and Concrete Research*, Vol. 29, 1999, pp. 71-78.
36. Ferraris, C.F. Connection between the Rheology of Concrete and Rheology of Cement Paste, 89-M43, *Journal of ACI Materials*, 1992, pp. 388-393.
37. Ferraris, C.F. Measurement of the Rheological Properties of Cement Paste: A New Approach, Role of Admixture in High Performance Concrete, *RILEM International Symposium*, Monterrey, Mexico, March, 1999.
38. Struble, L.J., R. Szecsy, W.G. Lei, and G.K. Sun. Rheology of Cement Paste and Concrete, *Cement, Concrete and Aggregates*, Vol. 20, No. 2, 1998, pp. 269-277.
39. Nehdi, M., and M.A. Rahman. Estimating Rheological Properties of Cement Pastes Using Various Rheological Models for Different Test Geometry, Gap and Surface Friction, *Cement and Concrete Research*, Vol. 34, 2004, pp. 1993-2007.
40. Bhattacharja, S., and F.J. Tang. Rheology of Cement Paste in Concrete with Different Mix Designs and Interlaboratory Evaluation of the Mini-Slump Cone Test, PCA R&D, Serial No.2412, *Portland Cement Association*, Skokie, Illinois, 2000.

41. Barnes, H.A. A Review of the Slip of Polymer Solutioins, Emulsions and Particle Suspensions in Viscometers; Its Cause, Character, and Cure, *Journal of Non-Newtonian Fluid Mechanics*, Vol. 56, 1995, pp. 221-225.
42. Wesche, K., H. Flaatten, and W. Vom Berg. On the Influence of Separations on the Rheological Investigations of Cement Paste and Mortar in the Rotational Rheometers, Fresh Concrete, Important Properties and their Measurement, Vol. 2, *RILEM Symposium*, Leeds, England, 1973.
43. Ferraris, C.F. Measurement of the Rheological Properties of Cement Paste: A New Approach, Role of Admixture in High Performance Concrete, *RILEM Proceedings, 5 (Role of Admixture in HPC)*, National Institute of Standards and Technology, Gaithersburg, Maryland, 1999, pp. 333-342.
44. Saak, A.W., H.M. Jennings, and S.P. Shah. The Influence of Wall Slip on Yield Stress and Viscoelastic Measurements of Cement Paste, *Cement and Concrete Research,* Vol. 31, No. 2, 2001, pp. 205-212.
45. Roy, D.M., and K. Asaga. Rheological Properties of Cement Mixes: The Effects of Mixing Procedures on Viscometric Properties of Mixes Containing Superplasticizers, *Cement and Concrete Research*, Vol. 9, 1979, pp. 731-739.
46. Orban, J., P. Parcevaux, and D. Guillot. Influence of Shear History on the Rheological Properties of Oil Well Cement Slurries, *8th International Conference on the Chemistry of Cement*, Vol. 6, Rio de Janeiro, 1986.
47. Helmuth, R.A. Structure and Rheology of Fresh Cement Paste, *Proceedings of the 7th International Conference on the Chemistry of Cement*, Vol. 6, Paris, 1980.
48. Yang, M., and H.M. Jennings. Influence of Mixing Methods on the Microstructure and Rheological Behavior of Cement Paste, *Advanced Cement Based Materials*, Vol. 2, No. 2, 1995, pp. 70-78.
49. Helmuth, R.A. *Fly Ash in Cement and Concrete*, Portland Cement Association, Skokie, Illinois, 1987.
50. Ramachandran, V.S. *Concrete Admixtures Handbook: Properties, Science and Technology.* 2nd Edition. Noyes Publications, Park Ridge, New Jersey, 1995.
51. Guo, Cheng-ju. Early Age Behavior of Portland Cement Paste, *Journal of ACI Materials*, Vol. 91, No. 1, 1994, pp. 13-25.

52. Hersey, A.T. Slump Loss Caused by Admixtures, *Journal of ACI Materials*, Vol. 972, No. 10, 1975, pp.526-527.
53. Stein, H.N. Influence of Some Additives on the Hydration Reactions of Portland Cement: Non-Ionic Organic Additives, *Journal of Applied Chemistry*, Vol. 11, 1961, pp. 474-482.
54. Pang, Y., H. Lou, X. Qiu, and D. Yang. Influences of Modified Lignosulfonate Superplasticizer on Cement Hydration and the Durability of Concrete, *Journal of Sichuan University*, Chengdu, China, Vol. 37, No.1, 2005, pp.74-77.
55. Neville, A.M. *Properties of Concrete.* 4th edition, Essex: Pearson Education, Limited, Burnt mill, Harlow, England, 1995.
56. Khalil, S.M., and M.A. Ward. Effect of Sulphate Content of Cement Upon Heat Evolution and Slump Loss of Concretes Containing High-range Water Reducer, *Magazine of Concrete Research*, Vol. 32, No. 110, 1980, pp. 28-38.
57. Haque, M.N., M.A. Ward, and B.W. Langen. Effect of Sulphate Content on the Hydration and Strength Development of Cement/Fly ash Systems With and Without a Water Reducing Admixture, *Magazine of Concrete Research*, Vol. 39, No. 139, 1987, pp. 102-108.
58. Jawed, I., and J. Skalny. Alkalis in Cement: A Review II. Effect of Alkalis on Hydration and Performance of Portland Cement, *Cement and Concrete Research*, Vol. 8, 1978, pp. 37-52.
59. Odler, I., and R. Wonneman. Effect of Alkalis on Portland Cement Hydration: II. Alkalis Present In Form of Sulphates, *Cement and Concrete Research*, Vol. 13, 1983, pp. 771-777.
60. Aitcin, P.C., and A.M. Neville. *High Performance Concrete Demystified*, Concrete International, Vol. 15, No. 1, 1993, pp. 21-26.
61. ASTM C 191, Standard Test Method For Time of Setting of Hydraulic Cement by Vicat Needle, ASTM International, West Conshohocken, Pennsylvania, 2004, pp. 181-187.
62. ASTM C 494, Standard Specification for Chemical Admixtures for Concrete, ASTM International, West Conshohocken, Pennsylvania, 2005, pp. 277-286.
63. Schindler, A.K., and K.J. Folliard. Heat of Hydration Models for Cementitious Materials, *Journal of ACI Materials*, Vol. 102, No. 1, 2005, pp. 72-81.

APPENDIX A

PRELIMINARY TESTS

FOR CEMENT PASTE RHEOLOGY

Table A-1 Rheological parameters and coefficient of variation from DSR (Bohlin).

Experimental Design #	Repeating Test No.	Plastic Viscosity	Plastic Viscosity Average	CV(%)	Yield Stress	Yield Stress Average	CV(%)
(P1) 0.2%D17 Gap:0.2mm	1	0.541	0.8879	35.73	168.85	264.88	34.76
	2	0.9593			273.4		
	3	1.1633			352.38		
(P2) 0.5%D17 Gap:0.2mm	1	0.6402	0.6901	14.18	141.17	124.27	21.96
	2	0.8029			138.84		
	3	0.6273			92.79		
(P3) 1%D17 Gap:0.2mm	1	0.6608	0.6401	9.65	100.94	90.44	24.06
	2	0.6888			104.96		
	3	0.5706			65.423		
(P1) 0.2%D17 Gap:0.5mm	1	0.5694	0.5002	36.26	396.22	398.78	10.51
	2	0.6367			358.21		
	3	0.2944			441.91		
(P2) 0.5%D17 Gap:0.5mm	1	0.3478	0.3221	8.00	88.832	71.59	25.21
	2	0.2963			52.838		
	3	0.3221			73.085		
(P3) 1%D17 Gap:0.5mm	1	0.2112	0.2186	6.13	24.505	24.61	8.39
	2	0.2106			22.595		
	3	0.2341			26.72		
(P1) 0.2%D17 Gap:1mm	1	0.3432	0.3640	10.72	289.4	324.13	9.68
	2	0.409			350.44		
	3	0.3398			332.54		
(P2) 0.5%D17 Gap:1mm	1	0.1931	0.1925	3.36	58.476	58.29	3.39
	2	0.1857			56.227		
	3	0.1986			60.163		
(P3) 1%D17 Gap:1mm	1	0.0853	0.0845	2.50	17.13	18.79	18.77
	2	0.0821			16.402		
	3	0.0861			22.844		
(P1) 0.2%D17 Gap:1.2mm	1	0.1489	0.1767	16.78	47.106	52.56	16.07
	2	0.2079			62.284		
	3	0.1732			48.277		
(P2) 0.5%D17 Gap:1.2mm	1	0.1486	0.1496	8.98	47.142	42.79	21.18
	2	0.1367			32.37		
	3	0.1635			48.857		
(P3) 1%D17 Gap:1.2mm	1	0.0978	0.1255	24.42	2.2917	3.15	30.36
	2	0.1202			2.9786		
	3	0.1584			4.1811		
(P1) 0.2%D17 Gap:1.5mm	1	0.1383	0.1454	7.77	16.65	15.50	8.02
	2	0.1584			14.181		
	3	0.1394			15.679		
(P2) 0.5%D17 Gap:1.5mm	1	0.1145	0.1139	5.81	11.821	11.82	9.85
	2	0.1202			12.978		
	3	0.107			10.651		
(P3) 1%D17 Gap:1.5mm	1	0.089	0.0902	7.90	4.19	3.47	29.70
	2	0.0978			2.2917		
	3	0.0837			3.942		

APPENDIX B

HEAT OF HYDRATION FOR

THE STUDIED CEMENT PASTES

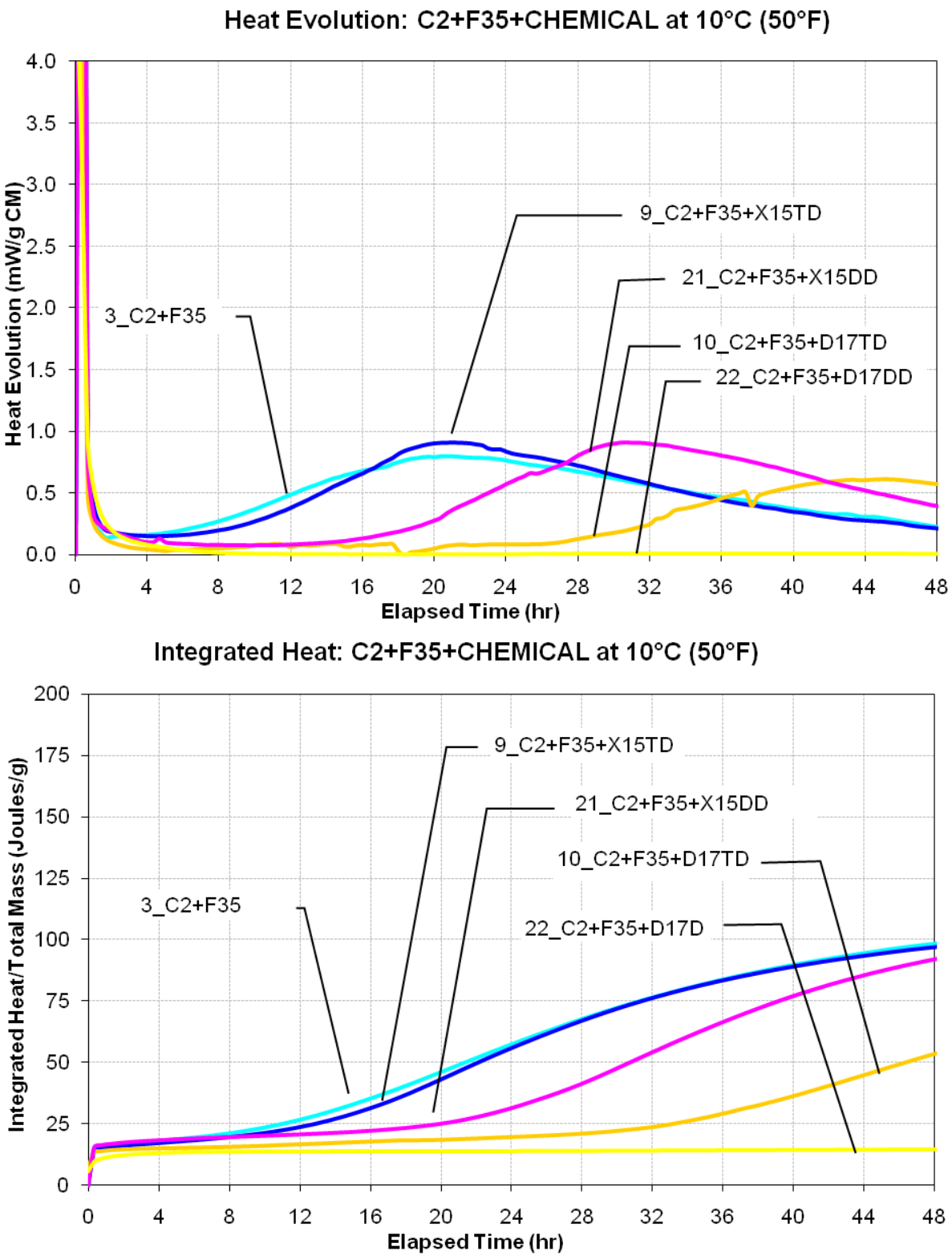

Figure B-1 Heat evolution (top) and integrated heat evolution (bottom) for C2 with F fly ash system at 10°C.

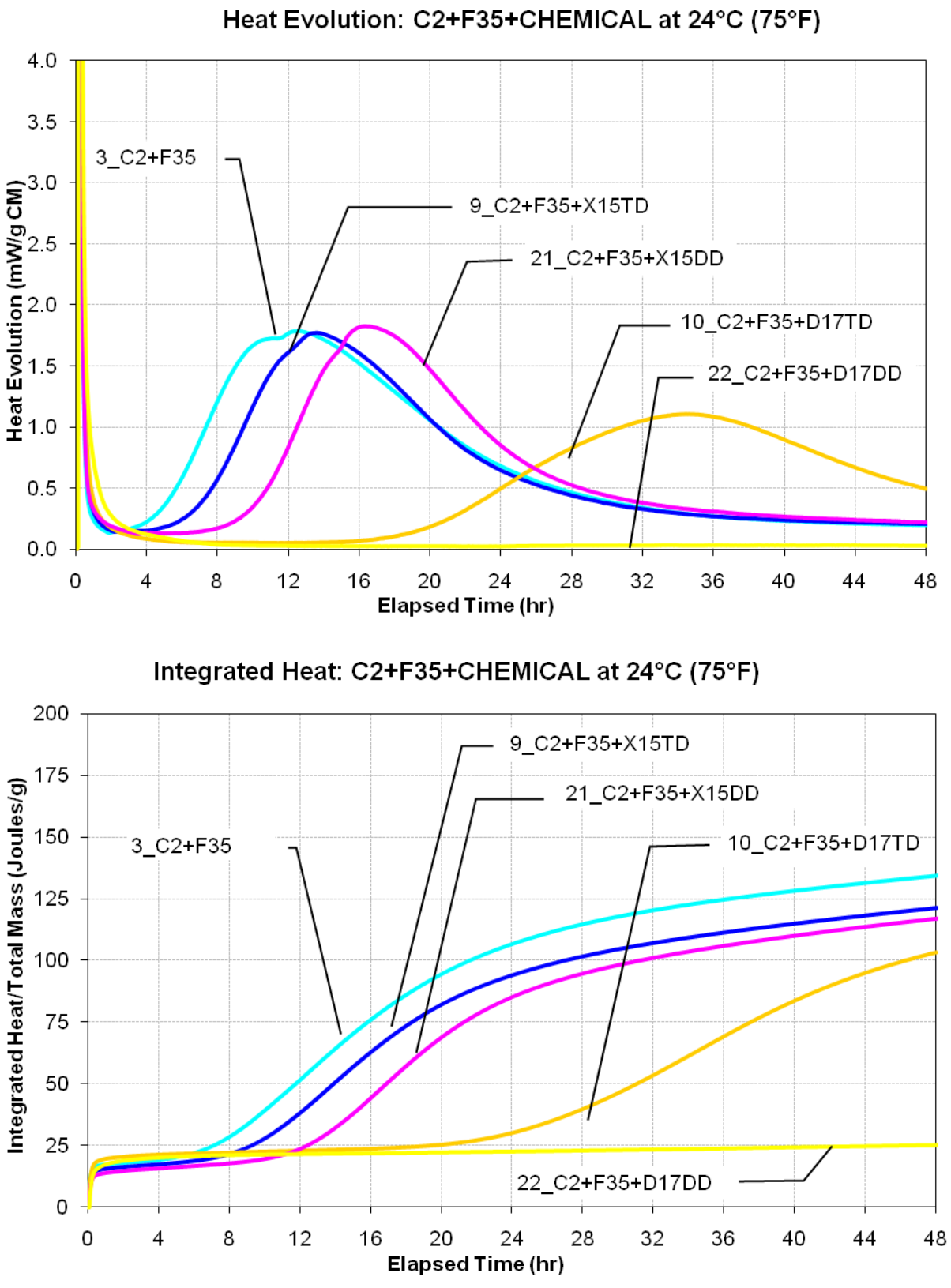

Figure B-2 Heat evolution (top) and integrated heat evolution (bottom) for C2 with F fly ash system at 24°C.

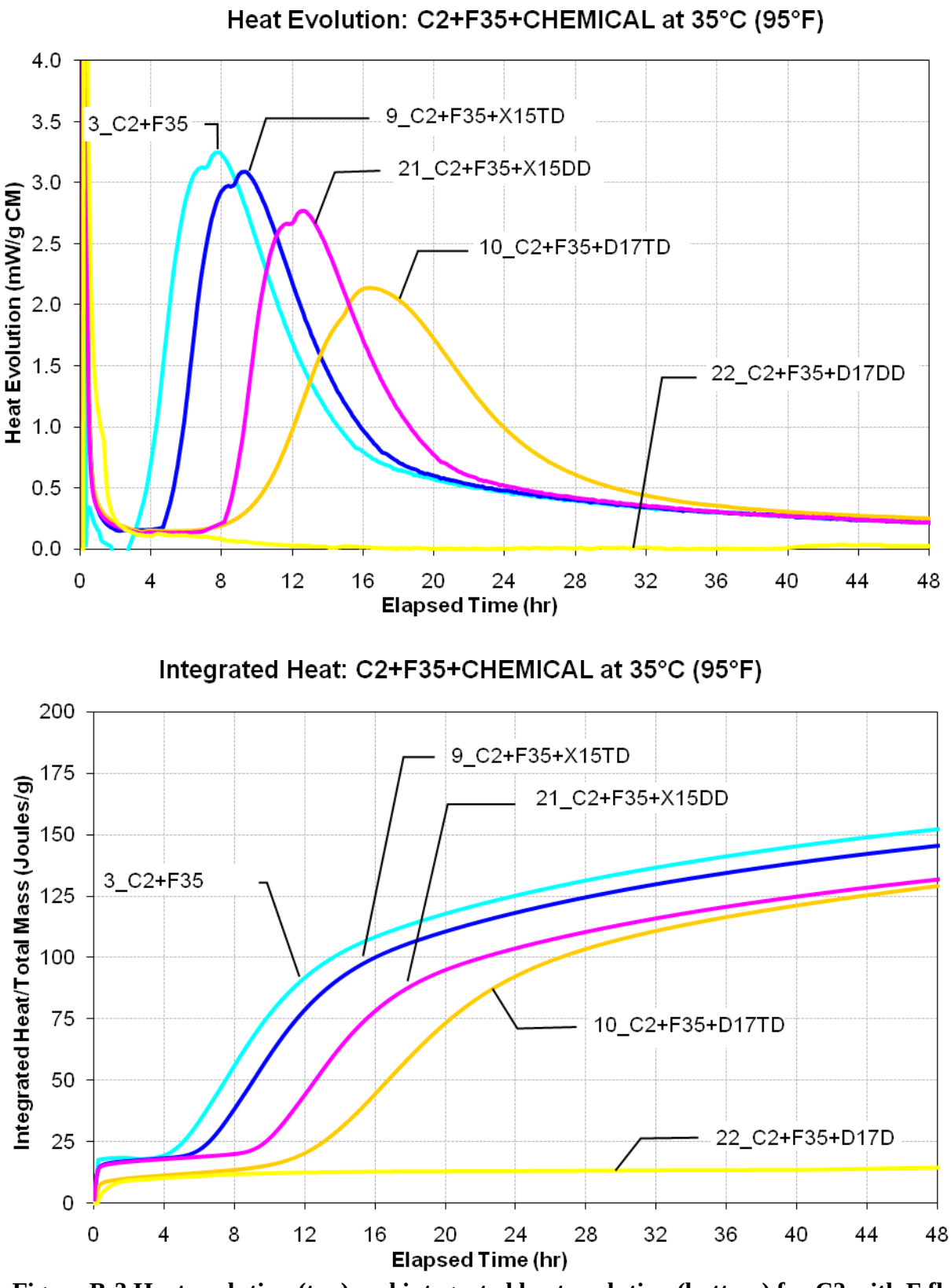

Figure B-3 Heat evolution (top) and integrated heat evolution (bottom) for C2 with F fly ash system at 35°C.

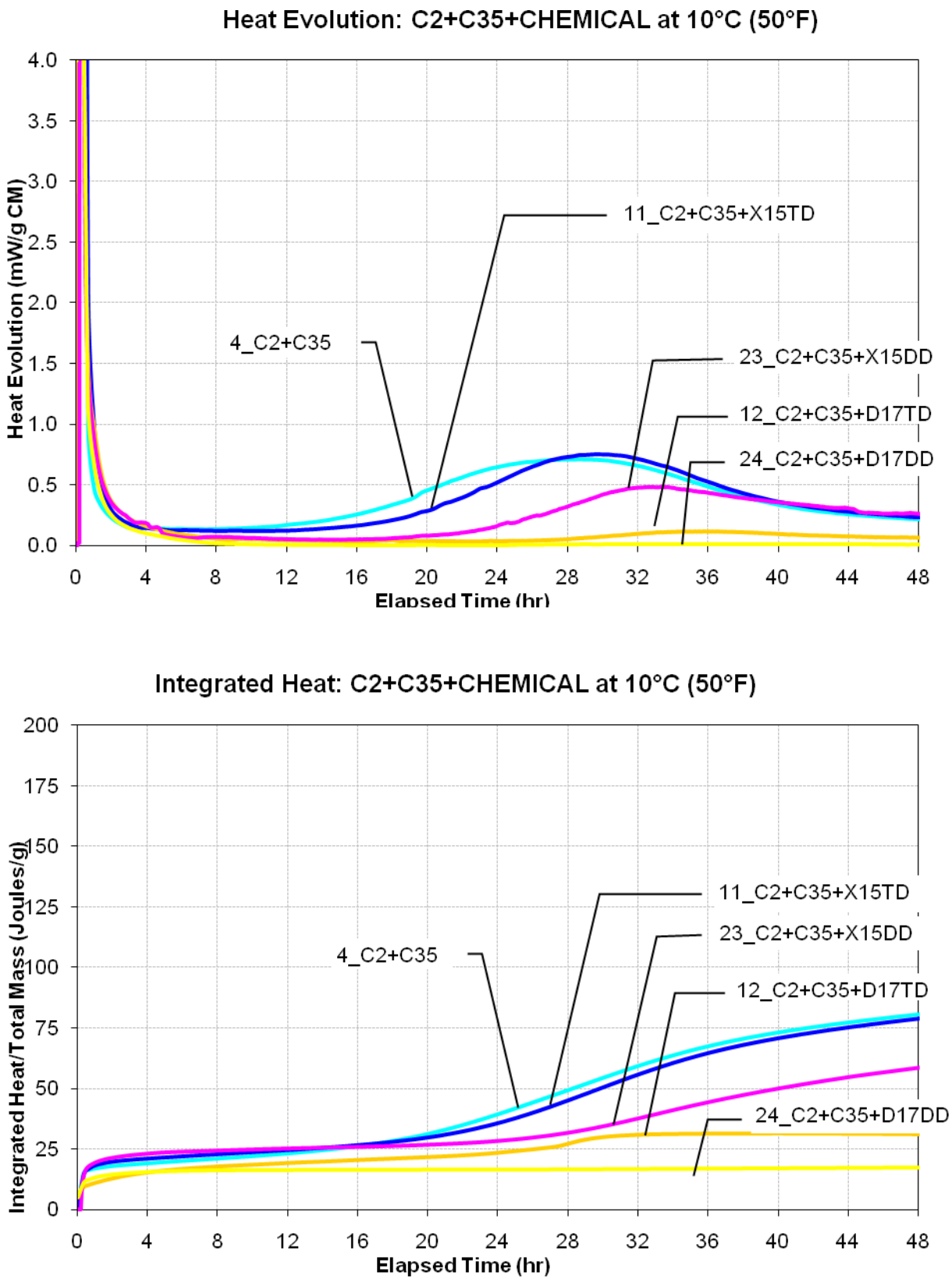

Figure B-4 Heat evolution (top) and integrated heat evolution (bottom) for C2 with C fly ash system at 10°C.

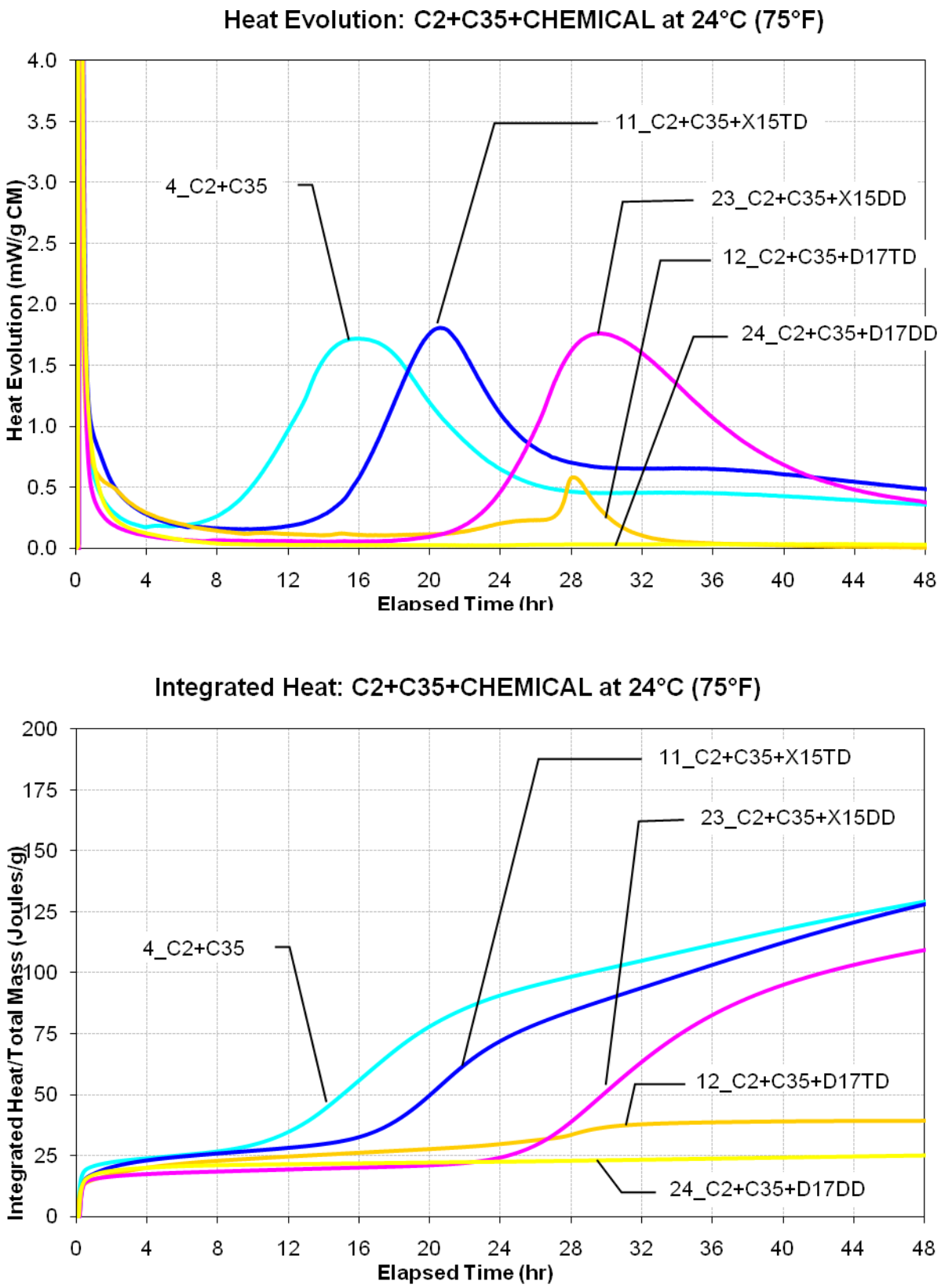

Figure B-5 Heat evolution (top) and integrated heat evolution (bottom) for C2 with C fly ash system at 24°C.

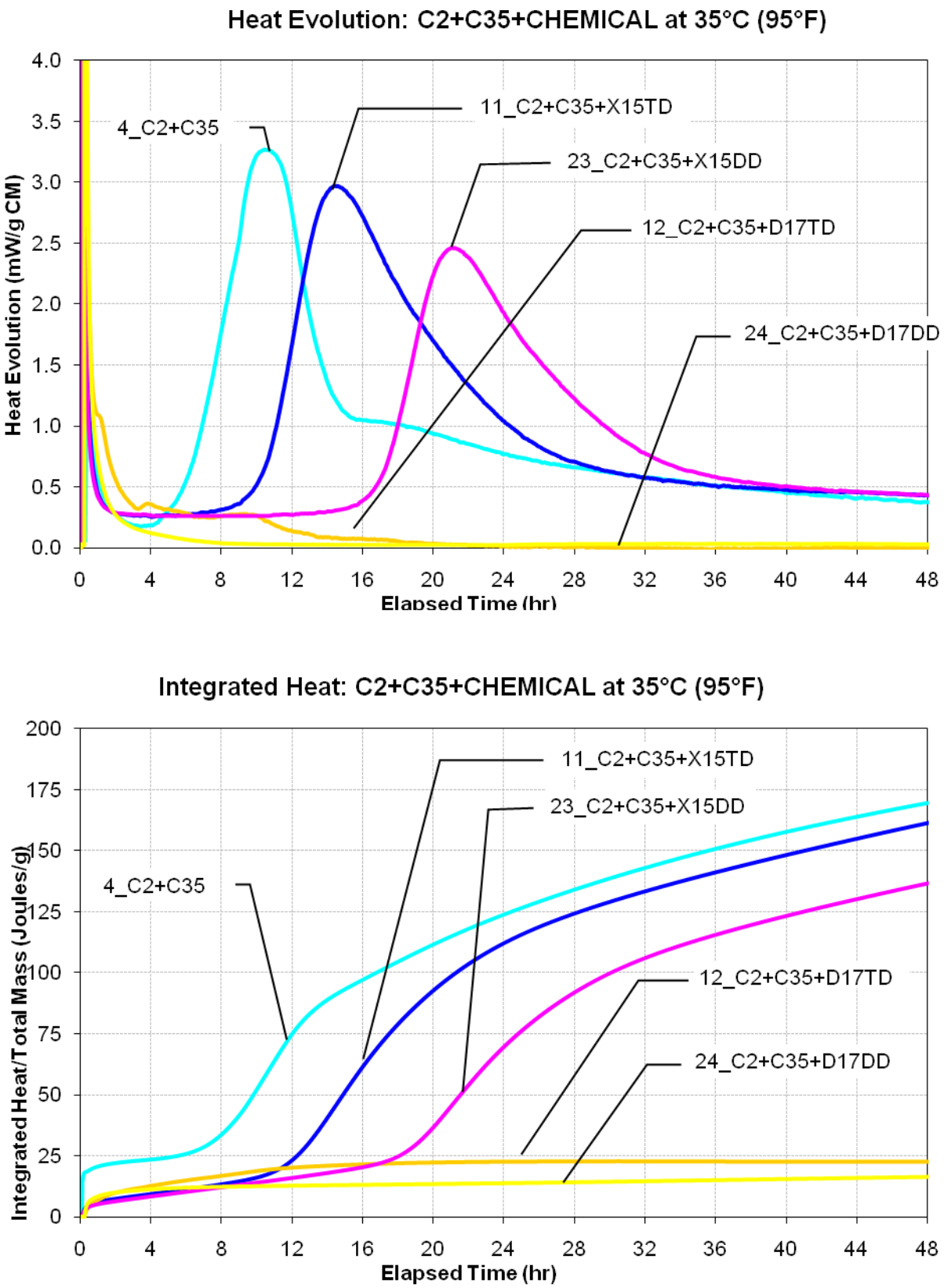

Figure B-6 Heat evolution (top) and integrated heat evolution (bottom) for C2 with C fly ash system at 35°C.

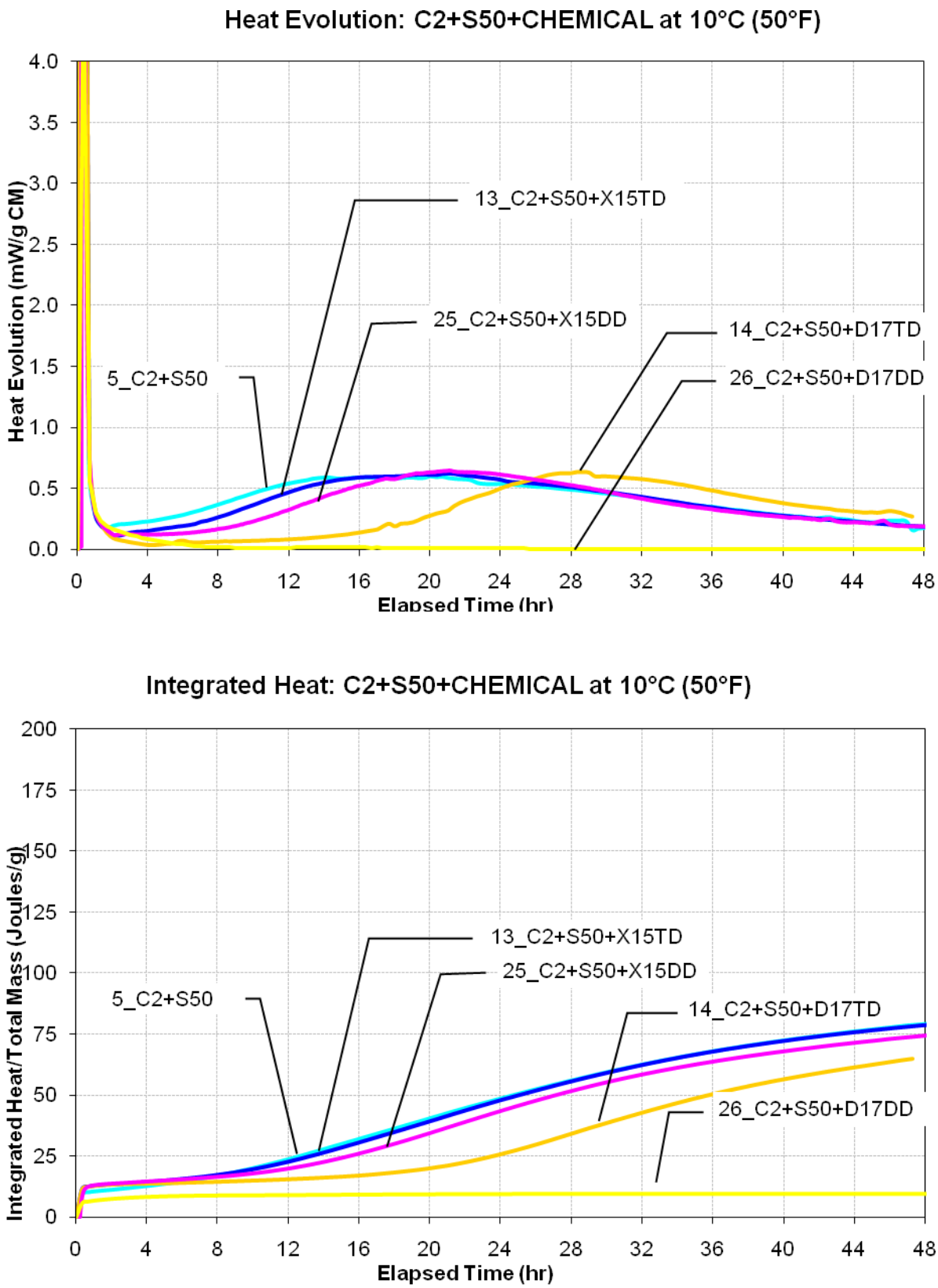

Figure B-7 Heat evolution (top) and integrated heat evolution (bottom) for C2 with granulated slag system at 10°C.

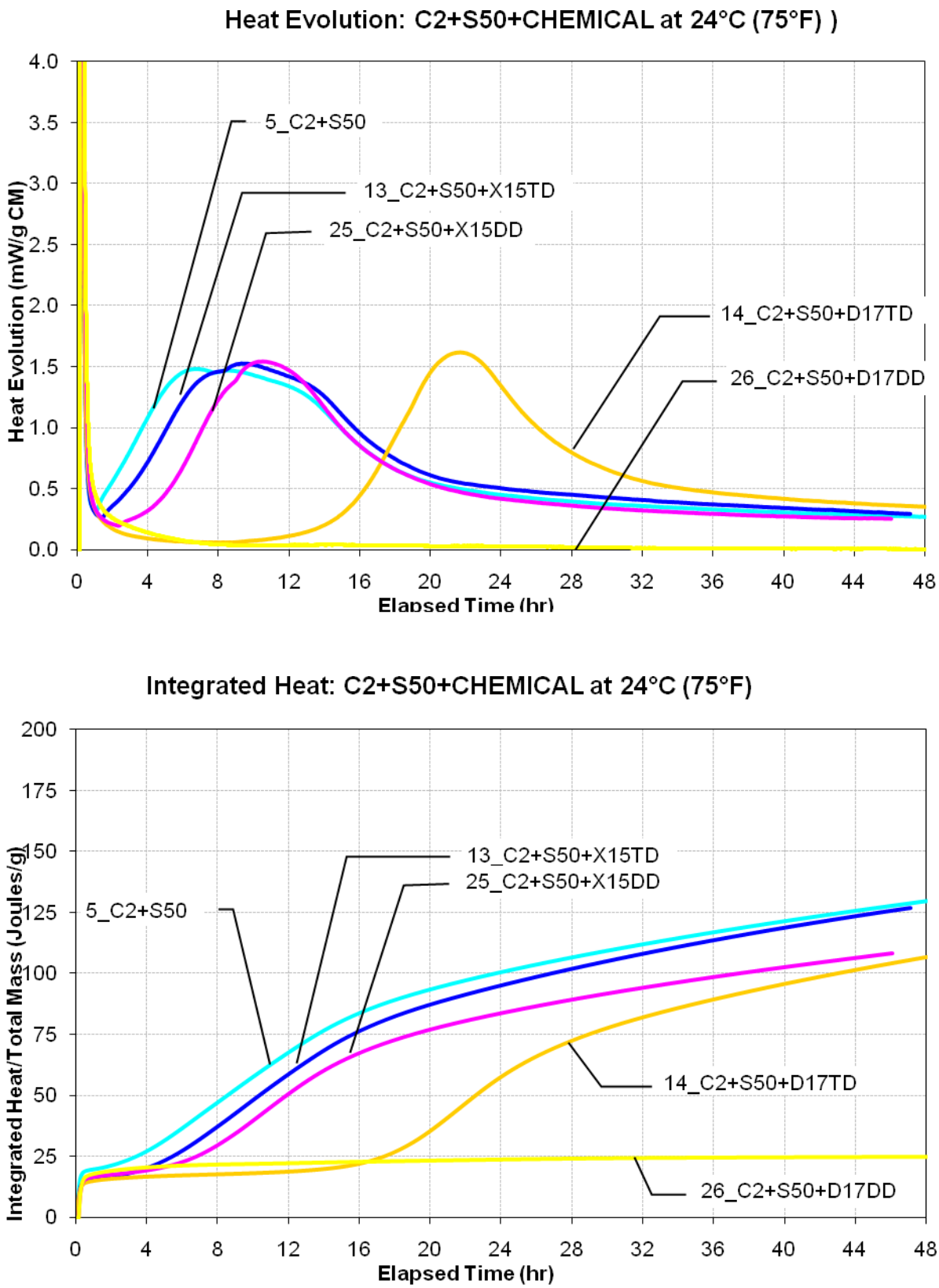

Figure B-8 Heat evolution (top) and integrated heat evolution (bottom) for C2 with granulated slag system at 24°C.

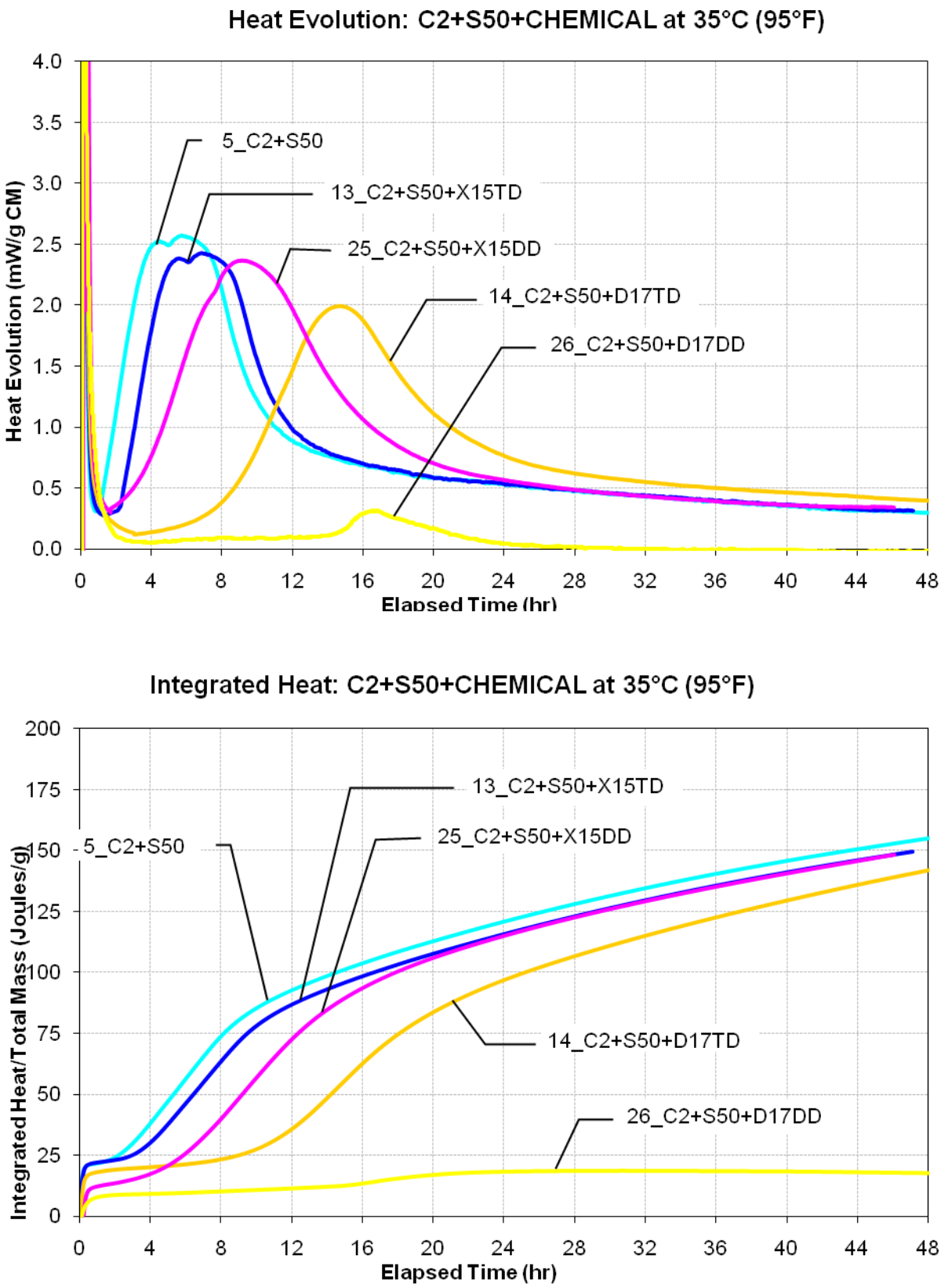

Figure B-9 Heat evolution (top) and integrated heat evolution (bottom) for C2 with granulated slag system at 35°C.

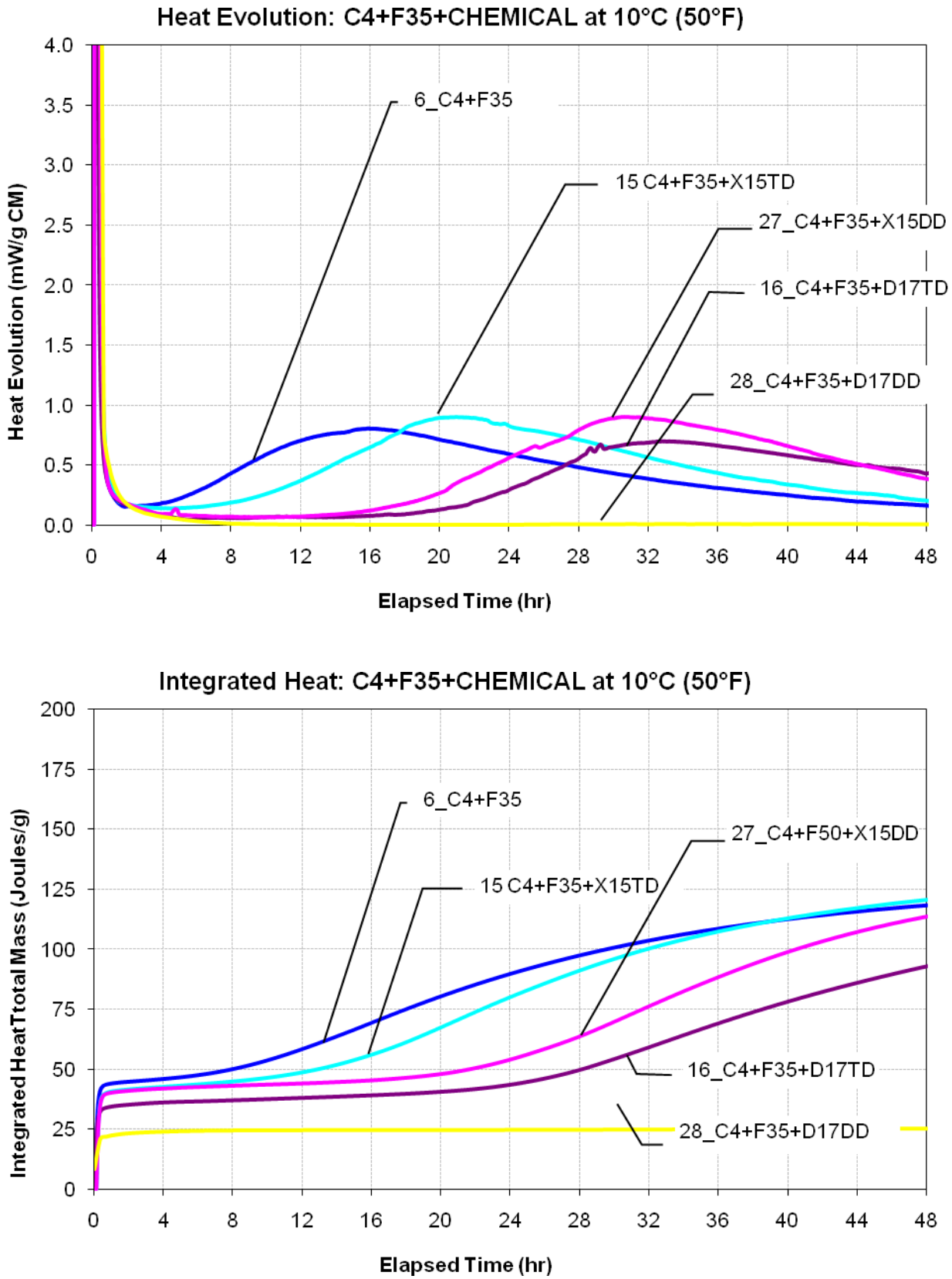

Figure B-10 Heat evolution (top) and integrated heat evolution (bottom) for C4 with F fly ash system at 10°C.

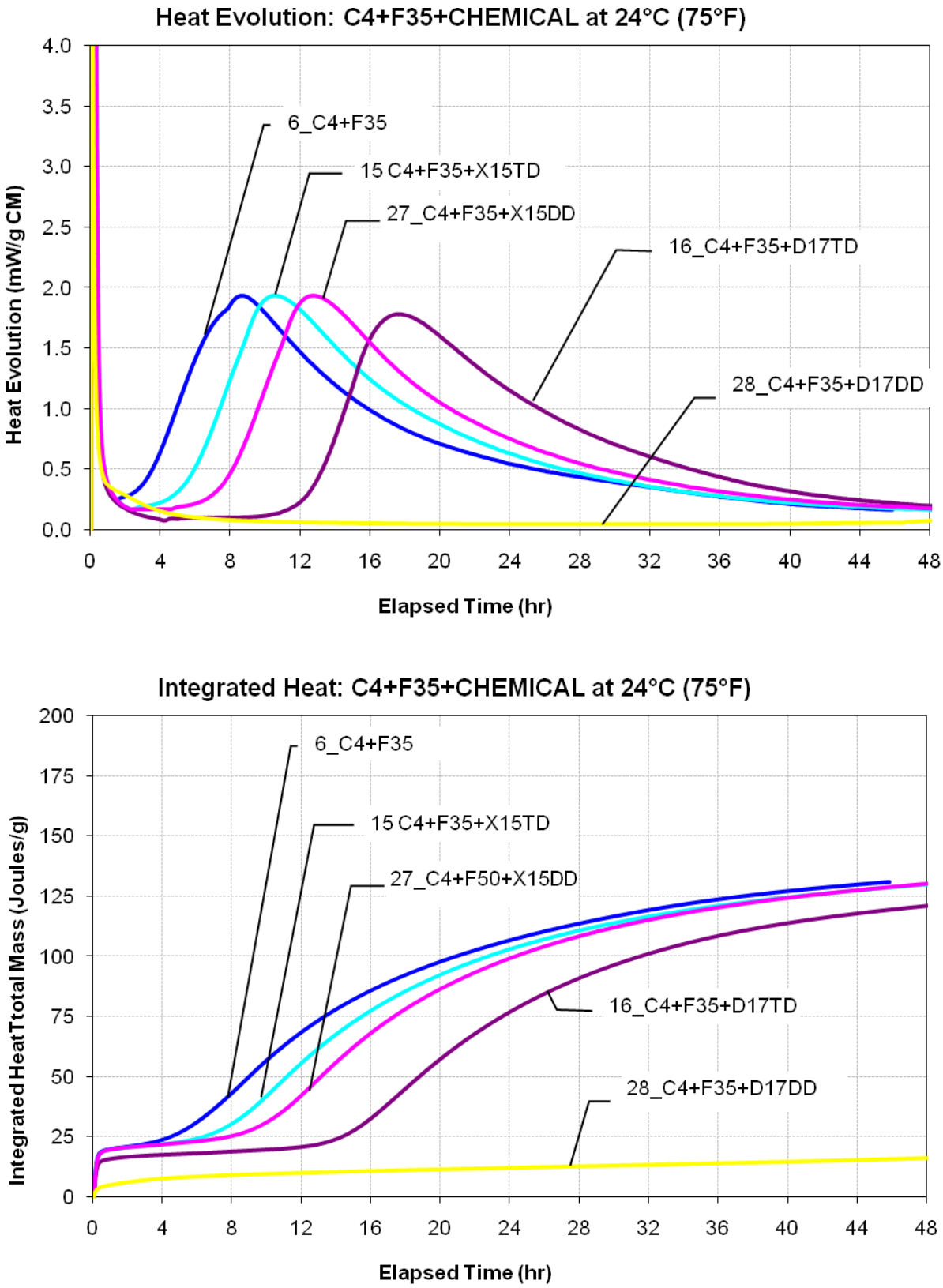

Figure B-11 Heat evolution (top) and integrated heat evolution (bottom) for C4 with F fly ash system at 24°C.

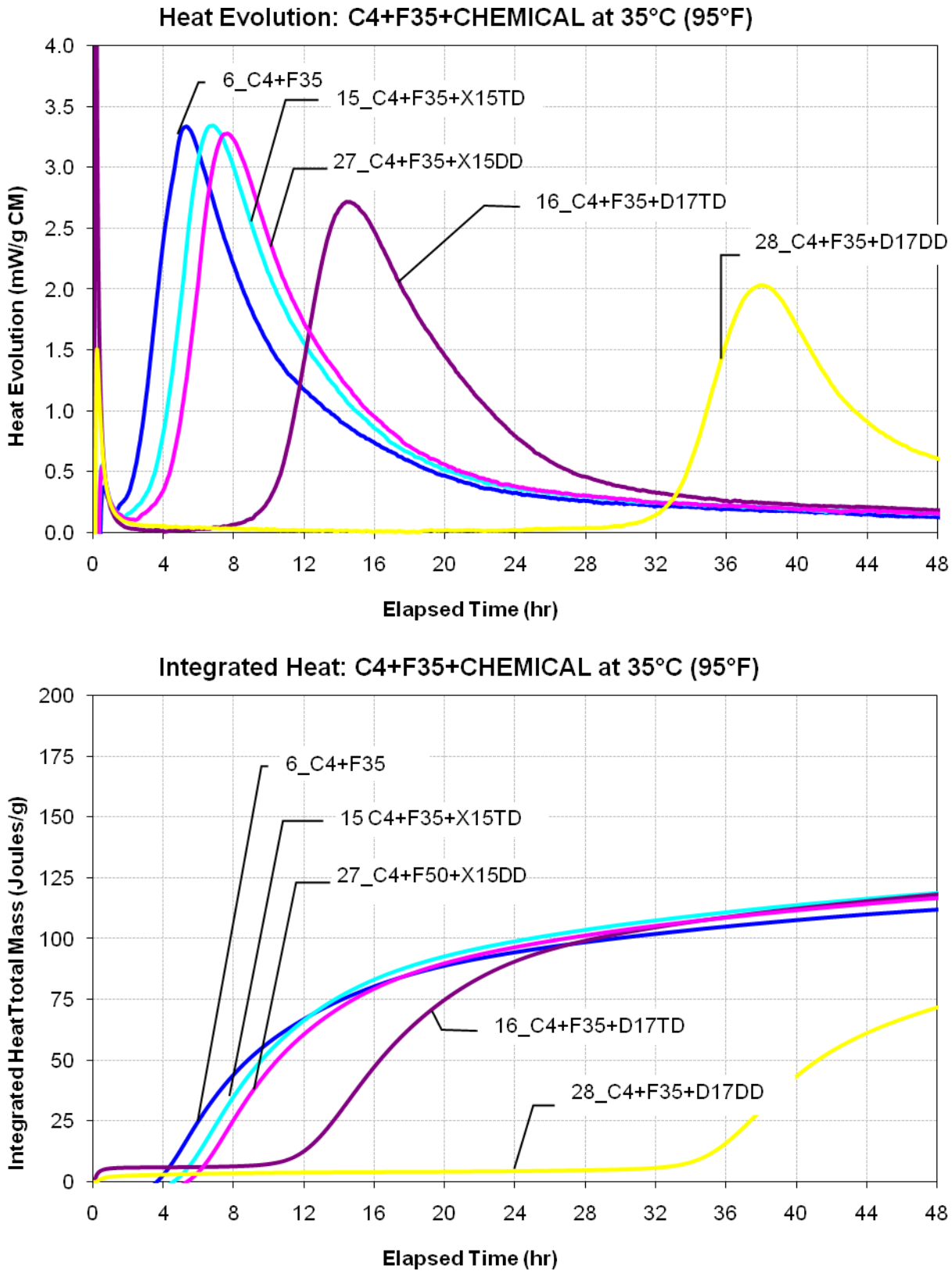

Figure B-12 Heat evolution (top) and integrated heat evolution (bottom) for C4 with F fly ash system at 35°C.

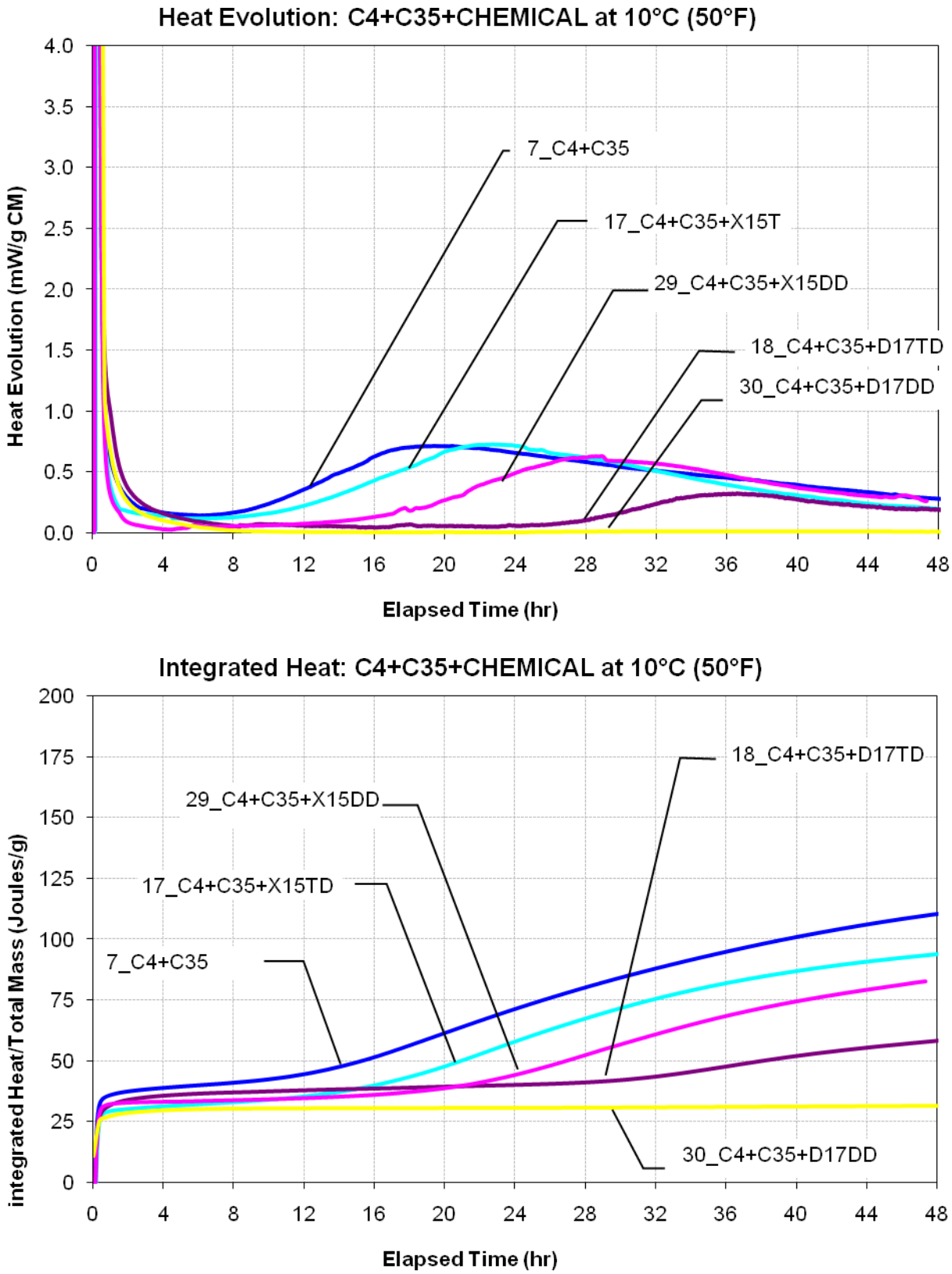

Figure B-13 Heat evolution (top) and integrated heat evolution (bottom) for C4 with C fly ash system at 10°C.

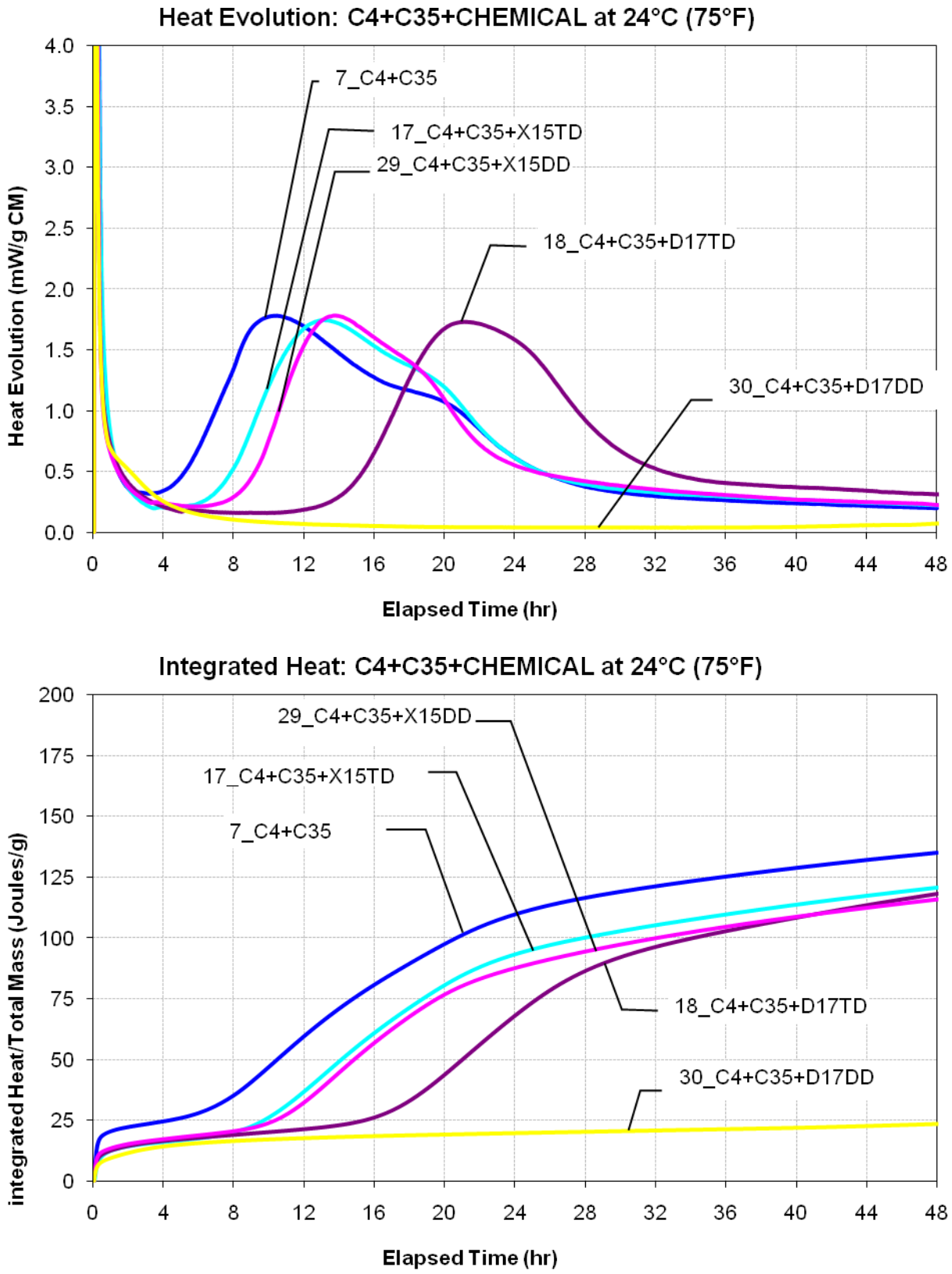

Figure B-14 Heat evolution (top) and integrated heat evolution (bottom) for C4 with C fly ash system at 24°C.

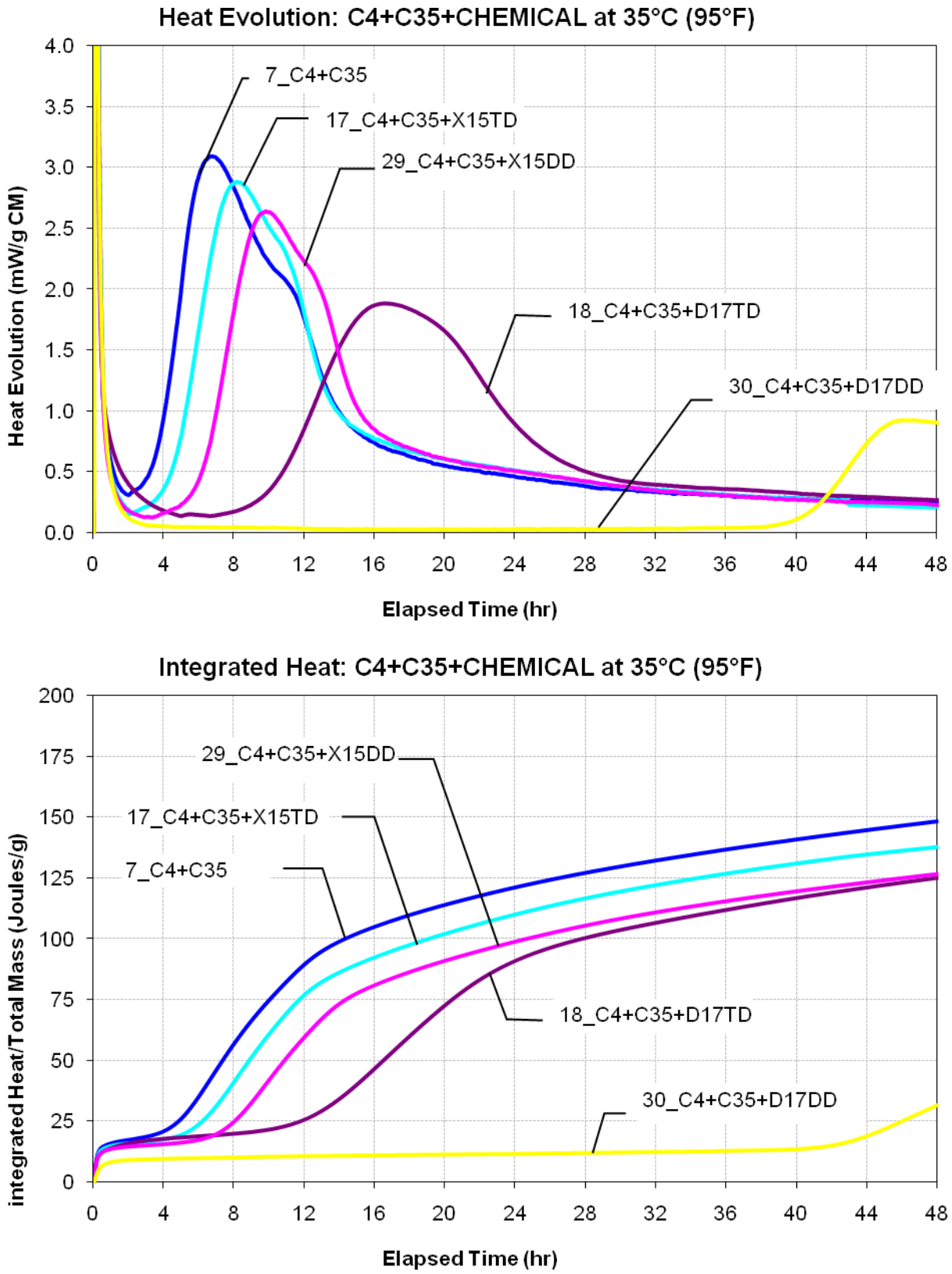

Figure B-15 Heat evolution (top) and integrated heat evolution (bottom) for C4 with C fly ash system at 35°C.

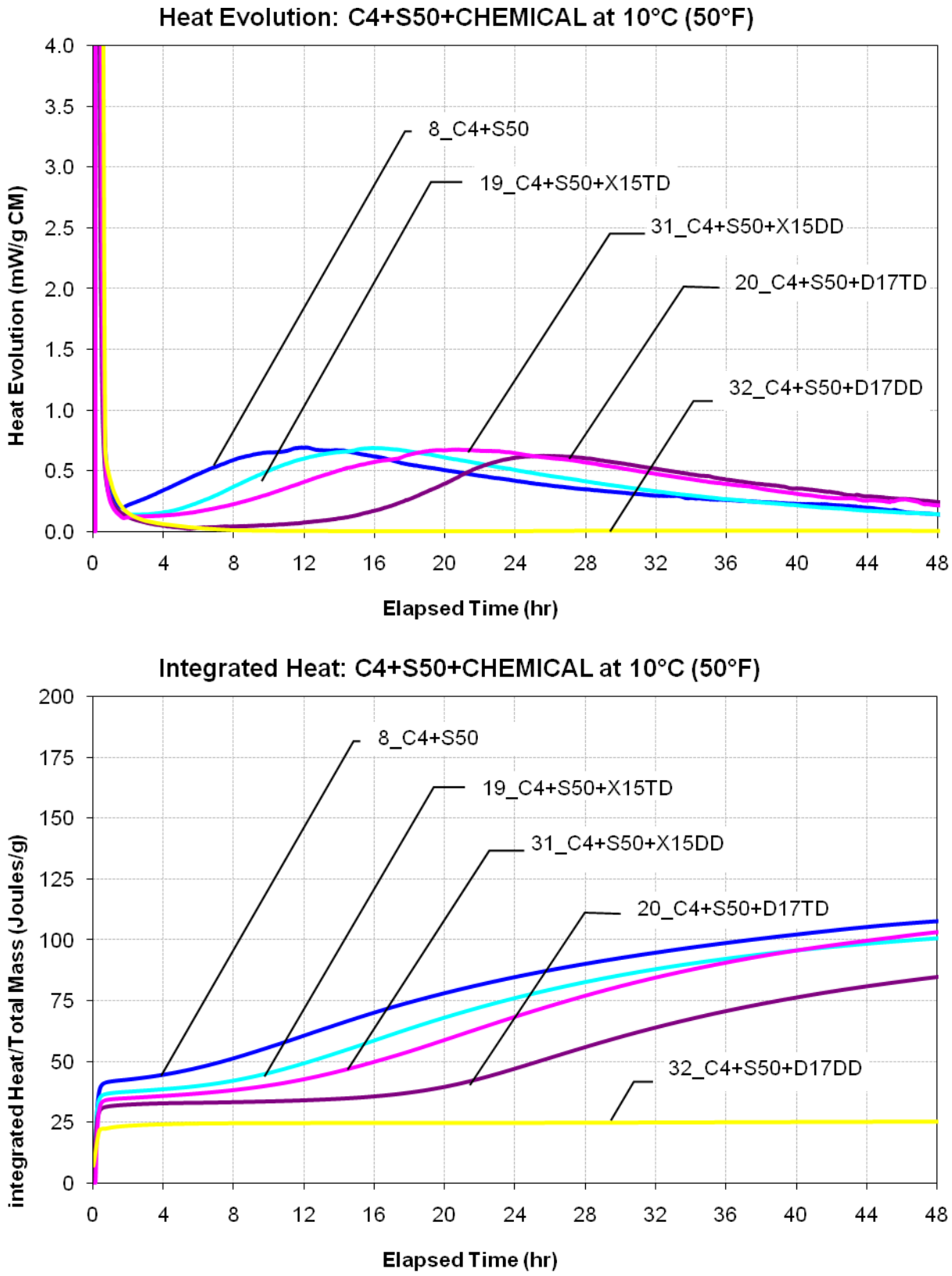

Figure B-16 Heat evolution (top) and integrated heat evolution (bottom) for C4 with granulated slag system at 10°C.

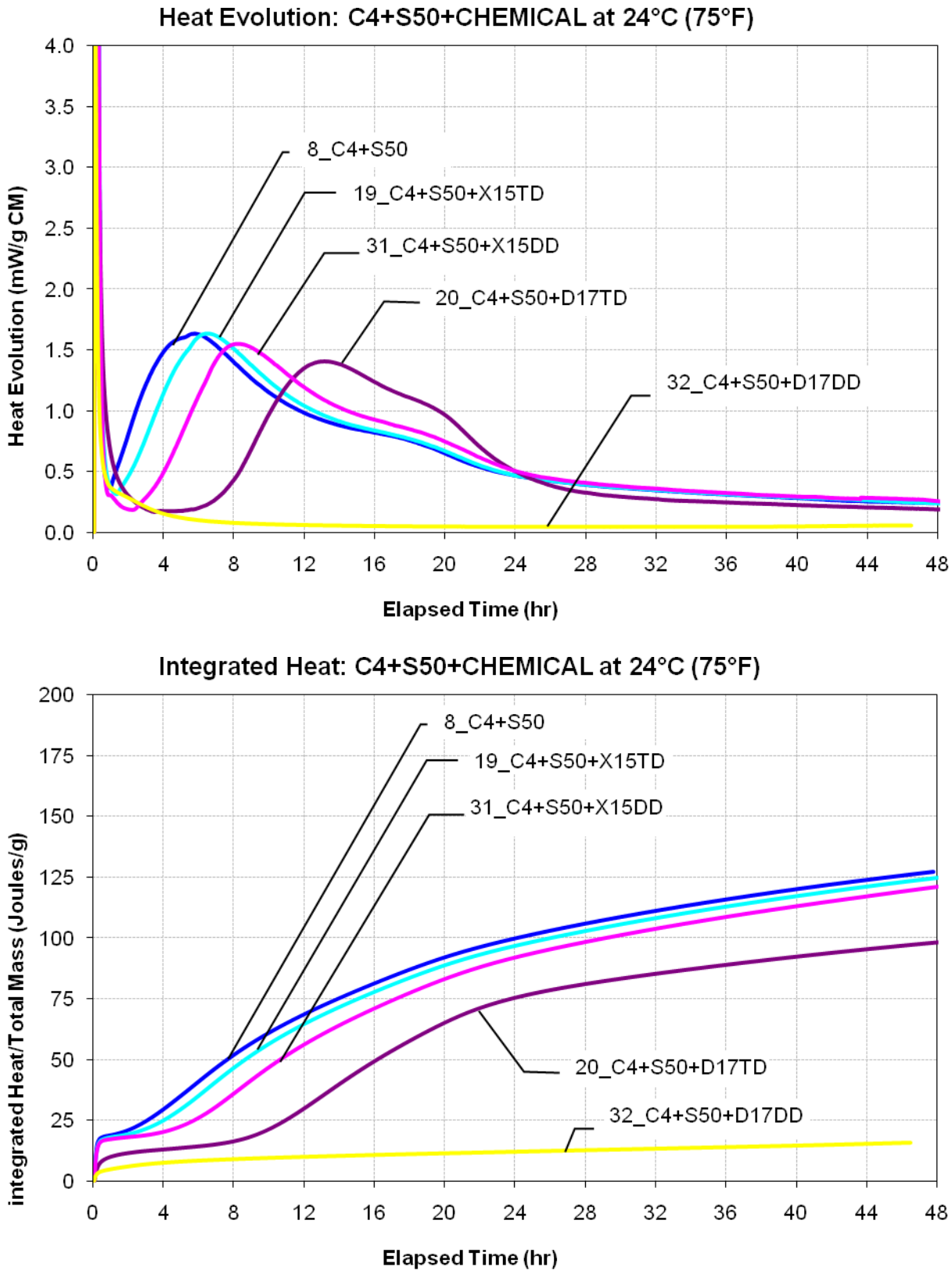

Figure B-17 Heat evolution (top) and integrated heat evolution (bottom) for C4 with granulated slag system at 24°C.

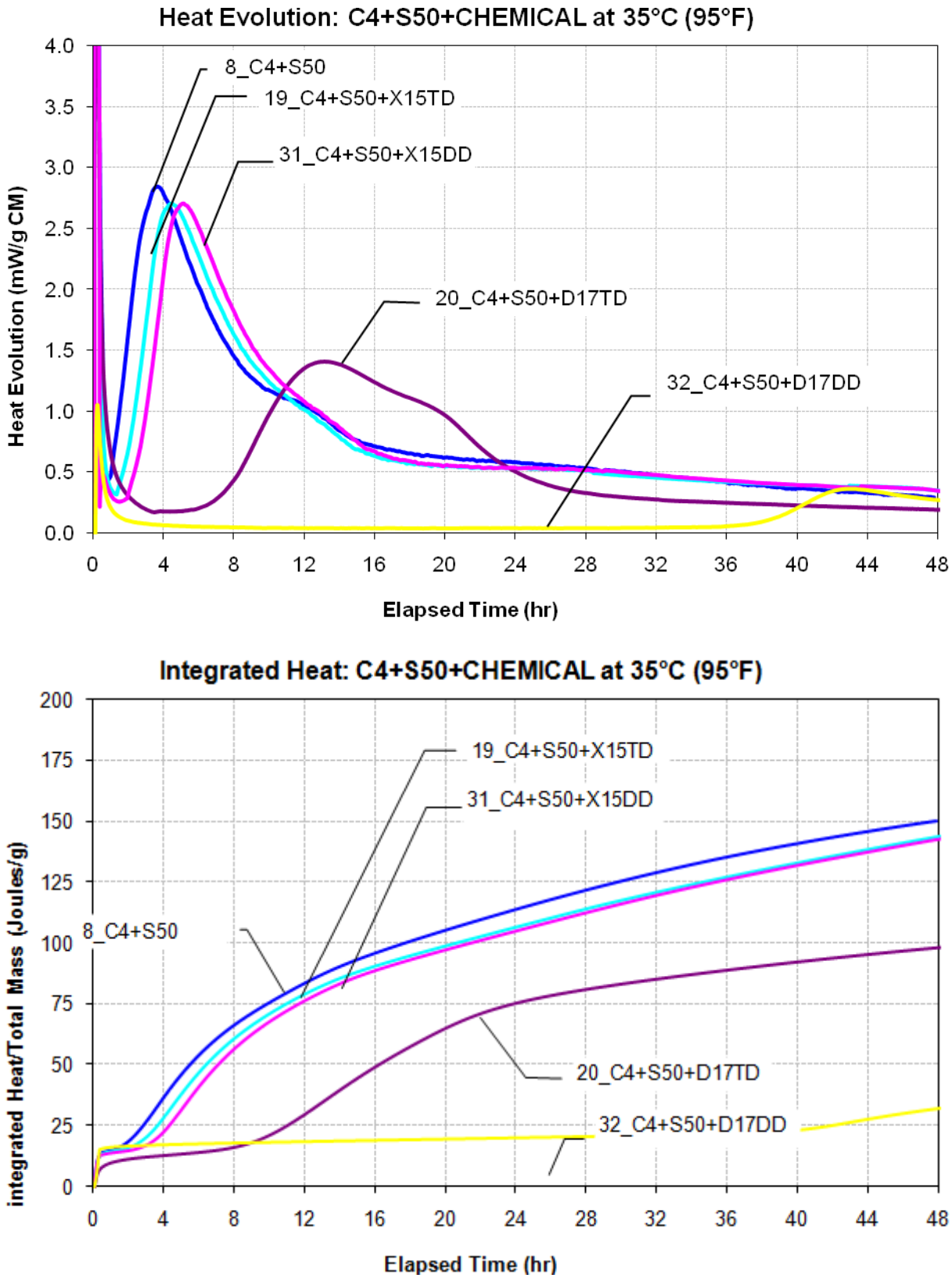

Figure B-18 Heat evolution (top) and integrated heat evolution (bottom) for C4 with granulated slag system at 35°C.

APPENDIX C

STATIC RHEOLOGICAL PARAMETERS

BY THE MODIFIED DSR

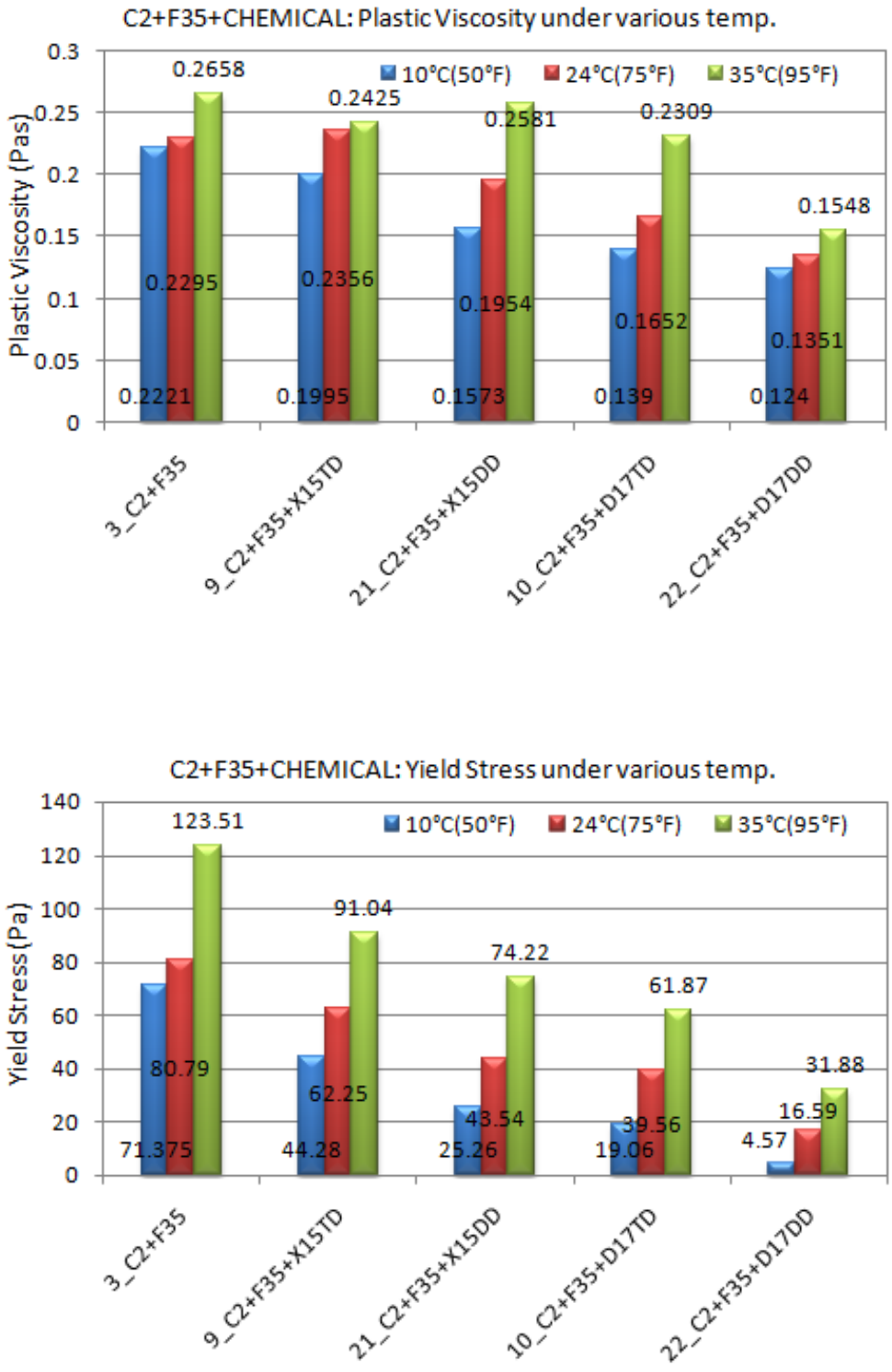

Figure C-1 PV (top) and YS (bottom) for C2+F35 system as a function of temperature, admixture type and dosage.

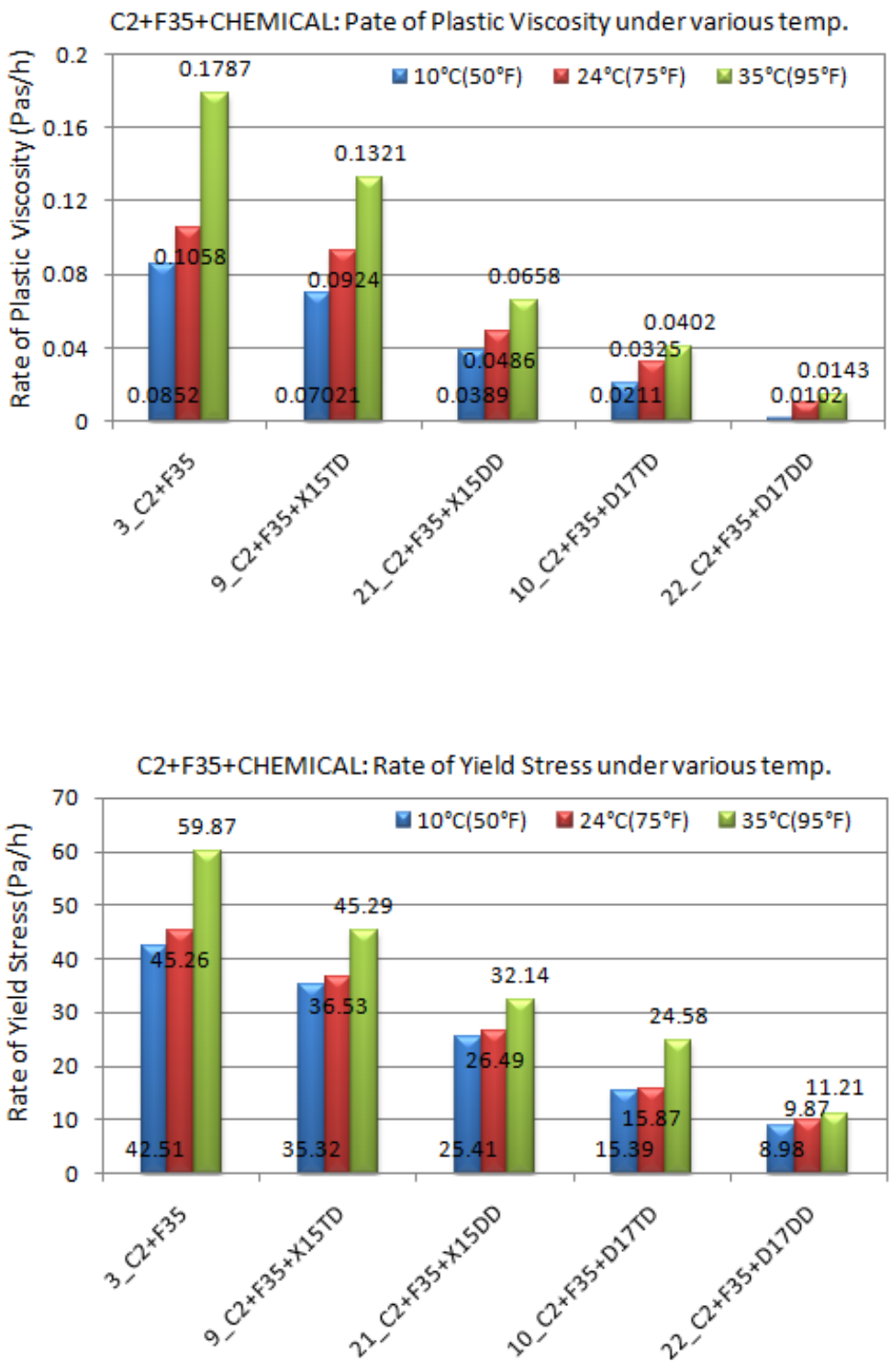

Figure C-2 RPV (top) and RYS (bottom) for C2+F35 system as a function of temperature, admixture type and dosage.

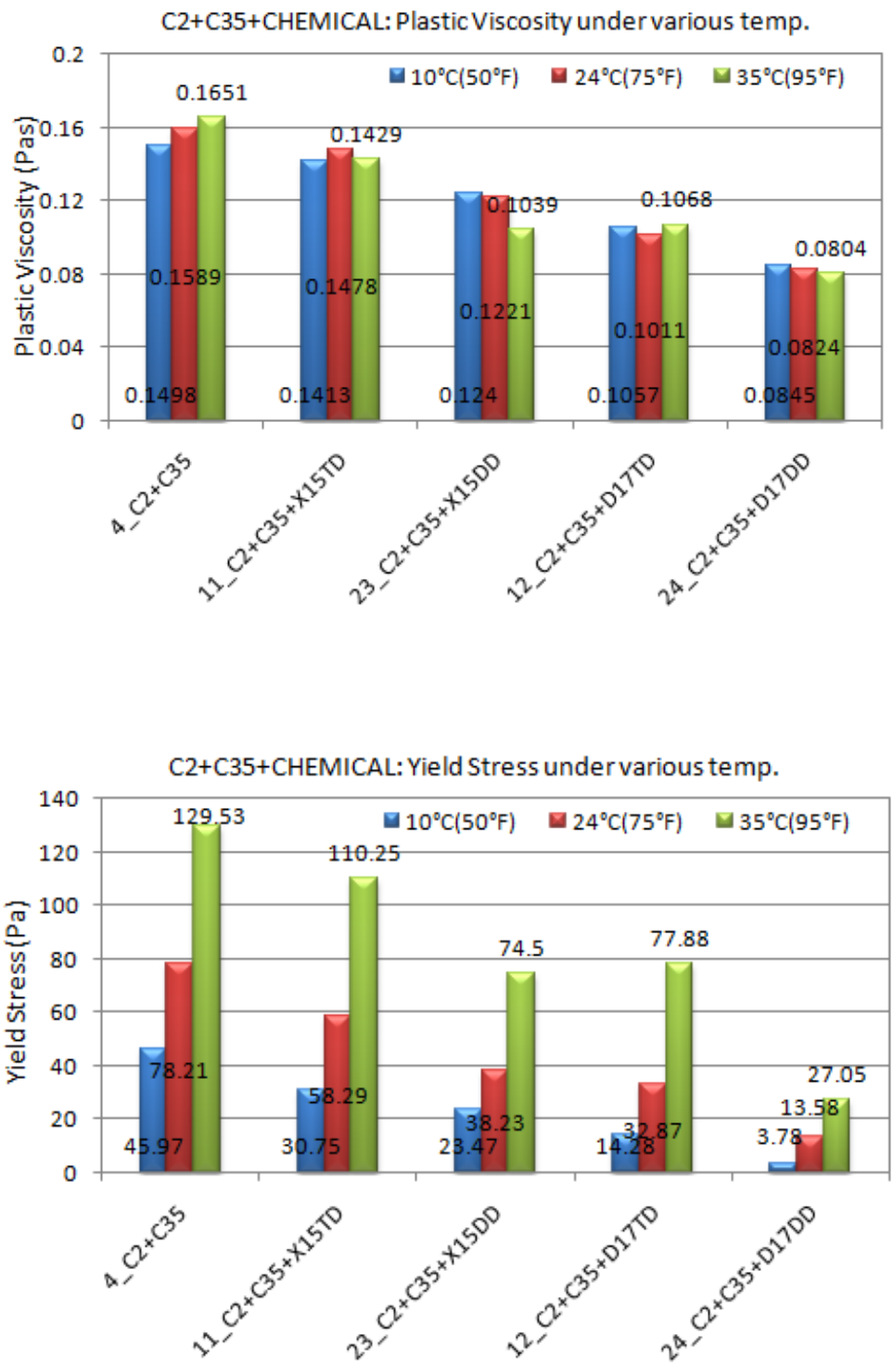

Figure C-3 PV (top) and YS (bottom) for C2+C35 system as a function of temperature, admixture type and dosage.

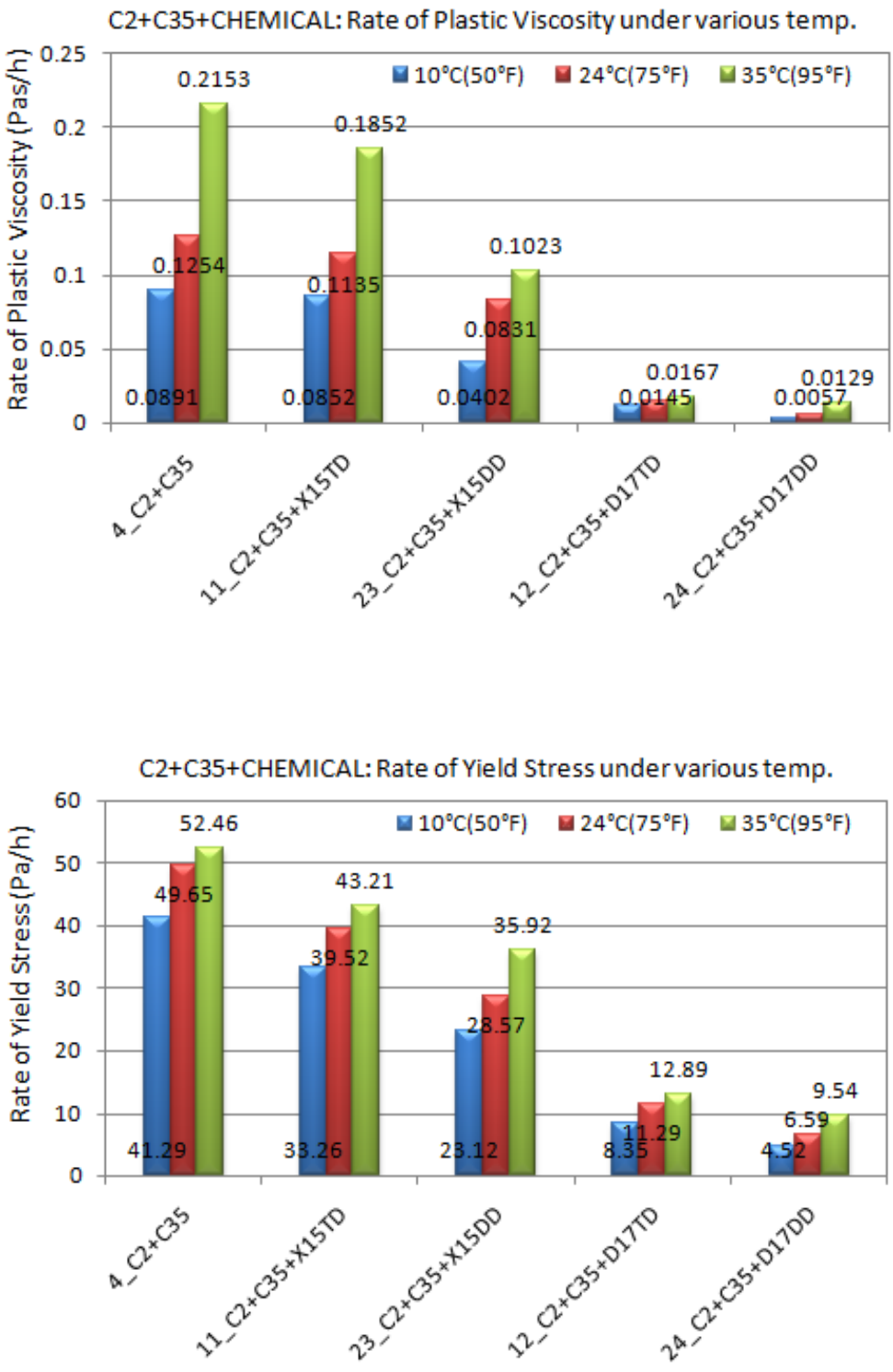

Figure C-4 RPV (top) and RYS (bottom) for C2+C35 system as a function of temperature, admixture type and dosage.

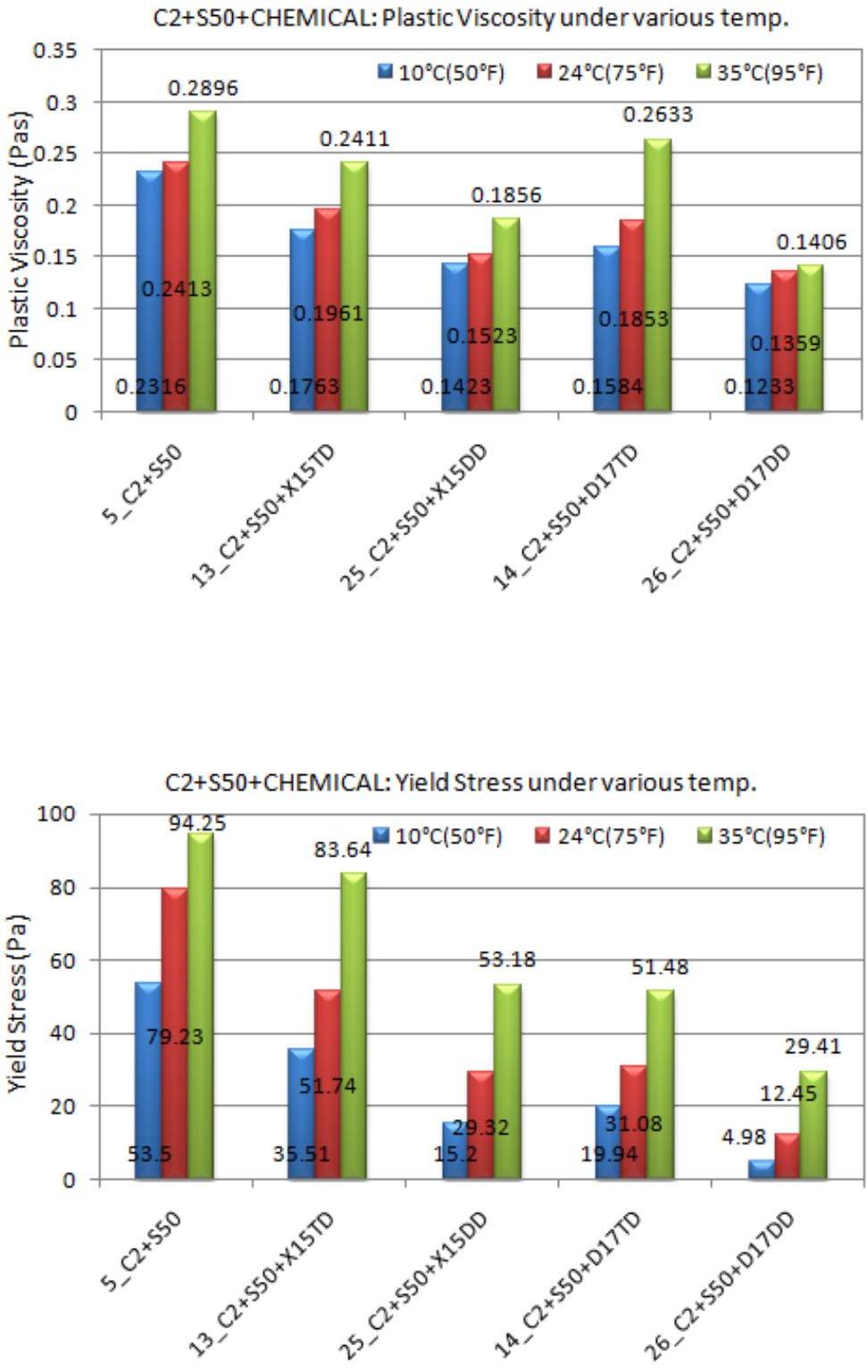

Figure C-5 PV (top) and YS (bottom) for C2+S50 system as a function of temperature, admixture type and dosage.

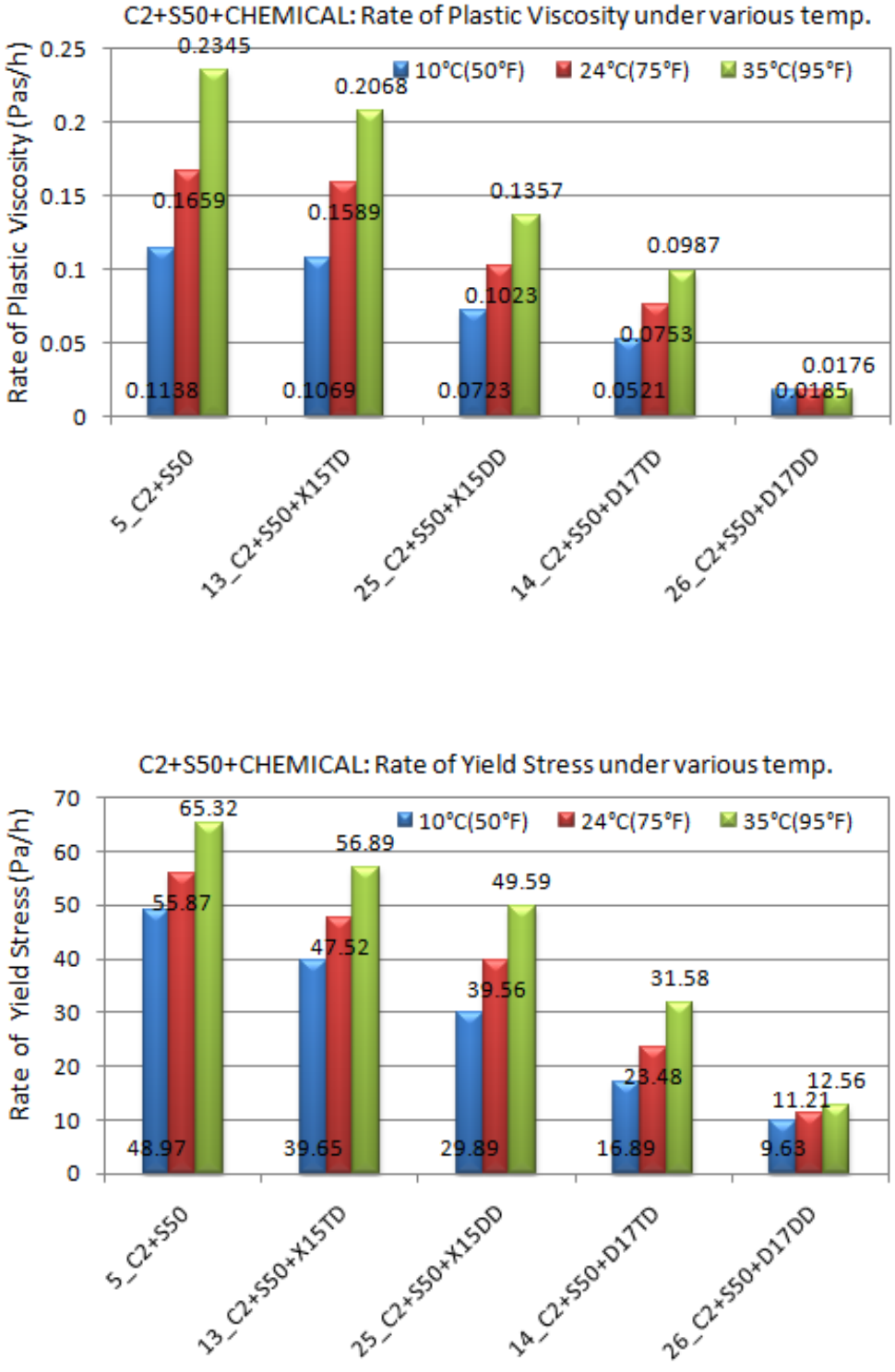

Figure C-6 RPV (top) and RYS (bottom) for C2+S50 system as a function of temperature, admixture type and dosage.

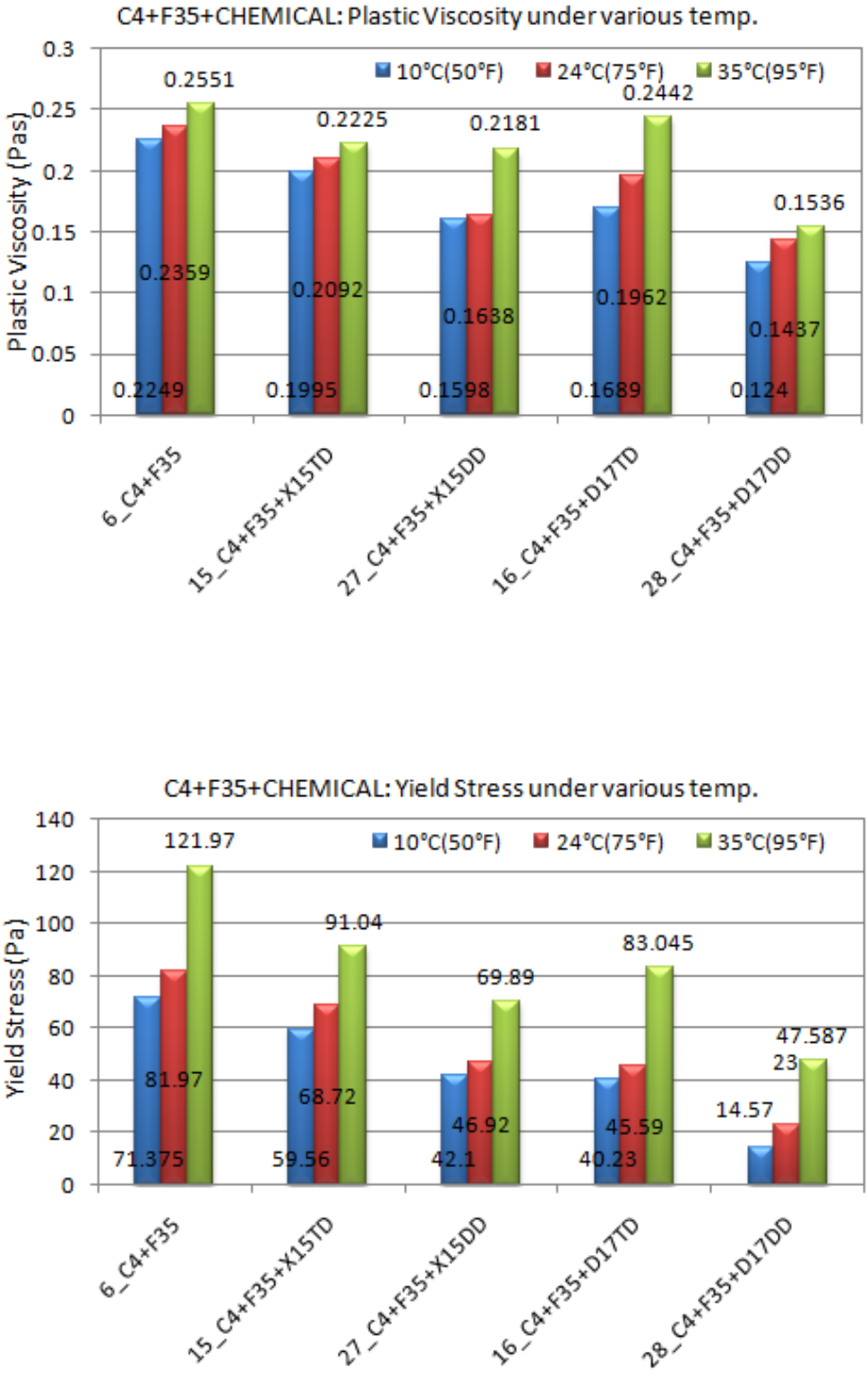

Figure C-7 PV (top) and YS (bottom) for C4+F35 system as a function of temperature, admixture type and dosage.

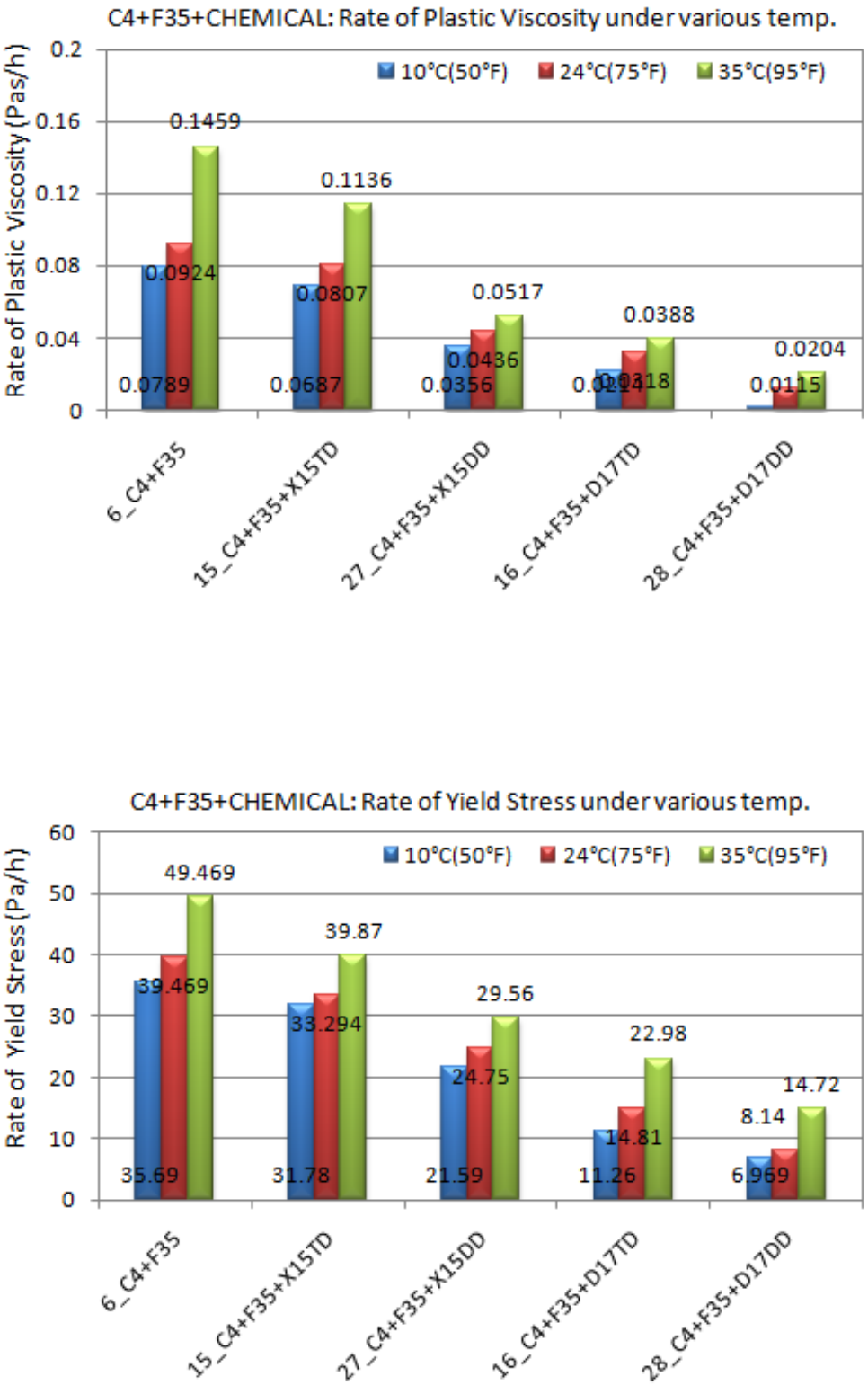

Figure C-8 RPV (top) and RYS (bottom) for C4+F35 system as a function of temperature, admixture type and dosage.

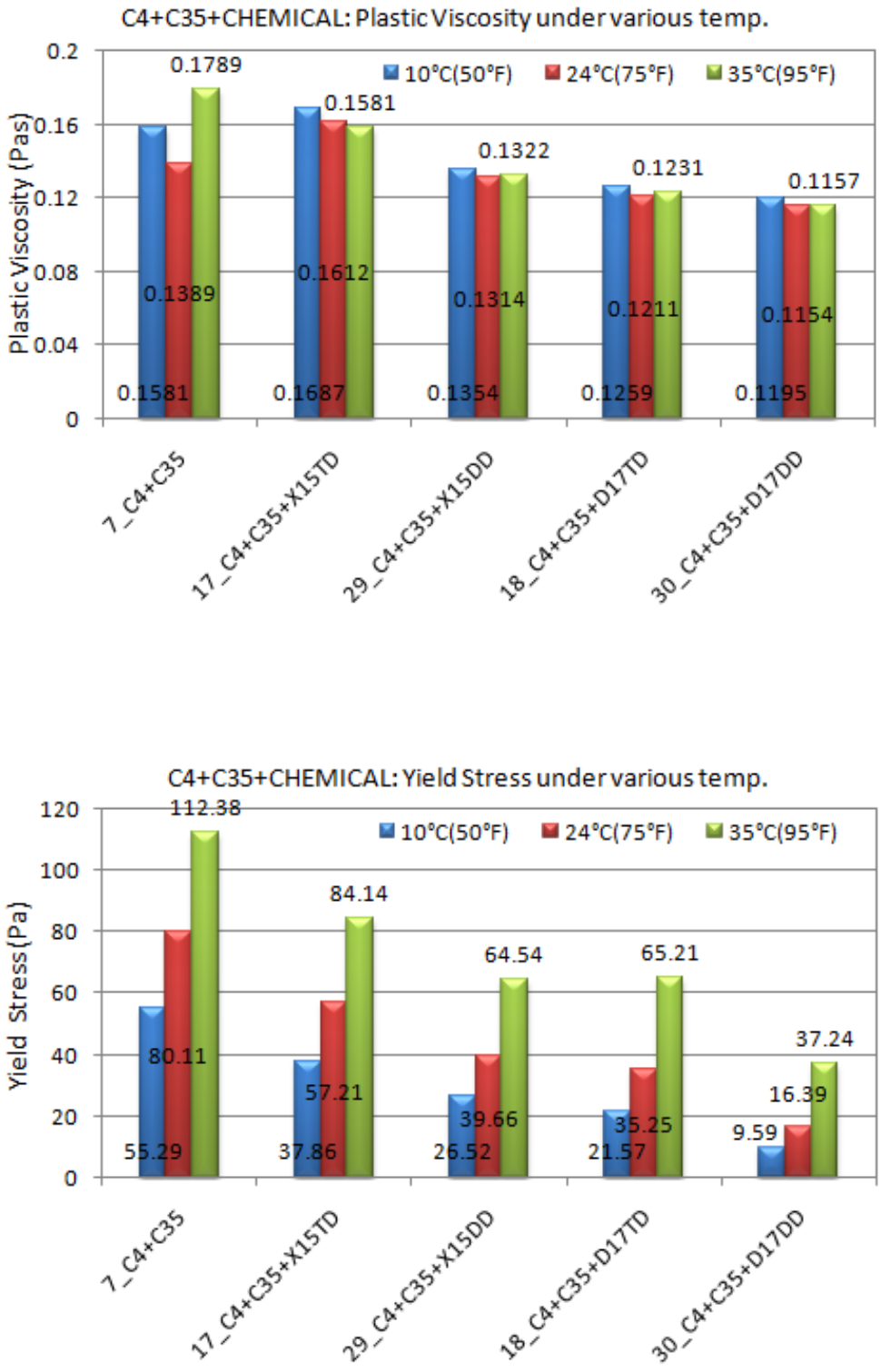

Figure C-9 PV (top) and YS (bottom) for C4+C35 system as a function of temperature, admixture type and dosage.

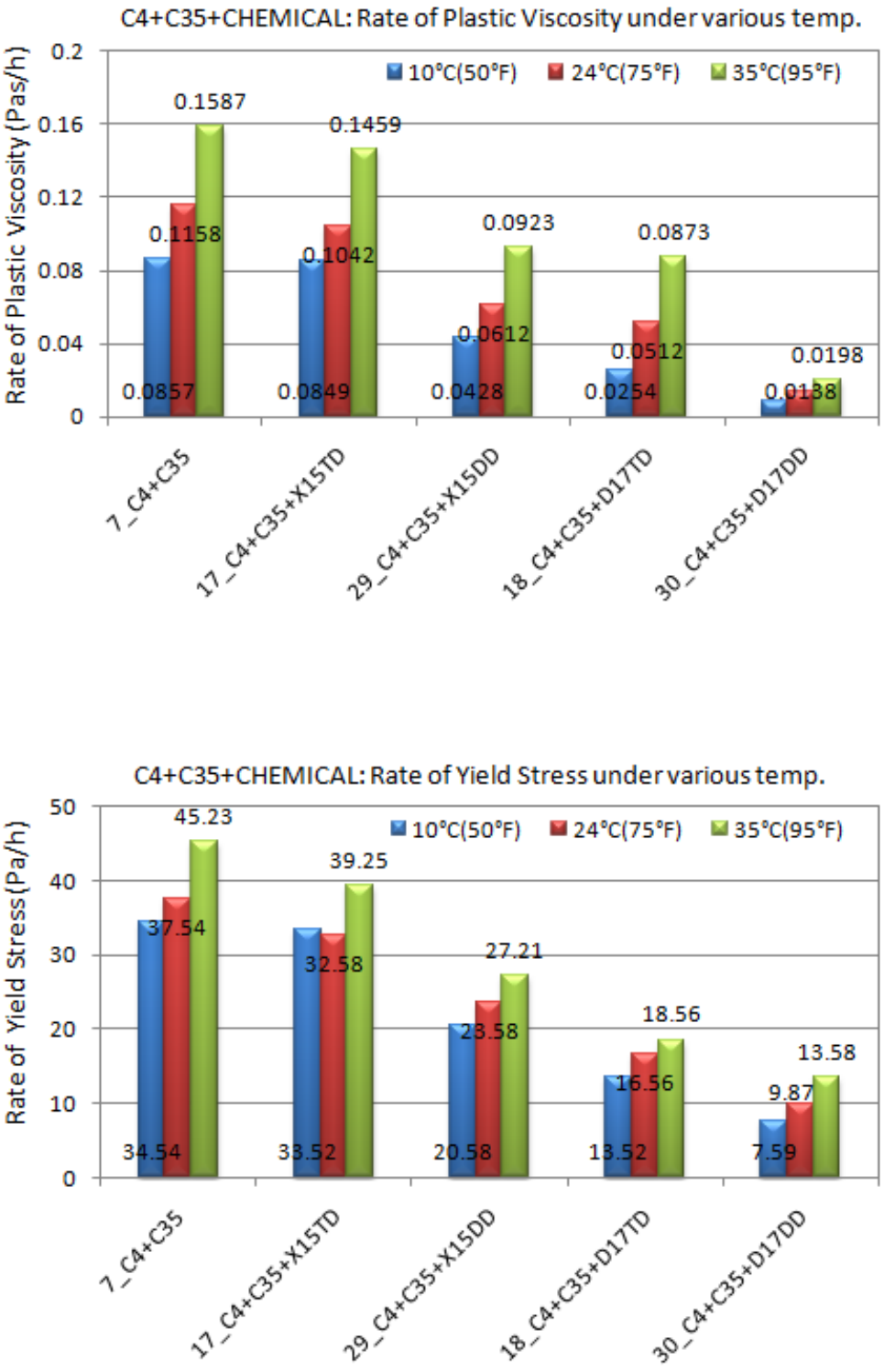

Figure C-10 RPV (top) and RYS (bottom) for C4+C35 system as a function of temperature, admixture type and dosage.

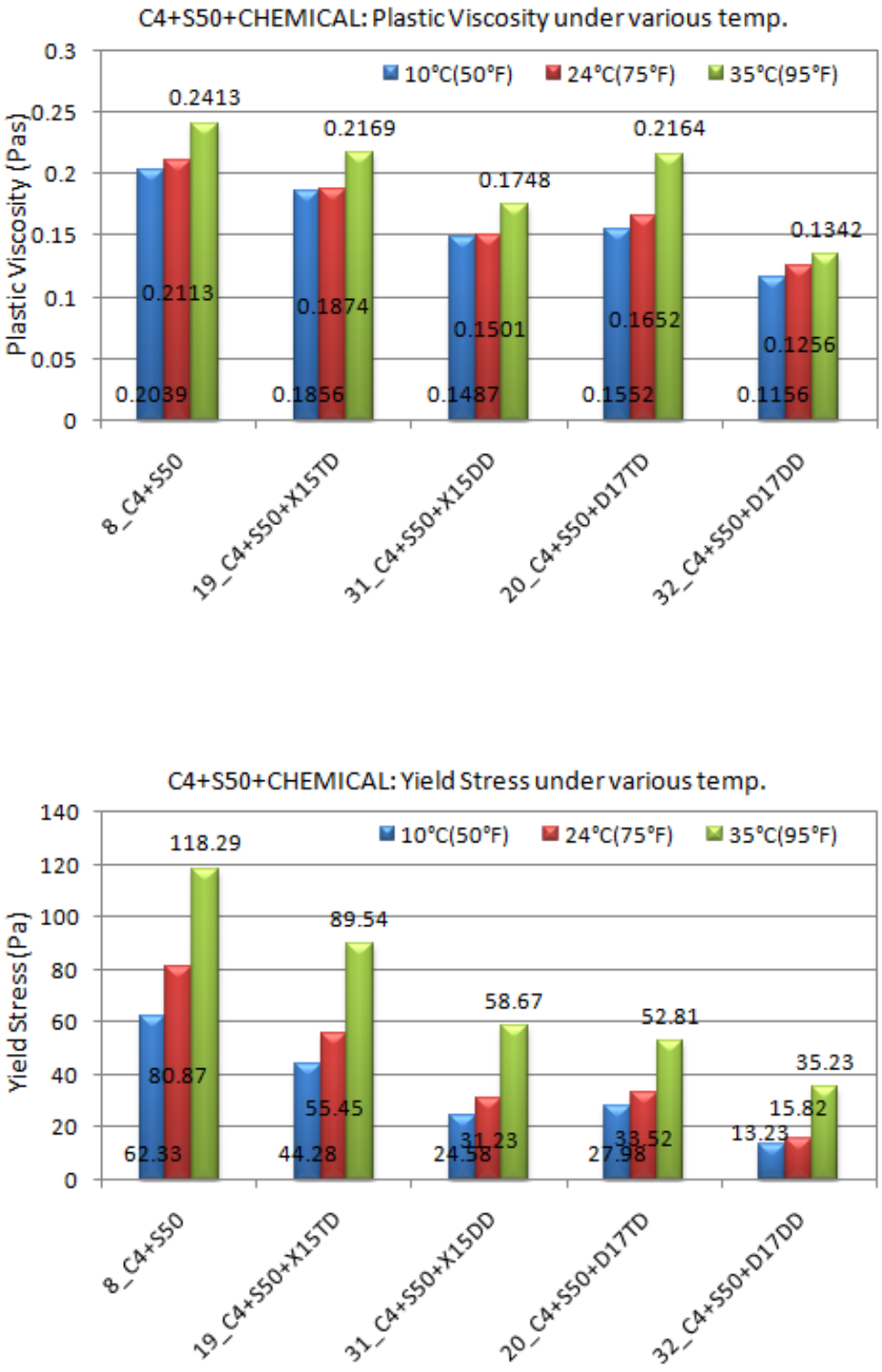

Figure C-11 PV (top) and YS (bottom) for C4+S50 system as a function of temperature, admixture type and dosage.

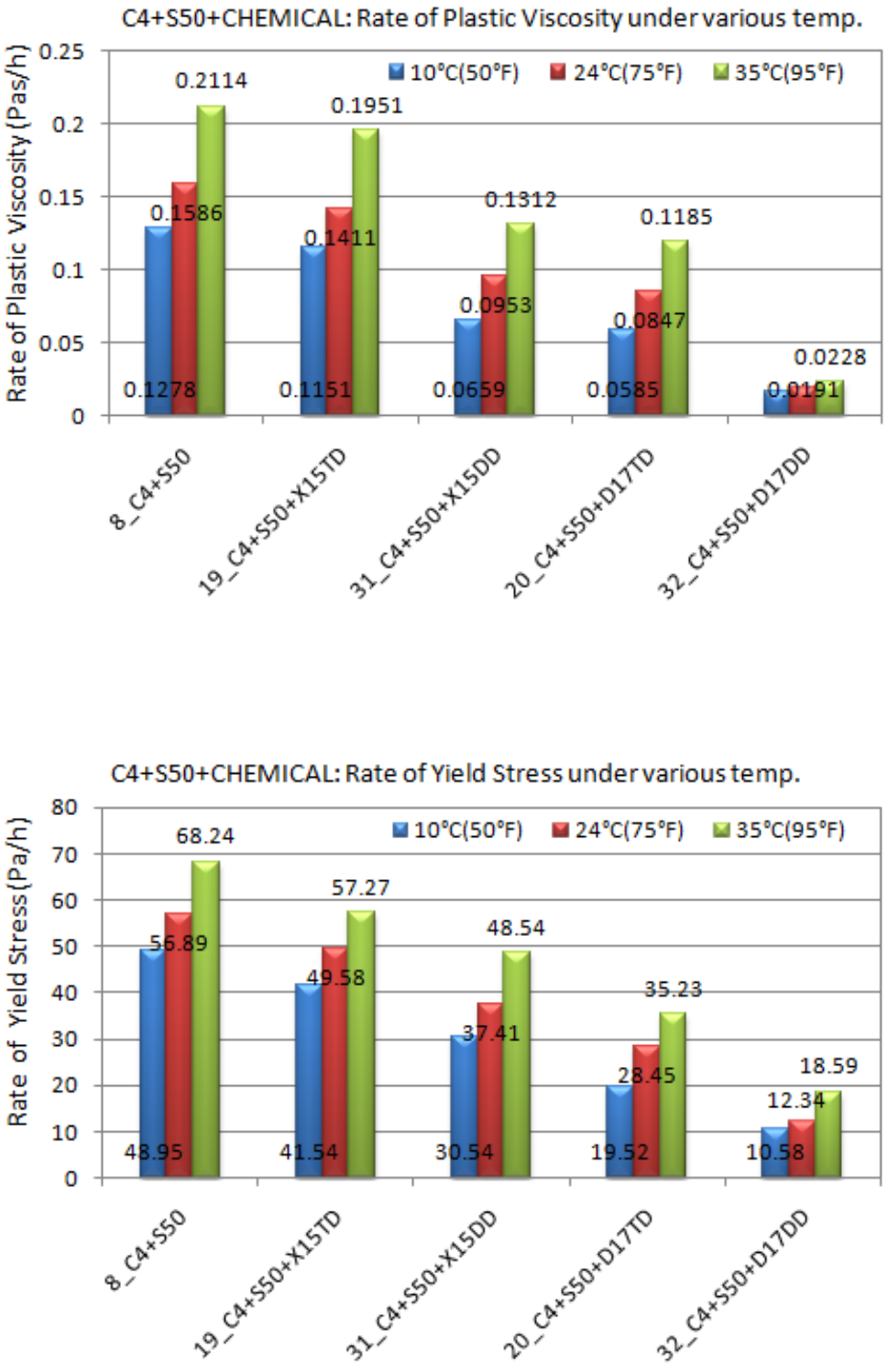

Figure C-12 RPV (top) and RYS (bottom) for C4+S50 system as a function of temperature, admixture type and dosage.

APPENDIX D

STATIC RHEOLOGICAL PARAMETERS

VS. PERCENT OF HEAT EVOLUTION

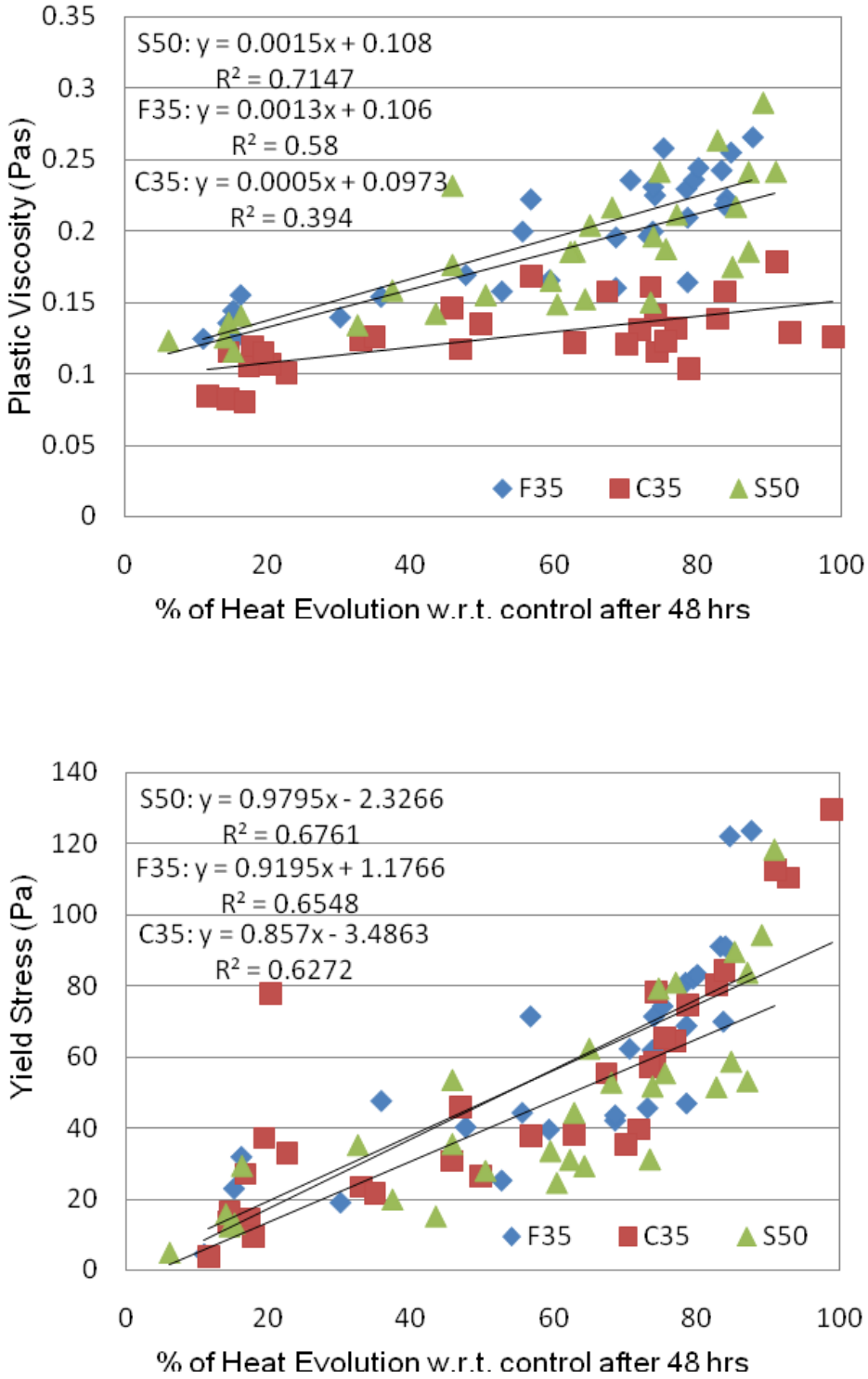

Figure D-1 Regression of PV (top) and YS (bottom) vs. percent of heat evolution as a function of SCMs.

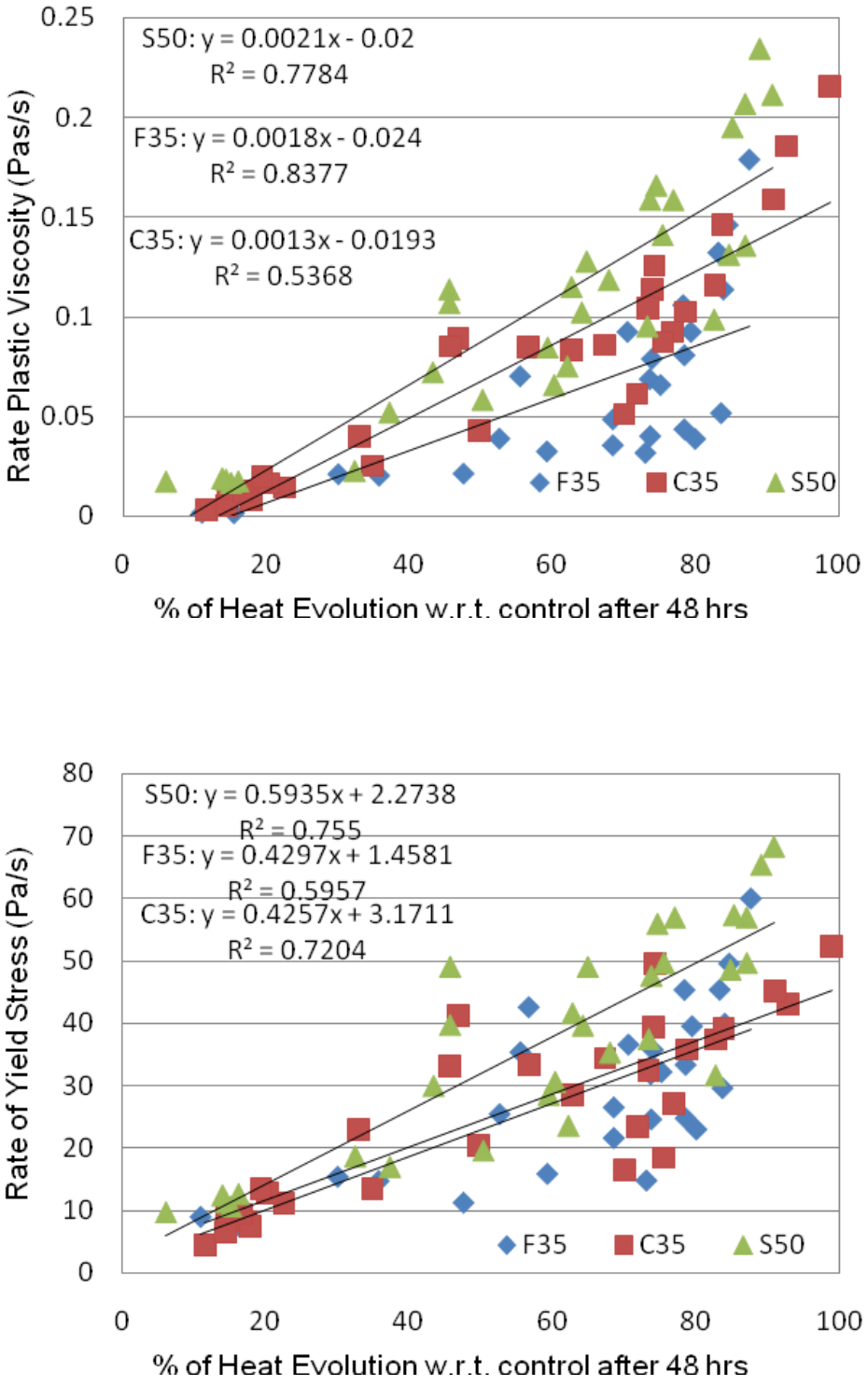

Figure D-2 Regression of RPV (top) and RYS (bottom) vs. percent of heat evolution as a function of SCMs.

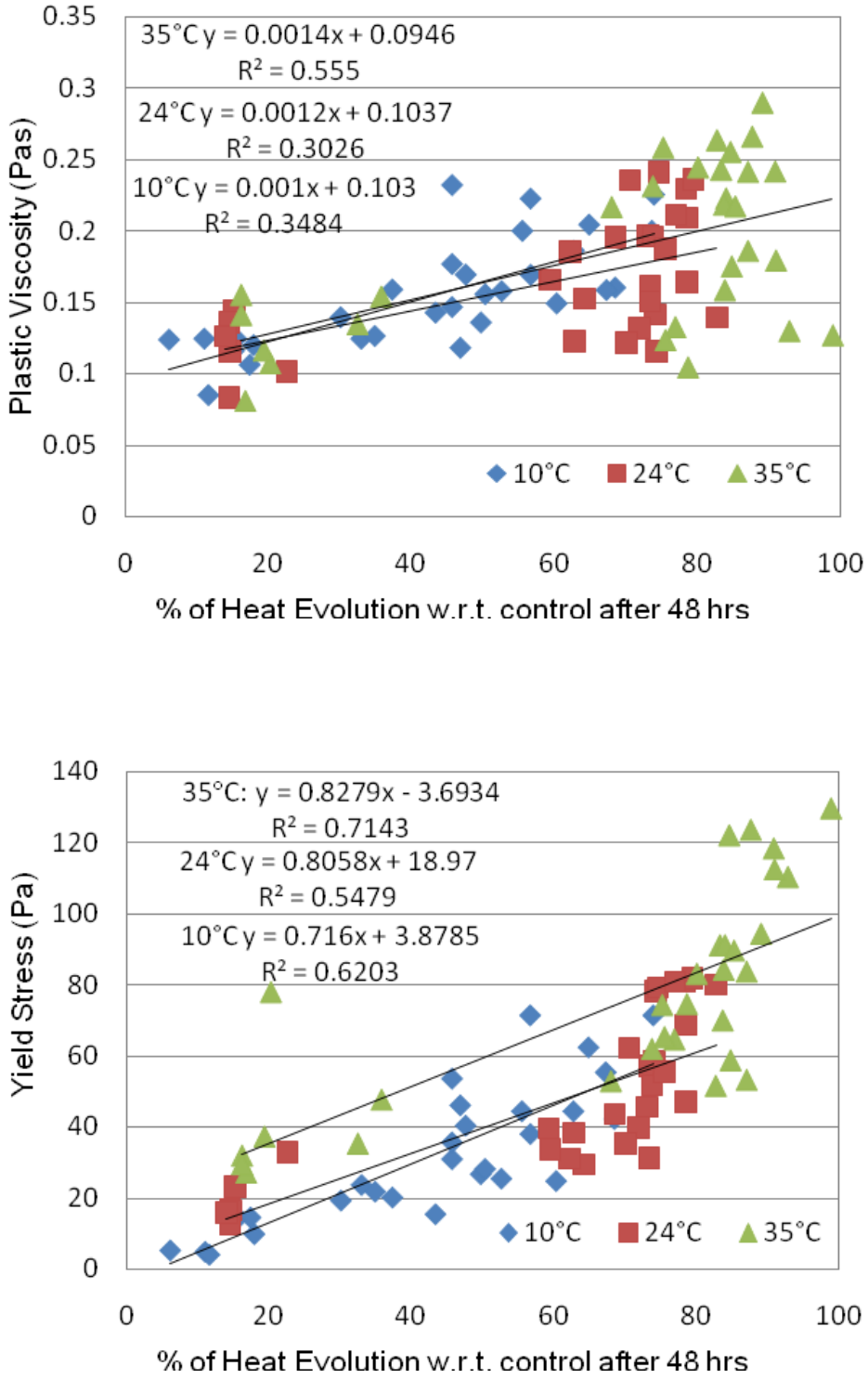

Figure D-3 Regression of PV (top) and YS (bottom) vs. percent of heat evolution as a function of temperature conditions.

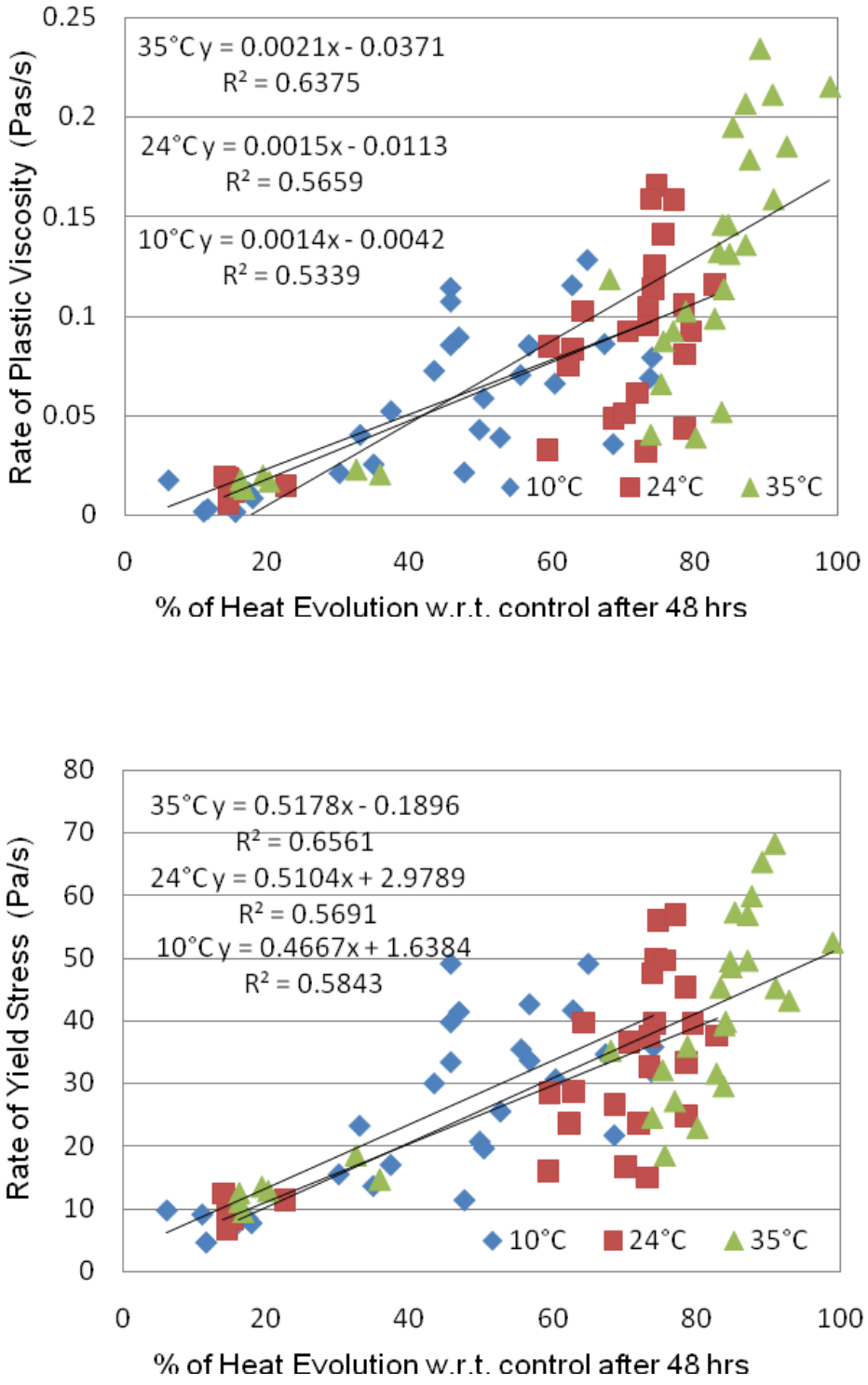

Figure D-4 Regression of RPV (top) and RYS (bottom) vs. percent of heat evolution as a function of temperature conditions.

APPENDIX E

DYNAMIC RHEOLOGICAL PARAMETERS

BY THE MODIFIED DSR

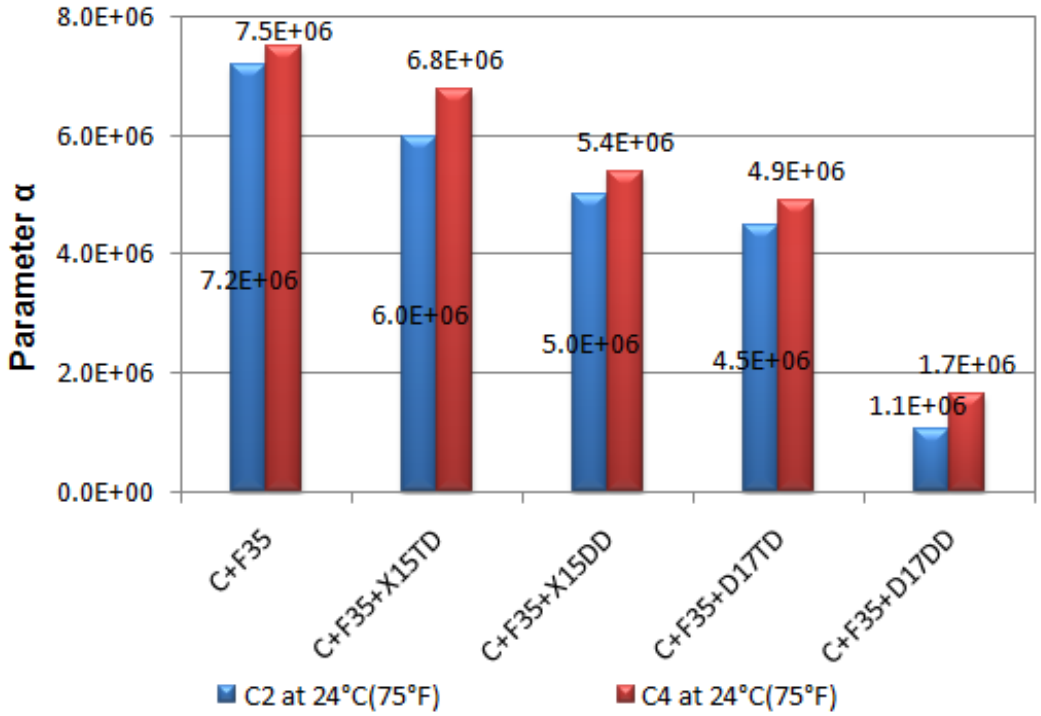

Figure E-1 Parameter α of the storage modulus curve for cements + F35 system at 24°C.

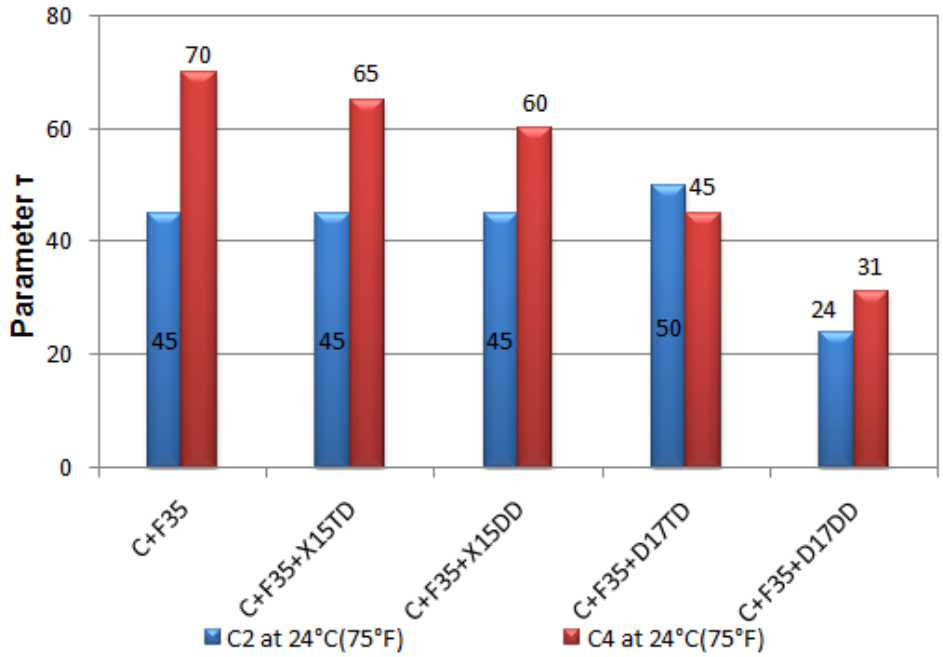

Figure E-2 Parameter τ of the storage modulus curve for cements + F35 system at 24°C.

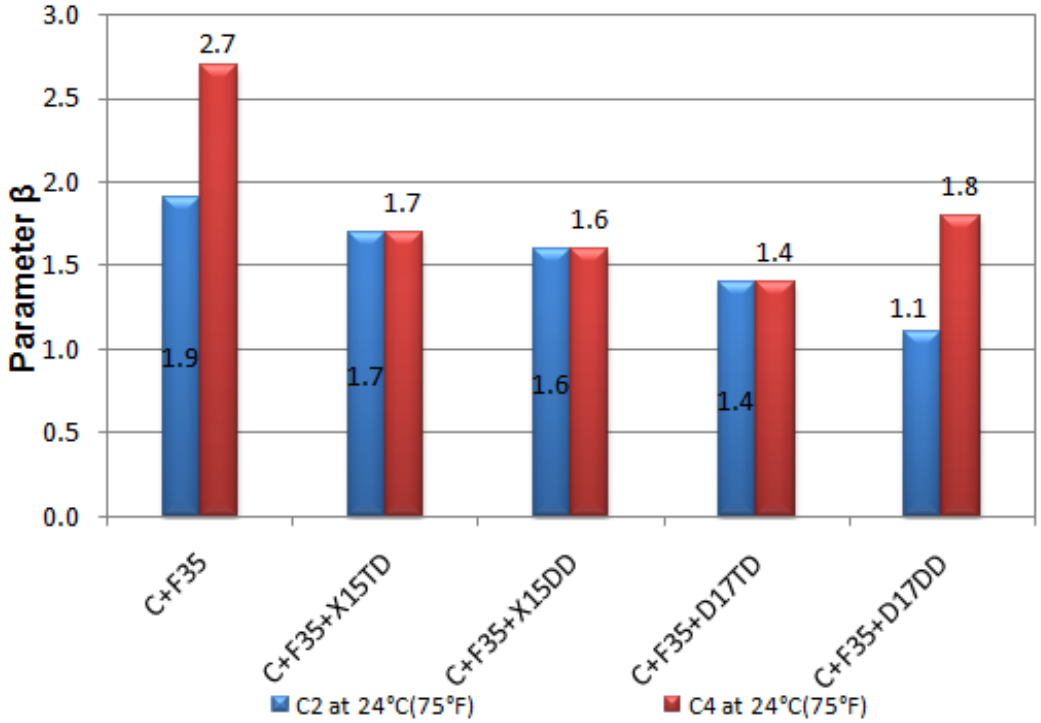

Figure E-3 Parameter β of the storage modulus curve for cements + F35 system at 24°C.

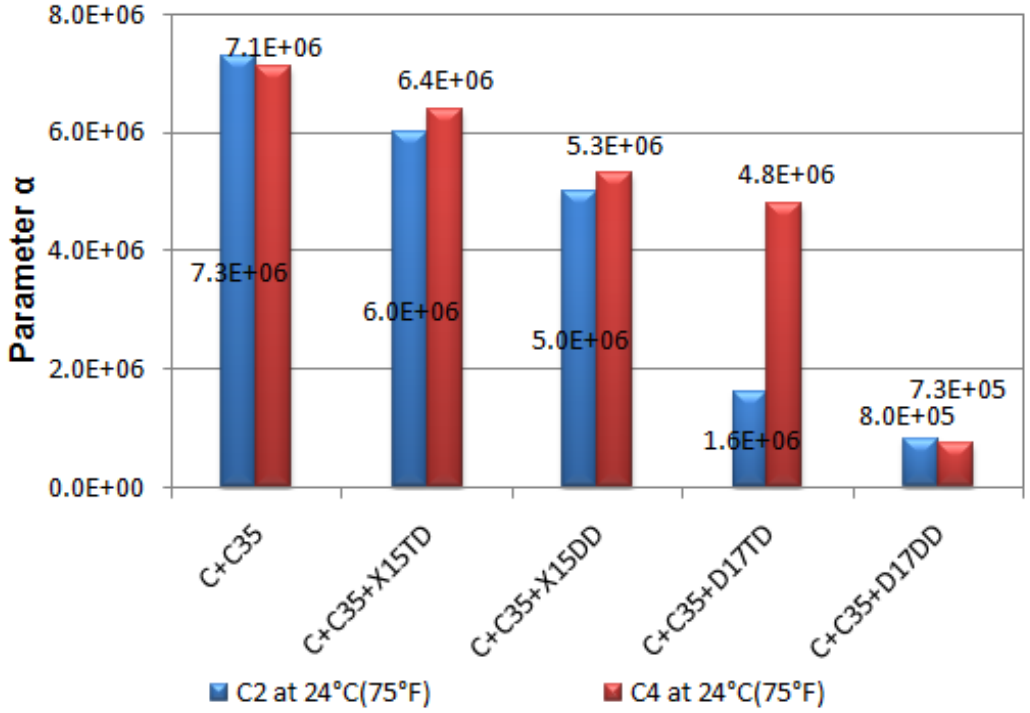

Figure E-4 Parameter α of the storage modulus curve for cements + C35 system at 24°C.

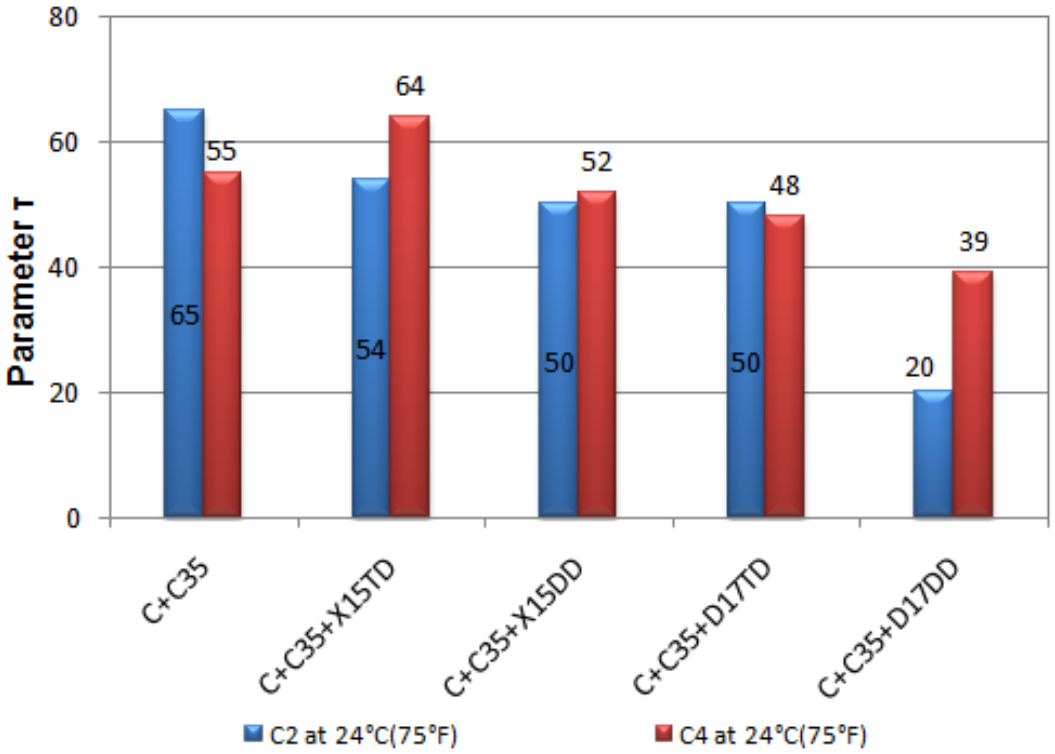

Figure E-5 Parameter τ of the storage modulus curve for cements + C35 system at 24°C.

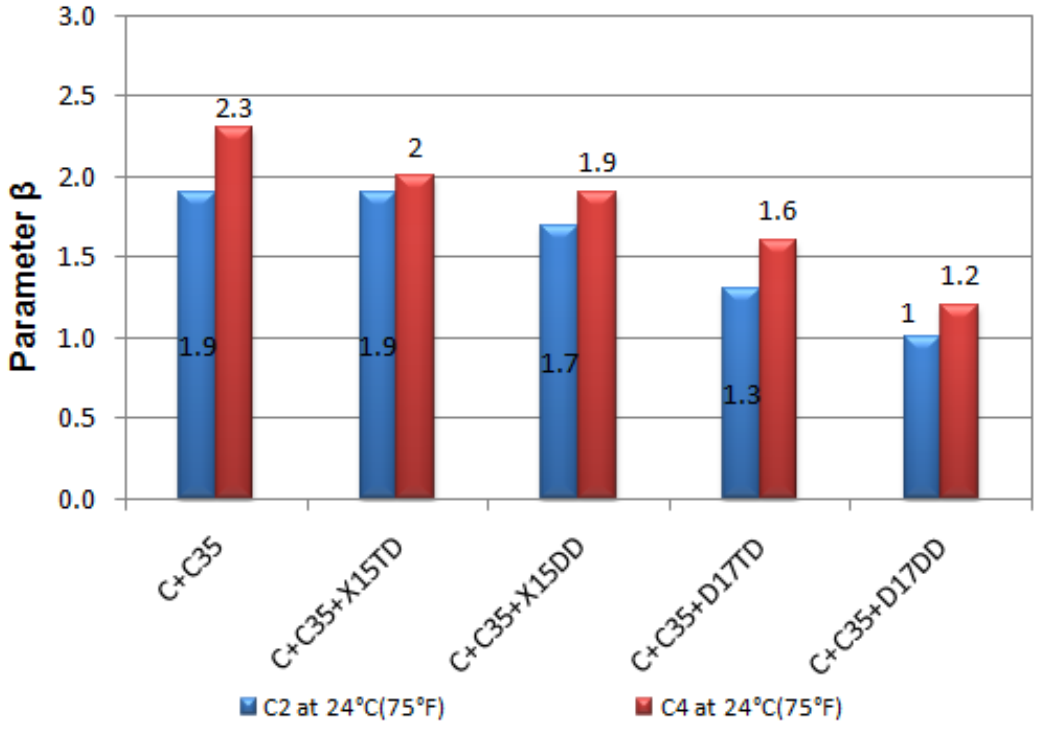

Figure E-6 Parameter β of the storage modulus curve for cements + C35 system at 24°C.

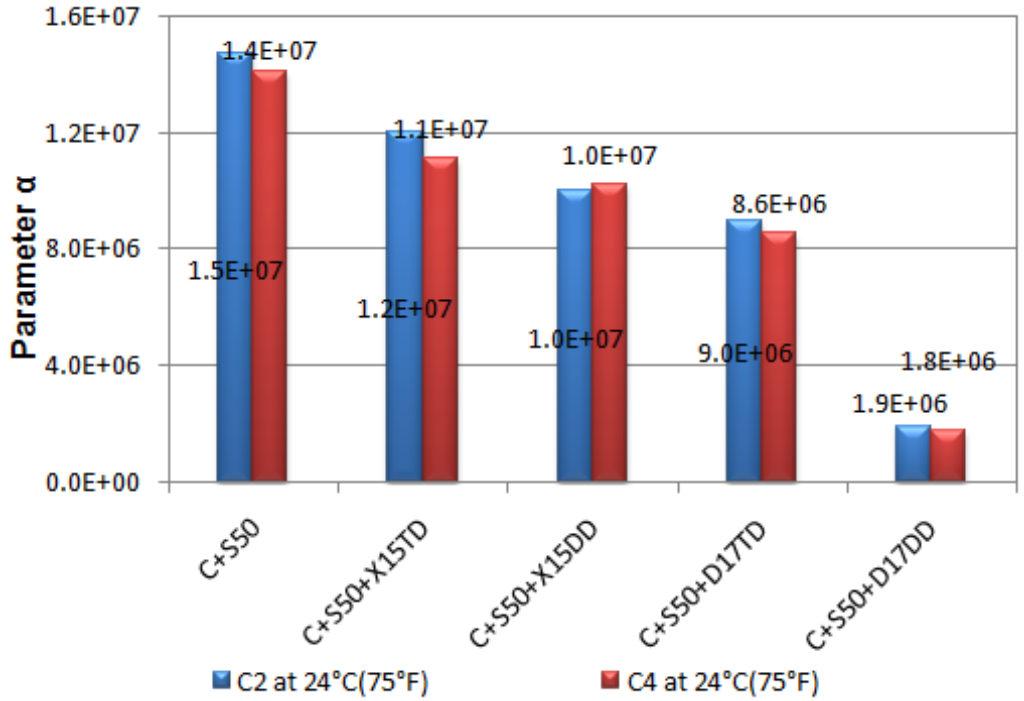

Figure E-7 Parameter α of the storage modulus curve for cements + S50 system at 24°C.

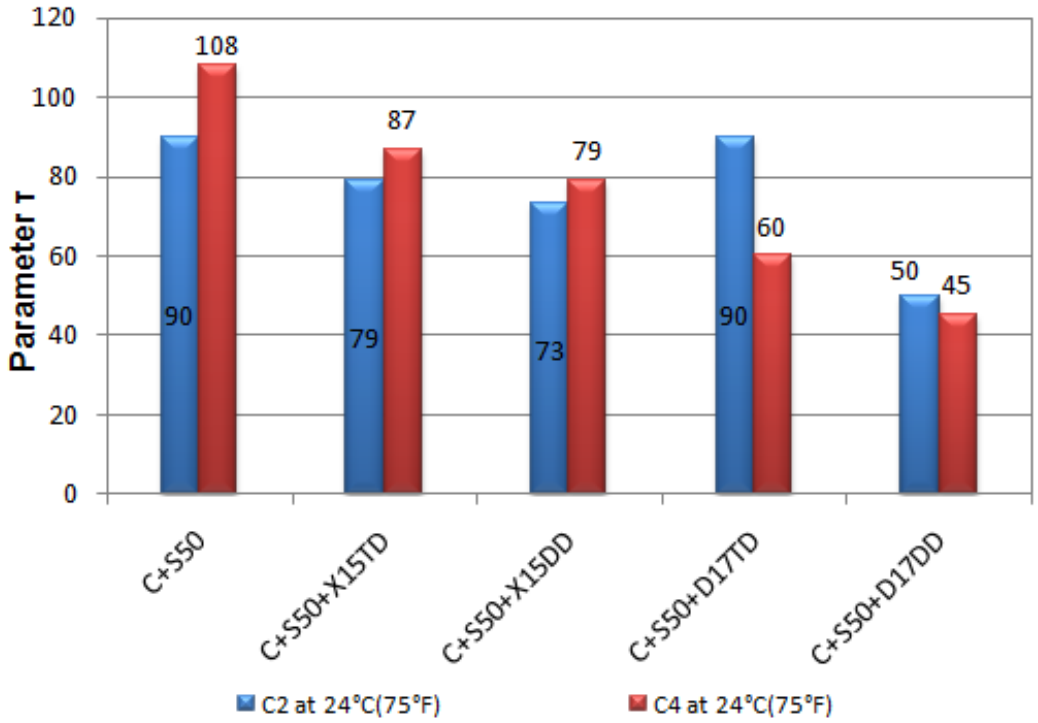

Figure E-8 Parameter τ of the storage modulus curve for cements + S50 system at 24°C.

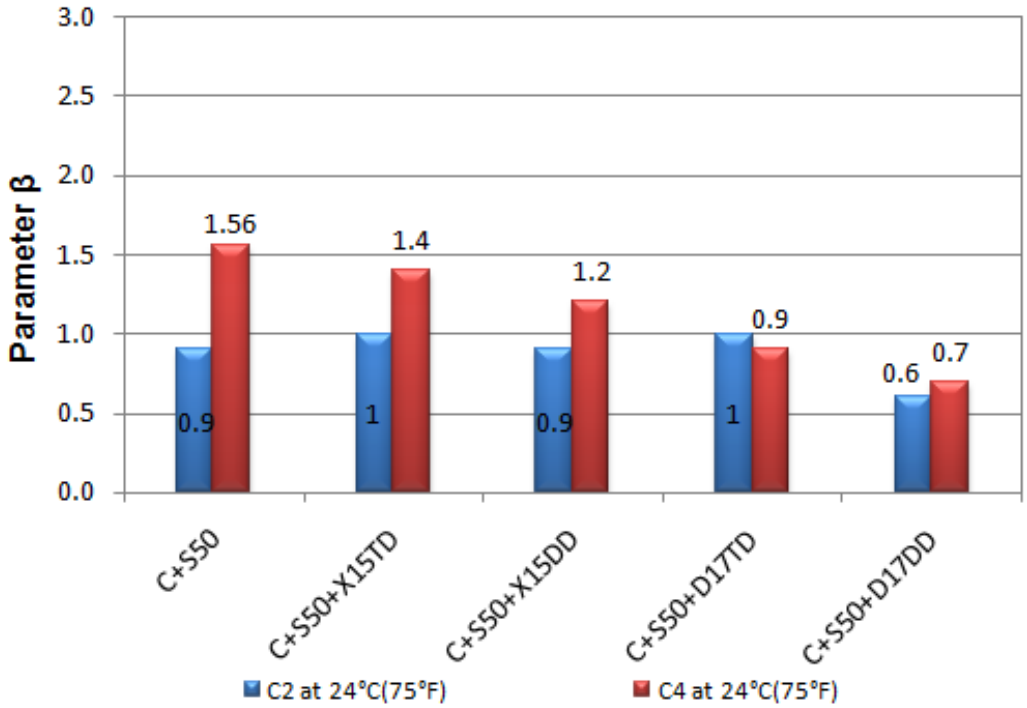

Figure E-9 Parameter β of the storage modulus curve for cements + S50 system at 24°C.

APPENDIX F

MINI SLUMP PAT AREA

AS A FUNCTION OF TIME

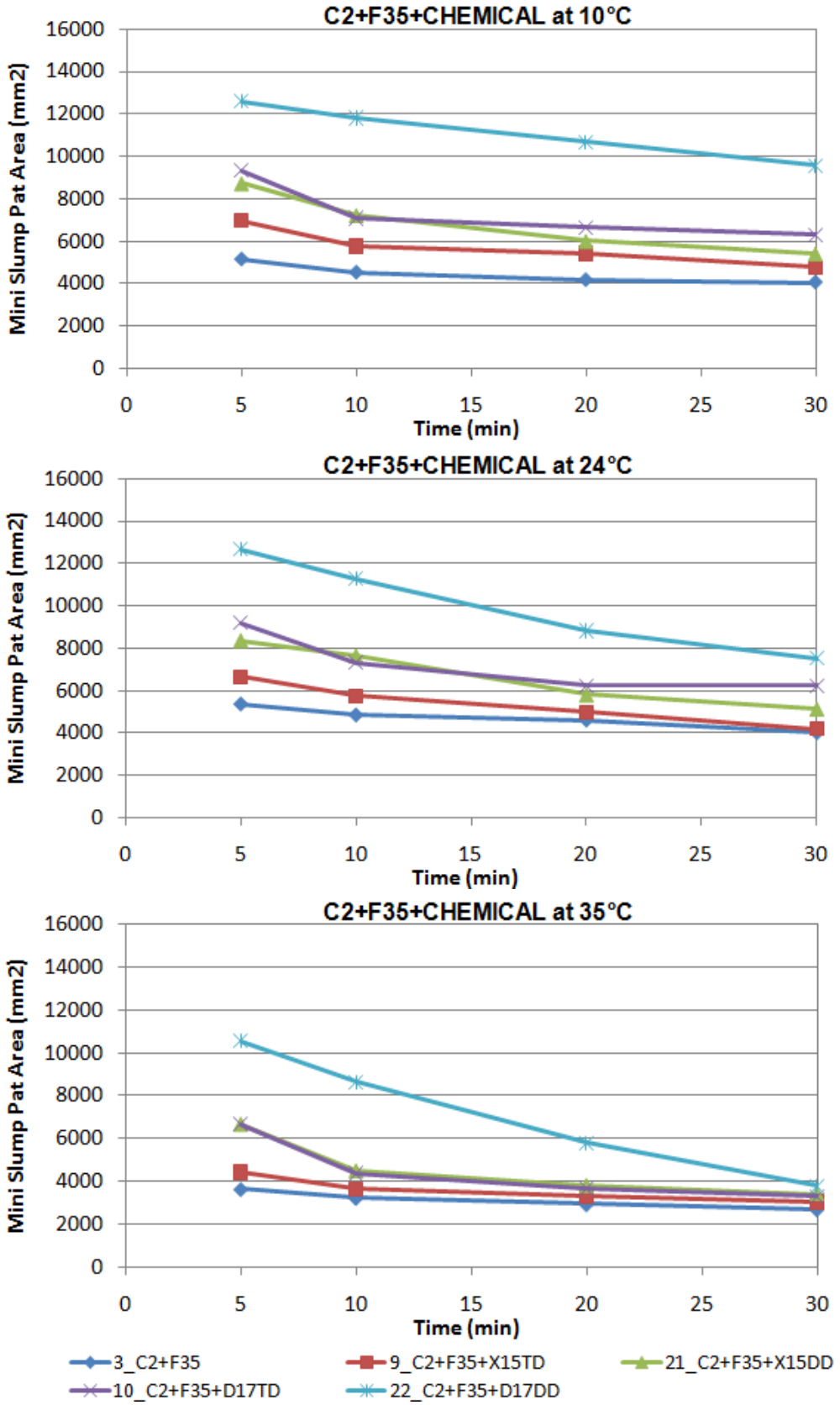

Figure F-1 Mini slump pat area for C2+F35 system under different temperatures.

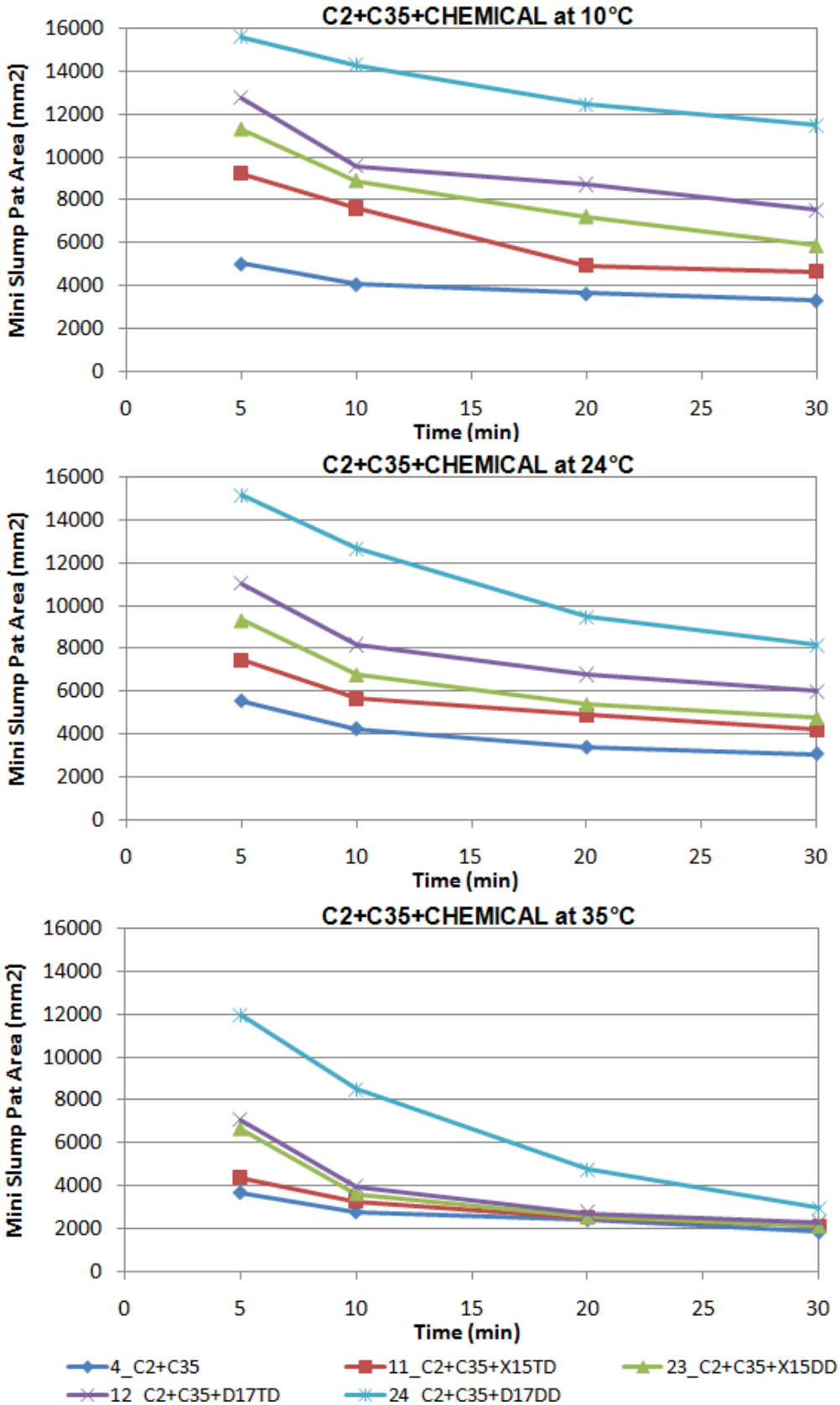

Figure F-2 Mini slump pat area for C2+C35 system under different temperatures.

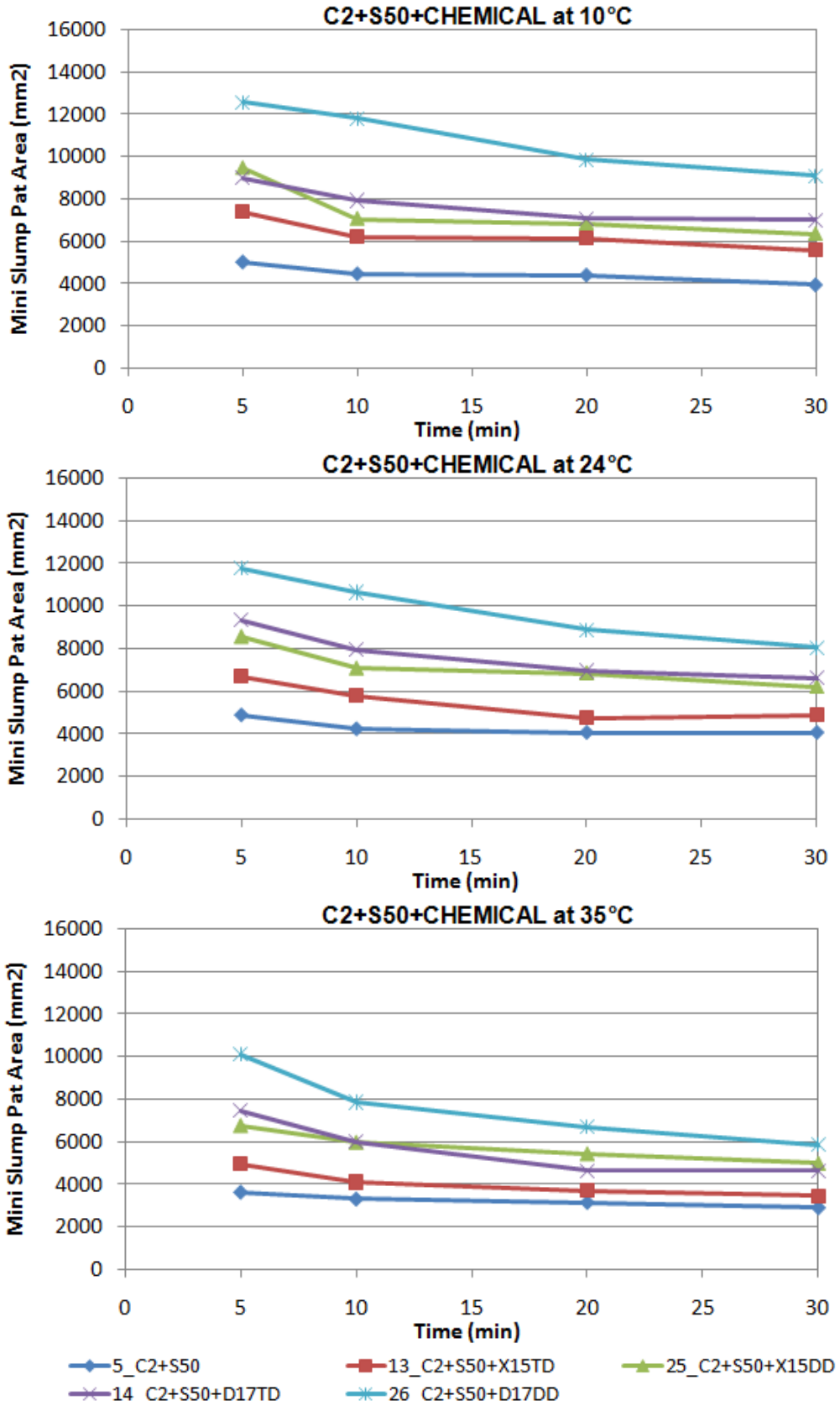

Figure F-3 Mini slump pat area for C2+S50 system under different temperatures.

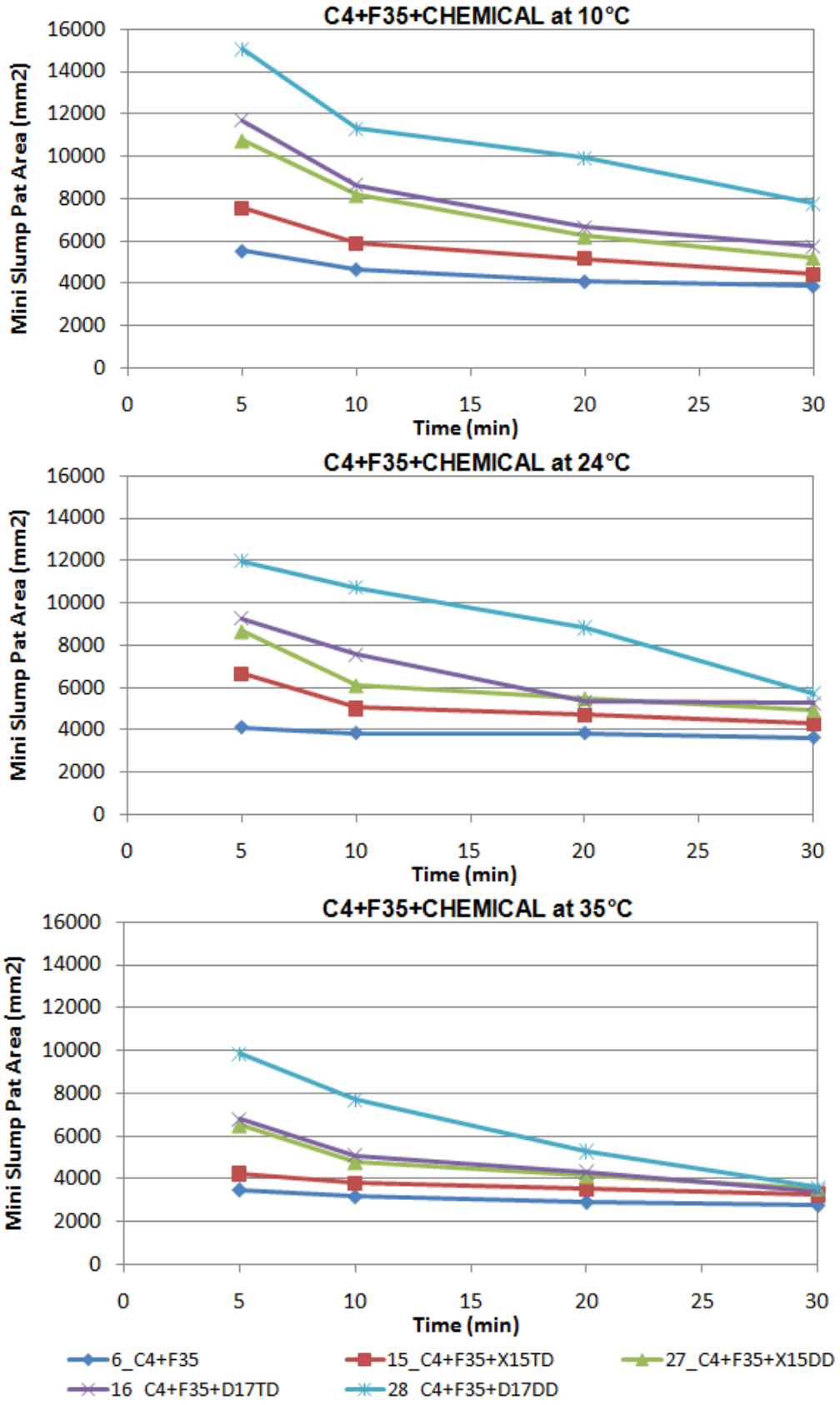

Figure F-4 Mini slump pat area for C4+F35 system under different temperatures.

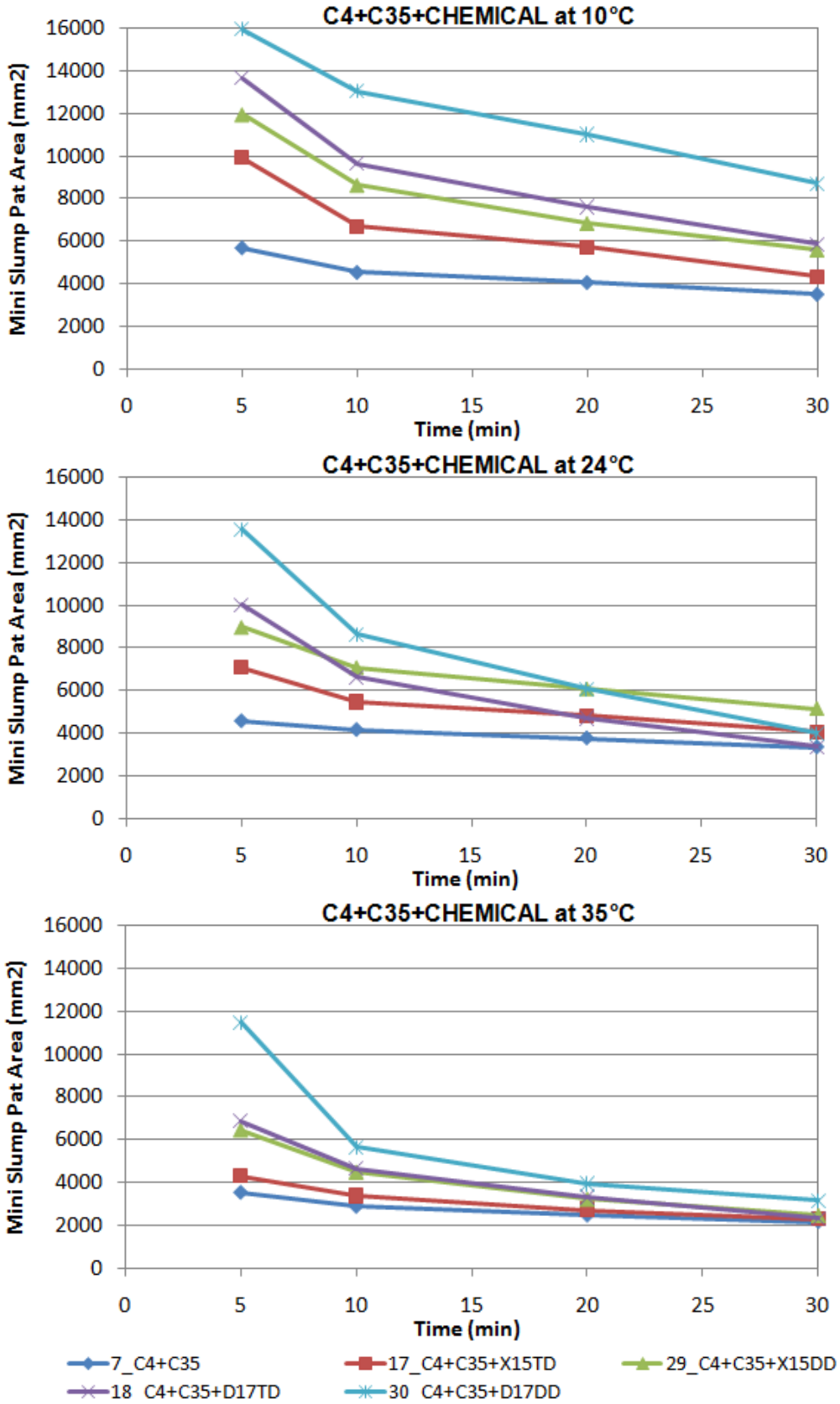

Figure F-5 Mini slump pat area for C4+C35 system under different temperatures.

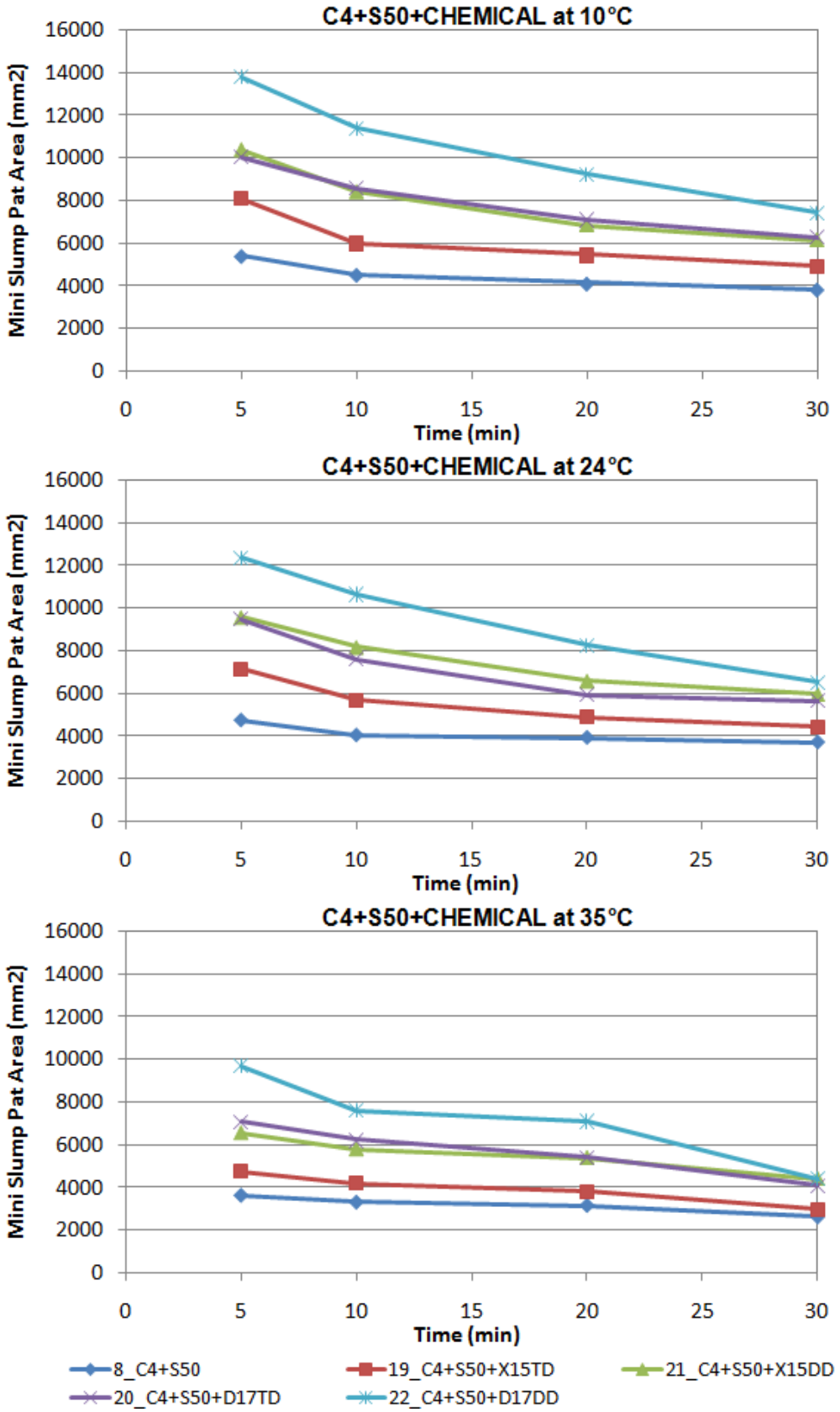

Figure F-6 Mini slump pat area for C4+S50 system under different temperatures.

APPENDIX G

RATE OF PAT AREA LOSS

AS A FUNCTION OF

TEMPERATURE AND SCMs

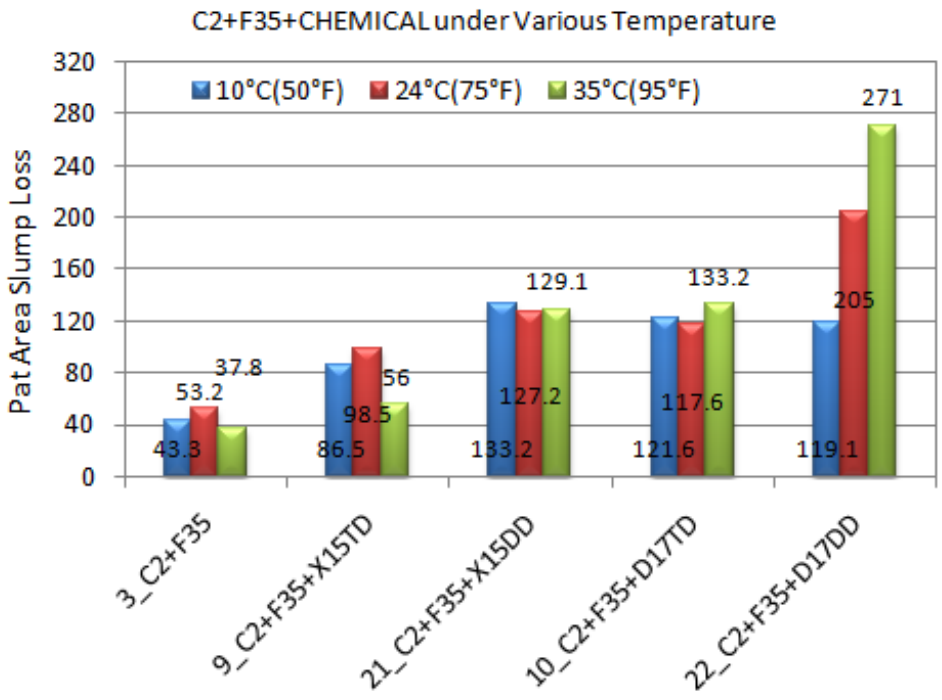

Figure G-1 Rate of pat area loss for C2+F35 system under different temperatures.

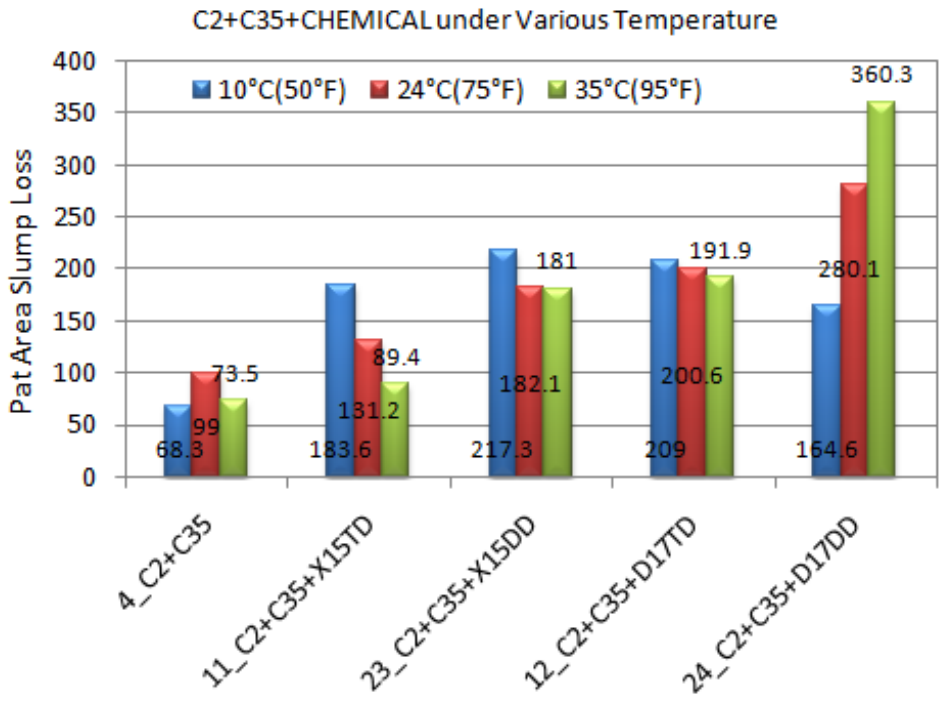

Figure G-2 Rate of pat area loss for C2+C35 system under different temperatures.

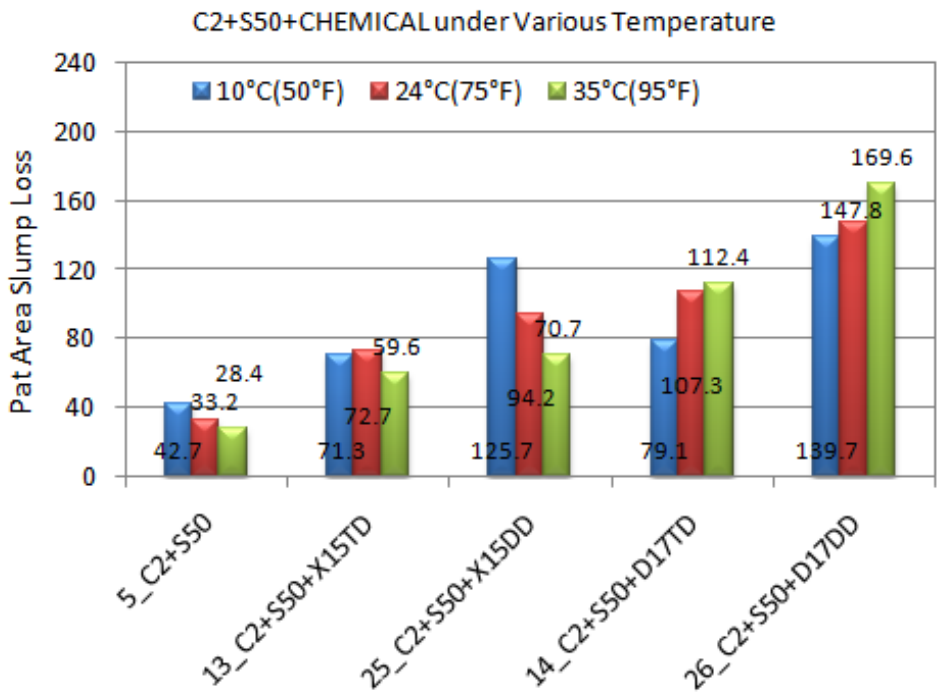

Figure G-3 Rate of pat area loss for C2+S50 system under different temperatures.

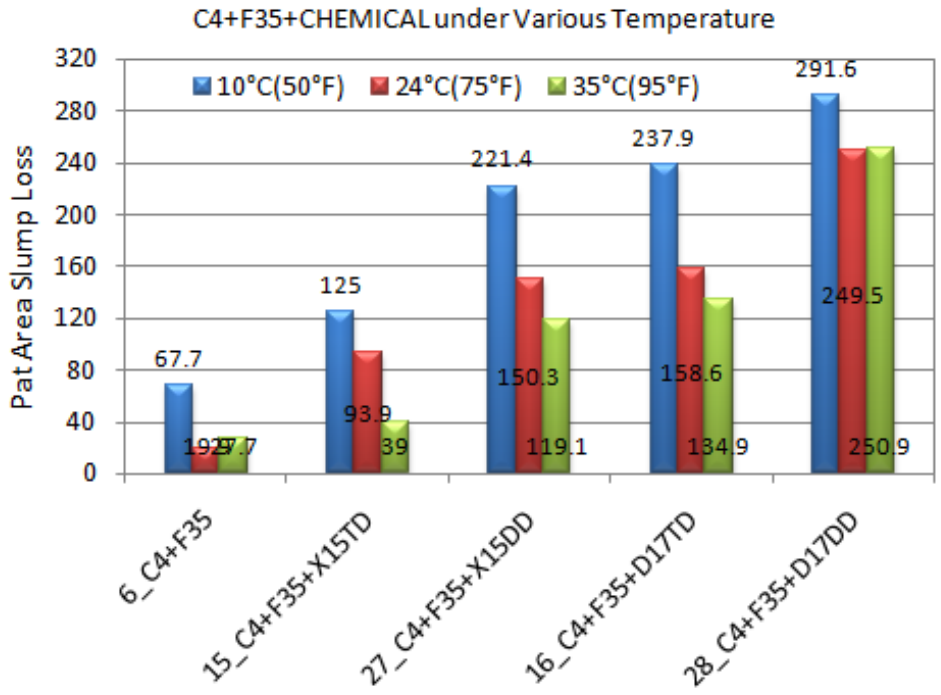

Figure G-4 Rate of pat area loss for C4+F35 system under different temperatures.

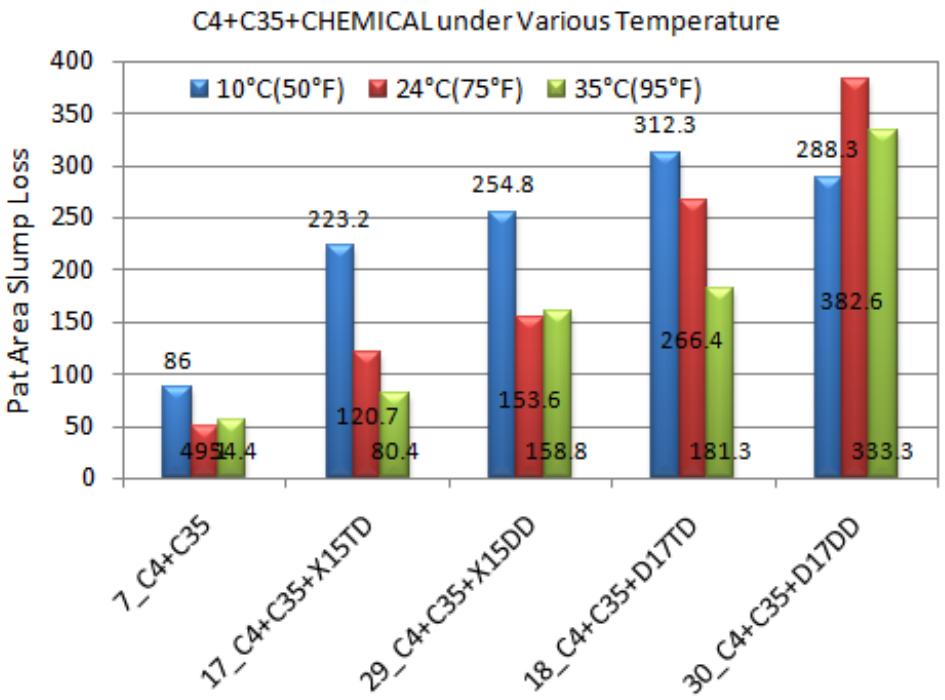

Figure G-5 Rate of pat area loss for C4+C35 system under different temperatures.

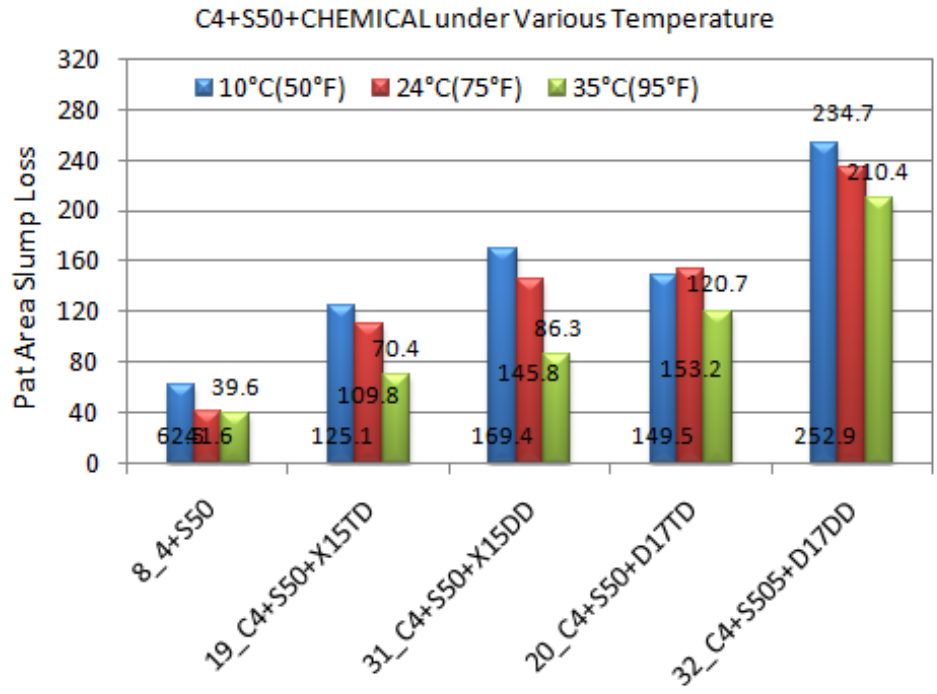

Figure G-6 Rate of pat area loss for C4+S50 system under different temperatures.

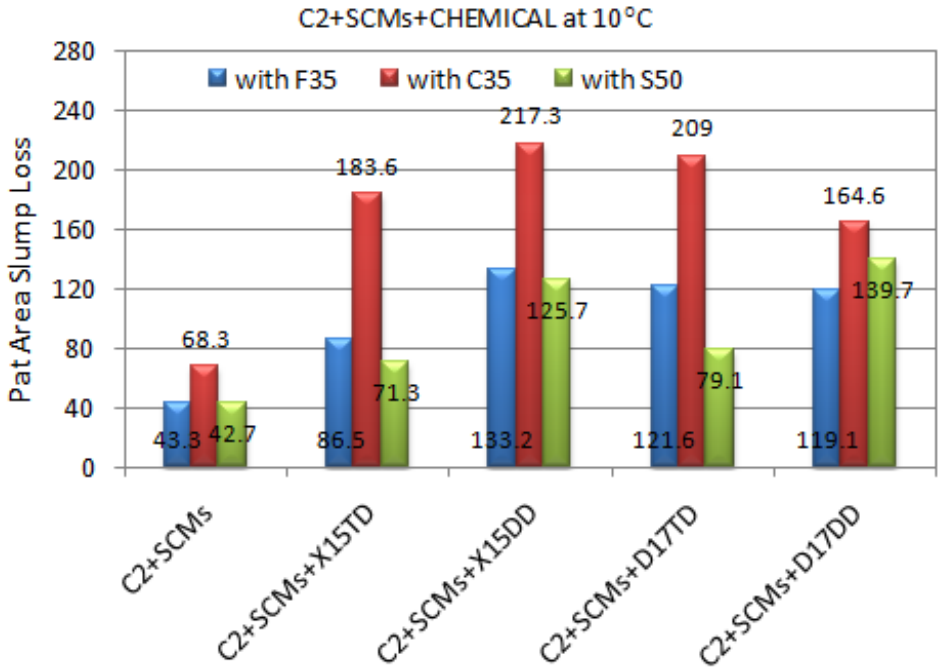

Figure G-7 Rate of pat area loss for C2 with different SCMs system at 10°C.

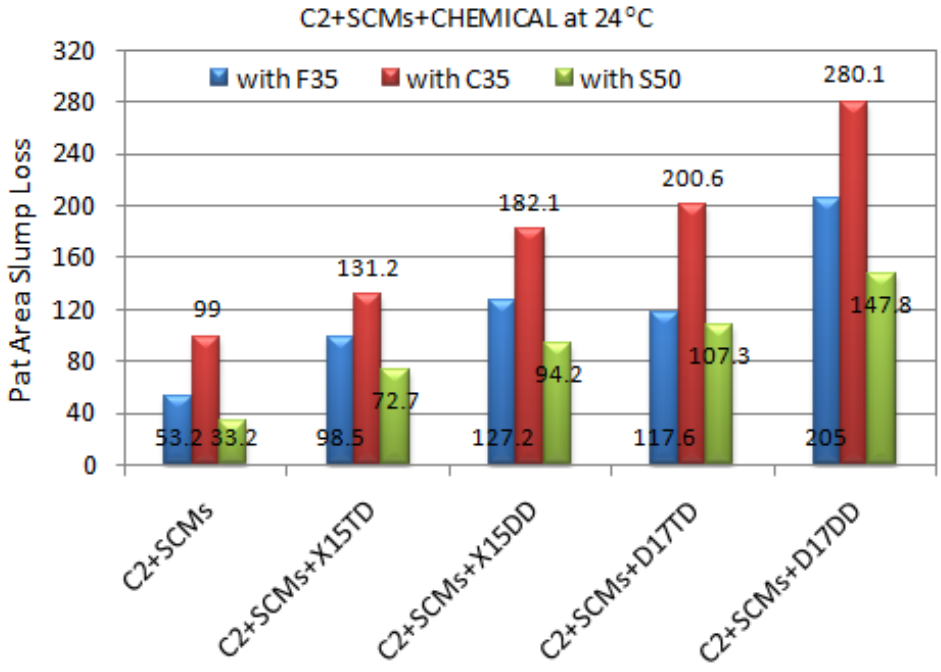

Figure G-8 Rate of pat area loss for C2 with different SCMs system at 24°C.

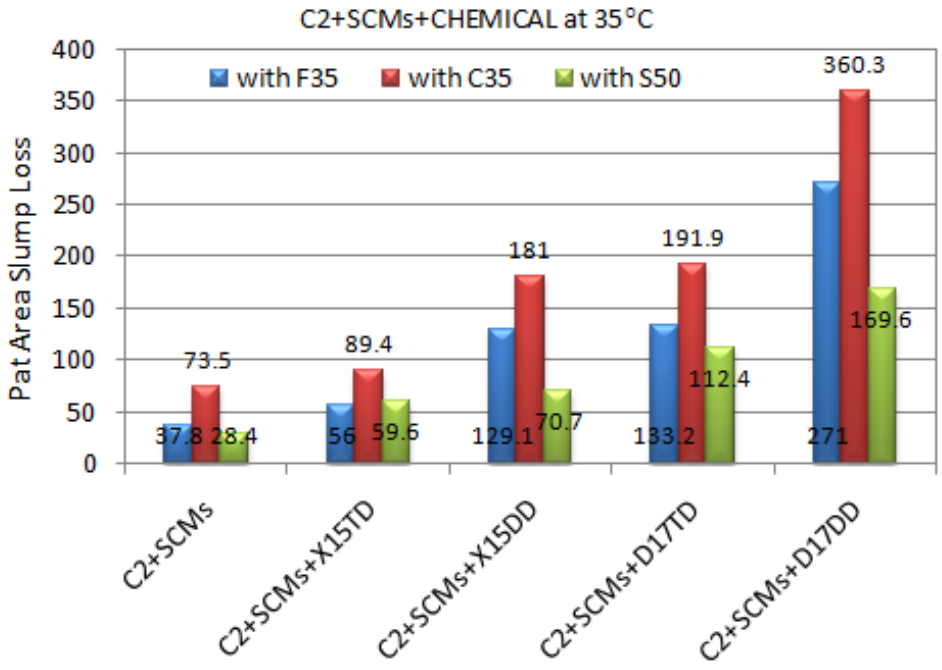

Figure G-9 Rate of pat area loss for C2 with different SCMs system at 35°C.

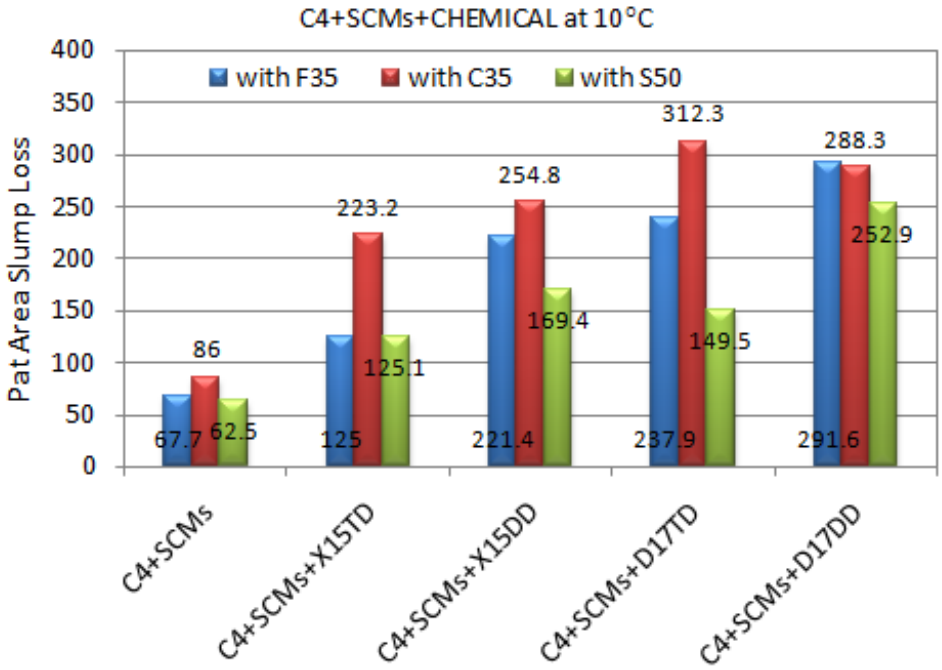

Figure G-10 Rate of pat area loss for C4 with different SCMs system at 10°C.

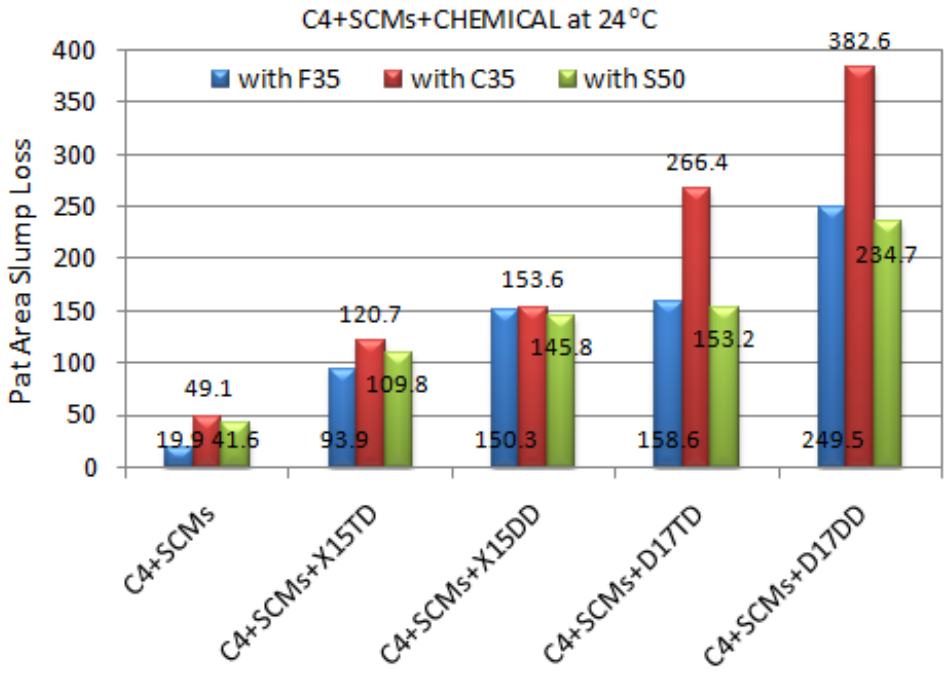

Figure G-11 Rate of pat area loss for C4 with different SCMs system at 24°C.

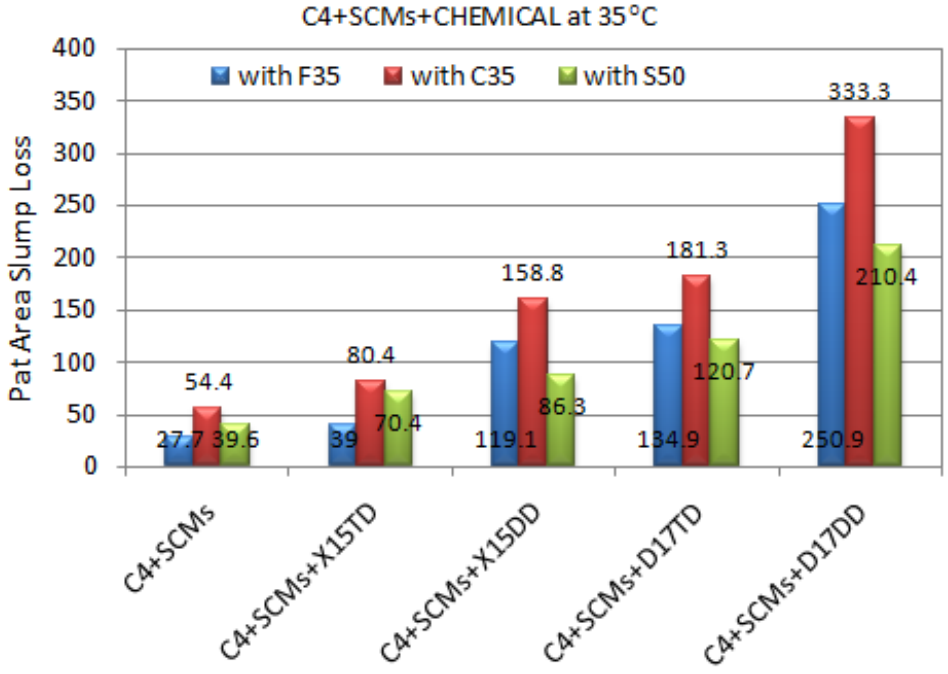

Figure G-12 Rate of pat area loss for C4 with different SCMs system at 35°C.

VITA

Se Hoon Jang obtained his B.S. degree in civil engineering from Kyungpook National University in Daegu, South Korea. After receiving his B.S. degree in 2002, he went to the Zachry Department of Civil Engineering at Texas A&M University in College Station, Texas and received his M.S. degree in August 2005. He was admitted as a Ph.D. candidate in the construction material division in the Zachry Department of Civil Engineering at Texas A&M University in College Station, Texas. He served as a graduate assistant researcher at the Texas Transportation Institute (T.T.I.) for five years and a graduate assistant teacher at the Zachry Department of Civil Engineering for half a year. He is a member of the American Concrete Institute (ACI) and the International Society on Concrete Pavements (ISCP). He was also president of the Korean-American Scientists and Engineers Association (KSEA) at Texas A&M University from August 2007 to August 2008.

Address: CE/TTI Building 501G Materials TAMU System 3135

College Station, TX 77840-3135 USA

E-mail: jangsehoon@gmail.com